SANDIA REPORT
SAND2004-0730
Unlimited Release
Printed February 2006

DRSPALL: Spallings Model for the Waste Isolation Pilot Plant 2004 Recertification

David L. Lord, David K. Rudeen, John F. Schatz, Amy P. Gilkey, Clifford W. Hansen

Prepared by
Sandia National Laboratories
Albuquerque, New Mexico 87185 and Livermore, California 94550

Sandia is a multiprogram laboratory operated by Sandia Corporation,
a Lockheed Martin Company, for the United States Department of Energy's
National Nuclear Security Administration under Contract DE-AC04-94AL85000.

Issued by Sandia National Laboratories, operated for the United States Department of Energy by Sandia Corporation.

Available to DOE and DOE contractors from
U.S. Department of Energy
Office of Scientific and Technical Information
P.O. Box 62
Oak Ridge, TN 37831

Telephone: (865)576-8401
Facsimile: (865)576-5728
E-Mail: reports@adonis.osti.gov
Online ordering: http://www.osti.gov/bridge

Available to the public from
U.S. Department of Commerce
National Technical Information Service
5285 Port Royal Rd
Springfield, VA 22161

Telephone: (800)553-6847
Facsimile: (703)605-6900
E-Mail: orders@ntis.fedworld.gov
Online order: http://www.ntis.gov/help/ordermethods.asp?loc=7-4-0#online

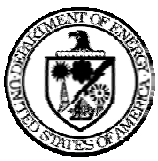

SAND2004-0730
Unlimited Release
February 2006

DRSPALL: Spallings Model for the Waste Isolation Pilot Plant 2004 Recertification

David L. Lord[1], David K. Rudeen[2], John F. Schatz[3], Amy P. Gilkey[2], Clifford W. Hansen[1]

[1]Performance Assessment and Decision Analysis Department
Sandia National Laboratories
Carlsbad Programs Group
Carlsbad, NM 88220

[2]GRAM, Inc.
Albuquerque, NM 87112

[3]John F. Schatz Research & Consulting, Inc.
Del Mar, CA 92014

Abstract

This report presents a model to estimate the spallings releases for the Waste Isolation Pilot Plant Performance Assessment (WIPP PA). A spallings release in the context of WIPP PA refers to a portion of the solid waste transported from the subsurface repository to the ground surface due to inadvertent oil or gas drilling into the WIPP repository at some time after site closure. Some solid waste will be removed by the action of the drillbit and drilling fluid; this waste is referred to as cuttings and cavings. If the repository is pressurized above hydrostatic at the time of intrusion, solid waste material local to the borehole may be subject to mechanical failure and entrainment in high-velocity gases as the repository pressure is released to the borehole. Solid material that fails and is transported into the wellbore and thus to the surface comprise the spallings releases. The spallings mechanism is analogous to a well blowout in the modern oil and gas drilling industry. The current spallings conceptual model and associated computer code, DRSPALL, were developed for the 2004 recertification because the prior spallings model used in the 1996 WIPP Compliance Certification Application (CCA) was judged by an independent peer review panel as inadequate (DOE 1996, 9.3.1).

The current conceptual model for spallings addresses processes that take place several minutes before and after a borehole intrusion of a WIPP waste room. The model couples a pipe-flow wellbore model with a porous flow repository model, allowing high-pressure gas to flow from the repository to the wellbore through a growing cavity region at the well bottom. An elastic stress model is applied to the porous solid domain that allows for

mechanical failure of repository solids if local tensile stress exceeds the tensile strength of the waste. Tensile-failed solids may be entrained into the wellbore flow stream by a fluidized bed model, in which case they are ultimately transported to the land surface comprising a release. In July 2003, DOE/SNL presented the spallings conceptual model to a independent peer review panel in accordance with NUREG 1297 guidelines (NRC, 1988). The panel ultimately judged the model as adequate for implementation in WIPP PA (Yew et al., 2003).

This report documents the spallings model history from 1997 to the implementation of DRSPALL in the 2004 Compliance Recertification Application (CRA) (DOE, 2004). The scope of this report includes descriptions of the conceptual model, numerical model, verification and validation techniques, model sensitivity studies, and WIPP PA spallings results as presented in the 2004 CRA.

Acknowledgements

The principal authors wish to acknowledge the following individuals for their contributions to the spallings project:

Technical contributions:

T.W. Thompson	Carlsbad Technical Assistance Contractors
F.D. Hansen	Sandia National Laboratories, Dept 6820
S.W. Webb	Sandia National Laboratories, Dept. 6142
T. Hadgu	Sandia National Laboratories, Dept. 6852

Project resources and logistics:

D.S. Kessel	Sandia National Laboratories, Dept 6821
S. Casey	US Department of Energy
D. Mercer	US Department of Energy
P. Shoemaker	Sandia National Laboratories, Dept 6820
K. Wahi	GRAM, Inc.

Quality assurance support:

M.J. Chavez	Sandia National Laboratories, Dept 6820
M.B. Gross	Carlsbad Technical Assistance Contractors
T. Kirchner	Sandia National Laboratories, Dept 6821
E. Vugrin	Sandia National Laboratories, Dept 6821

Table of Contents

APPENDICES

List of Figures

List of Tables

List of Acronyms

Acronym	*Definition*
CCA	Compliance Certification Application
CCDF	Complimentary Cumulative Distribution Function
CDB	CAMDAT file (binary format)
CMPRP	Conceptual Model Peer Review Panel
CMS	Configuration Management System
CRA	Compliance Recertification Application
DDZ	Drilling-damaged zone
DOE	U.S. Department of Energy
DRSPALL	Computer code that implements the new conceptual model for spallings
DRZ	Disturbed Rock Zone
EPA	U.S. Environmental Protection Agency
GTI	Gas Technology Institute, formerly Gas Research Institute (GRI)
LHS	Latin Hypercube Sampling and the computer code that implements it
NAS	National Academy of Sciences
NRC	Nuclear Regulatory Commission
PA	Performance Assessment
SNL	Sandia National Laboratories
TRU	Transuranic Waste
VVP/VD	Verification and Validation Plan / Validation Document
WIPP	Waste Isolation Pilot Plant

1 Executive Summary

This report documents the development of the Waste Isolation Pilot Plant Performance Assessment (WIPP PA) spallings model from the April, 1997 meeting of the Conceptual Model Peer Review Panel (CMPRP) (Wilson et al., 1997, Hansen et al., 1997) to the model's application in the 2004 Compliance Recertification Application (CRA) (DOE, 2004). The spallings model is one of twenty-four conceptual models that underlie the WIPP PA. Each one of these conceptual models was subjected to independent peer review during the review of the 1996 Compliance Certification Application (CCA). The review by the CMPRP of the end-state erosional spalling model used in the CCA found this model inadequately represented key physical elements of the spalling process. As a result, a preliminary mechanistically based model was developed (Hansen et. al., 1997) and following review the CMPRP determined that this model addressed many of their concerns and also showed that the values for spall releases used in the CCA were conservative. This model was preliminary and required further development for use in compliance calculations. This report covers that development.

Under the direction of the U.S. Department of Energy (DOE), Sandia National Laboratories (SNL) continued model development from 1997-2003 during which time a new computer code, DRSPALL, was developed to execute the spallings calculations. In July 2003, DOE/SNL presented a revised spallings model to an independent review panel which judged the new model as "adequate" for implementation in WIPP PA (Yew et al., 2003). The DRSPALL model was soon thereafter qualified for use in WIPP compliance calculations according to procedure NP 19-1 (Chavez, 2003), and integrated into the CRA Performance Assessment for submission to the U.S. Environmental Protection Agency (EPA) in 2004.

1.1 Introduction and Problem Description

The requirement for a WIPP spallings model is rooted in regulations (EPA, 1996) drawn up by the EPA that require a risk analysis of releases of WIPP waste due to inadvertent human intrusion of the repository sometime during the 10,000-year regulatory period. The intrusion in this context is an exploratory oil or gas borehole that intersects a waste room, and thus creates a pathway for direct release of radioactive material to the land surface. A WIPP spallings event is a special case of the drilling intrusion in which the repository contains gas at high (> 8MPa) pressure that causes localized mechanical failure and entrainment of solid WIPP waste into and up the borehole, carried ultimately to the land surface. This phenomenon, encountered occasionally in the oil and gas industry, is known as a gas kick leading to a blowout.

1.2 Description of Conceptual Model

The conceptual model for a WIPP spallings event is based largely on an understanding of two phenomena: (1) state of the degraded waste at the time of intrusion, and (2) the physics of a "blowout" event. Much of the basis for the conceptual model for the state of the waste is

described in the report by Hansen et al. (2003). The basic concepts for the repository model were established by Berglund (1992) and the fundamentals of the mechanistically based spallings model were developed by Hansen et al (1997).

The current approach to modeling a blowout event divides the model into two primary domains, the wellbore and repository, coupled by a growing cavity region. The wellbore is treated using an unsteady one-dimensional, compressible pipe flow model for a mixture of mud, gas, and solids. The repository is modeled as a radially symmetric porous solid with unsteady, compressible, isothermal, ideal gas flow. The cavity that couples the bottom of the well with the repository is a mixing region that is allowed to grow in volume with drilling or spalling.

Several key sub-models are also described, including an elastic stress law to determine regions of tensile failure, and a fluidized bed model to calculate how much failed repository solid may be transported from the cavity up the wellbore to the land surface due to gas flow from the repository to the wellbore.

1.3 Numerical Model: DRSPALL

The conceptual model is implemented in the FORTRAN code DRSPALL. The code is run in WIPP PA on the Open VMS 7.3-1 operating system and Compaq Alpha ES40 and ES45 machines.

The code design uses a finite difference numerical technique with variable zone sizes. The wellbore equations are solved with explicit integration in time, while the repository equations are solved with implicit integration in time. The inlet boundary for the wellbore annulus is the pressure of a cavity that is common to both the wellbore and repository. The outlet boundary condition is constant pressure at atmospheric pressure. The repository outer boundary is no flow, while the interior boundary is common pressure with the cavity.

1.4 Zone Size Sensitivity Study

Zone size studies are used to determine that the zone size used in calculations is small enough to reasonably capture a numerical solution. The objective of this particular study is to demonstrate the effect of repository zone size, Δr, characteristic tensile failure length, L_t, and wellbore zone size, Δz, on the spall release. Analysis of the results indicate that Δr= 0.004m, Δz= 2.0m and L_t=0.02m are appropriate for the sensitivity studies and CRA spalling release calculations presented in this report. These values show a significant gain in efficiency (a factor of 4 reduction in run time) over the base case (Δr=0.002m, Δz= 1.0m and L_t=0.02m) without sacrificing accuracy.

1.5 Code Verification and Validation

NP19-1 guidelines require that WIPP PA codes pass rigorous verification and validation testing as a condition of qualification. The DRSPALL code was subjected to four test problems that explicitly address code design requirements. The test problems for DRSPALL included:

1. Wellbore Flow Verification – Flow properties in the wellbore such as pressure distribution, fluid velocity, and phase distribution were simulated with DRSPALL and the commercial computational fluid dynamics code FLUENT for simple test problems. The results were compared and found to match closely, thus verifying that the DRSPALL code was solving the wellbore flow equations accurately.

2. Repository Flow Verification – The transient pressure distribution in the repository was simulated with DRSPALL and compared with a solution of the same problem from an alternate code. The results were found to match closely, thus verifying that the DRSPALL code was solving the porous flow equations correctly.

3. Internal Logic Checks Verification – Selected sub-models that were not previously verified through the wellbore flow and repository flow test problems were examined by setting up special flags to output sub-model results directly to text files that were subsequently analyzed with EXCEL spreadsheet tools. This highly resolved analysis of intermediate output variables allowed for verification of proper sub-model performance.

4. Coalbed Methane Validation – A field analog to the WIPP spallings phenomenon called "dynamic open hole cavitation" is occasionally employed to stimulate natural gas production from coal formations. The process involves intentionally pressurizing the coal formation with gas pumped down from the surface and then suddenly releasing the pressure to cause mechanical failure and ejection of solids up the borehole, ultimately forming a cavity near the wellbore. Some field monitoring data for such a process were available for a partial validation test of DRSPALL. The test demonstrated that DRSPALL could calculate, within a reasonable tolerance, a cavity volume comparable to the observed volume from the field data.

1.6 Model Sensitivity Study 1

The DRSPALL code was examined for sensitivity to subjective parameter uncertainty. This study was necessary to (i) provide reassurance that the model would behave stably when run in the broad parameter space encountered in WIPP total system performance assessment, and (ii) allow close inspection for proper implementation of the conceptual model by illustrating the relationships between key inputs and outputs.

Fifteen input parameters were sampled using Latin Hypercube Sampling (LHS) to build a set of 50 independent input parameter sets or "vectors." These vectors were each run with

DRSPALL, and the output were analyzed and correlated to input values using scatter plots. This process arrived at a set of six input variables to which code sensitivity was possibly significant, and nine that were screened out as not influential. The six potentially important variables were then re-examined in a second sensitivity study. These parameters include initial repository pressure, waste permeability, waste porosity, waste tensile strength, waste particle diameter, and particle shape factor.

The primary observations from this sensitivity study indicate that a pressure greater than 12.5 MPa coupled with repository permeability near the middle of its sampled range is required to cause spalling.

1.7 Model Sensitivity Study 2

The DRSPALL code sensitivity study was refined to sample on just 5 parameters based on the results of Sensitivity Study 1. Of these five sampled parameters, sampling range was the same as sensitivity study 1 for pressure, permeability, and porosity. The range of waste tensile strength was expanded to two orders of magnitude. Also, the particle diameter range was changed from 0.001-0.01m to 0.001-0.1 m while holding the particle shape factor constant at 0.1 in order to achieve the same effective product of shape factor × particle diameter as sensitivity study 1 while lowering the number of sampled parameters.

The results of the refined sensitivity analysis demonstrated several model features to add to those observed in sensitivity study 1:

1. Expanding the sampled range of tensile strength around the original range (0.12-0.17 MPa) led to larger mean spallings release due to the low strength vectors.

2. In spite of larger mean releases at low tensile strength, model behavior was stable at tensile strength as low as 0.01 MPa.

1.8 Compliance Recertification Approach

The qualified DRSPALL model was exercised as part of the total system performance assessment in the 2004 Compliance Recertification Application for WIPP. The six uncertain input parameters that emerged as most important from the sensitivity study were grouped into four sampled variables (waste permeability, waste porosity, waste tensile strength, particle size × shape factor) and one master variable, repository pressure. LHS (WIPP PA, 1996f) was run on the four sampled variables to create 50 vectors. These vectors were run in DRSPALL at four selected repository pressure scenarios (10, 12, 14, and 14.8 MPa), resulting in a table of 50 vectors × 4 pressures = 200 single (drilling) intrusion spall volumes. DRSPALL vectors were paired randomly with PA vectors so that only two independent variables were required to determine the spallings contribution to a particular drilling intrusion: vector index and repository pressure.

The effect of the new spallings model on the Complementary Cumulative Distribution Functions (CCDFs), the standard performance metric for WIPP PA, was a general downward shift in release levels relative to those simulated for the 1996 Compliance Certification Application. The lower CCDF releases stem primarily from lower single-intrusion spall values, with both the mode and median spall volume for a given intrusion actually zero. Only when an appropriate combination of uncertain material properties such as low waste porosity, low waste permeability, small particle size, was coupled with high repository pressure, were spallings releases observed.

2 Introduction

This chapter describes the context for the spallings model within the framework of the Waste Isolation Pilot Plant Performance Assessment (WIPP PA).

2.1 Historical Perspective

Located in southeastern New Mexico, WIPP is the world's first deep geologic repository certified for disposal of transuranic[1] (TRU) wastes generated during defense-related atomic energy activities since the 1940's. The U.S. Congress assigned regulatory responsibility over WIPP to the U.S. Environmental Protection Agency (EPA) through the Land Withdrawal Act of 1992 (Public Law 102-579, 1992) and its amendment in 1996. In response, the EPA drafted "WIPP Compliance Criteria" (EPA, 1996) that describe what information the operator of the site, the U.S. Department of Energy (DOE), must submit in order to comply with federal disposal standards for radioactive wastes. Part of these requirements call for the DOE to present calculations that assess the performance of the WIPP repository over the next 10,000 years relative to federal environmental safety standards. The WIPP PA, which estimates the cumulative releases of radionuclides to the environment due to significant processes and events over the 10,000-year regulatory period following site closure, is designed to meet this requirement. The releases predicted by the WIPP PA are directly compared against regulatory standards and, therefore, serve as a critical measure of compliance.

The WIPP PA comprises a suite of process models that address the various mechanisms affecting repository performance. The Compliance Certification Application (DOE, 1996) identifies human intrusion as the only mechanism potentially leading to significant radionuclide releases from the repository system. Leading in importance among possible human intrusions is the direct release of radionuclides to the surface through an oil or gas exploration borehole that intersects a waste room. These direct releases are accounted for in WIPP–PA through four mechanisms, listed below and shown schematically in Figure 2.1-1.

1. Cuttings: Solid waste material removed by direct cutting action of the drillbit

2. Cavings: Solid waste material removed by the shear forces exerted by drilling mud moving within the borehole.

3. Spallings: Solid waste material local to the borehole that is subject to tensile stresses leading to mechanical failure of the borehole walls, and subsequent transport of this disaggregated material up the borehole.

[1] TRU waste is defined by the US EPA as "waste containing more than 100 nanocuries of alpha-emitting transuranic isotopes, with half-lives greater than twenty years, per gram of waste…" with several exceptions (US EPA, 1993).

4. Direct Brine Release: Dissolved radionuclides transported up the borehole in brine flowing from WIPP waste rooms

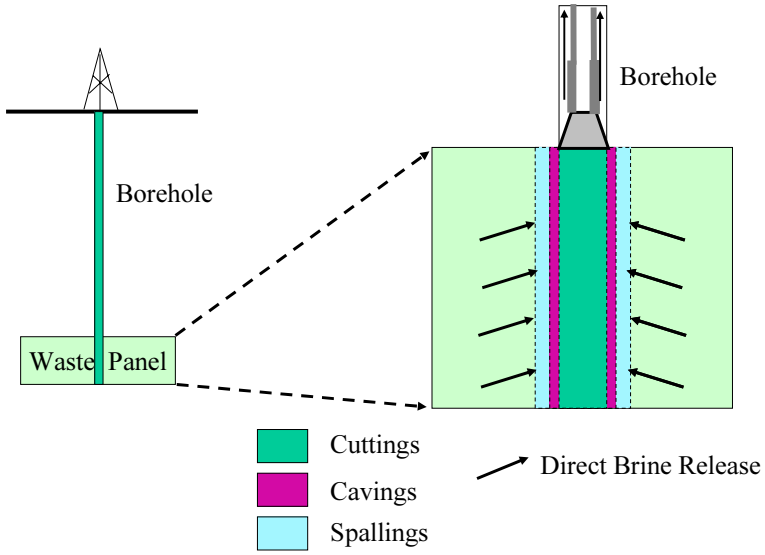

Figure 2.1-1. Schematic of Direct Releases.

While conceptual models for the cuttings, cavings, and direct brine release mechanisms used in WIPP PA in 1996 were approved by the CMPRP, the end-state erosional spallings model used in the PA calculations was judged to inadequately represent key physical elements of the spalling process. As a result a preliminary mechanistically based model was developed (Hansen et. al., 1997), and following review the CMPRP determined this model addressed many of their concerns, and showed that the values for spall releases used in the CCA were conservative. . In the interim period between the 1997 peer review and the 2004 Compliance Recertification Application, this preliminary mechanistic conceptual model was further developed by the US DOE, Sandia National Laboratories (SNL) and their contractors. The purpose of this report is to describe this conceptual model for spallings and its associated computer code, DRSPALL, developed for the 2004 WIPP CRA (DOE, 2004).

2.1.1 WIPP Spallings Defined

The spallings release mechanism in the WIPP PA is defined as a human drilling intrusion that intersects a high-pressure WIPP repository, allowing solid waste material local to the borehole to fail under mechanical stress and transport rapidly up the borehole to the land surface. This is known as a "blowout" in the oil and gas exploration business where the high-pressure fluids literally blow the contents of the wellbore out to the land surface. Blowouts pose a danger to workers and may lead to potentially costly damage to equipment though they are rare with modern drilling practices. Current drilling operations monitor downhole conditions closely for evidence of high-pressure pockets and resulting "gas kicks" that can lead to blowouts if not controlled properly. Various processes at WIPP such as iron

corrosion, biodegradation, and creep closure of the repository will lead to pressurization of the waste rooms over the 10,000-year regulatory period. If the pressure in the waste rooms is higher than the fluid pressure in an intersecting borehole, repository fluids will flow toward and enter the borehole. If the pressure difference is sufficiently high, the resulting mechanical stress state may fracture the solid material comprising the walls of the borehole, leading to disaggregation and potential transport of these failed solids to the surface. The critical issue in the WIPP PA is to determine how much radioactive solid waste may be expelled to the surface in such an event.

2.2 Requirements of Spallings Model

The spallings model must ultimately calculate a mass or volume of WIPP waste transported to the surface in a potential spalling event. This mass or volume is multiplied by the concentration of radionuclides in the waste panel at the time of intrusion to yield a "release" value.

Building an effective conceptual model for use in compliance calculations at WIPP requires, at a minimum, the following elements:

- Knowledge of the state of the waste, including mechanical properties such as permeability, tensile strength, density, porosity.

- Knowledge of applicable oil and gas drilling practices including typical borehole geometry and drilling mud properties.

- Knowledge of the mechanical and chemical conditions of the repository at the time of intrusion including fluid pressure and stress state in the repository at the time of intrusion.

- Engineering models for (1) transient, compressible, single-phase gas through the porous repository domain, coupled to (2) transient mud, gas, and solids flow in the borehole, (3) mechanical stress state of waste in the repository, and (4) transport of disaggregated waste from the repository domain to the wellbore domain.

- Review and approval from a conceptual model peer review panel conducted in accordance with NUREG 1297 guidelines (NRC, 1988).

In addition, for the computational model to be functional in WIPP PA, the spallings computer code must:

- Execute on the current Open VMS 7.3-1 operating system and Compaq Alpha ES40 and ES45 machines.

- Be capable of many (400+) executions on the current operating system in the space of one week or less.

- Obtain input data from the WIPP PA database.

- Write output to binary CAMDAT files that are retained in the Configuration Management System (CMS).

- Meet NP19-1 Software Requirements guidelines (Chavez, 2003). The NP 19-1 procedure was developed by SNL to implement the regulatory requirements contained in 40 CF194.22 (EPA, 1996) and NQA-2a-1990 addenda, Part2.7 (ASME 1990)

2.2.1 Conceptual Model Peer Review

A conceptual model is a statement of how important features, events, and processes such as fluid flow, chemical processes, or intrusion scenarios are to be represented in performance assessment. To be used in performance assessment, the conceptual model must be successfully translated into analytical statements and mathematical analogs. The peer review process is used to assure that the conceptual model reasonably represent possible future states of the disposal system and adequately assesses the long-term performance. For WIPP compliance analyses, the conceptual model peer review process is guided by EPA regulation 40 CFR Part 194.27 (EPA, 1996), and NUREG-1297 (ASME, 1990).

As stated previously, the conceptual models for the cuttings, cavings, and direct brine release mechanisms were approved for use in WIPP PA in 1997 by the conceptual model peer review panel, but the end-state erosional spallings model used in the CCA was judged inadequate (Wilson et al., 1997). A mechanistic model developed at that time, and described in Hansen et al, 1997, addressed many of the panel's concerns and successfully demonstrated that the CCA spall releases were conservative. However this was a very preliminary model and the DOE committed to further develop the model for use in the CRA.

In July 2003, the spallings model documented herein was presented to the peer review panel. Over the period July to October 2003 the panel reviewed the spallings conceptual model in detail, including the assumptions and scientific information used to develop the model, alternative models considered, uncertainties, adequacy, accuracy, and validity of conclusions (Yew et al, 2003). The panel also made an assessment of whether the conceptual model is adequate for implementation in an overall WIPP PA. The review evaluated the structure of the conceptual model and the mathematics used to embody the model in code. The review also included an assessment of the reasonableness of outputs based on sensitivity to parameter inputs.

Based on the review the panel found that the supporting assumptions, mathematical implementation and integration of this conceptual model with the other conceptual models are expected to be adequate and concluded:

- The new spallings conceptual model appears generally sound in its structure and reasonableness.
- The proposed implementation of the new spallings model appears reasonable.

3 Conceptual Model for Spallings

3.1 Geologic Setting for WIPP Spallings Model

The principal design concept of WIPP is to isolate nuclear waste from the accessible environment by entombing it in salt formations deep in the ground, a waste management approach endorsed by the National Academy of Sciences since 1957 (NAS/NRC, 1957). Salt is attractive for isolation of long-lived nuclear wastes because it exhibits a very low permeability, providing an effective barrier to transport of contaminated brine to the land surface. Salt also exhibits plastic properties and "creep closure" under stress, allowing it to literally entomb wastes that are placed underground for many years.

The WIPP repository, operational since March 1999, is located in a large rock salt deposit in the Delaware Basin in southeast New Mexico, as indicated in the map shown in Figure 3.1-1.

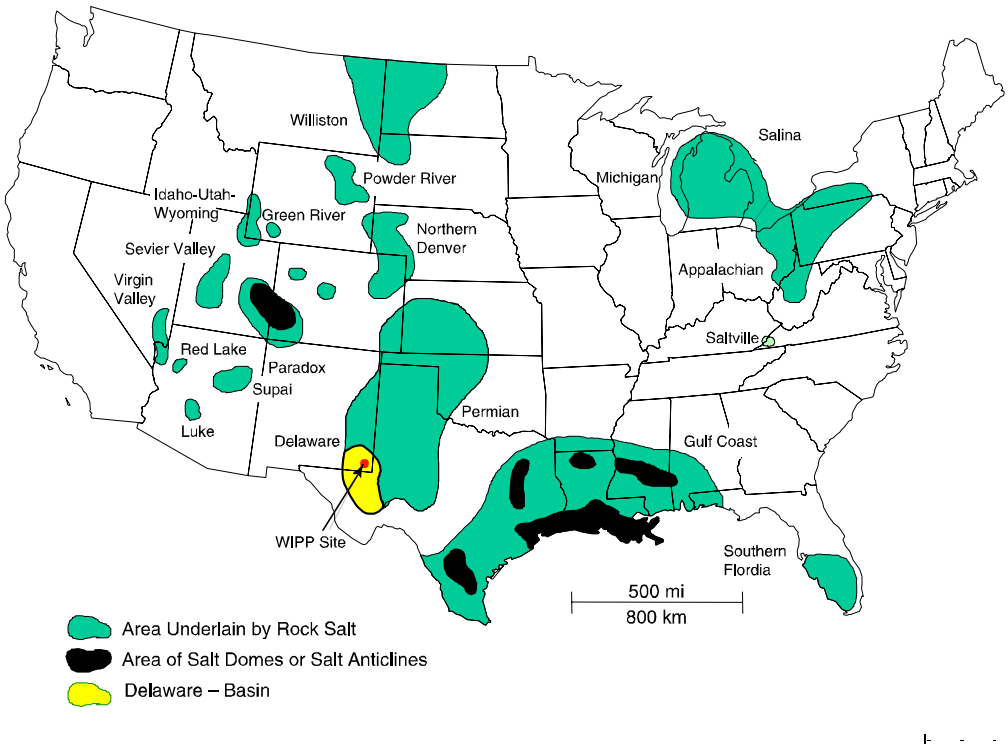

Figure 3.1-1. Map of Salt Deposits in the U.S.

The excavated region of WIPP that contains waste is located about 655m below the ground surface in bedded salt that is estimated to have been in place for about 255 million years (Swift and Corbet, 2000). A cross-section view of the geologic strata is given in Figure 3.1-2.

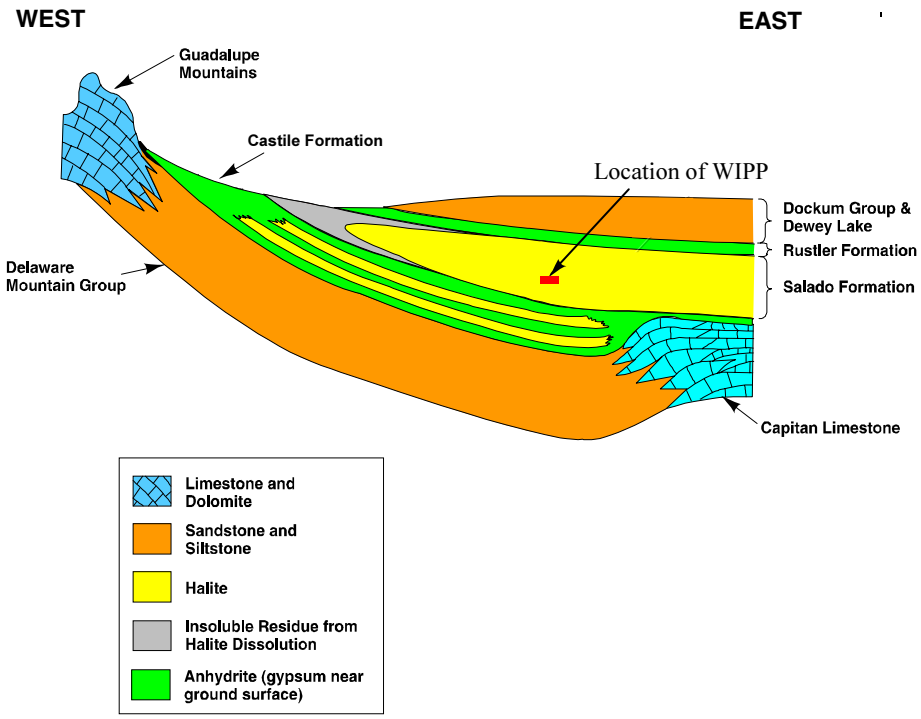

Figure 3.1-2. East-West Geologic Cross-Section Through the Delaware Basin at the WIPP Site.

3.1.1 WIPP Waste Rooms

A plan view of the WIPP repository at 655m below ground surface is given in Figure 3.1-3. Waste is stored in the areas marked "Panel 1" through "Panel 8." Some of the connecting drifts will also be used for waste storage, resulting in a total of 10 panels planned for waste storage. Each panel contains seven waste "rooms," which measure 10.1 m wide × 33 m long × 4 m deep at the time of excavation (DOE, 1996). The creep closure mechanism will reduce the volume of these rooms over time, but for the purpose of the WIPP PA, the length and width remain constant while the height decreases according to the room closure model. The rooms are surrounded by a "disturbed rock zone" (DRZ), which is salt that is in the process of healing after excavation.

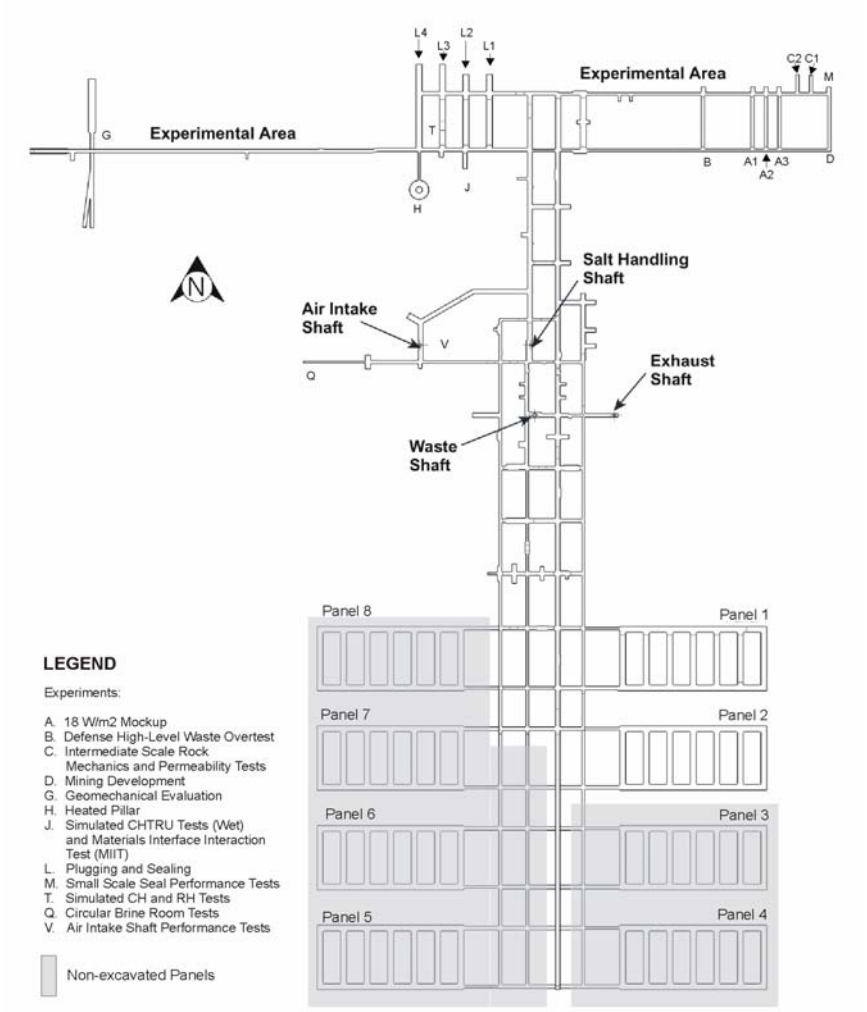

Note: Circa 2003. Excavated panels not current. As of publication Panel 3 has also been excavated.

Figure 3.1-3. Plan View of WIPP Excavation at 655m Below Land Surface.

3.1.2 Well Blowout Analog

The spallings phenomenon is effectively a blowout that occurs when a borehole intersects a high-pressure WIPP repository. The probability that any particular intrusion of WIPP will result in a blowout is small, but the possibility exists and must be investigated. Some general background from observations of oil and gas blowouts is therefore relevant to formulating a conceptual model for the WIPP spallings.

The potential for a blowout occurs when formation fluid pressure exceeds that expected for a given exploration area. Fluid pressure at the bottom of the well is actively manipulated by the driller and typically exceeds the local formation pressure to create a slightly "overbalanced" state. This creates stable drilling conditions and only minor losses of mud to the formation. If the drillbit encounters an over pressured zone, the system may become

"underbalanced" in which formation pressure exceeds the bottomhole pressure causing formation fluids to move toward and into the wellbore. This can become problematic for drilling and potentially very destructive, costly, and dangerous if not properly controlled. A sufficiently high pressure gradient may cause mud to accelerate up and out of the wellbore, fail and entrain solids local to the wellbore wall, and lead to rapid expulsion of contents at the surface. The contemporary oil and gas exploration and drilling industry attempts to prevent well blowouts, motivated by a combination of safety, economic, and regulatory concerns. This is known as the practice of "well control" (Baker, 1998). The most common approach to well control is to monitor the drilling mud return rate closely for changes. Entrance of high-pressure fluid into the wellbore, known as a "kick," causes an increase in the mud return rate. The driller may choose to shut the well in at this time by closing the blowout preventer, continuing to pump mud in order to circulate the kick fluids out of the wellbore. Once shut in, the well pressure may be bled off slowly and mud density increased to offset the higher formation pressure before resuming drilling.

3.1.3 Previous WIPP Spallings Models

Previous efforts to develop a spallings model for use in WIPP PA compliance calculations failed to produce a peer review-sanctioned model. Nonetheless, the background information collected and developed during this period (1990-1998) formed a basis for the conceptual model underlying DRSPALL.

The first study of record (Berglund, 1992) concerning the direct release of WIPP wastes by drilling activity presented two mechanisms for direct removal of wastes other than the cutting action of the drillbit: (1) erosion within the borehole annulus due to shear forces from the drilling mud, and (2) waste-gas-induced borehole spall. The shear force erosion model within the borehole annulus was eventually approved by peer review and adopted by WIPP PA as the "cavings" mechanism. The waste-gas-induced spalling mechanism was also eventually employed as part of the DRSPALL model, though the first generation spallings model presented in the 1996 CCA relied more on empirical laboratory observations (Lenke et al., 1997) than the theory presented in Berglund (1992).

Berglund's work built a preliminary conceptual model for the transient pore pressure and stress response of a pressurized WIPP waste-storage room to a sudden borehole intrusion. He presented problem setups and solutions for seven types of calculations, ranging in complexity from a "one-dimensional cylindrical elastic approximation," to an "inelastic dynamic response of the waste." Berglund's analyses did not assess material failure or transport from the repository to the wellbore, as was ultimately done in DRSPALL. Nonetheless, he established the basic concepts for the repository model and demonstrated basic solutions to various test scenarios. Several of Berglund's concepts were eventually implemented in the DRSPALL model: (1) a radially symmetric domain with origin at borehole axis or point of intrusion and impermeable outer boundary, (2) Darcy's Law for transient ideal gas flow in porous waste (Forchheimer effect added in DRSPALL. See section 3.5), and (3) homogeneous, elastic response model for waste with effective stress law ("seepage stress" added in DRSPALL).

The spallings model implemented in the 1996 CCA diverged from the theoretical approach presented in Berglund (1992) and was formed largely upon experimental observations from a laboratory-scale blowout model described in Lenke et al. (1997). The experimental apparatus comprised a cylindrical-shaped pressure cell that was filled with silica sand and subjected to a steady pore pressure difference between the outer circumference and the axis of symmetry. The resulting gas flow caused some sand to evacuate the cell through a "borehole" into a separate measuring device, with the removed material interpreted as spalled waste. From these data, the researchers developed a mathematical model for volume of sand (spalled waste) removed based on a "fracture erosion" model. They hypothesized that fractures, formed local to the borehole under the imposed pore pressure gradient, channeled high-velocity gas that eroded sand, transporting it up the borehole and out of the domain. The critical gas velocity for erosion was based on the terminal velocity of a falling sphere in a viscous fluid.

The sand erosion model did not pass conceptual model peer review, however. This development initiated an effort by Hansen et al. (1997) to support the conservatism of the results of the erosion approach to spallings by presenting a new mechanistic model which provided independent experimental results that predicted the same or lower releases. Through this model and the experimental an analog support for it, Hansen and co-workers were able to demonstrate to the satisfaction of the panel and EPA that, in the words of the peer review panel "…the spallings volumes used in the CCA are reasonable, and in fact appear to overestimate the actual waste volumes that would be expected to be released by the spallings process." (Wilson et al., 1997). The EPA implemented the recommendation of the peer review panel by specifying that the WIPP PA use a range of spall release volumes from 0.5-4.0 m^3 if repository pressure at the time of intrusion exceeds 8 MPa, the approximate hydrostatic pressure at repository depth. In doing so, the conceptual model for spallings was still technically rejected, but the results were deemed acceptable for compliance purposes.

Spallings model development continued from 1998 through 2003, building on the approach taken in Hansen et al. (1997). This effort resulted in a new computer code, DRSPALL, and culminated in a conceptual model peer review that yielded a positive outcome (Yew et al., 2003).

The current report presents the spallings model development, qualification, and implementation from just after the 1997 peer review (Wilson et al., 1997) to the 2004 CRA.

3.2 Key Model Assumptions

Since any engineering model is an abstraction of a real system, some assumptions must be stated in order to frame the conceptual model. Primary assumptions for the spallings model are as follows:

- Isothermal
- One-dimensional geometry with two coupled domains
    - Wellbore domain: linear geometry oriented parallel with gravity
    - Repository domain: radially symmetric around either wellbore axis (cylindrical) or intrusion point (spherical)

- Single-phase, compressible, ideal gas in repository
    - Darcy flow with Forchheimer correction (accounts for inertial resistance effects on flowing gas)
- Multiple-phase (gas, liquid, solid) homogeneous mixture in wellbore
    - Standard Navier-Stokes compressible flow
    - Colebrook pipe flow friction model
    - Power law slurry viscosity model
- Elastic stress model for intact repository solids
    - Based on linear poro-elasticity (waste skeleton behaves elastically, displacement and strains are small, waste grains are incompressible and Terzaghi effective intergranular stress principle holds)
    - Radial Tensile failure model
        - Failure is evaluated over one "characteristic length" from cavity wall
    - Strain not evaluated
    - Shear failureis not evaluated.
- Fluidized bed model for transport of disaggregated solids from cavity to wellbore
    - Based on Ergun (1952) model
    - Failed waste assumes uniform particle size and shape
- Waste properties (solids in repository domain)
    - Fully-degraded granular material cemented into an aggregate
        - Property values estimated by measurements on laboratory surrogates (Hansen et al., 2003)
    - Homogeneous, isotropic, constant with time
- Drilling parameters
    - Use values representative of current practices in Delaware Basin
    - No driller intervention during blowout (no shut-in or use of blowout preventer)

3.3 Defining the Spallings Model Domain

The domain encompassed by the spallings model includes an intrusion wellbore and the WIPP waste room intersected by the wellbore. Boundary conditions for the wellbore include a mud pump and mud return line outlet at the land surface, and a cavity at the bottom of the wellbore where pressure and flow are coupled with those in the waste room. Boundary conditions for the waste room are no-flow at the outer boundary and coupled flow and pressure at the origin where the waste room contacts the wellbore. This is depicted schematically in Figure 3.3-1.

The nature of the coupling between the wellbore and repository domains depends on whether the model is operating prior to or after the drillbit penetrates the repository. Prior to penetration, gas from an over pressured repository will flow toward the wellbore through the intervening porous rock. Here it is assumed that the flow path is constrained to a cylinder

directly beneath the approaching wellbore in a region called the drilling-damaged zone[2] (DDZ). This coupling method is depicted in Figure 3.3-2. Here mud flows down the drill pipe, through the drillbit nozzles, and up the annulus to the land surface. Simultaneously, gas flows from the repository through the DDZ and mixes into the mud traveling up the annulus to the surface.

After the wellbore penetrates the repository, a coupling region called the "cavity" forms a common boundary pressure for the lower end of the wellbore and the inner wall of the repository. This configuration is illustrated in Figure 3.3-3. Here mud flows down the drill pipe, through the bit nozzles, into the cavity and up the annulus to the land surface. Also mixed into the flow in the cavity are gas from the repository and waste solids drilled or spalled from the cavity wall. This three-phase mixture is transported to the surface up the wellbore annulus.

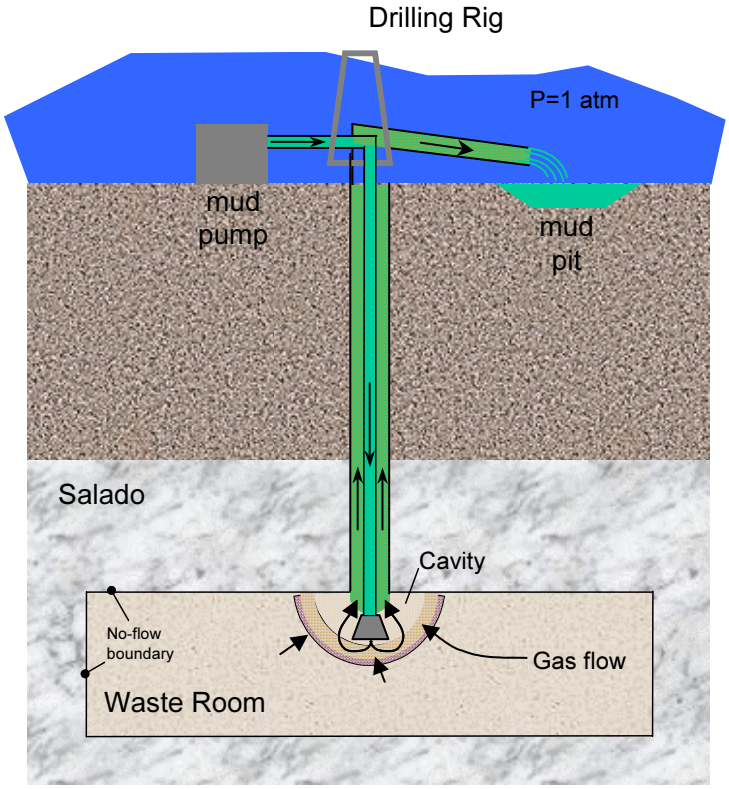

Figure 3.3-1. Schematic of the Spallings Model Domain.

[2] The drilling-damaged zone is defined as rock immediately ahead of the borehole that suffers mechanical fracture damage due to the stresses of drilling and therefore exhibits increased permeability relative to the surrounding rock. See Hansen et al. (2003) for a more detailed description of the DDZ.

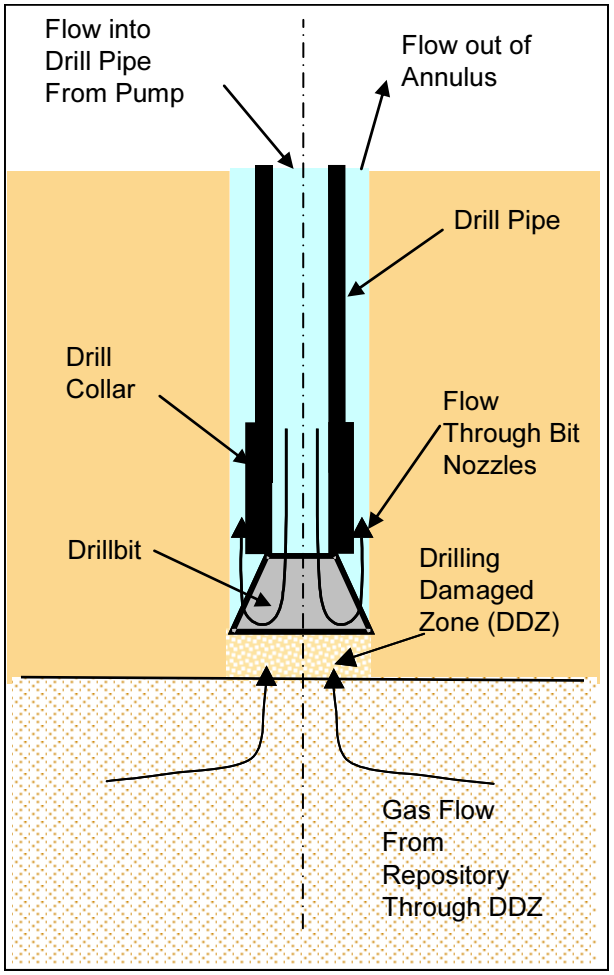

Figure 3.3-2. Schematic Diagram of the Flow Geometry Prior to Repository Penetration

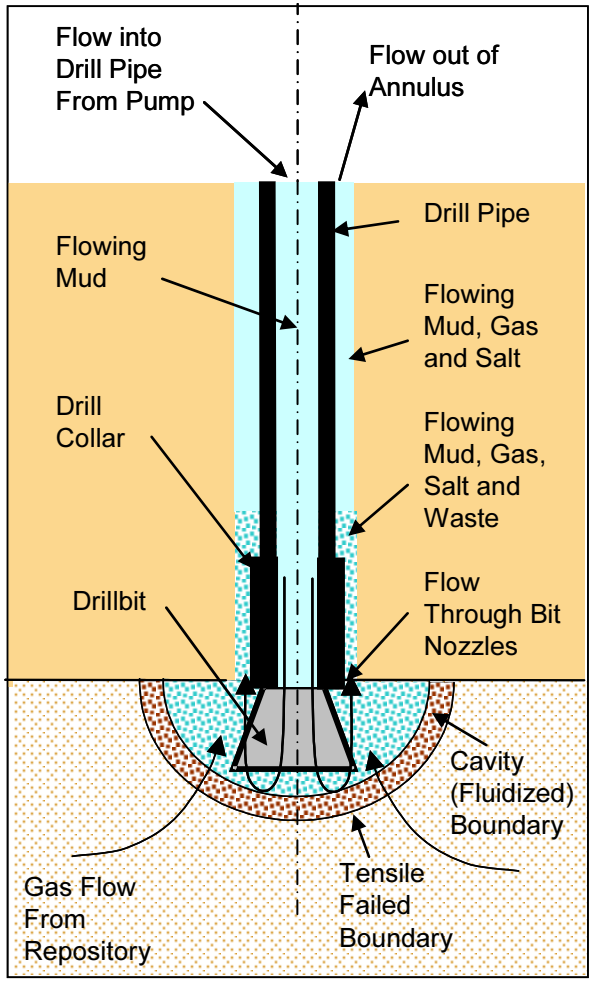

Figure 3.3-3. Schematic Diagram of the Flow Geometry after Repository Penetration. Spherical Case Is Shown.

3.3.1 Wellbore Flow Prior to Penetration

Flow in the well prior to drillbit penetration into the repository is treated as shown in Figure 3.3-4.

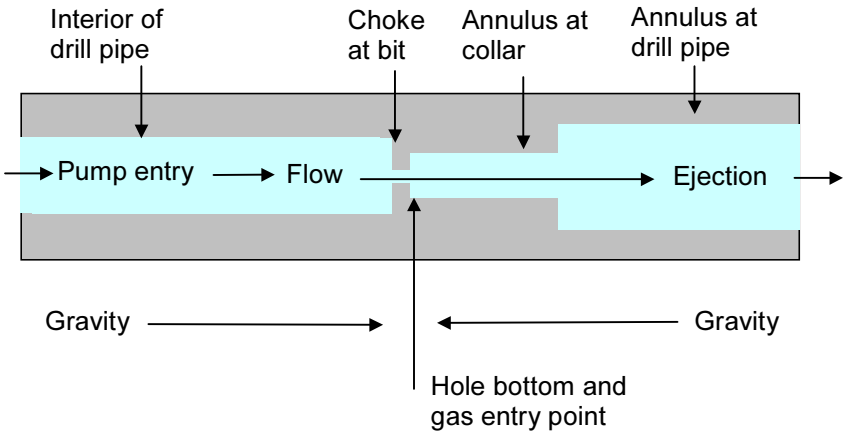

Figure 3.3-4. Effective Wellbore Flow Geometry Before Bit Penetration.

In concept this model is similar to that proposed by Podio and Yang (1986), which is currently in use in the oil and gas industry. The pump input is controlled by volume flow rate (with a maximum pressure), and may be stopped or started. Flow is one dimensional pipe flow with cross sectional areas corresponding to the appropriate flow area at a given position in the well. The drillbit is treated as a choke with cross-sectional area appropriate to the bit nozzle area. Immediately below the bit, gas from the repository can flow through drilling-damaged salt into the well, as described in section 3.3. After the bit, return flow to the surface is treated as pipe flow in the annulus separating the drill string and the outer hole boundary. At the annulus output to the surface, mud ejection is to a constant atmospheric pressure. The gravitational body force acts in its appropriate direction based on position before or after the bit. The well fluid is Newtonian. Viscosity of the phase mixture is determined by an approximation as discussed in section 3.4.2. Flow friction may be either laminar or turbulent, also based on an approximation given in section 3.4.1.

3.3.2 Repository Flow Prior to Penetration

The flow in the repository is one-dimensional radial, either hemispherical or cylindrical with its origin at the centerline of the well. Darcy flow of an isothermal ideal gas in a porous medium allows the simplifying pseudo-pressure approach to be taken, as is commonly done in the field of petroleum reservoir engineering (Rath and Podio, 2000). A modification allowing for non-Darcy inertial resistance effects at high flow velocities is included. Near the well, the boundary pressure is determined as discussed in the next section on coupling.

The outer boundary of the repository is set to a no flow condition, consistent with repository far-field conditions.

In order to avoid forcing gas to flow to a point in the 1-D, radially symmetric repository domain prior to bit penetration, a preliminary cavity, referred to throughout the DRSPALL documentation as the "pseudo-cavity," is formed where the repository meets the DDZ. The volume of this cavity is small, with a surface area equal to that of a circle with a diameter equal to the bit diameter. The purpose of this pseudo-cavity is to avoid forcing gas flow to converge to a single point (spherical geometry) or line (cylindrical geometry) at the origin of the radial coordinate system.

Solid stresses in the repository are treated as elastic and with an effective stress law. Flow-related forces are included. A homogeneous solid is assumed. Solid stresses are not relevant prior to penetration, but play a key role in determining failure and fluidization after penetration, as discussed later.

3.3.3 Coupling of Wellbore and Repository Flow Prior to Penetration

Prior to penetration, it is assumed that the drilling action creates a cylinder of altered-permeability salt material with diameter equal to the drillbit that moves ahead of the drillbit. This material allows limited porous gas flow from the repository to the wellbore. This is shown simply as the DDZ, in Figure 3.3-2. Additional conceptual detail is shown in Figure 3.3-5. The permeability of this altered zone is greater than that of the intact salt and the DRZ and is based on a composite model as described in the section 3.5.1.1.

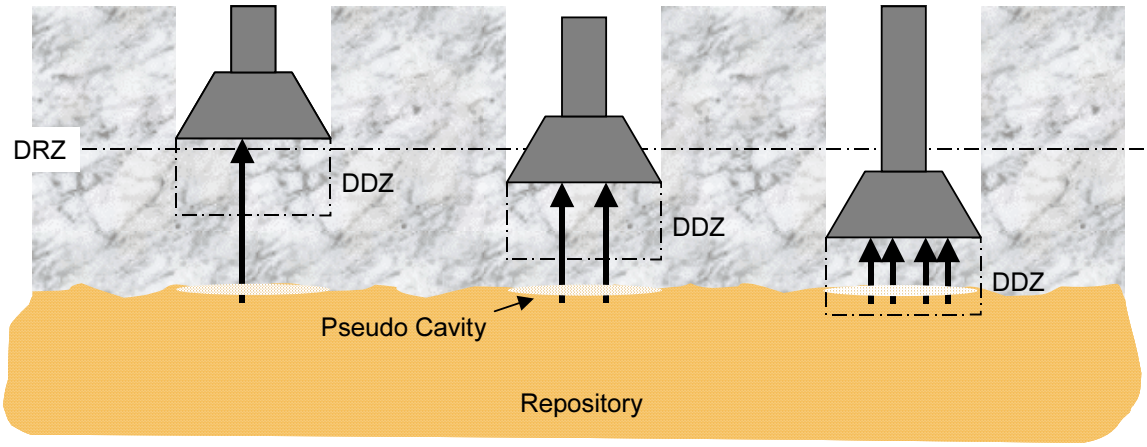

Figure 3.3-5. Coupling of the Repository and Wellbore Prior to Drillbit Penetration.

Porous flow through this cylindrical volume is determined by the boundary pressures and flow areas of the volume. The boundary pressure on the well side is the pressure immediately below the bit. The area is the bit cross-sectional area (also assumed to be the wellbore area). The boundary pressure on the repository side is the pressure in a small

pseudo-cavity at the wellbore face of the waste with the same surface area as the end of the drillbit. The pseudo-cavity provides continuity between the wellbore and repository and does not play a material role in total flow.

3.3.4 Wellbore Flow after Penetration

After drillbit penetration, the pseudo-cavity at the waste face becomes a real cavity and is connected to the flow area of the wellbore as shown in Figure 3.3-6. The cavity is now representative of the material removed from the repository by drilling, material failure, and subsequent fluidization.

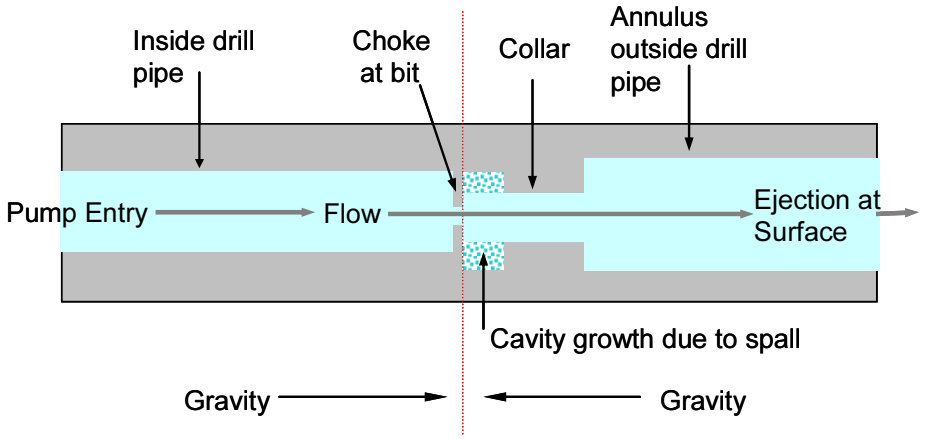

Figure 3.3-6. Effective Wellbore Flow Geometry After Bit Penetration

After penetration, the cavity is treated as a mixing volume connecting the wellbore and the repository, and is used to provide the pressure boundary conditions at the inner wall of the repository. The volume of the cavity zone shown in Figure 3.3-6 is constantly adjusted so that it is equal to the growing volume of the actual hemispherical or cylindrical cavity. Fluidized waste solids mix with the mud/gas/salt flow and are moved up the wellbore and possibly out at the surface. An approximate model for the viscosity of the multi-phase mixture is used. All phases in the wellbore are assumed to move at the same velocity. The assumption of a single-phase velocity greatly simplifies the mathematics and speeds numerical execution time. This assumption should be conservative with respect to waste release to the surface because a lagging waste particle velocity is expected in the wellbore, leading to a lower surface release rate and lower total release. The viscosity model causes the mixed fluid to act as a dense slurry for high solids concentrations, and there is a relative solids volume which causes complete choking. Treating the fluidized cavity as a region in one-dimensional series with the wellbore flow is a simplification. However, it is consistent with the one-dimensional nature of the flows in both wellbore and repository and is a simple and convenient way of introducing the boundary coupling.

3.3.5 Repository Flow after Penetration

The flow model is basically the same after penetration as before. Without failure, the inner surface area of the repository is the same as the surface area of the true drilled borehole cavity. If radial tensile failure occurs as a result of pressure relief at the inner boundary and flow-related forces, the waste material is deemed susceptible to fluidization in the region of tensile failure. Then the pore fluid flow velocity is compared to a limiting velocity based on fluidized bed theory. If this fluidization velocity is exceeded, material is assumed to disaggregate and move into the cavity, thus enlarging the cavity and adding waste solids to it. The cavity volume is determined by cavity radius. The cavity radius is the sum of two components: the drilling radius and the spallings depth. The drilling radius is the radius of the volume with surface area equivalent to the surface area of the cylinder removed by drilling, as explained in section 3.6. The spallings depth is the depth to which fluidization extends beyond the current cavity radius, as explained in section 3.5.5.3.

3.3.6 Coupling of Wellbore and Repository after Penetration

As mentioned above, the coupling of the wellbore and the repository following penetration is achieved by treating the cavity as a mixing volume (Figure 3.3-6). If no fluidization occurs but drilling continues, the cavity grows at a rate equivalent to the volume being drilled. If fluidization occurs, the cavity volume may be greater than the drilled volume. Waste moves into the cavity when it is fluidized. Mass balance is maintained at all times. Mud flows into the cavity through the nozzles at the bit. Gas, waste and salt are moved into the cavity as drilling and fluidization occur. Subsequently, all components progress up the well. Salt and waste solids are treated as incompressible. Volumes of the compressible phases (gas and mud) are calculated based on their equations of state and the current pressure.

3.4 Wellbore Equations

Flow in the well is modeled as one-dimensional pipe flow with cross-sectional areas corresponding to the appropriate flow area at a given position in the well, as shown in Figure 3.3-4 and Figure 3.3-6. In concept, this model is similar to that proposed by Podio and Yang (1986) and now in use in the oil and gas industry. Drilling mud is added at the wellbore entrance by the pump. Flow through the drillbit is treated as a choke with cross-sectional area appropriate for the bit nozzle area. At the annulus output to the surface, mixture ejection is to a constant atmospheric pressure. The gravitational body force acts in its appropriate direction based on position before or after the bit.

Prior to drillbit penetration into the repository, gas from the repository can flow through drilling-damaged salt into the well. After penetration, the cavity at the bottom of the wellbore couples the wellbore flow and the repository flow models; gas and waste material can exit the repository domain into the cavity. The cavity radius increases as waste materials are moved into the wellbore.

The system of equations representing flow in the wellbore includes: four equations for mass conservation, one for each phase (salt, waste, mud and gas); one equation for conservation of total momentum; two equations relating gas and mud density to pressure; the definition of density for the fluid mixture; and one constraint imposed by the fixed volume of the wellbore. The conservation of mass and momentum are described by:

$$\frac{\partial}{\partial t}\left(\rho_q V_q\right)+\frac{\partial}{\partial z}\left(\rho_q V_q u\right)=S_q \tag{3.4.1a}$$

$$\frac{\partial}{\partial t}\left(\rho V u\right)+\frac{\partial}{\partial z}\left(\rho V u^2\right)=-V\left(\frac{\partial P}{\partial z}-\rho g+F\right)+S_{mom} \tag{3.4.1b}$$

where

q	=	phase (w for waste, s for salt, m for mud, and g for gas)
V_q	=	volume (m^3) of phase q
V	=	total volume (m^3)
ρ_q	=	density (kg/m^3) of phase q, constant for salt and waste and pressure-dependent for gas and mud (see Eqs. (3.4.2) and (3.4.3))
ρ	=	density of fluid mixture (kg/m^3) determined by Eq. (3.4.4)
u	=	velocity (m/s) of fluid mixture in wellbore
t	=	time (s)
z	=	distance (m) from inlet at top of well
S_q	=	rate of mass (kg/s) of phase q entering and exiting wellbore domain at position z (Eq. (3.4.14))
S_{mom}	=	rate of momentum (kg m / s^2) entering and exiting wellbore domain at position z (Eq. (3.4.17))
P	=	pressure (Pa) at position z
g	=	gravity constant (kg/m s^2)
F	=	friction loss using pipe flow model (kg/m^2 s^2) determined by Eq. (3.4.6)

Gas is treated as isothermal and ideal, so

$$\frac{\rho_g}{\rho_{g,0}}=\frac{P}{P_{atm}} \tag{3.4.2}$$

where $\rho_{g,0}$ is the density of the gas at atmospheric pressure, P_{atm}.

The mud is assumed to be a compressible liquid, so

$$\rho_m=\rho_{m,0}\left[1+c_m\left(P-P_{atm}\right)\right] \tag{3.4.3}$$

where $\rho_{m,0}$ is the density of the mud at atmospheric pressure and c_m is the compressibility of the mud.

The density of the fluid mixture is determined from the densities and volumes occupied by the phases:

$$\rho = \frac{\rho_g V_g + \rho_m V_m + \rho_s V_s + \rho_w V_w}{V} \tag{3.4.4}$$

The volume of each phase is constrained by the fixed volume of the wellbore:

$$V = V_g + V_m + V_s + V_w \tag{3.4.5}$$

3.4.1 Wellbore Friction Factor

The friction loss is a standard formulation for pipe flow (Fox and McDonald, 1985), where the head loss per unit length is given as:

$$F = f \frac{\rho}{d_h} \frac{u^2}{2} \tag{3.4.6}$$

The hydraulic diameter d_h is given by

$$d_h = \frac{4A}{\pi \left(D_i + D_o \right)} \tag{3.4.7}$$

The area A is calculated as either the cross-sectional area inside the pipe or the area of the annulus between the outer and inner radii. The inner diameter, $D_{i,}$ and outer diameter, $D_{o,}$ are a function of location along the flow path.

The friction factor f is determined by a classical method for laminar flow and by the method of Colebrook (Fox and MacDonald, 1985) for turbulent flow. In the laminar regime (Re < 2100)

$$f = \frac{64}{\mathrm{Re}} \tag{3.4.8}$$

and in the turbulent regime (Re > 2100)

$$\frac{1}{\sqrt{f}} = 1.0 \log \left(\frac{\varepsilon / d_h}{3.7} + \frac{2.51}{\mathrm{Re}\sqrt{f}} \right) \tag{3.4.9}$$

where ε is the wall roughness, $\mathrm{Re} = \dfrac{u\rho d_h}{\eta}$ is the Reynolds number of the mixture, and η is the viscosity calculated by Eq. (3.4.10).

3.4.2 Viscosity of Wellbore Slurry

As the wellbore mixture becomes particle-laden, the viscosity of the mixture is determined from an empirical relationship developed for proppant slurry flows in channels for the oil and gas industry (Barree and Conway, 1995). Viscosity is computed by an approximate slurry formula based on the volume fraction of waste solids:

$$\eta = \eta_0 \left(1 - \frac{w}{w_{\max}} \right)^s \tag{3.4.10}$$

where η_0 is a base mixture viscosity , $w = V_w / V$ is the current volume fraction of waste solids, w_{max} is an empirically determined maximal volume fraction above which flow is choked, and s is an empirically determined constant.

3.4.3 Wellbore Initial Conditions

Initial conditions in the wellbore approximate mixture flow conditions just prior to penetration into the waste. The wellbore is assumed to contain only mud and salt. Initial conditions for the pressure, fluid density, volume fractions of mud and salt, and the mixture velocity are set by the following algorithm.

Step 1. Set pressure in the wellbore to hydrostatic: $P(z) = P_{atm} + \rho_{m,0} g z$

Step 2. Set mud density using Eq. (3.4.3)

Step 3. Set mixture velocity: $u(z) = \dfrac{R_m}{A(z)}$, where R_m is the volume flow rate of the pump and $A(z)$ is the cross-sectional area of the wellbore

Step 4. Set volume of salt in each cell: $V_{s,i} = R_{drill} A_{bit} \dfrac{\Delta z_i}{u_i}$, where R_{drill} is the rate of drilling, $A_{bit} = \dfrac{\pi d_{bit}^2}{4}$ is the area of the bottom of the wellbore, d_{bit} is the diameter of the bit, Δz_i is the wellbore zone size and u_i is the flow velocity.

Step 5. Set volume fraction of mud in each cell: $V_{m,i} = V_i - V_{s,i}$

Step 6. Recalculate mixture density using Eq. (3.4.4), assuming no waste or gas in the wellbore.

The initial conditions set by this algorithm approximate a solution to the wellbore flow (Eq. (3.4.1)) for constant flow of mud and salt in the well. The approximation rapidly converges to a solution for wellbore flow if steady-state conditions are maintained (WIPP PA, 2003g).

3.4.4 Wellbore Boundary Conditions and Source Terms

Mass can enter the wellbore at the pump inlet and below the drillbit, and can exit at the wellbore outlet. Mud enters at the pump inlet, and salt, gas, and waste enter below the bit.

Mud enters the well at the pump inlet based on the volume flow rate of the pump and the mud density:

$$S_{m,in} = \rho_m R_m \tag{3.4.11}$$

Until the drillbit penetrates the repository, salt enters the wellbore at a constant rate:

$$S_{s,in} = \rho_s R_{drill} A_{bit} \tag{3.4.12}$$

Additional mass enters the wellbore by gas flow from the repository ($S_{gas,in}$) or by drilling or spalling of waste material ($S_{w,in}$); these mass sources are discussed in Section 3.5.1. The outlet of the wellbore is set to atmospheric pressure. Mass exiting the wellbore is determined from the mixture velocity, the area of the outlet A_{out}, and the density and volume fraction of each phase at the outlet of the wellbore:

$$S_{q,out} = \rho u_{out} A_{out} \frac{V_q}{V} \tag{3.4.13}$$

Finally, the net change in mass for phase q is

$$S_q = S_{q,in} - S_{q,out} \tag{3.4.14}$$

The outlet of the wellbore is set to atmospheric pressure. Momentum exiting the wellbore is determined from the fluid velocity and the area of the outlet A_{out}:

$$S_{mom,in} = \frac{\rho_{0,m}}{A_p} R_m^2 \tag{3.4.15}$$

$$S_{mom,out} = -\rho A_{out} u_{out}^2 \tag{3.4.16}$$

No momentum is added by mass flow into the wellbore from the repository, thus:

$$S_{mom} = S_{mom,in} - S_{mom,out} . \tag{3.4.17}$$

3.5 Repository Equations

The repository is modeled as a radially symmetric domain. A spherical coordinate system is used for this presentation and for most DRSPALL calculations. In a few circumstances, cylindrical coordinates are used where spall volumes are large enough that spherical coordinates are not representative of the physical process. Cylindrical coordinates are also available; the Design Document for DRSPALL (WIPP PA, 2003a) provides details on the implementation of the repository flow model in cylindrical coordinates.

Flow in the repository is assumed to be transient, compressible, viscous, and single phase (gas) flow in a porous medium. Gas is treated as isothermal and ideal. The equations governing flow in the repository are the equation of state for gas, conservation of mass, and Darcy's law with the Forchheimer correction (Aronson 1986; Whitaker, 1996):

$$\frac{\rho_g}{\rho_{g,0}} = \frac{P}{P_{atm}} \tag{3.5.1a}$$

$$\phi \frac{\partial \rho_g}{\partial t} + \nabla \cdot \left(\rho_g \boldsymbol{u} \right) = 0 \tag{3.5.1b}$$

$$\nabla P = -\frac{\eta_g}{k} \left(1 + F \right) \boldsymbol{u} \tag{3.5.1c}$$

where

P = pressure in pore space (Pa)

ρ_g = density of gas (kg/m^3)

$\boldsymbol{u}$ = $u\boldsymbol{i}$, gas velocity vector

u = velocity of gas in pore space (m/s)

ϕ = porosity of the solid (unitless)

η_g = gas viscosity (Pa s)

k = permeability of waste solid (m^2)

F = Forchheimer coefficient (unitless)

The Forchheimer correction is included to account for inertial resistance effects in the flowing gas, which becomes important at high gas velocities (Ruth and Ma, 1992). When the Forchheimer coefficient is zero, Eq. (3.5.1c) reduces to Darcy's Law. A derivation of Eq. (3.5.1c) from the Navier-Stokes equations is given by Whitaker (1996); the derivation suggests that F is a linear function of gas velocity for a wide range of Reynolds numbers.

The Forchheimer coefficient takes the form

$$F = \frac{\beta_{nd} \rho u k}{\eta_g} \tag{3.5.2}$$

where β_{nd} is the non-Darcy coefficient, which depends on material properties such as the tortuosity and area of internal flow channels, and is empirically determined (Belhaj et al., 2003). The current default value is from a study by Li et al. (2001) that measured high-velocity nitrogen flow through porous sandstone wafers, giving the result

$$\beta_{nd} = \frac{1.15 \times 10^{-6}}{k\phi} \tag{3.5.3}$$

Eq.(3.5.1) combines into a single equation for pressure in the porous solid:

$$\frac{\partial P}{\partial t} = \frac{k'}{2\phi\eta_g} \nabla^2 P^2 + \frac{1}{2\phi\eta_g} \nabla P^2 . \nabla k' \tag{3.5.4}$$

where

$$k' = \frac{k}{1+F} = \frac{k}{1+\frac{\beta_{nd}\rho u k}{\eta_g}} = \frac{k}{1+\frac{1.15x10^{-6}\rho u}{\phi\eta_g}} \tag{3.5.5}$$

and the operator in a radially-symmetric coordinate system is given by

$$\nabla^2 = \frac{1}{r^{m-1}} \frac{\partial}{\partial r} \left(r^{m-1} \frac{\partial}{\partial r} \right) \tag{3.5.6}$$

where r denotes radius, and m = 2 for cylindrical coordinates or m = 3 for spherical coordinates.

The permeability of the waste solid is constant for waste material that has not failed and fluidized. In a region of waste that has failed, the permeability is assumed to increase as the waste fluidizes by a factor of $1 + 4F_f$, where F_f is the fraction of failed material that has fluidized and is based on the fluidization relaxation time. This approximately accounts for the bulking of material as it fluidizes.

Initial pressure in the repository is set to a constant value P_{ff}. A no-flow boundary condition is imposed at the outer boundary ($r = R$):

$$\nabla P(R) = 0 \tag{3.5.7}$$

The outer boundary to the repository domain exhibits sufficiently low permeability relative to the waste that a no-flow boundary was reasonable and simple to implement. In addition, there is sufficient distance between the borehole and outer boundary that the impact of the boundary condition is not felt during the time scale of normal DRSPALL executions. At the inner boundary ($r = r_{cav}$), the pressure is specified as $P(r_{cav}, t) = P_{cav}(t)$, where $P_{cav}(t)$ is defined in the next section. The cavity radius r_{cav} increases as drilling progresses and as waste material fails and moves into the wellbore; calculation of r_{cav} is described in Section 3.5.1.3.

3.5.1 Wellbore to Repository Coupling

Prior to penetration, a cylinder of altered-permeability salt material with diameter equal to the drillbit is assumed to connect the bottom of the wellbore to the repository. At the junction of the repository and this cylinder of salt, a small, artificial cavity is used to determine the boundary pressure for repository flow. After penetration, the cavity merges with the bottom of the wellbore to connect the wellbore to the repository.

3.5.1.1 Flow Prior to Penetration

Prior to penetration, the cylinder of altered permeable salt connecting the wellbore and the repository has a permeability and gas flow rate determined by the series connection of the salt, DRZ, and DDZ permeability (Gross and Thompson, 1998) (Figure 3.3-5). Since the DDZ permeability is the greatest of these, the DRZ boundary is fixed while the DDZ boundary advances with drilling, and the distance between the bit and the repository is decreasing with time, the permeability of this zone increases with time and becomes unbounded as the repository is penetrated. However, since the cavity and borehole pressures converge as the repository is penetrated, the overall mass flow remains bounded.

To couple the repository to the DRZ or DDZ, the model uses an artificial pseudo-cavity in the small hemispherical (or cylindrical) region of the repository below the wellbore, with the same surface area as the bottom of the wellbore (Figure 3.3-6). The pseudo-cavity is a numerical device that avoids the singularity if flow were to a point. Coupled with the DDZ it serves to smooth the discontinuities in pressure and flow that would otherwise occur upon bit penetration of the repository. The pseudo-cavity contains only gas and is initially at repository pressure. The mass of gas in the cavity m_{cav} is given by:

$$\frac{dm_{cav}}{dt} = S_{rep} - S_{g,in}, \tag{3.5.8}$$

where

S_{rep} = gas flow from repository into pseudo-cavity (kg/s); see Eq. (3.5.9),

$S_{g,\,in}$ = gas flow from pseudo-cavity through DRZ and/or DDZ into wellbore (kg/s); see Eq. (3.5.10).

Flow from the repository into the pseudo-cavity is given by:

$$S_{rep} = \rho_{g,rep} u_{rep} \phi A_{cav} \tag{3.5.9}$$

where

$\rho_{g,rep}$ = gas density in repository at cavity surface (kg/m^3) = $\rho_g\left(r_{cav}\right)$

u_{rep} = gas velocity (m/s) in repository at cavity surface = $u\left(r_{cav}\right)$

ϕ = porosity of waste (unitless)

A_{cav} = surface area of hemispherical part of the cavity (m^2)

= $\frac{\pi}{4} d_{bit}^2$, where d_{bit} is the diameter of the bit (m)

Flow out of the pseudo-cavity through the DRZ and DDZ and into the wellbore is modeled as steady-state using Darcy's Law:

$$S_{g,in} = \frac{k_{eff} \pi \left(\frac{d_{bit}}{2}\right)^2}{2\eta_g R_0 T L}\left(P_{cav}^2 - P_{BH}^2\right) \tag{3.5.10}$$

where

$$k_{eff} = \frac{L}{\frac{L_{DDZ}}{k_{DDZ}} + \frac{L_{DRZ}}{k_{DRZ}}} \tag{3.5.11}$$

η_g = gas viscosity (Pa s)

R_0 = ideal gas constant for hydrogen (J / kg °K)

T = repository temperature (°K)

L = $L_{DDZ} + L_{DRZ}$ or length (m) from bottom of borehole to top of repository

L_{DDZ} = length (m) of DDZ

L_{DRZ} = length (m) of DRZ

P_{cav} = pressure in pseudo-cavity (Pa)

P_{BH} = pressure at bottom of wellbore (Pa)

There is no need to start this process while there is intact salt between the DDZ and repository, as the flow is too small to have noticeable effect. In the numerical analysis, a series of steady-states (one for each timestep) is used with time-varying pressure boundary conditions. The wellbore pressure boundary is the pressure at the point of entry (just below the bit), and the repository pressure is that of the small pseudo-cavity at the face of the repository. Although the flow is not truly steady-state, this approach is justified as follows: When the distance L is large (that is, drilling is at or above the DRZ) the steady state assumption will somewhat overestimate the flow, but the flow itself is so small that the error is small. When the distance L becomes small, the steady-state assumption becomes more and more accurate, since equilibrium is rapidly achieved. Thus the stepwise steady state approach becomes sufficiently accurate at the time and position of the bit where accuracy is most required. These conclusions are established by inspection of the results of Gross and Thompson (1998)

The pseudo-cavity is initially filled with gas at a pressure of P_{ff}. The boundary pressure on the well side (P_{BH}) is the pressure immediately below the bit, determined by Eq (3.4.1). The pressure in the pseudo-cavity (P_{cav}) is determined by the ideal gas law:

$$P_{cav} = \frac{m_{cav} R_0 T}{V_{cav}} \tag{3.5.12}$$

where the volume of the spherical cavity V_{cav} is given by

$$V_{cav} = \left(\frac{\pi}{24\sqrt{2}} \right) d_{bit}^3 \quad . \tag{3.5.13a}$$

and in the cylindrical case

$$V_{cav} = \left(\frac{\pi}{64H} \right) d_{bit}^4 \tag{3.5.13b}$$

Recall that the surface area of the enclosed geometry dependent volume is equal to the circular area of the bit – the flux area is conserved. If the pseudo-cavity volume is small compared to physical volumes in the system, it will act to provide compatible boundary conditions prior to penetration and should have no other effect on the solution. For example, once the bit has penetrated the repository by about 1/10 its diameter, the volume actually drilled in the repository exceeds that volume of the pseudo cavity.

3.5.1.2 Flow after Penetration

After penetration of the waste, the bottom of the wellbore is modeled as a hemispherical cavity in the repository, the radius of which grows as drilling progresses and as material fails and moves into the cavity. Gas, drilling mud and waste are assumed to thoroughly mix in this cavity; the resulting mixture flows around the drill collars and then up the annulus between the wellbore and the drill string. Gas flow from the repository into the cavity is

given by Eq. (3.5.9); however, A_{cav} is now dependent on the increasing radius of the cavity (see Section 3.5.1.3). Waste flow into the cavity is possible if the waste fails and fluidizes; these mechanisms are discussed in Sections 3.5.2 and 3.5.3. Pressure in the cavity is equal to the pressure at the bottom of the wellbore and is computed by Eq. (3.5.12).

3.5.1.3 Cavity Volume after Penetration

The cylindrical cavity of increasing depth created by drilling is mapped to a hemispherical volume at the bottom of the wellbore to form the cavity. This mapping maintains equal surface areas in order to preserve the gas flux from the repository to the wellbore. The cavity radius from drilling is thus

$$r_{drill} = \sqrt{\frac{d_{bit}^2 + 4 d_{bit} \Delta H}{8}} \tag{3.5.14}$$

where ΔH is the depth of the drilled cylinder.

.

The cavity radius, r_{cav}, is increased by the radius of failed and fluidized material r_{fluid}, which is the depth to which fluidization has occurred beyond the drilled radius. That is,

$$r_{cav} = r_{drill} + r_{fluid} \tag{3.5.15}$$

3.5.2 Elastic Response and Failure

Gas flow from the waste creates a pressure gradient within the waste, which induces elastic stresses in addition to the far-field confining stress. These stresses may lead to tensile failure of the waste material, assumed to be a prerequisite to spallings releases. While the fluid calculations using Eq. (3.5.1) are fully transient, the elastic stress calculations are assumed to be quasi-static (i.e., sound-speed phenomena in the solid are ignored). The equations for elastic effective stresses are derived from the linear elastic relationships for a porous body (presented in Jaeger and Cook (1969) by developing flow or pore pressure induced stress terms analogous to the thermal induced stresses of Timoshenko and Goodier (1970), which gives:

$$\sigma_r'(r) = \sigma_{sr}(r) + \sigma_{ff}\left(1 - \left(\frac{r_{cav}}{r}\right)^m\right) + P(r_{cav})\left(\frac{r_{cav}}{r}\right)^m - \beta P(r) \tag{3.5.16}$$

$$\sigma_\theta'(r) = \sigma_{s\theta}(r) + \sigma_{ff}\left[1 + \frac{1}{m-1}\left(\frac{r_{cav}}{r}\right)^m\right] - \frac{P(r_{cav})}{m-1}\left(\frac{r_{cav}}{r}\right)^m - \beta P(r) \tag{3.5.17}$$

where β is Biot's constant and σ_{ff} is the confining far-field stress, m is 2 or 3 for cylindrical or spherical geometry, respectively, and the flow-related radial and tangential stresses (σ_{sr} and $\sigma_{s\theta}$, respectively) are:

$$\sigma_{sr}(r) = (m-1)\beta\left(\frac{1-2\upsilon}{1-\upsilon}\right)\frac{1}{r^m}\int_{r_{cav}}^{r}\left(P(s)-P_{ff}\right)s^{m-1}ds \tag{3.5.18}$$

$$\sigma_{s\theta}(r) = -\beta\left(\frac{1-2\upsilon}{1-\upsilon}\right)\left(\frac{1}{r^m}\int_{r_{cav}}^{r}\left(P(s)-P_{ff}\right)s^{m-1}ds - \left(P(r)-P_{ff}\right)\right) \tag{3.5.19}$$

where P_{ff} is the far field repository pressure and υ is Poisson's ratio.

Since stresses are calculated as quasi-static, an initial stress reduction caused by an instantaneous pressure drop at the cavity face propagates instantaneously through the waste. The result of calculating Eq. (3.5.16) can be an instantaneous early-time tensile failure of the entire repository if the boundary pressure is allowed to change suddenly. This is non-physical and merely a result of the quasi-static stress assumption combined with the true transient pore pressure and flow-related stress equations. To prevent this non-physical behavior, tensile failure propagation is limited by a tensile failure velocity. This limit has no quantitative effect on results other than to prevent non-physical tensile failure.

At the cavity face, Eqs. (3.5.16) and (3.5.18) evaluate to zero, consistent with the quasi-static stress assumption. This implies that the waste immediately at the cavity face cannot experience tensile failure; however, tensile failure may occur at some distance into the waste material. Consequently, the radial effective stress $\sigma_r'(r)$ is averaged from the cavity boundary into the waste over a characteristic length L_t. If this average radial stress $\bar{\sigma}_r'$ is tensile and its magnitude exceeds the material tensile strength ($\left|\bar{\sigma}_r'\right| > TENSLSTR$), the waste is no longer capable of supporting radial stress and fails, permitting fluidization.

Eqs (3.5.17) and (3.5.19) evaluate shear stresses in the waste. The shear stresses in the waste are not used in the calculation of waste failure for spalling releases. These stresses are included in this discussion for completeness.

3.5.3 Fluidization

In a region where tensile failure has occurred, the waste material is first assumed to be disaggregated, but not in motion. It remains as porous, bedded material lining the cavity face, and is treated as a continuous part of the repository from the perspective of the porous flow calculations. The bedded material is subject to mobilization and removal to the flow stream in the cavity by fluidized bed theory. As such, solids are allowed to flow into the

cavity if the superficial gas velocity, u_{repos}, at the cavity face exceeds a minimum fluidization velocity, U_f. Superficial gas velocity is defined as the average velocity across the entire surface area of the cavity (u_{repos} = pore velocity × ϕ). The cavity radius will increase corresponding to the volume of solid material removed by fluidization. The minimum fluidization velocity is determined by solving the following quadratic equation (Cherimisinoff and Cherimisinoff, 1984; Ergun, 1952).:

$$\frac{1.75}{a\phi^3}\left(\frac{d_p U_f \rho_g}{\eta_g}\right)^2 + 150\left(\frac{1-\phi}{a^2\phi^3}\right)\left(\frac{d_p U_f \rho_g}{\eta_g}\right) = \frac{d_p^3 \rho_g \left(\rho_w - \rho_g\right) g}{\eta_g^2} \tag{3.5.20}$$

where

a = particle shape factor (unitless)

d_p = particle diameter (m)

If fluidization occurs, the cavity is allowed to grow until the cavity radius equals the depth of the first intact (non tensile-failed) material. New tensile failure is allowed from the boundary into the intact repository material. Once the entire region of length L_t nearest boundary fluidizes, a new region of length L_t is defined and evaluated for failure as discussed above. With cavity growth, the gas and waste particles in the newly fluidized region must mix into the cavity in such a way as to conserve mass. To account for the fact that this mixing cannot be instantaneous, which would be non-physical and lead to numerical instability later (much as allowing instantaneous tensile failure propagation), a small artificial relaxation time, equal to the cavity radius divided by the superficial gas velocity, is imposed upon the mixing phenomenon. As fluidization occurs, the permeability of the failed waste in that region is allowed to grow according to

$$k'_f = k'(1 + 4F_f) \tag{3.5.21}$$

where F_f is the fraction fluidized and is based on the fluidization relaxation time. This approximately accounts for the bulking of material as it fluidizes. It is interesting to note that the Ergun equation, which leads to Eq. (3.5.20), can also be used to derive a non-Darcy coefficient for particulate beds (Narayanaswamy et al., 1999). This takes a form similar to Eq. (3.5.3).

3.5.4 Repository Boundary Conditions

The porous flow equations are solved with a pressure (flow) boundary condition at the inner (cavity) wall and a zero pressure gradient (no-flow) condition at the outer wall. For the inner wall, the cavity pressure (either pseudo or real) sets a pressure outside the porous solid. The inner cavity wall propagates radially outward as material is drilled or failed and fluidized and moved from the repository to the cavity. Thus, the boundary condition is subsequently applied to the adjacent non-fluidized but possibly failed material. The pressure inside the

porous solid then develops a gradient, which is used to calculate a pore velocity at the boundary using Darcy's Law:

$$u_{repos} = \frac{k'}{\eta\phi}\frac{\partial p}{\partial r}\bigg|_{r=r_c} \tag{3.5.22}$$

Material (gas) loss across the boundary as a function of time can then be calculated using Eq. (3.5.9).

3.5.5 Implementation of Conceptual Submodels in DRSPALL

Some of the features of the conceptual and mathematical model discussed earlier require special implementation procedures in a finite difference code. The purpose of this section is to elucidate the implementation steps that are not necessarily clear in a discussion of the conceptual model alone.

3.5.5.1 Characteristic Length and Tensile Failure

A review of the effective stress formulation (Eq. (3.5.16)) reveals several issues that require careful consideration when applying this model to a repository domain divided into discrete computational zones. A typical radial effective stress curve is drawn in Figure 3.5-1.

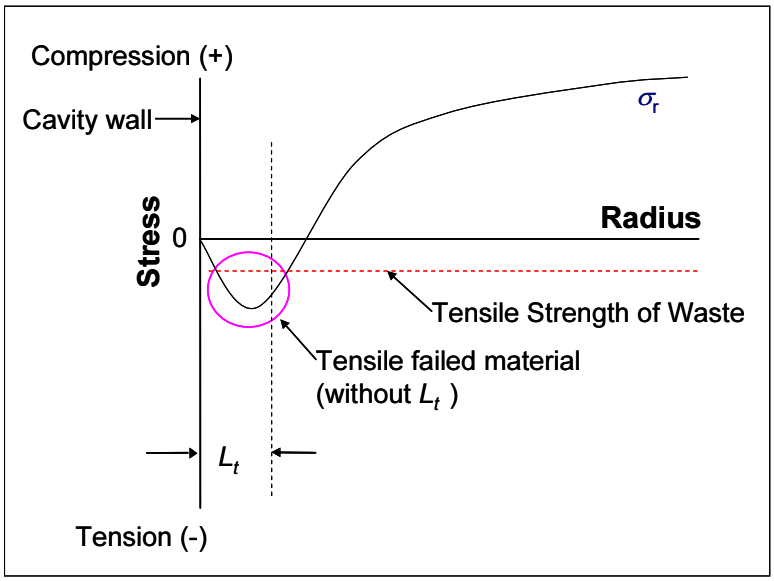

Figure 3.5-1. Drawing of Typical Radial Effective Stress Curve in DRSPALL Repository Domain at Some Time During Drill Penetration.

The tensile strength of the waste is shown in the figure as well. Effective radial tensile stresses (negative values on the stress axis) are shown to develop near to, but not exactly at the cavity wall. In fact, the effective stress exactly at the cavity wall is always $\sigma_r'(r_{cav}) = 0$.

As such, a region of tension develops that may exceed the tensile strength at radii greater than, but not at, the cavity wall. The region of material subject to tensile failure, without consideration of the characteristic length concept, is circled in Figure 3.5-1. Note that material between the failed region and the cavity wall is still intact according to the current stress model.

Failed regions trapped between intact shells cannot, by themselves, be removed from the repository domain without first removing the intact cavity wall. It is assumed here that once a tensile-failed region exists, the cavity wall is likely to eventually succumb to buckling failure. A simple approach to this is implemented in DRSPALL by introducing a characteristic failure length, L_t, in which the mean tensile stress is evaluated over a region that extends from the cavity wall ($r = r_{cav}$) to a depth of one characteristic length ($r = r_{cav} + L_t$) into the repository domain. This characteristic length must be large enough to encompass several computational zones, but not so large that it masks the tensile region. If the mean tensile stress over L_t exceeds the tensile strength, all the zones in L_t fail, and they are flagged as "failed" in DRSPALL. Zones outside of L_t are not allowed to fail until all the disaggregated, bedded waste is fluidized.

3.5.5.2 Cavity Growth by Drilling

During normal drilling, when the bit penetration depth passes the outer edge of a computational zone, that zone (gas and solids) is removed from the repository domain and put into "storage." From storage, the drilled mass is then released to the cavity over a mixing time $t_m = (r_{c1}/u_{repos})$ where r_{c1} is the radius to the center of the cell that forms the cavity wall ($r_{c1} = r_{cav} + \Delta r/2$). This is done because instantaneously adding the entire contents of a computational zone to the cavity causes numerical noise, and the controlled release from storage dampens the numerical shock.

3.5.5.3 Cavity Growth by Fluidization

In the event that a group of zones comprising L_t fails, the zones are individually tested for fluidization potential using the Ergun (1952) model given in Eq. (3.5.20). If the superficial gas velocity exceeds the minimum fluidization velocity ($u_{repos} > U_f$), a failed zone is flagged for fluidization. The fluidization process requires a finite fluidization time $t_f = r_{c1}/u_{repos}$. Zones must begin fluidization sequentially so that the zone comprising the cavity wall starts first, after which the next zone can start fluidization. This proceeds until all zones flagged for fluidization are removed from the repository domain and thus incorporated into the wellbore domain. The cavity thus grows in zone-by-zone increments as subsequent zones complete fluidization.

3.5.5.4 Repository Thickness

Repository thickness H at the time of intrusion is determined from the current repository porosity ϕ, and the height H_o and porosity ϕ_o of a waste-filled room prior to closure:

$$H = \frac{(1-\phi_o)H_o}{1-\phi} \tag{3.5.23}$$

3.6 One Dimensional Geometry Considerations

In a real three-dimensional system, the drilling process creates a cylindrical borehole through the waste repository that constantly increases in length and possibly grows radially due to caving and spalling processes. To rigorously simulate a borehole that grows axially, radially, or both, under isotropic homogenous conditions would require a large, computationally intensive two-dimensional axial-symmetric model. The probabilistic framework in which the spallings model is applied requires many executions, resulting in a necessary balance between model sophistication and computational efficiency. Development of a one-dimensional model geometry was seen as a strategy that would promote computational speed but still include all of the critical mechanisms proposed in the conceptual model. Therefore, two one-dimensional geometric models (hemispherical, cylindrical) are implemented in DRSPALL, with the geometry selected by the user. At early time just prior to and just after penetration, the repository domain is best modeled with hemispherical flow and stress state assumptions. As the bit approaches the floor of the repository the one-dimensional cylindrical assumption is more appropriate. In spite of this, only one geometry may be used per execution in the current DRSPALL model.

The true cylindrical cavity of increasing height formed during the drilling process must be mapped each computational step to an equivalent cavity radius in the specified one-dimensional spherical or cylindrical geometry. This mapping assumes conservation of surface area in order to preserve the early time repository pressure gradients and gas flux from the repository to the wellbore. Note that the drilled volume will not be conserved.

The surface area of the true cylinder cut from the waste takes the shape of a soup can with one end removed. The surface area of this cut cylinder is therefore:

$$A_{cut} = \frac{\pi d_{bit}^2}{4} + \pi d_{bit} \Delta H \tag{3.6.1}$$

In spherical geometry the equivalent radius is determined by equating A_{cut} with the surface area of a hemisphere ($A = 2\pi r_{eq}^2$). Solving for r_{eq} gives:

$$r_{eq} = \left(\frac{A_{cut}}{2\pi} \right)^{\frac{1}{2}} \tag{3.6.2}$$

In cylindrical geometry the equivalent radius is determined by equating A_{cut} with the surface of a cylinder with fixed height H and open ends ($A = \pi d_b H$). Solving for r_{eq} in this case gives:

$$r_{eq} = \left(\frac{A_{cut}}{2\pi H} \right) \tag{3.6.3}$$

For small penetration depths this implies a very small diameter equivalent cylinder with a height equal to the repository thickness.

Equivalent volumes are calculated from the equivalent radius using the volume equation appropriate for the assumed geometry. When the bit reaches the floor of the repository, drilling is stopped and in cylindrical geometry the actual drilled and equivalent volumes will be the same. But, in spherical geometry the equivalent volume will be greater than the drilled volume.

The effect of the geometry on specific model setup parameters is demonstrated in Figure 3.6-1, which compares equivalent radius and enclosed volume for the two geometries as a function of drillbit penetration depth. Recall that the equivalence to the actual wellbore geometry drilled into the repository assumes conservation of cavity surface area. The result is that neither the drilled radius nor the drilled volume is conserved. At early times for cylindrical geometry, the wellbore cavity is modeled as a very small diameter cylinder with a length equal to the repository height. As drilling proceeds, the actual 3-D wellbore cavity in the repository increases while radius remains constant. In the one-dimensional DRSPALL model, however, the wellbore cavity length is fixed and the radius increases to conserve surface area. When the drillbit reaches the repository floor at a depth of about 1.5 m, the radius and volume of the DRSPALL model wellbore for cylindrical geometry is slightly larger than the actual 3-D wellbore because the circular surface area at the bottom of the wellbore is included in the circumferential surface area used to compute the effective wellbore radius for the model. In spherical geometry the equivalent radius and volume are considerably larger than that of the actual 3-D wellbore cavity.

Figure 3.6-2 shows the effect of geometry on the radial elastic stress. A spreadsheet was used to calculate the stress profiles using boundary conditions that are representative. There are two major factors contributing to the differences in the stress profiles. One factor is the geometry. For the same cavity radius, the cylindrical geometry has lower stresses and gradients near the wellbore than the spherical (compare curves with r_{cav} = 0.35m). The other factor arises from conservation of area, which results in a much smaller equivalent radius in cylindrical geometry. In this example, r_{cav} = 0.082m for the cylindrical case versus r_{cav} = 0.35 for the spherical case for the same cavity area. The smaller equivalent cavity radius in cylindrical geometry results in larger radial elastic stress and gradients near the wellbore. The latter case is representative of the sensitivity results presented in section **7**.

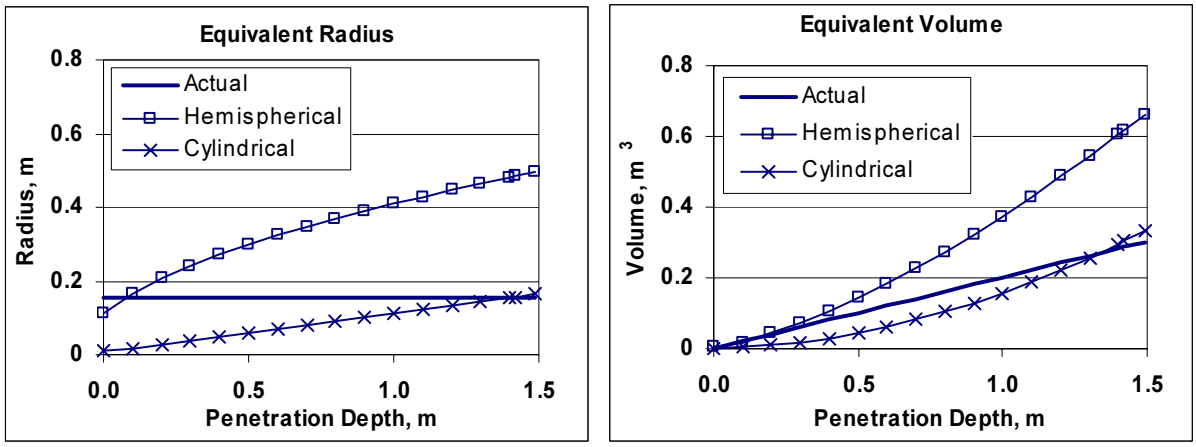

Figure 3.6-1. Equivalent Radius and Volume for One-Dimensional Hemispherical and Cylindrical Geometries

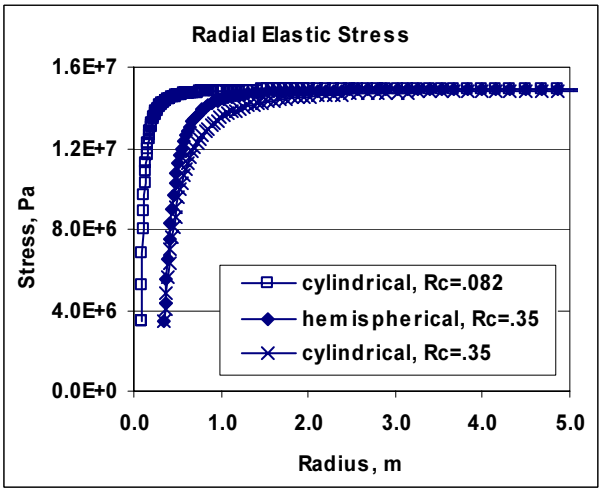

Figure 3.6-2. Radial Elastic Stress Profiles for One-Dimensional Hemispherical and Cylindrical Geometries

4 Numerical Model: DRSPALL

4.1 Code Design

Both the wellbore and the repository calculations use classical Eulerian, time-marching, central finite difference schemes which are similar but not identical. The two domains are coupled through boundary conditions and source terms but their governing equations are solved independently. However, the solution algorithms are part of a single computational loop and therefore use the same timestep. No formal consistency or stability analyses have been performed on the solution algorithms, but extensive verification (section 6) and zone size studies (section 5) provide confidence, but not proof, that the solution algorithms are consistent and stable.

4.2 Wellbore Numerical Methods

The wellbore is zoned for finite differencing as shown Figure 4.2-1. This shows zones, zone indices, grid boundaries, volumes, and interface areas. The method is Eulerian. That is, zone boundaries are fixed, and fluid moves through the interfaces by convection. Quantities are zone-centered and integration is explicit in time. The following detailed discussion will be specific to the mass balance given by Eq. (3.4.1a). However, the differencing method for the momentum balance given by Eq. (3.4.1b) is the same.

The equations shown below are for constant zone size. DRSPALL actually implements difference equations that allow for the zone size to vary from cell to cell. The intent is to use small zones near regions where there are geometry changes and increase zone size geometrically away from those regions.

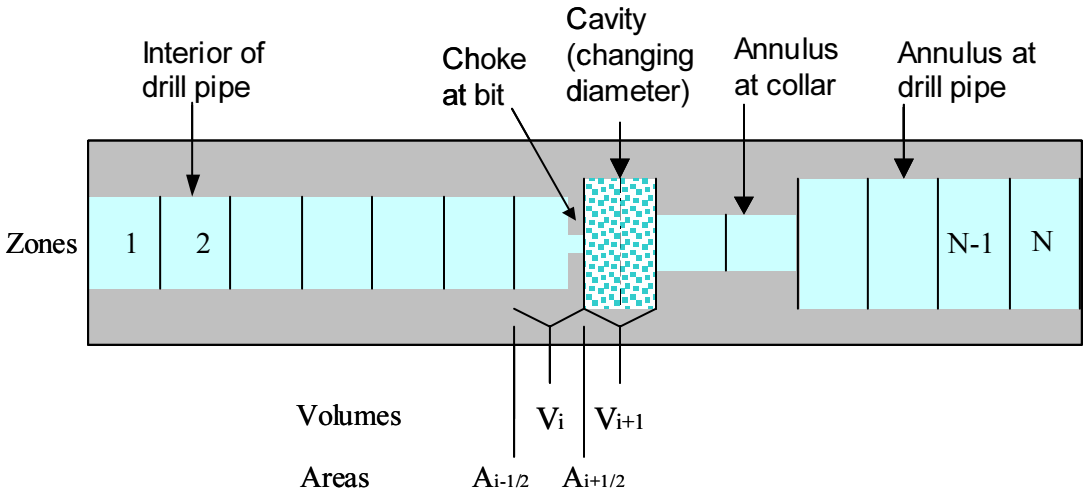

Figure 4.2-1. Finite Difference Zoning for Wellbore.

All of the materials (mud, salt, gas, and waste) are assumed to move together as a mixture. Since fluid moves through the grid boundaries, calculation requires values for the flow through these boundaries during a timestep. This is obtained from the difference between the fluid velocities at the zone centers, given by

$$u_{i+1/2} = \frac{1}{2}\left(u_{i+1}^{n-1} + u_i^{n-1}\right) \tag{4.2.1}$$

The mass balance equation, prior to any volume change, becomes

$$V_i\ \rho_i^* = V_i\ \rho_i^{n-1} - \Delta t\left(A_{i+1/2}\rho_{i+1/2}^{n-1}u_{i+1/2} - A_{i-1/2}\rho_{i-1/2}^{n-1}u_{i-1/2}\right) + \Delta t S_{m,i} \tag{4.2.2}$$

Here the source terms($S_{m,i}$) are set to correspond to material entering or exiting at the pump, cavity, and surface. The "upwind" zone centered densities are used for the interface values, $\rho_{i+1/2}^{n-1}$ and $\rho_{i-1/2}^{n-1}$.

Finally we incorporate any changed volumes and add numerical mass diffusion for stability:

$$V_i\ \rho_i^n = V_i\ \rho_i^* + \Delta z_i \sum_{m=1}^{N_c} \zeta_m \left[A_{i+1/2}\left(\left(\rho f_m\right)_{i+1}^{n-1} - \left(\rho f_m\right)_i^{n-1}\right) - A_{i-1/2}\left(\left(\rho f_m\right)_i^{n-1} - \left(\rho f_m\right)_{i-1}^{n-1}\right)\right] \tag{4.2.3}$$

The densities, ρf_m, are for the particular constituent, m, being diffused and are calculated from the mixture density, ρ, times the mass fraction, f_m, of the constituent in the referenced cell. The numerical diffusion coefficient ζ_m is chosen empirically for stability. Separate diffusion coefficients could be used for the different materials (mud, gas, etc.). However, sufficient stability is obtained by only diffusing mud and salt using the same coefficient. This better preserves the accuracy of the location of gases and waste in the well.

Momentum is differenced as

$$\begin{aligned} V_i\ \left(\rho u\right)_i^* = V_i\ \left(\rho u\right)_i^{n-1} &- \Delta t\left(A_{i+1/2}\left(\rho u\right)_{i+1/2}^{n-1} u_{i+1/2} - A_{i-1/2}\left(\rho u\right)_{i-1/2}^{n-1} u_{i-1/2}\right) \\ &- V_i\ \left(\frac{P_{i+1}^{n-1} - P_{i-1}^{n-1}}{2\Delta z} - \rho_i^{n-1} g + F_i^{n-1}\right) + \Delta t S_{mom,i} \end{aligned} \tag{4.2.4}$$

where the dissipation term F_i^{n-1} is obtained from Eq. (3.4.6) and is constrained as follows:

$$\left|F_i^{n-1}\right| \le \left|\frac{P_{i+1}^{n-1} - P_{i-1}^{n-1}}{2\Delta z} - \rho_i^{n-1} g\right| \tag{4.2.5}$$

and the sign F_i^{n-1} is chosen such that it opposes flow.

Finally, numerical momentum diffusion is added without distinguishing between phases in the mixture (ρ is the mixture density).

$$V_i\ (\rho u)_i^n = V_i\ (\rho u)_i^* - \zeta_p \Delta x_i \left[A_{i+1/2} \left((\rho u)_{i+1}^{n-1} - (\rho u)_i^{n-1} \right) - A_{i-1/2} \left((\rho u)_i^{n-1} - (\rho u)_{i-1}^{n-1} \right) \right] \quad (4.2.6)$$

Eqs (3.4.2), (3.4.3), and (3.4.4) comprise a simultaneous system of equations for the volumes of gas and mud, and the pressure in the wellbore. The volumes of salt and waste will be known, since they are considered incompressible. Solving Eq. (3.4.2) for P; substituting P and ρ_m from Eq. (3.4.3) into Eq. (3.4.4) and rearranging terms results in the following quadratic equation for gas volume:

$$aV_g^2 + bV_g - c = 0 \quad (4.2.7)$$

where

$$a = 1 - c_m P_{atm}$$
$$b = c_m P_{atm} V_{g,0} - aV^* + V_{m,0}$$
$$c = V^* c_m P_{atm} V_{g,0}$$
$$V_{g,0} = m_g / \rho_{g,0}$$
$$V_{m,0} = m_m / \rho_{m,0}$$

and

$$V^* = V_m + V_g = V - V_s - V_w$$

The volume of the mud phase follows from Eq. (3.4.3) and the pressure from Eq. (3.4.2). Once mixture density in each cell (ρ_i) is updated by Eq. (3.4.4), mixture velocity in each cell (u_i) is computed by

$$u_i = \frac{(\rho u)_i}{\rho_i} \quad (4.2.8)$$

where the quantity ρu is determined by Eq. (4.2.6).

An approximate solution for Colebrook's f (Eq. 3.4.9) in the turbulent regime is given by Serghides (1984):

$$f = \left[a - \frac{(b-a)^2}{c + a - 2b} \right]^{-2} \quad (4.2.9)$$

where

$$a = -2\log\left[\frac{\varepsilon / d_h}{3.7} + \frac{12}{\mathrm{Re}}\right]$$

$$b = -2\log\left[\frac{\varepsilon / d_h}{3.7} + \frac{2.51a}{\mathrm{Re}}\right]$$

$$c = -2\log\left[\frac{\varepsilon / d_h}{3.7} + \frac{2.51b}{\mathrm{Re}}\right]$$

4.3 Repository Numerical Methods

The time integration method for the repository flow is implicit, with spatial derivatives determined after the time increment. This method requires the inversion of a matrix for the entire repository, which is usually straightforward. The implicit scheme is unconditionally stable. However, it is still necessary to use small timesteps to ensure gradient accuracy.

We start with Eq. (3.5.10), and employ a numerical method described by Press et al. (1989). The equations presented below are for constant zone size. DRSPALL actually implements difference equations that allow for a variable zone size. Near the cavity, a small, constant zone size is used, and then zones are allowed to grow geometrically as the outer boundary is approached. This procedure greatly increases computational efficiency without sacrificing accuracy in the region of interest.

For an isothermal ideal gas, the pseudo-pressure (Rath and Podio, 2000) is defined as

$$\psi = \frac{P^2}{\eta_g} \quad \text{or} \quad P = \sqrt{\eta_g \psi}\ . \tag{4.3.1}$$

Using Eq. (4.3.1), Equation (3.5.4) is expanded to

$$\frac{\partial \psi}{\partial t} = D(\psi)\left[\frac{\partial^2 \psi}{\partial r^2} + \frac{(m-1)}{r}\frac{\partial \psi}{\partial r} + \frac{1}{k'}\frac{\partial k'}{\partial r}\frac{\partial \psi}{\partial r}\right] \tag{4.3.2}$$

where

$$D(\psi) = \frac{k'}{\phi}\sqrt{\frac{\psi}{\eta_g}} = \frac{k'P}{\phi\eta_g}$$

Eq. (4.3.2) is then converted to a difference equation by assuming $D(\psi)$ is constant over a zone which simplifies the numerical implementation. Using its zone-centered value at the current time, D_j^n, gives:

$$\frac{\psi_j^{n+1}-\psi_j^n}{\Delta t}=\frac{D_j^n}{\Delta r}\left[\frac{\psi_{j+1}^{n+1}-2\psi_j^{n+1}+\psi_{j-1}^{n+1}}{\Delta r}+\frac{(m-1)\left(\psi_{j+1}^{n+1}-\psi_{j-1}^{n+1}\right)}{2r_j}+\frac{\left(k'^{n+1}_{j+1}-k'^{n+1}_{j-1}\right)\left(\psi_{j+1}^{n+1}-\psi_{j-1}^{n+1}\right)}{4k'\Delta r}\right] \quad (4.3.3)$$

Now, rearrange, collecting similar terms in ψ.

$$-\alpha_1\psi_{j-1}^{n+1}+(1+2\alpha)\psi_j^{n+1}-\alpha_2\psi_{j+1}^{n+1}=\psi_j^n \quad j=1,2\ldots. \quad (4.3.4)$$

where

$$\alpha=\frac{D_j^n\Delta t}{(\Delta r)^2}$$

$$\alpha_1=\left(\frac{D_j^n}{\Delta r}\right)\left(\frac{1}{\Delta r}-\frac{(m-1)}{2r_j}-\frac{k'^{n+1}_{i+1}-k'^{n+1}_{i-1}}{4k'\Delta r}\right)\Delta t$$

$$\alpha_2=\left(\frac{D_j^n}{\Delta r}\right)\left(\frac{1}{\Delta r}+\frac{(m-1)}{2r_j}+\frac{k'^{n+1}_{i+1}-k'^{n+1}_{i-1}}{4k'\Delta r}\right)\Delta t$$

Eq. (4.3.4) is a tridiagonal system that may be solved by simplified LU decomposition as presented in Press (1989).

4.3.1 Boundary Conditions.

The boundary condition at the inner radius is implemented by noting that for i =1 (the first intact or non-fluidized cell) , ψ_{i-1} is the cavity pseudo-pressure, which is known and, therefore, can be moved to the right hand side of Eq. (4.3.4).

$$(1+2\alpha)\psi_1^{n+1}-\alpha_2\psi_2^{n+1}=\psi_1^n+\alpha_1\psi_{cav}^{n+1} \quad (4.3.5)$$

The far field boundary condition is a zero gradient, which is implemented by setting $\psi_{j+1}^{n+1}=\psi_j^{n+1}$ in Eq. (4.3.4), recognizing that $1+2\alpha=1+\alpha_1+\alpha_2$ and rearranging, which gives

$$-\alpha_1\psi_{j-1}^{n+1}+(1+\alpha_1)\psi_j^{n+1}=\psi_j^n \quad (4.3.6)$$

where j is the index of the last computational cell.

4.3.2 Repository Stress State.

Once pore pressure is known, evaluation of the repository stress state, Eqs. (3.5.16) and (3.5.17), is algebraic except for the integral in the seepage stress calculations in Eqs. (3.5.18) and (3.5.19). The integrals are evaluated using trapezoidal integration with trapezoids formed between the cell centers where pore pressure and stress components are evaluated. Radii are evaluated at cell centers. .

$$\int_{r_{cav}}^{r_j} \left[P\left(r_j\right) - P_{ff} \right] s_j^{m-1} ds = \sum_{i=1}^{j} 0.5\left(\left(P_{i-1} - P_n\right) r_{i-1}^{m-1} + \left(P_i - P_n\right) r_i^{m-1} \right) \left(r_i - r_{i-1}\right) \quad (4.3.7)$$

where i=1 is the first intact cell (non-fluidized); j is index of the cell for which stress components are being evaluated; r_j is radius to the center of cell j; p_0 is the cavity pressure; r_0 is the radius of cavity cell next to the interface; and n is the index of the last computational cell.

4.4 Coupling Region

The calculation of gas flux from the repository to the cavity (Eqs 3.5.9) requires the gas velocity at the cavity interface, u_{repos} .The velocity is evaluated numerically as follows:

$$u_{repos} = \frac{k_1'}{\eta\phi}\left(\frac{p_1 - p_{cav}}{\Delta r_1} \right) \quad (4.4.1)$$

The mass of gas flowing from the repository to the cavity at the bottom of the wellbore is then evaluated from:

$$\Delta m_{cav} = \rho_{g,rep} u_{rep} \phi A_{cav} \Delta t \quad (4.4.2)$$

4.5 Timestep Determination

For the wellbore, which uses a conditionally stable explicit method, the Courant condition

$$ss_m \frac{\Delta t}{\Delta z} < constant \quad (4.5.1)$$

is the basis of timestep determination, where Δz is the zone size and ss_m is the sound speed in the mud:

$$ss_m = \sqrt{\frac{1}{c_m \rho_m}} \tag{4.5.2}$$

The wellbore timestep is calculated by replacing the inequality in (4.5.1) with equality, solving for Δt using a user specified *constant* and finding the minimum over all computational cells

$$\Delta t = \min\left(constant \frac{\Delta z_i}{ss_{m_i}} \right) \tag{4.5.3}$$

Normally, the value of the *constant* is taken as 1.0 for the "standard" Courant condition. However, due to the addition of the numerical diffusion terms and the extreme conditions in the present problem, especially where mass feeds from the repository into the wellbore, *constant* might be much be less than 1 for a stable solution and is found by trial and error. A value that produces stable results (free of cell-to-cell oscillations) will typically work across a range of model parameter values.

For the repository, which uses an unconditionally stable implicit method, a constant timestep would typically be specified by the user. DRSPALL actually implements the timestep selection as a user specified factor, F_{rep}, that is multiplied by the Courant criteria that would normally be used by an explicit algorithm.

$$\Delta t = \min\left(F_{rep} \frac{\Delta r_i^2}{\frac{k_i'}{\varphi}\left(\frac{\psi_i}{\eta_{g,i}}\right)^{1/2}} \right), i = 1, n_{\max} \tag{4.5.4}$$

where Δt is the minimum over all cells in the repository domain ($n_{\max}$). Trial and error or convergence testing can be used to find a timestep factor (usually greater than 1) that gives suitable results and gradient definitions.

The final timestep used is the lesser of the wellbore-determined and repository-determined timestep.

5 Zone Size Sensitivity Study

5.1 Objective

The objective of this study is to demonstrate the effect of repository zone size, Δr, characteristic tensile failure length, L_t, and wellbore zone size, Δz, on the spall release. The dependence of spall release on a combination of mechanisms (stress, failure, fluidization) requires that stress and failure be examined explicitly, in addition to spall release, in order to gain a meaningful understanding of the impacts of zone size on the DRSPALL model performance. The wellbore provides the inner pressure boundary condition to the reporsitory by accurately modeling the transport of mud, injected gas and mobilized waste to the surface. Repository zone size is discussed in detail and the wellbore zone size effect is briefly demonstrated. The results from this study facilitated selection of appropriate set of DRSPALL zone size parameters and justified the values used in the CRA spalling release calculations documented in sections 7, 8, and 9.

5.2 Background

The characteristic length (section 3.5.5.1) is the distance from the wellbore interface over which radial effective stress is averaged and then compared to the tensile cutoff in order to determine material failure from spalling. This characteristic length is used to allow failure of a shell of material next to the wellbore to occur, even though actual material failure is always at some finite distance into the solid. This situation occurs because the radial effective stress is always zero at the boundary between the wellbore and repository where both the radial elastic stress and pore pressure are equal to the bottomhole pressure (boundary condition), and the seepage stress is zero. This implies that the cell-centered radial effective stress will decrease toward zero near the wellbore boundary, and that this stress always will be less than the tensile cutoff at the boundary zone at some sufficiently small zone size. These small zones near the boundary will never fail, leading to the conclusion that grid refinement always leads to zero spalling under the assumption that failure propagates into the waste from the cavity interface. The use of a characteristic length over which failure is evaluated allows an internal failure to lead to failure of a shell of material. This is, in fact, a realistic approach, since solid material next to a wellbore does not tend to fail continuously from the wellbore interface into the waste on a particulate scale. Instead, discrete chunks will fail whose size is determined by the characteristics of the waste, such as the type of waste material, its original size, its degree of compaction at the time of the borehole intrusion, and its tensile strength. Failure of material close to the wellbore will therefore lead to loss of strength of the shell between this failure point and the wellbore, provided the thickness of the shell is not too large.

The average radial effective stress over the characteristic length therefore is used to evaluate tensile failure in DRSPALL. With the characteristic length, grid refinement leads to a "converged" radial effective stress profile, resulting in similar tensile failure behavior for

different zone sizes. The theoretical background for the stress model discussed above is presented in detail in section 3.5.2.

5.3 Problem Description.

The problem parameters used to evaluate the effects of the zone size and characteristic length were chosen to be within the typical sampling range for WIPP intrusion analyses and to yield reasonable spall release volume. Thus, DRSPALL sensitivities should be more visible than in a zero release problem or for a randomly chosen set of parameters. The base case (BC1) input (.DRS) file used for this zone size study is shown in Table 5.3-1. The parameters controlling zone size and characteristic length are highlighted in the table.

Table 5.3-1. Input File for the Zone Size Sensitivity Study.

REPOSITORY		
Land Elevation	(m):	1037.3
Repository top	(m):	385.31
Total Thickness	(m):	1.4898
DRZ Thickness	(m):	0.85
DRZ Permeability	(m^2):	1.00E-15
Outer Radius	(m):	19.2
Initial Gas Pressure	(m):	1.35E+07
Far-Field In-Situ Stress	(m):	1.49E+07
WASTE		
Porosity	(-):	0.6013
Permeability	(m^2):	1.78E-13
Forchheimer Beta	(-):	1.15E-06
Biot Beta	(-):	1
Poissons Ratio	(-):	0.3703
Cohesion	(Pa):	1.30E+05
Friction Angle	(deg):	44.4
Tensile Strength	(Pa):	1.20E+05
Failure Characteristic Length	(m):	0.02
Particle Diameter	(m):	1.48E-03
Gas Viscosity	(Pa-s):	8.93E-06
MUD		
Density	(kg/m^3):	1324
Viscosity	(Pa-s):	0.0107
Wall Roughness Pipe	(m):	1.52E-04
Wall Roughness Annulus	(m):	1.52E-04
Max Solids Vol. Frac.	(Pa-s):	0.6123
Solids Viscosity Exp.	(Pa-s):	-1.208

WELLBORE/DRILLING		
Bit Diameter	(m):	0.3112
Pipe Diameter	(m):	0.1143
Collar Diameter	(m):	0.2032
Pipe Inside Diameter	(m):	0.0972
Collar Length	(m):	182.9
Exit Pipe Length	(m):	0
Exit Pipe Diameter	(m):	0.2032
Drilling Rate	(m/s):	4.96E-03
Bit Above Repository	(m):	0.15
Mud Pump Rate	(m^3/s):	0.0194
Max Pump Pressure	(Pa):	2.75E+07
DDZ Thickness	(m):	0.156
DDZ Permeability	(m^2):	3.16E-15
Stop Drill Exit Vol Rate	(m^3/s):	1000
Stop Pump Exit Vol Rate	(m^3/s):	1000
Stop Drilling Time	(s):	1000

COMPUTATIONAL		
Spherical/Cylindrical	(S/C):	S
Allow Fluidization	(Y/N/A):	Y
Max Run Time	(s):	500
Repository Cell Length	(m):	0.002
Radius, Growth Rate	(m,-):	0.5, 1.01
Wellbore Cell Length	(m):	1
Wellbore Cell Growth Rate	(-):	1.01
First Wellbore Zone	(-):	387
Well Stability factor	(-):	0.1
Repository Stability factor	(-):	5
Mass Diffusion factor	(-):	0
Momentum Diffusion factor	(-):	0.01

PARAMETERS		
Pi	(-):	3.1416
Atmospheric Pressure	(Pa):	1.01E+05
gravity	(m/s^2):	9.8067
Gas Constant	(J/kg K):	4116
Repository Temperature	(K):	300
Water Compressibility	(1/Pa):	1.24E-09
Waste Density	(kg/m^3):	2650
Salt Density	(kg/m^3):	2201
Shape Factor	(-):	0.2932
Tensile Velocity	(m/s):	1000
Bit Nozzle Number	(-):	3
Bit Nozzle Diameter	(m):	0.0111
Choke Efficiency	(-):	0.9

5.4 Test Procedure

Six spherical DRSPALL configurations were compared to determine the sensitivity of cavity radius, pore pressure and solid stress profiles to various combinations of zone sizes and characteristic lengths. One additional run was used to evaluate wellbore zone size effect on bottomhole pressure. Three of the cases (BC1, DR2, DRH) were run a second time with a large tensile failure limit in order to analyze the development of the radial tensile stress profiles without the complication of failure and fluidization. The same three cases were repeated a third time using cylindrical geometry. All other material and problem specification parameters remained the same. The suite of configurations is outlined in Table 5.4-1, which also provides the nomenclature used to identify the runs in the figures presented below. Cavity radius was chosen as the primary basis for evaluation because it is directly related to tensile failure and fluidization. Pore pressure and radial stress profiles are also compared because they are the primary numerical solution variables.

Table 5.4-1. Spherical Geometry Run Descriptions

Case	Description
BC1	Base Case, Δr=0.002 m out to R1=0.2 m; then grow at 1.01; L_t = 0.02 m, Wellbore Δz=1 m
DR2	Base Case 1 with twice Δr, 0.004 m
DRH	Base Case 1 with one-half Δr, 0.001m
LT2	Base Case 1 with twice L_t, 0.04 m
LT4	Base Case 1 with four times L_t, 0.08 m
LTH	Base Case 1 with one-half L_t, 0.01 m
DZ2	Base Case with twice the wellbore zone size, Δz, 2.0 m

5.5 Results

5.5.1 Cavity Radius History with Zone Size

Cavity radius provides the most global measure of zone size convergence because it is the final result from tensile failure and fluidization of the waste. Cavity radius (CAVRAD) histories are shown in Figure 5.5-1 and Figure 5.5-2 for the spherical geometry. The drill radius history is included as a reference curve. Drilling is identical regardless of material failure and thus provides a baseline minimum radius for comparison to cavity radius. Any difference between a test case cavity history and the drill history (CAVRAD > DRILLRAD) is due to tensile failure and fluidization and will be referred to as the spall radius.

The effect of variations in repository zone size, Δr, is demonstrated in Figure 5.5-1, which compares cavity radius at double (Δr = 0.004m)(DR2) and half (Δr = 0.001m)(DRH) the base case zone size (Δr = 0.002m)(BC1). The drillbit penetrates the repository at about 35

seconds. Cavity growth due to spallings starts at around 150 seconds, with drilling completed by 350 seconds. The data for the three zone size cases overlay quite closely. Final cavity radius values and equivalent spall volumes are given in Table 5.5-1. The zone sizes chosen for this study do not impact the growth of the cavity or the final cavity radius in a significant manner. Spall volumes compare reasonably well considering that failure and fluidization are discreet rather than continuous phenomena that occur over increments of the zone size and can be switched on or off with only minute changes in critical values relative to cutoff values. The effect of zone size on more continuous results such as pore pressure and effective stresses are demonstrated in Section 5.5.3.

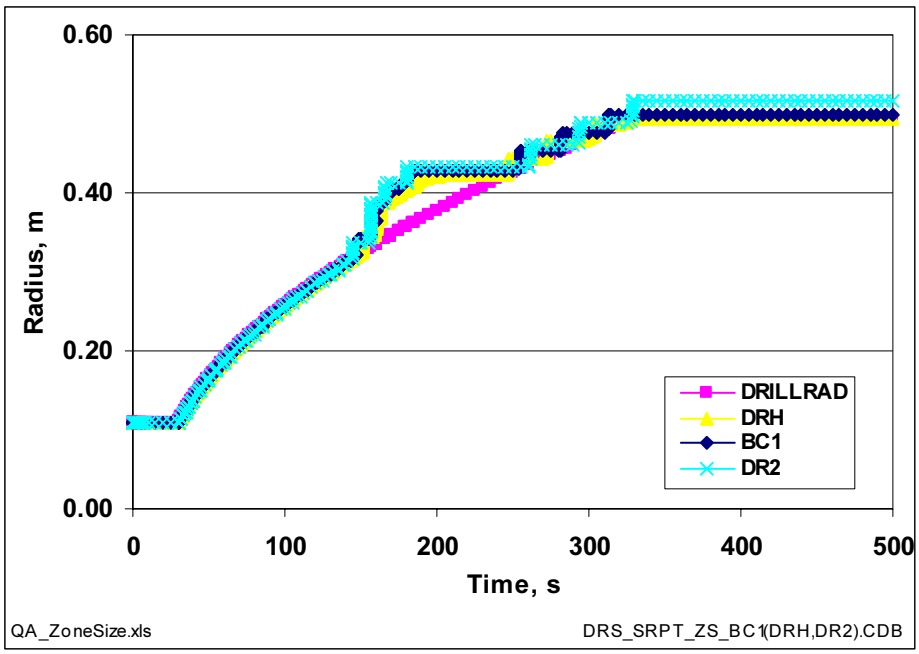

Figure 5.5-1. Cavity Radius History for Three Repository Zone Sizes in Spherical Geometry.

Table 5.5-1. Final Cavity Radius in Spherical Geometry.

Case	Final radius (m)	Spall Volume (m^3)
BC1	0.500	0.483
DR2	0.516	0.544
DRH	0.494	0.420
Drilled	0.494	0.0

5.5.2 Cavity Radius History with Characteristic Length

The effect of characteristic tensile failure length, L_t, on cavity radius is illustrated in Figure 5.5-1 for spherical geometry, which compares cavity radius histories using double (LT2), quadruple (LT4) and one-half (LTH) the base case characteristic length (L_t = 0.02m). . Drilling occurs through the same time frame as in Figure 5.5-1. Note that the discrete failure lengths can be seen for the BC1 and LT2 cases by examining the size of the incremental jumps in cavity radius between 250 and 320 s. For example, the jumps for LT2 are roughly twice as large as those for BC1. Between 150 and 200s for case BC1 and LTH cavity radius is increasing without visible delay between incremental jumps. But in spite of this difference, L_t variations do not have a significant impact on the final cavity radius. However, there was no tensile failure with for LT4 (L_t =0.08m) indicating that this characteristic failure length was much larger than the tensile pulse width and it therefore masked failure.

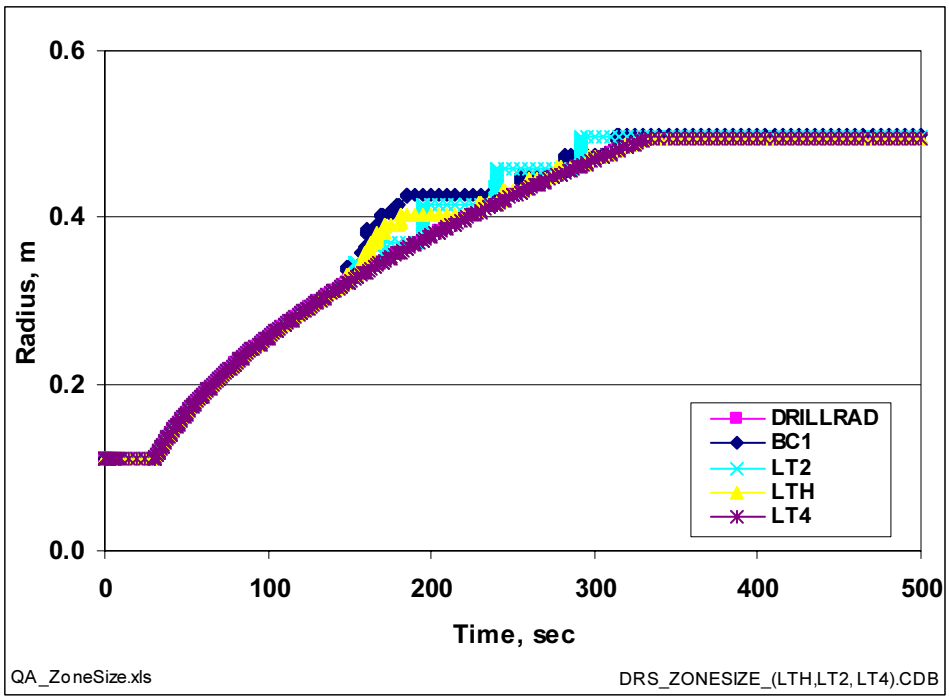

Figure 5.5-2. Cavity Radius History for Four Characteristic Length Variations in Spherical Geometry.

5.5.3 Pore Pressure and Radial Stress Profiles with Failure Suppressed

Failure and fluidization, represented collectively by the cavity radius, are actually evaluated by post processing the solutions for porous flow and the mechanical stress state at each timestep. A more detailed measure of solution convergence with decreasing zone size is the comparison of radial profiles for the primary solution variables (pressure and stress). However, profiles prior to failure do not show the fully developed tensile phases, and are difficult to interpret once failure has started, because failure occurs over different shell sizes and with different cavity radii.

To facilitate comparison of the profiles, a new set of calculations were run using the same problem setup discussed above but with a large tensile strength to preclude tensile failure and spall. This approach allows comparisons of pore pressure and stress across all zone sizes with almost identical boundary conditions for the well bottomhole pressure and the cavity radius. These results, presented in Figure 5.5-3 for the spherical geometry, show pore pressure and radial stress profiles in the repository at 160 seconds, soon after failure would have occurred. At this time the tensile region of the radial effective stress near the cavity interface is fairly well developed. These comparisons show essentially identical results for all zone sizes. The bottom figure in Figure 5.5-3 has zoomed in on the tensile region and shows essentially the same profiles with decreasing zone size, implying convergence for the radial effective stress, which is a numerically sensitive parameter. The slight shift in the tensile pulse for DR2 is due to the discrete mechanism used to remove cells from the repository domain as the drillbit penetrates the repository - a cell is removed when the equivalent 1-D drill radius exceeds a cell's far boundary radius. Smaller cells are therefore removed more rapidly.

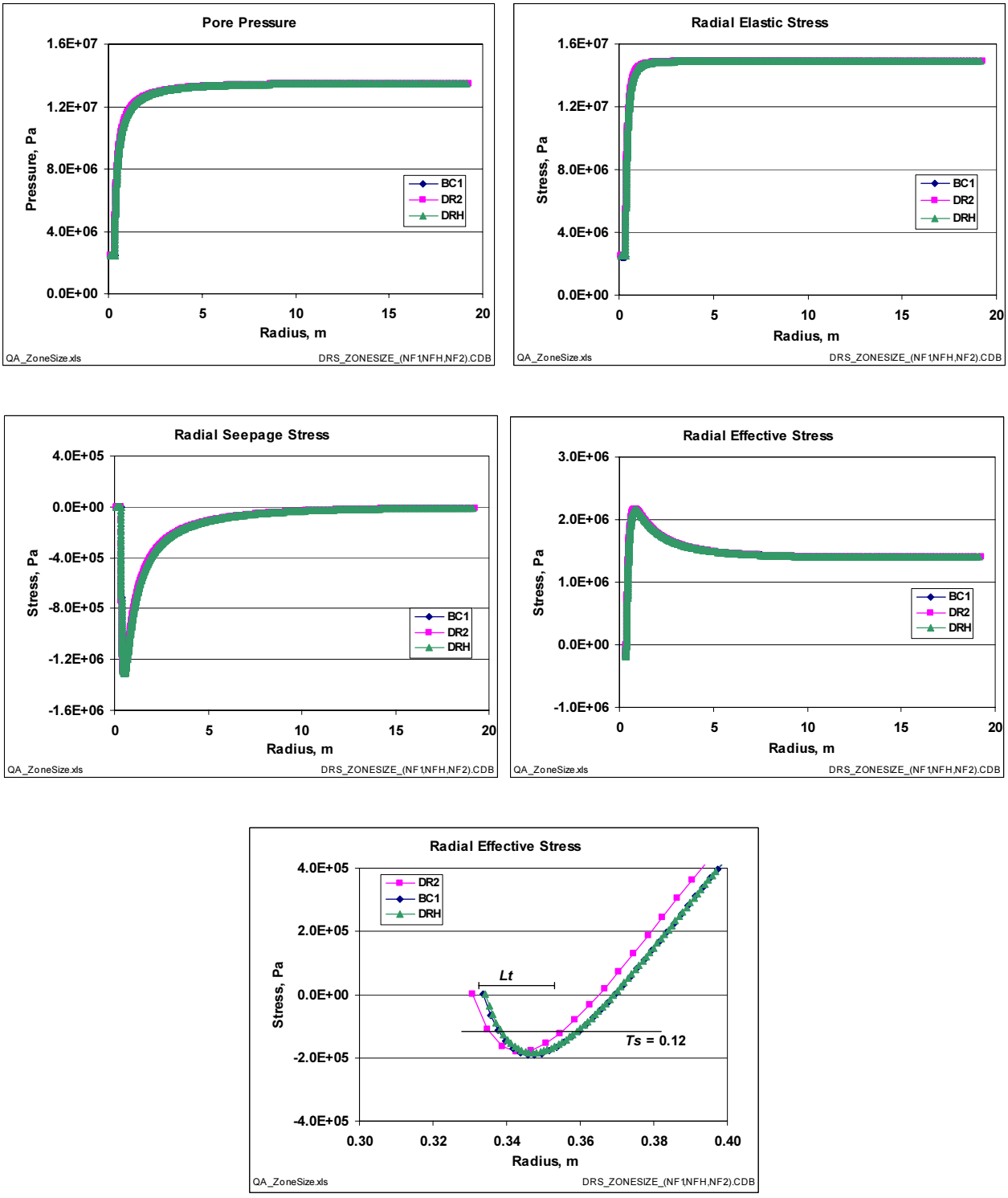

Figure 5.5-3. Pore Pressure and Radial Stress Profiles at 160 Seconds With No Failure, Spherical Geometry.

While the data in Figure 5.5-3 show that the stress and pressure profiles are essentially the same for all zone sizes studied, this is only at one time, 160 seconds, in simulations that encompass several hundred seconds. To examine the evolution of the radial effective stress profiles, data for the three zone sizes DR2, BC1, and DRH are plotted every 20 seconds from 100 to 400 seconds in Figure 5.5-4. Thus, proceeding from left to right, along the "Radius" axis, the first set of three stress curves is taken at 100 sec, while the next set is taken at 120 sec, etc. out to 400 sec. The curves shift to the right along the radial axis because the cavity expands due to drilling. Note that the last several curves on the right end overlay because drilling stopped and cavity expansion stops at 0.49 m. Also displayed is the tensile strength T_s = 0.12 MPa used to generate the cavity radius histories in Figure 5.5-1 and Figure 5.5-2. The profiles at 160 seconds for all cases exceed the tensile strength indicating that failure should be initiated between 140 and 160 seconds. Examination of the cavity radius plots in Figure 5.5-1 confirms that this is so. After 160 seconds, the evolution of cavity sizes in Figure 5.5-4 does not coincide with those given in Figure 5.5-1 because failure is suppressed in Figure 5.5-4. What is clear, however, is that the stress profile in Figure 5.5-4 has stabilized after 300 seconds for all cases, that further failure is not expected, and that the profiles may be considered converged for the given zone sizes.

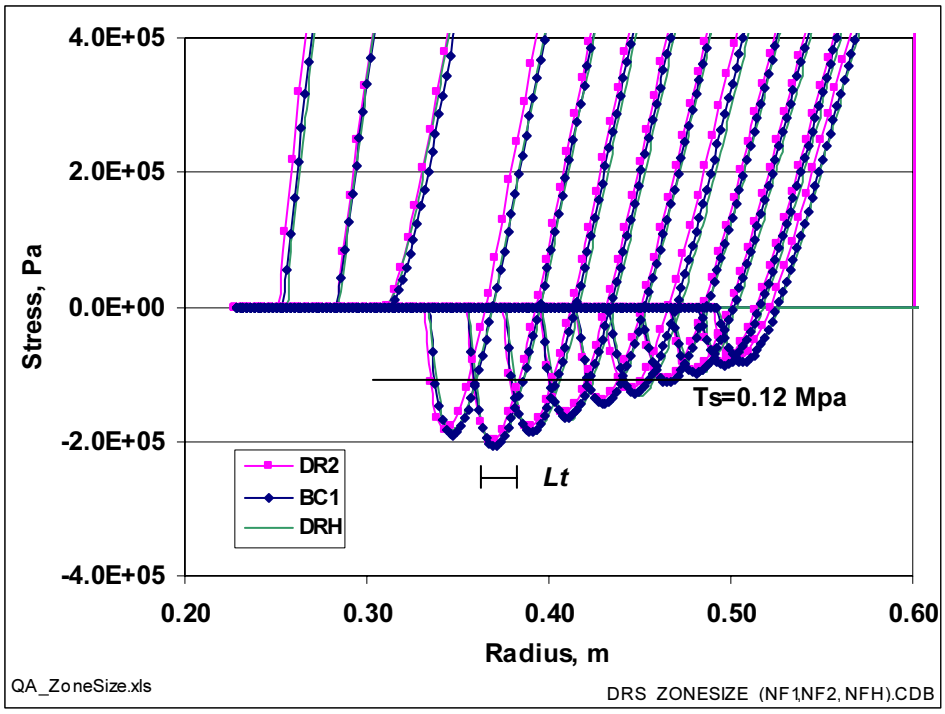

Note: Spherical geometry is shown.

Figure 5.5-4. Radial Effective Stress Profiles for the Three Zone Sizes Shown as They Evolve Though Time Every 20 Seconds from 100 to 400 Seconds.

Cylindrical Geometry. The calculations that precluded failure were repeated in cylindrical geometry using the same three zone sizes (BC1, DRH and DR2). Results are summarized with the radial effective stress profiles at 100 to 400 by 20 second

increments in Figure 5.5-5. The results essentially overlay with only a very slight shift in radius for case DR2 at a few of the plot times because of the discrete way cavity radius increases during drilling. Removal of the larger DR2 zone size is a slightly delayed resulting in a slightly smaller cavity radius. A tensile region never develops at any time in the cylindrical geometry, so that failure and spalling never occur.

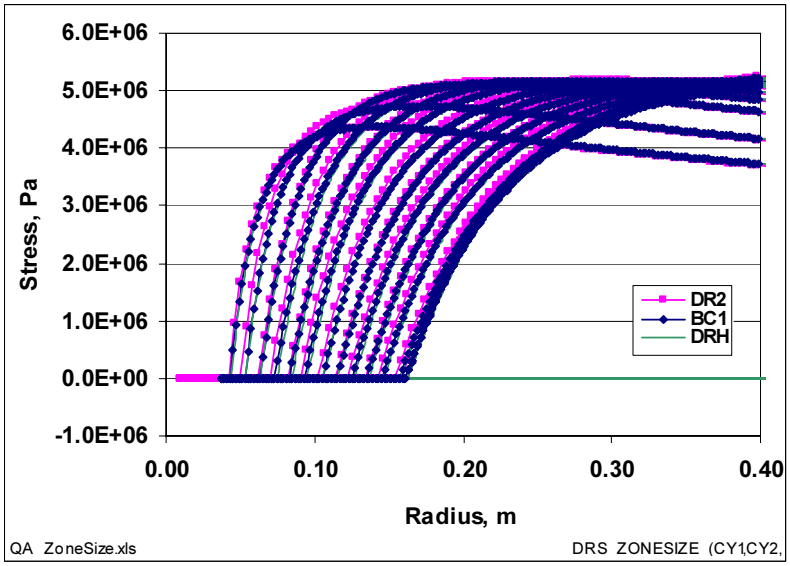

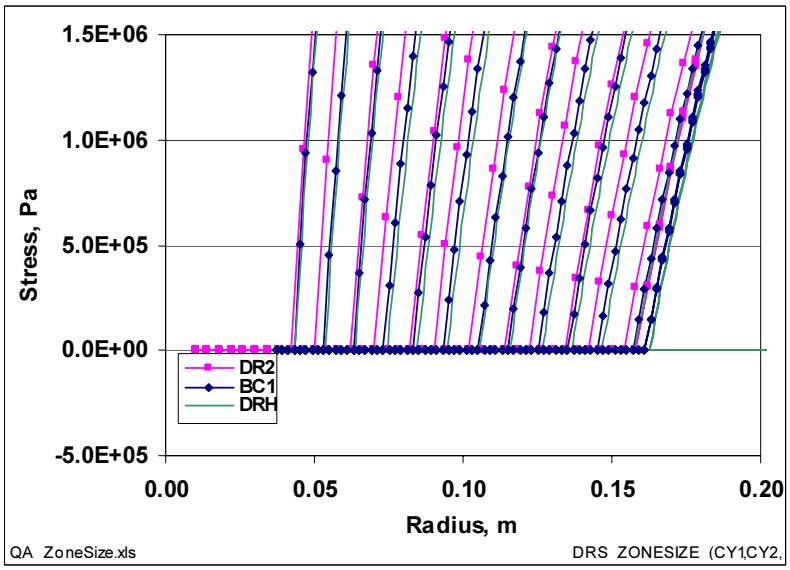

Note: The lower figure shows the same data, but zoomed in for more detail near the cavity wall. Cylindrical geometry Is shown.

Figure 5.5-5. Radial Effective Stress Profiles for the Three Zone Sizes Shown as They Evolve Though Time Every 20 Seconds from 100 to 400 Seconds.

5.6 Wellbore Zone Size

The bottomhole pressure (BOTPRS), which results from the distribution of mud, waste and gas over the full length of the wellbore, provides a boundary condition for repository gas flow and waste solid stress calculations. The pressure difference between the repository and the wellbore drives gas flow in the pore space of the repository waste and can lead to waste failure and spall through the development of tensile effective stress. Therefore, sensitivity of BOTPRS to wellbore zone size (Δz) could have a significant impact on the overall sensitivity of DRSPALL. The effect of wellbore zone size is shown in Figure 5.6-1 where BOTPRS is compared for zone sizes of 1 and 2 m. BOTPRS shows reasonable convergence for these zone sizes with only slight timing differences of the pressure spikes around 150 to 180 sec when failed waste is released into the wellbore flow.

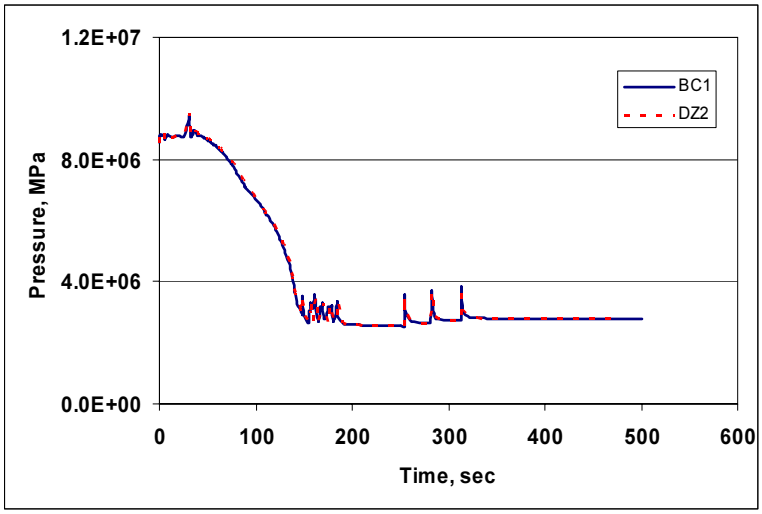

Figure 5.6-1. Bottomhole Pressure (BOTPRS) History for Two Wellbore Zone Sizes.

5.7 Summary

Zone size studies are used to determine that the zone size being used for calculations is small enough to reasonably capture a solution. The cavity radii in DRSPALL showed excellent convergence with zone size refinement over the range investigated, while the primary solution variables of pore pressure and solid stress also showed convergence as zone size is reduced over the same range (Figure 5.5-3). This provides confidence that the repository zone sizes of 0.001 to 0.004 m would be appropriate for the calculations reported herein.

The characteristic length variations showed similar behavior except for the largest value (L_t= 0.08 m) that resulted in no tensile failure. Recall that tensile failure is evaluated using the average tensile stress over the characteristic length. As the characteristic length increases and approaches the width of tensile region in the radial effective stress, failure becomes less likely because the average stress will become less tensile. Decreasing the characteristic

length could also reduce the likelihood of tensile failure as it approaches the zone size of the cell nearest the boundary (radial effective stress is zero at the wellbore interface).

Also, the criteria has been established for DRSPALL that the zone size should be less than 1/5 the characteristic length over the region where failure might occur. In other words, there should be 5 or more zones per characteristic length. This study used a range of 5 to 20 zones per characteristic length. The results indicate that a minimum of 5 zones over characteristic length of 0.02 m would be reasonable. The 0.02 m value seemed to best capture the tensile pulse width.

Based on the data presented in this zone size study, the following ranges are likely to give very similar and reasonably accurate results:

- Repository zone size $\Delta r = 0.001 – 0.004$m
- Characteristic length $L_t = 0.02$ m with 5-10 zones per characteristic length
- Wellbore zone size, $\Delta z = 1$-2 m

The parameters for the DR2 and DZ2 calculations ($\Delta r = 0.004$m, $\Delta z = 2.0$m and $L_t = 0.02$m) have been selected as the standard configuration for DRSPALL calculations. These values shown a significant gain in efficiency (a factor of 4 reduction in run time) over the base case values without sacrificing accuracy.

6 Code Verification and Validation

This chapter describes the verification and validation testing of the DRSPALL code. The test methodology is governed by Nuclear Waste Management Program Procedure NP19-1 Software Requirements (Chavez, 2003), implemented for all WIPP PA codes used in compliance calculations. The NP 19-1 procedure was developed by SNL to implement the regulatory software quality assurance requirements contained in 40 CF194.22 (EPA, 1996) and NQA-2a-1990 addenda, Part2.7 (ASME 1990).

The testing is described in greater detail in the DRSPALL VVP/VD (WIPP PA, 2003g). Consult the VVP/VD to see listings of most input and output files.

Three test cases were used to verify selected DRSPALL functionality, and a fourth test case was designed to validate DRSPALL against observations from a field analog. The four test cases are summarized below and are presented in detail in following subsections:

- Porous flow – the transient, porous flow of gas through the repository waste material is verified, uncoupled from the wellbore flow model, with comparisons to a semi-analytical model developed by Djordjevic and Adams (2003).

- Wellbore flow –the flow of a multicomponent fluid in the wellbore is verified, uncoupled from the repository model, with comparisons against an independent computational fluid dynamics model, FLUENT (*FLUENT 6.1 User's Guide*, 2003). Results from six calculations with different combinations of fluid constituents (mud, gas, solid) are compared.

- Internal Logic checks – the following submodels are verified by spreadsheet calculations and visual examination of special detailed output files created during execution of this test case:

    - Coupling of wellbore and repository flow
    - Tensile failure
    - Fluidized bed transport of disaggregated waste
    - Expulsion of disaggregated waste at the ground surface

- Coalbed methane validation – This test case examines the suitability of DRSPALL to simulate coalbed cavitation, an analog to the WIPP spallings scenario. DRSPALL is run with input parameters derived from a field-scale coalbed cavitation experiment by Khodaverdian et al. (1996), and measured results are compared to the DRSPALL output.

6.1 Porous Flow Verification

6.1.1 Test Objective

The purpose of this test case is to determine whether DRSPALL can accurately calculate transient gas pressures in the repository during the first few seconds after a borehole intrusion. The porous flow test problem is implemented by comparing pressure profiles in cylindrical and spherical coordinates generated by DRSPALL to those calculated using the utility code developed by Djordjevic and Adams (2003) for an identical problem.

This test case was referred to as "Test Case #1" in the DRSPALL VVP/VD (WIPP PA, 2003g).

6.1.2 Problem Description

This test case involves solving the equations of transient, radial, isothermal, compressible gas flow through a porous medium. In this test case, no failure of the medium or transport of solids is allowed. Furthermore, the coupling of mass flow between the wellbore and repository is simplified to a zero pressure boundary condition. As such, the wellbore calculations in DRSPALL are ignored. The problem is solved in both cylindrical and spherical geometry.

6.1.2.1 Cylindrical Geometry Equations

The cylindrical domain comprises a porous solid with a given porosity φ and permeability k, shown in Figure 6.1-1. There is a cylindrical cavity of radius r_o aligned with the axis that represents a borehole that depressurizes the simulated repository. The domain begins filled with an ideal gas at an initial pressure of P_1 with viscosity η. At $t > 0$, the gas pressure p inside the borehole is set to zero, thus creating a pressure step that diffuses radially outward through the domain.

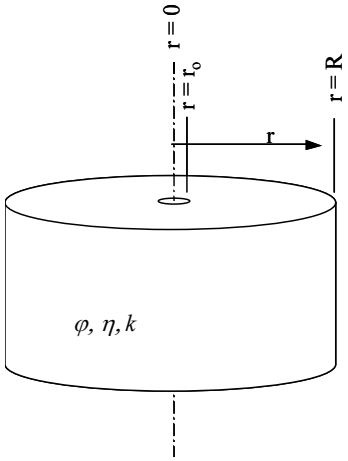

Figure 6.1-1. Schematic of Cylindrical Domain for Porous Flow Test Problem.

Starting with the governing equation for flow of gas through a porous material in a radially symmetric system gives:

$$\frac{\partial p}{\partial t} = \frac{k}{2\varphi\eta}\nabla^2 p^2, \quad p = p(r,t), \quad r \geq r_{0,} \quad t \geq 0 \tag{6.1.1}$$

where p is the gas pressure in the porous medium at radius r and time t. The boundary and initial conditions are expressed as:

$$p(r_0,t) = f(t), \quad \lim_{r\to\infty} p(r,t) = p_{ff}, \quad p(r,0) = p_{ff} \tag{6.1.2}$$

where p_{ff} is the far-field pressure at large r. For this problem, the pressure at the inner boundary r_o representing the wellbore wall is held constant at zero. As such, $f(t) = 0$ for $t > 0$.

A pseudopressure approach is introduced after Chan et al. (1993) utilizing the following change of variables:

$$\psi(p) = \frac{p^2}{\eta} \tag{6.1.3}$$

which leads to

$$\frac{\partial \psi}{\partial t} = \frac{k}{\varphi\sqrt{\eta}}\sqrt{\psi}\nabla^2\psi, \quad \psi = \psi(r,t), \quad r \geq r_{0,} \quad t \geq 0 \tag{6.1.4}$$

and

$$\psi(r_0,t) = \frac{f^2}{\eta}, \quad \lim_{r\to\infty}\psi(r,t) = \frac{p_{ff}^2}{\eta}, \quad \psi(r,0) = \frac{p_{ff}^2}{\eta} \tag{6.1.5}$$

Nondimensional parameters may be defined as follows:

$$\psi = \frac{p_{ff}^2}{\eta}\Psi \quad t = t_0\tau, \quad t_0 = \frac{\varphi\eta r_0^2}{k p_{ff}} \tag{6.1.6}$$

and for cylindrical coordinates:

$$z = \ln(\frac{r}{r_0}) \tag{6.1.7}$$

which upon substitution into Eq. (6.1.4) yields the transformed equation:

$$\frac{\partial \Psi}{\partial \tau} = e^{-2z} \Psi^{1/2} \frac{\partial^2 \Psi}{\partial z^2} \tag{6.1.8}$$

Eq. (6.1.8) is integrated numerically with the boundary and initial conditions

$$\Psi(0,\tau) = \frac{f^2}{p_{ff}^2}, \quad \lim_{z\to\infty} \Psi(z,\tau) \to 1, \quad \Psi(z,0) = 1 \tag{6.1.9}$$

6.1.2.2 Spherical Geometry Equations

For the spherical problem, the cavity is hemispherical in shape with radius r_o as depicted in Figure 6.1-2.

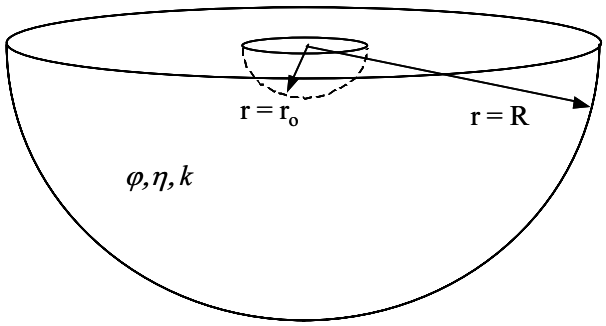

Figure 6.1-2. Schematic of Spherical Domain in Porous Flow Test Problem.

Eqs. (6.1.4) – (6.1.6) apply to the spherical geometry, but in order to proceed, z must be re-defined as:

$$z = \frac{r_o}{r} \tag{6.1.10}$$

The resulting transformed governing equation is then

$$\frac{\partial \Psi}{\partial \tau} = z^4 \Psi^{1/2} \frac{\partial^2 \Psi}{\partial z^2} \tag{6.1.11}$$

Eq. (6.1.11) is integrated numerically with the boundary conditions

$$\Psi(1,\tau) = \frac{f^2}{p_{ff}^2}, \quad \Psi(0,\tau) = 1, \quad \Psi(z,0) = 1 \tag{6.1.12}$$

6.1.2.3 Boundary Conditions

The Djordjevic and Adams (2003) solution, modeled after Chan et al. (1993), requires that (1) the gas pressure at $r = r_o$, the face of the borehole, is set to zero at all times, and (2) pressure in the far field, where $r >> r_o$, remains at the initial pressure, P_1. During normal execution of DRSPALL, the pressure at the inner boundary r_o is calculated by coupling mass flows from the repository and wellbore. However, for purposes of this test case, the cavity pressure variable is assigned a value of zero during each computational loop. This will cause the cavity mass to artificially increase but will not cause inaccuracy in the validation procedure since the cavity mass is irrelevant in this test case.

At the outer boundary ($r = R$), DRSPALL uses a no-flow condition. Djordjevic and Adams (2003) and Chan et al. (1993), however, use a constant pressure in the far-field, p_{ff}. This difference will not be recognized by the models for the short execution times used in this test case because the pressure impulse travels at a finite speed away from the borehole, and will not reach the outer boundary in the time specified for this test. This can be confirmed by computing the approximate depth of penetration of a "dividing surface" defined as the point inside which $P(r) < P_1$, and outside which $P(r) = P_1$.

Chan (1993) gives an approximate location of the dividing surface, $R(t)$, for small values of t in the cylindrical domain as follows:

$$\frac{R(t)}{a} = 1 + \sqrt{\frac{t}{t_o}} \tag{6.1.13}$$

The default outer radius in DRSPALL is 19.2m. Recognizing that $t/t_o = \tau$, the expression above evaluates to $R = 0.649$ m when $\tau = 10$ and $a = 0.156$ m. $\tau = 10$ represents the longest scaled time evaluated in this test problem. The dividing surface is therefore clearly interior to the outer boundary for this and shorter times.

Chan gives another expression for the approximate location of the dividing surface at large t:

$$\frac{R(t)}{a} \cong \frac{(t/t_o)^{0.5}}{[\log(t/t_o)]^{0.5}} \tag{6.1.14}$$

If the DRSPALL outer boundary of 19.2 m is substituted into Eq. (6.1.14) for R, and t_o is evaluated with the input values given in Table 6.1-1, the resulting time t that satisfies the expression is $t \approx 2600$ seconds. Thus, for the short times ($t < 4$ sec) examined in this test case, the pressure impulse will not reach the boundary of the domain and the specific boundary conditions are irrelevant.

6.1.2.4 Input Parameters

Relevant input parameters for this test case are given in Table 6.1-1. To avoid tensile failure of the repository material, tensile strength (T_s) is set to a high value of 0.690E+06 Pa (100

psi). The Forchheimer Beta input parameter was set to zero for this test case, resulting in a constant permeability by removing the velocity-dependence.

Table 6.1-1. Input Parameters for Porous Flow Verification.

Symbol	Definition	Units	Value
P_1	Initial gas pressure	Pa	0.145E+08
φ	Porosity	–	0.575
η	Gas viscosity	Pa-s	0.8934E-05
k	Permeability	m^2	2.400E-13
T_s	Tensile strength	Pa	0.690E+06

6.1.2.5 Repository Zoning

The zoning scheme in the repository domain in DRSPALL is set to a constant zone size of 0.002 m from the cavity wall to a radius of 0.50 m, and then increased geometrically using a multiplication factor of 1.01.

6.1.3 Analysis Methods

Chan et al., (1993) present numerical results as the dimensionless pseudo-pressure, Ψ, versus the dimensionless plotting parameter, ζ, for selected values of scaled time, τ. The dimensionless plotting parameter, comparable to a dimensionless radius, is defined as:

$$\text{cylindrical} \qquad \zeta = \frac{\left(e^{z} - 1\right)}{\tau^{1/2}} \tag{6.1.15}$$

$$\text{spherical} \qquad \zeta = \frac{\left(1/z - 1\right)}{\tau^{1/2}}$$

This analysis entails comparing DRSPALL and Djordjevic and Adams (2003) pseudopressure profiles at designated scaled times. DRSPALL output in the form *P(r, t)* are thus converted to $\Psi(\zeta,\tau)$ at the four scaled times 0.01, 0.1, 1.0, and 10. Output from DRSPALL and Djordjevic and Adams (2003) are displayed graphically.

6.1.3.1 Cylindrical Case Output from Djordjevic and Adams

The cylindrical case solutions were obtained using the independent utility code developed by Djordjevic and Adams (2003). Dimensionless pseudo-pressure profiles were produced at four dimensionless times, τ = 0.01, 0.1, 1.0, 10. The solutions are illustrated graphically in Figure 6.1-3. Tabular results are given in the DRSPALL VVP/VD (WIPP PA, 2003g).

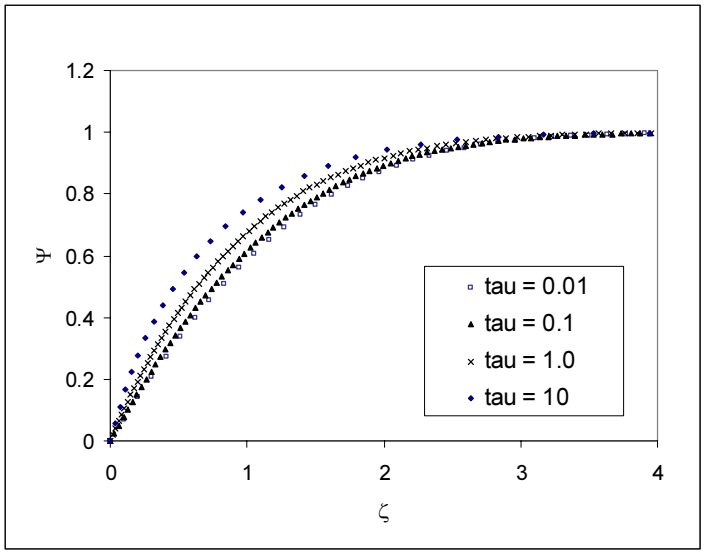

Figure 6.1-3. Numerical Solutions to the Dimensionless Pseudo-Pressure Profiles for Cylindrical Geometry.

Since the numerical grid used in DRSPALL may be different from that used in the comparison solutions shown in Figure 6.1-3, a curve was fit to the comparison data to facilitate visual inspection of the overlay of results. The general form of the function fit to the comparison data was:

$$\Psi(\zeta) = 1\text{-}\exp\{-(C_1\zeta+C_2\zeta^2+C_3\zeta^3)\} \qquad \text{for } 0 \le \zeta \le 1 \tag{6.1.16}$$

where C_1, C_2, and C_3 are constants determined by minimizing the sum of squares:

$$SUM = \sum_i \left[\Psi(\zeta)_a - \Psi(\zeta)_b\right]^2 \tag{6.1.17}$$

where the subscript *a* denotes the solution calculated by Djordjevic and Adams (2003), the subscript *b* denotes the value of the functional fit, and the sum is taken over all the reported grid indices *i*. The constants calculated for the four dimensionless times in the cylindrical geometry are given in Table 6.1-2. Details of the fitting procedure are provided in the DRSPALL VVP/VD (WIPP PA, 2003g).

Table 6.1-2. Constants for Functional Fit to Djordjevic and Adams Solution in Cylindrical Geometry.

τ	C_1	C_2	C_3
0.01	0.715	0.167	0.0
0.1	0.803	0.157	0.0
1.0	1.032	0.101	0.0
10.0	1.505	-0.017	0.0

6.1.3.2 Spherical Case Output from Djordjevic and Adams

The spherical case solutions were obtained using an independent utility code developed by Djordjevic and Adams (2003). Dimensionless pseudo-pressure profiles were produced at the same four dimensionless times (τ = 0.01, 0.1, 1.0, 10) as for the cylindrical case. The solutions are illustrated graphically in Figure 6.1-4. Tabular results are given in the DRSPALL VVP/VD (WIPP PA, 2003g). Functions in the form of Eq. (6.1.17) were fit to the data using a least squares method with associated constants reported in Table 6.1-3, and details of the fitting procedure are provided in the DRSPALL VVP/VD (WIPP PA, 2003g).

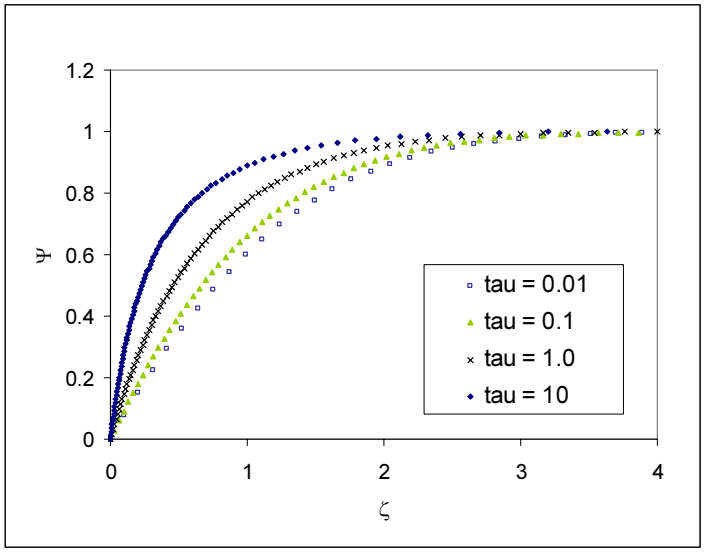

Figure 6.1-4. Numerical Solutions to the Dimensionless Pseudo-Pressure Profiles for Spherical Geometry.

Table 6.1-3. Constants for Functional Fit to Djordjevic and Adams Solution in Spherical Geometry.

τ	C_1	C_2	C_3
0.01	1.331	-0.073	0.000
0.10	1.000	0.126	0.000
1.0	1.537	-0.033	0.000
10.0	3.500	-2.229	0.858

6.1.4 Results

6.1.4.1 Cylindrical Geometry

Figure 6.1-5 and Figure 6.1-6 show the results of this test case in cylindrical geometry. The DRSPALL results are written to text file that is output for validation purposes for this test

case only. The output file is imported into a Microsoft EXCEL spreadsheet for post-processing and graphing. The plots display the dimensionless pseudo-pressure (Ψ) versus the dimensionless plotting parameter (ζ) at four selected values of dimensionless time (τ). The comparison curves on each figure were generated from the parameters in Table 6.1-2. Conceptually, the curves represent the evolution of the pore pressure profile. The initial condition is set to $\Psi = 1$ throughout the domain. For $\tau > 0$, Ψ at the inner boundary of the domain, $\zeta = 0$, is set to zero representing zero pressure in the wellbore. The outer boundary Ψ is held at unity representing a constant far-field pressure. The tendency of the curves at different τ to nearly overlay one another is related, in part, to the presence of the $t^{-0.5}$ in the plotting parameter function (Eq. (6.1.15)). For each set of axes, the results for two dimensionless times are given. Visual inspection of Figure 6.1-5 and Figure 6.1-6 indicates that the DRSPALL results overlay the Djordjevic and Adams (2003) solutions quite closely. The magnitude and shape of the curves match well over the entire range of interest. A simple statistical comparison between solution methods is also given in WIPP PA (2003g).

6.1.4.2 Spherical Geometry

Figure 6.1-7 and Figure 6.1-8 show the results of this test case for implicit solution in the spherical geometry. A close match to the comparison solution is observed for all times, as indicated visually in Figure 6.1-7 and Figure 6.1-8.

6.1.5 Conclusions

The Porous Flow Verification demonstrates that the DRSPALL solutions to transient, compressible, ideal gas flow compare favorably to those generated by an independent utility code developed by Djordjevic and Adams (2003). Both codes utilize an implicit solution algorithm to solve an initial boundary value problem that represents the evolution of pore pressure and resulting blowdown in a simplified gas repository following intrusion by an underbalanced (low-pressure) borehole.

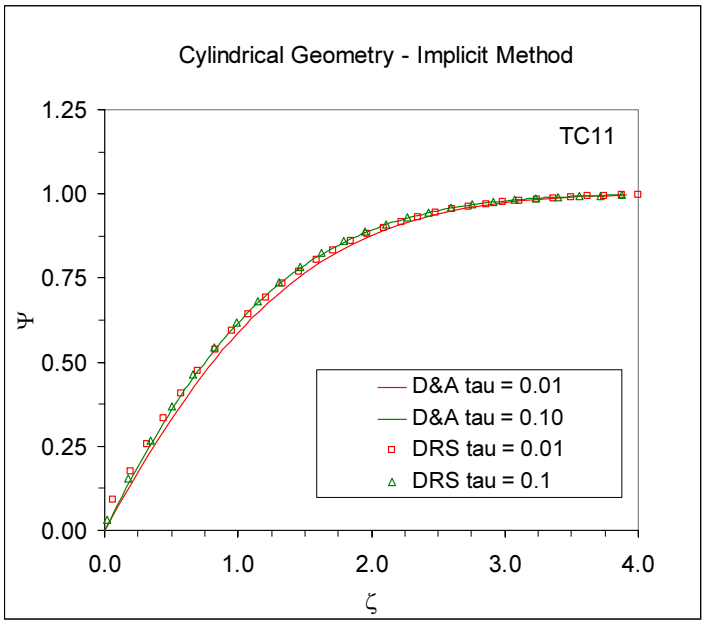

Figure 6.1-5. Overlay of DRSPALL with Djordjevic and Adams Solutions for the Cylindrical Geometry With τ = 0.01, 0.10.

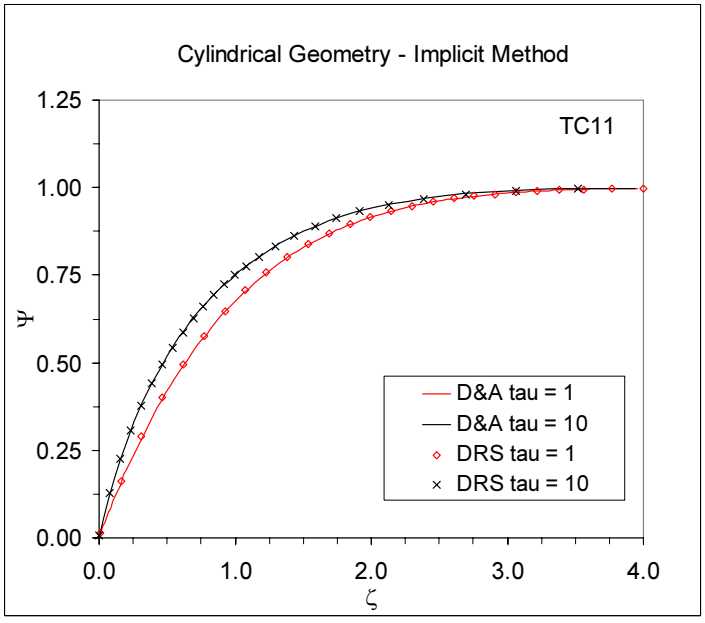

Figure 6.1-6. Overlay of DRSPALL with Djordjevic and Adams Solutions for the Cylindrical Geometry with τ = 1.0, 10.

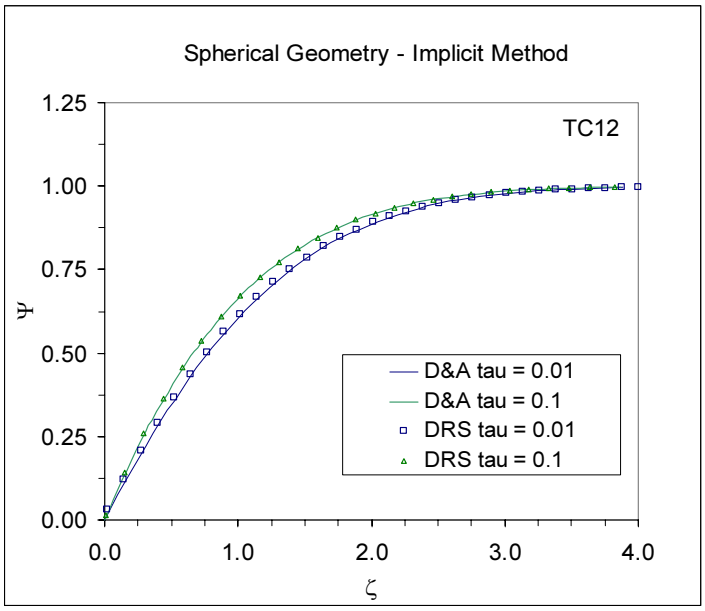

Figure 6.1-7. Overlay of DRSPALL with Djordjevic and Adams Solutions for the Spherical Geometry with τ = 0.01, 0.10.

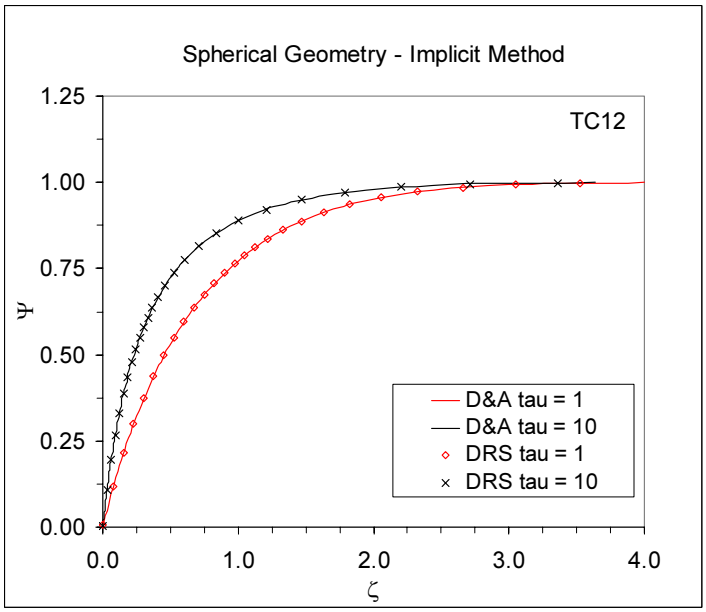

Figure 6.1-8. Overlay of DRSPALL with Djordjevic and Adams Solutions for the Spherical Geometry with τ = 1.0, 10.

6.2 Wellbore Flow Verification

6.2.1 Test Objective

The objective of this test case is to verify the wellbore flow model against an independent computational fluid dynamics model FLUENT.

This test case was referred to as "Test Case #5" in the DRSPALL VVP/VD (WIPP PA, 2003g).

6.2.2 Problem Description

This test case focuses on the wellbore model, and thus decouples its behavior from the repository. Known boundary conditions are imposed to observe the model's response to steady flow of:

1. mud
2. mud and gas
3. mud and gas and solids

Independent calculations are run in parallel with the commercial computational fluid dynamics code FLUENT (FLUENT 6.1 User's Guide, 2003).

The problem domain is the wellbore annulus in a typical WIPP intrusion. The geometric description of the wellbore is adapted from the DRSPALL Parameter Justification Report (Hansen et al., 2003). Typical WIPP values are used for most DRSPALL parameters (WIPP PA 2000g). A schematic of the domain is shown in Figure 6.2-1.

6.2.2.1 Boundary Conditions

Boundary conditions are set to simulate a WIPP intrusion scenario, however the bottom of the wellbore is decoupled from the repository and controlled directly to facilitate comparison between DRSPALL and the FLUENT code. The inlet boundary to the wellbore annulus is a constant volumetric flow rate. The outlet boundary to the wellbore annulus is constant at atmospheric pressure, 0.1 MPa. Gas and solids are added at pre-determined mass flow rates at the lower boundary to the annulus.

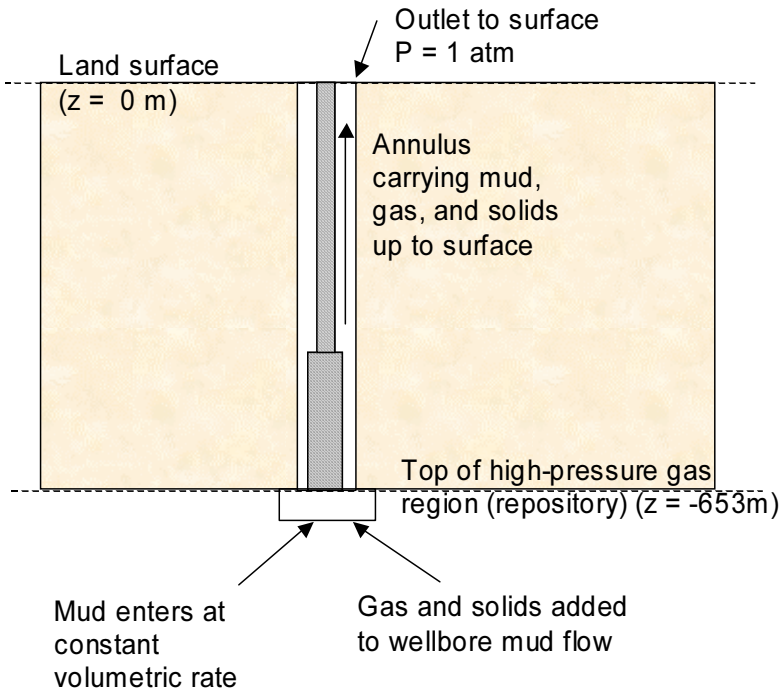

Figure 6.2-1. Schematic of Wellbore Flow Test Problem Domain.

6.2.2.2 Input Parameters

Input parameters for the wellbore domain represent a typical WIPP intrusion. Repository flow parameters are irrelevant since the domains are decoupled in this test case. There are several run-specific parameters such as mud density, mud pump rate, and gas/solids loading rate that vary among runs and are discussed below.

6.2.3 Analysis Method

Steady state runs are examined to establish that the steady pressure profiles in the wellbore are matched reasonably between DRSPALL and FLUENT. Three basic types of runs are required:

1. Mud only
2. Mud and gas
3. Mud and gas and solids

For mud only, two mud densities are examined. In addition, a static case is run with no mud pumping to assure that the mud column settles to an equilibrium hydrostatic distribution. For the mud and gas cases, gas input rate is controlled as the independent variable. For the three-phase run, gas and solid loading rates representative of near-steady conditions in a WIPP spallings intrusion are tested.

The run matrix is shown in Figure 6.2-1. Specific test run information is given below.

Table 6.2-1. Run Conditions for FLUENT Comparison

Case	Mud Density, kg/m^3	Mud Flow Rate, m^3/s	Gas Flow Rate, kg/s	Solid Flow Rate, kg/s	Description
5.1	1210	0	0	0	Static mud in wellbore
5.2	1210	0.02018	0	0	Mud-only, steady flow, nominal mud density
5.3	1380	0.02018	0	0	Mud-only, steady flow, high-end mud density
5.4	–	–	–	–	*Not used*
5.5	1210	0.02018	0.25	0	Steady mud flow, gas added to flow at low, constant rate
5.6	1210	0.02018	2.5	0	Steady mud flow, gas added to flow at medium, constant rate
5.7	1210	0.02018	2.5	2.5	Steady mud flow, gas added to flow at medium, constant rate; solids added at low constant rate

6.2.3.1 Case 5.1 – Static Mud in Wellbore

The mud pump is turned off and the pressure distribution is monitored to assure that it settles to a hydrostatic distribution. The boundaries at the pump inlet and annulus outlet are both set to atmospheric pressure. No gas or solids are added to the wellbore domain. Mud density is set to the DRSPALL default value 1210 kg/m^3. DRSPALL is a transient code, and the initial pressure distribution in the wellbore is not hydrostatic. The objective of this seemingly simple test is to see whether DRSPALL will eventually arrive at a stable solution demonstrating the hydrostatic pressure distribution.

6.2.3.2 Case 5.2 – Mud-Only, Steady Flow, Nominal Mud Density

Volumetric mud flow rate at the pump inlet and mud density are set to the DRSPALL default values of 0.02081 m^3/sec and 1210. kg/m^3, respectively. No gas or solids are added.

6.2.3.3 Case 5.3 – Mud-Only, Steady Flow, High-End Mud Density

This test run is the same as Case 5.2, section 6.2.3.2 above, except that the mud density is increased to ρ = 1380 kg/m^3, the highest value in its sampling range recommended in the Parameter Justification Report for DRSPALL (Hansen et al., 2003). The slightly higher density should lead to a proportionally higher pressure at the bottom of the well due to the weight of the mud column.

6.2.3.4 Case 5.5 – Gas Added to Flow at Low Constant Rate

This test run adds hydrogen gas to the flow stream at the bottom of the well. Mudflow rate and physical properties are set to defaults as in Case 5.2. The hydrogen mass flow rate is fixed at 0.25 kg/sec, a value representative of the gas flow rate into the wellbore through the DDZ just prior to bit penetration of the repository.

6.2.3.5 Case 5.6 – Gas Added to Flow at Medium Constant Rate

This test run adds hydrogen gas to the flow stream at the bottom of the well. Mud flow and physical properties are set to defaults as in Case 5.2. The hydrogen mass flow rate = 2.5 kg/sec, a value representative of the gas flow rate into the wellbore during a blowout while the mud column is accelerating.

6.2.3.6 Case 5.7 – Gas Added to Flow at Medium Constant Rate, Solids Added at Low Constant Rate

This test run is the same as Case 5.6, section 6.2.3.5, with gas flowing into the well bottom, except solids are also added. A solids loading rate of 2.5 kg/sec is selected to represent a slow, steady material failure case. In normal model executions where a spalling event occurs, this mass loading rate tends to spike early and diminish to zero. The constant rate was selected here for simplicity in implementation and comparison between models.

6.2.4 Test Procedure

FLUENT runs are executed independently and the data captured in tabular form. FLUENT is a commercial computational fluid dynamics code. FLUENT solves conservation equations for the fluids and solids phases in the pipe using the Navier-Stokes equations assuming no-slip wall boundary conditions. The pressure drop is evaluated from the momentum equation using the calculated velocity profiles and the effective fluid viscosity including turbulence and wall roughness. Friction factors are not employed. For this test problem, FLUENT was set up to apply a uniform velocity to all phases, as in DRSPALL and was run in 2-D cylindrical geometry. Two sections of the computational grid are shown in Figure 6.2-2 and illustrate the level of detail in the FLUENT models. Details of the FLUENT calculations are documented in a memo (Webb, 2003).

DRSPALL is run with the wellbore decoupled from the repository, and the mass loading function specific to the test case is specified internal to the code. DRSPALL is executed once for each of the six cases. Each execution results in output that is used to generate tables and graphs of the pressure, fluid velocities and volume fraction profiles in the wellbore. These data are compared with the corresponding data generated from FLUENT using basic Microsoft EXCEL capabilities.

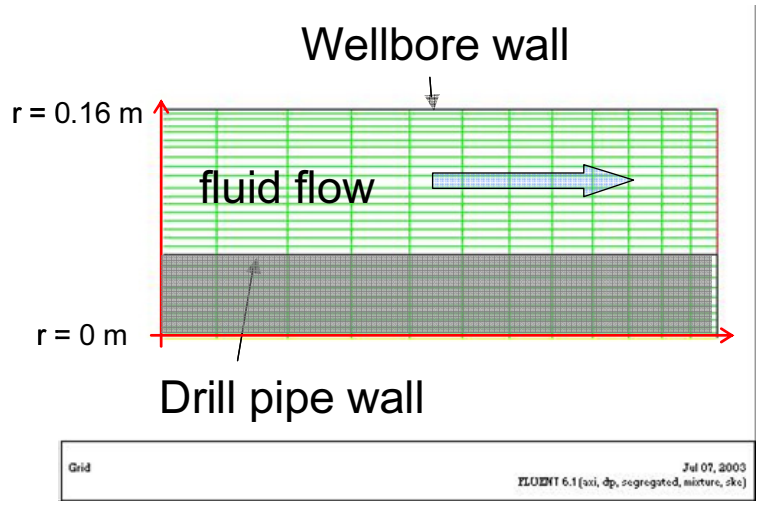

(a) Drill pipe grid section near outlet

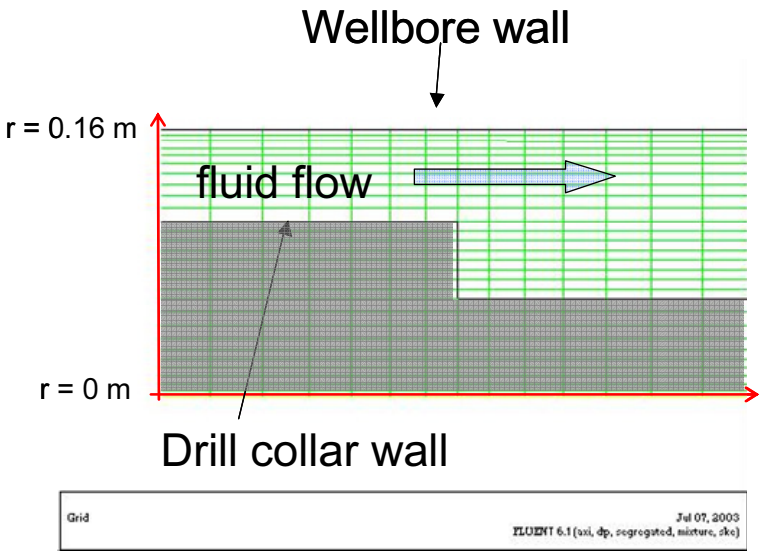

(b) Grid section at collar drill pipe transition

Figure 6.2-2. FLUENT Computational Grid

6.2.5 Results

Results for each case are presented individually in the following subsections. Results consist of graphical comparisons of pressure, fluid velocity and volume fractions as a function of wellbore position. The bottom of the wellbore is located at 0.0 and the land surface is located at 653 m. FLUENT actually solves the steady state problem. DRSPALL solves the transient problem for constant boundary conditions. DRSPALL cases are run until pressure and velocity maintained a relatively constant value; therefore, run time varied for each subcase.

6.2.5.1 Case 5.1 – Static with Nominal Mud Density

Results for Case 5.1 are summarized by the pressure and velocity profile comparisons shown in Figure 6.2-3. DRSPALL results are at 90 s because it takes some time for the code to settle to a steady pressure profile after the arbitrary starting profile. The results visually overlay. A simple hydrostatic model gives the expected bottomhole pressure as ρgh = 7.7 MPa, where ρ = 1210 kg/m^3 is the mud density, g = 9.81 m/s^2, and h = 653 m is the wellbore height. In the code results, the pressure decreases linearly to 0.1 MPa at the land surface. FLUENT calculated a bottomhole pressure value of 7.84 MPa. DRSPALL calculated a value of 7.77 MPa. The velocities for this test case should be zero. But, because DRSPALL uses a transient algorithm, a small residual velocity can be expected. While this test problem may seem trivial, stable behavior of a transient code under steady-state conditions is not guaranteed. Correct and stable solution of this problem lends confidence that the differencing scheme and mass balance are working as designed.

6.2.5.2 Case 5.2 – Steady Flow with Nominal Mud Density

The results for Case 5.2 (mud pumping rate = 0.02018 m^3/s and mud density = 1210 m) are summarized by the pressure and fluid velocity profiles at 90 s shown in Figure 6.2-4. The results from FLUENT and DRSPALL visually overlay. The pressure profiles are similar to Case 5.1, section 6.2.5.1, with only very minor differences due to dynamic effects. The velocity profiles show the effects of the two annulus areas – one for the collar region just above the well bottom and the other for the drill pipe extending to the land surface. Fluid velocities, u_i, can be determined analytically from the pumping rates, R = 0.02018 m^3/s, and the annulus cross sectional areas, A_1 = 0.044 m^2, A_2 = 0.066 m^2, as follows: $u_i = R/A_i$, where, i=1 is the collar region and 2 is the drill pipe region. This gives analytic values for the fluid velocities of 0.46 m/s and 0.31 m/s for the collar and drill pipe regions, respectively.

6.2.5.3 Case 5.3 – Steady Flow with High Mud Density

The results for Case 5.3 (constant mud pumping rate = 0.02018 m^3/s and a high mud density = 1380 kg/m^3) are summarized by the pressure and fluid velocity profiles at 90 s shown in Figure 6.2-5. The results from FLUENT and DRSPALL visually overlay. The pressure profiles are similar to Case 5.2, section 6.2.5.2, except for an increase in bottomhole pressure due the increase in mud density. The estimated value of bottomhole pressure is ρgh = 8.83 MPa, where ρ = 1380 kg/m^3 is the mud density, g = 9.82 m/s^2, and h = 653 m is the wellbore height. The calculated values for bottomhole pressure were 8.84 MPa and 8.95 MPa for FLUENT and DRSPALL, respectively.

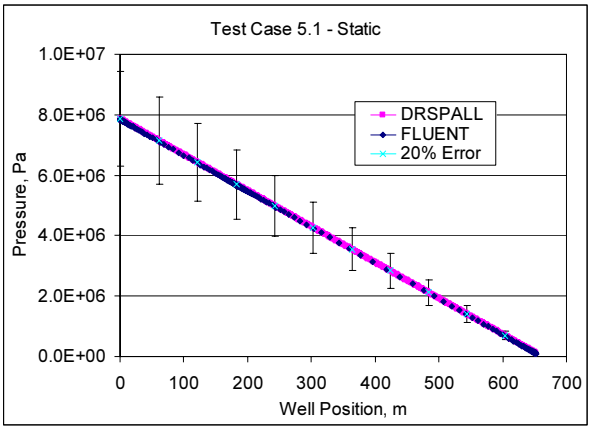

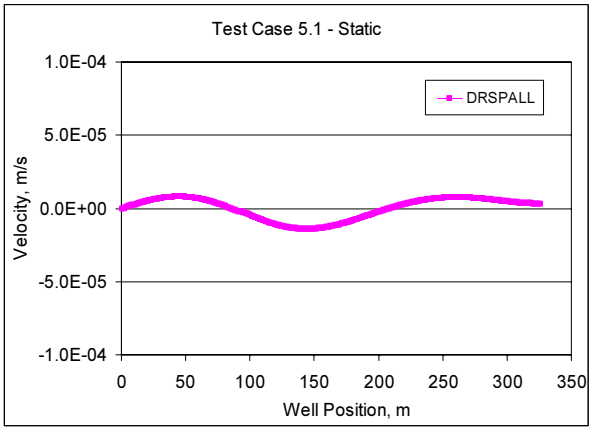

Figure 6.2-3. Pressure and Velocity Profiles for Static Wellbore, Case 5.1

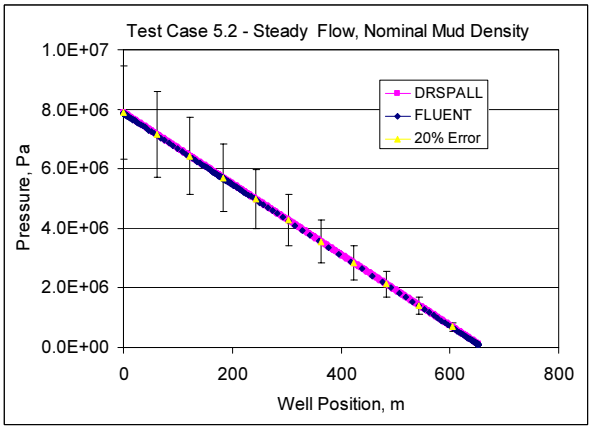

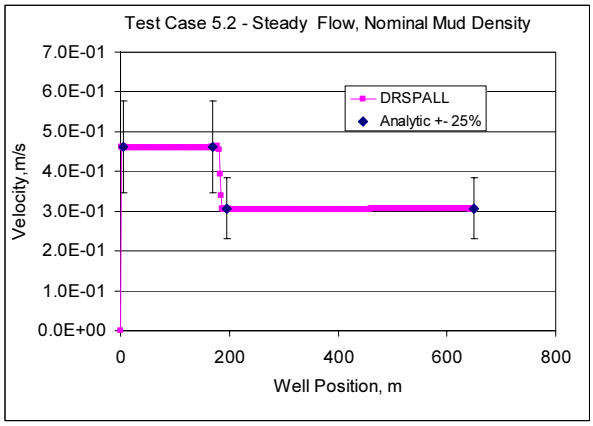

Figure 6.2-4. Pressure and Velocity Profiles for Steady State and Nominal Mud Density, Case 5.2.

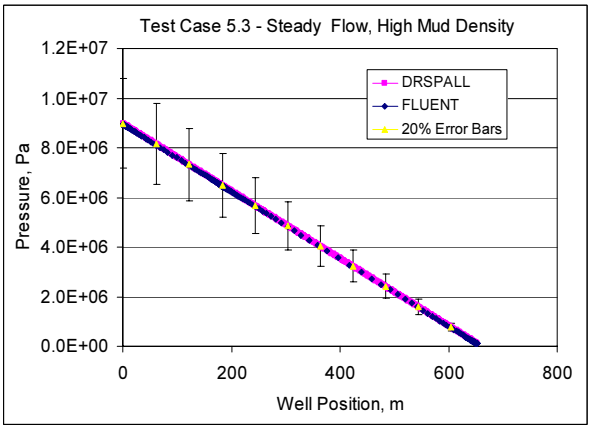

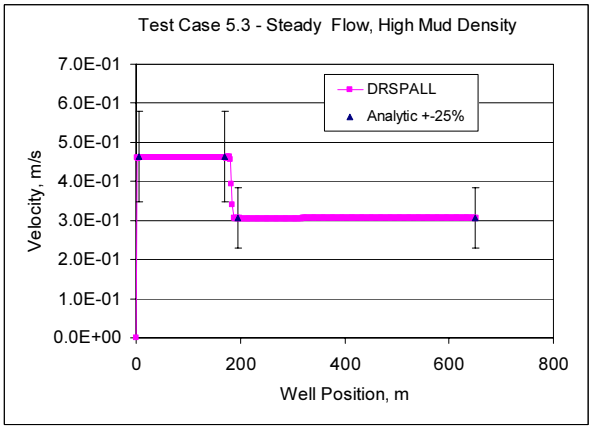

Figure 6.2-5. Pressure and Velocity Profiles for Steady State and High Mud Density, Case 5.3.

The velocity profiles show the effects of the two annulus areas – one for the collar region just above the well bottom and another for the drill pipe extending to the land surface. The expected values of fluid velocities are the same as in Case 5.2.

6.2.5.4 Case 5.5 – Low Gas Injection Rate

The results for Case 5.5 (constant mud pumping rate = 0.02018 m^3/s, mud density = 1210 kg/m^3 and gas injection rate = 0.25 kg/s) are summarized by the pressure, fluid velocity and gas volume fraction profiles at 450 s shown in Figure 6.2-6. The pressure profile results from FLUENT and DRSPALL visually overlay. Note that the bottomhole pressures have dropped from 8 MPa to 0.4 MPa because of the large amount of gas in the wellbore. Gas volume fractions are around 98% with differences between FLUENT and DRSPALL less than 0.02. The fluid velocity profiles show increasing fluid acceleration with height because of the decrease in gas density and pressure. The drop in velocity at about 180 m is at the collar drill pipe interface and indicates the increase in annulus area.

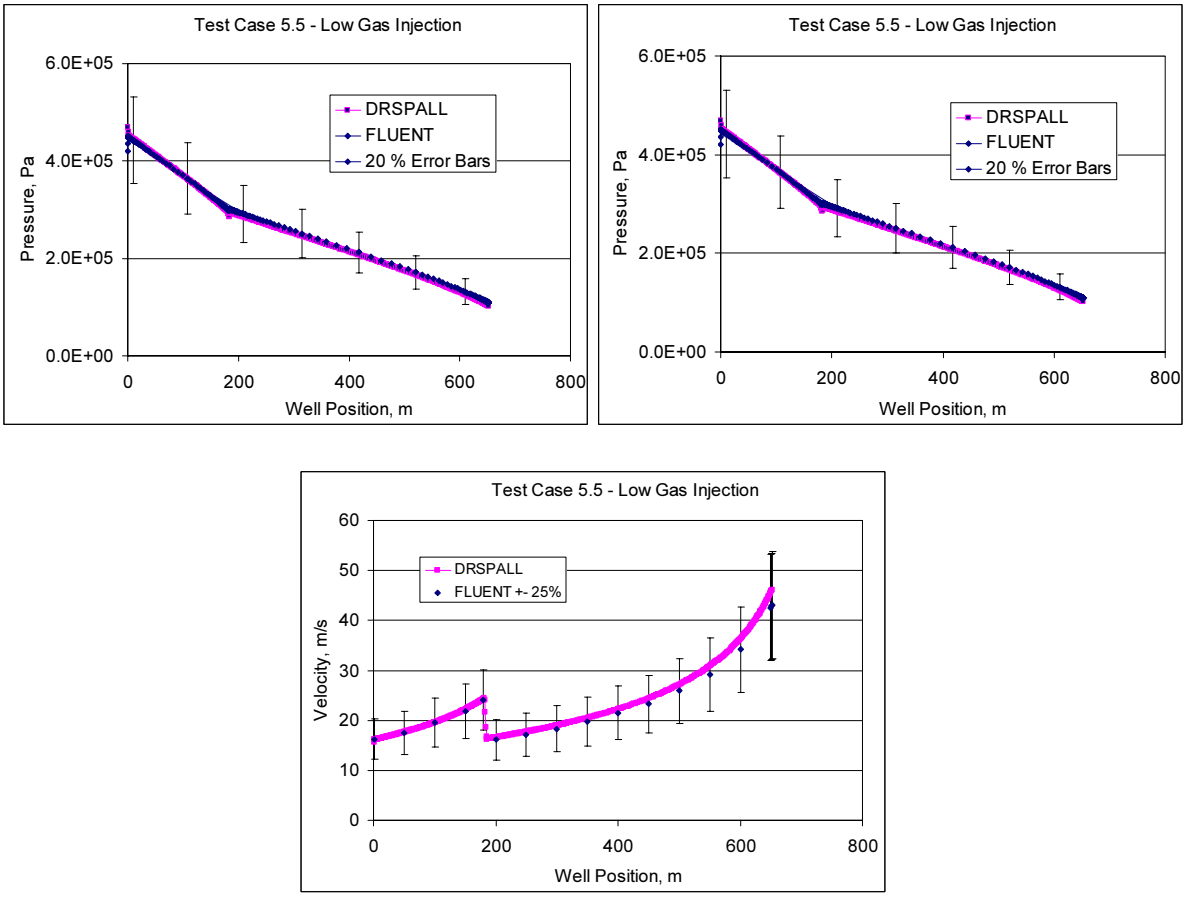

Figure 6.2-6. Pressure, Gas Volume Fraction and Velocity Profiles for Steady State, Nominal Mud Density and Low Gas Injection Rate, Case 5.5.

6.2.5.5 Case 5.6 – Medium Gas Injection

The results for Case 5.6 (constant mud pumping rate = 0.02018 m^3/s; mud density = 1210 kg/m^3; and a gas injection rate = 2.5 kg/s) are summarized by the pressure, fluid velocity and gas volume fraction profiles at 450s shown in Figure 6.2-7. The gas injection rate is ten times larger than in Case 5.5, section 6.2.5.4. The bottomhole pressure, gas volume fraction and fluid velocity have increased relative to Case 5.5 because of the increased gas injection rate. Pressure profiles compare very well. Gas volume fractions are above 99% for both DRSPALL and FLUENT. DRSPALL fluid velocities are slightly low relative to FLUENT because of the slightly lower gas volume fraction.

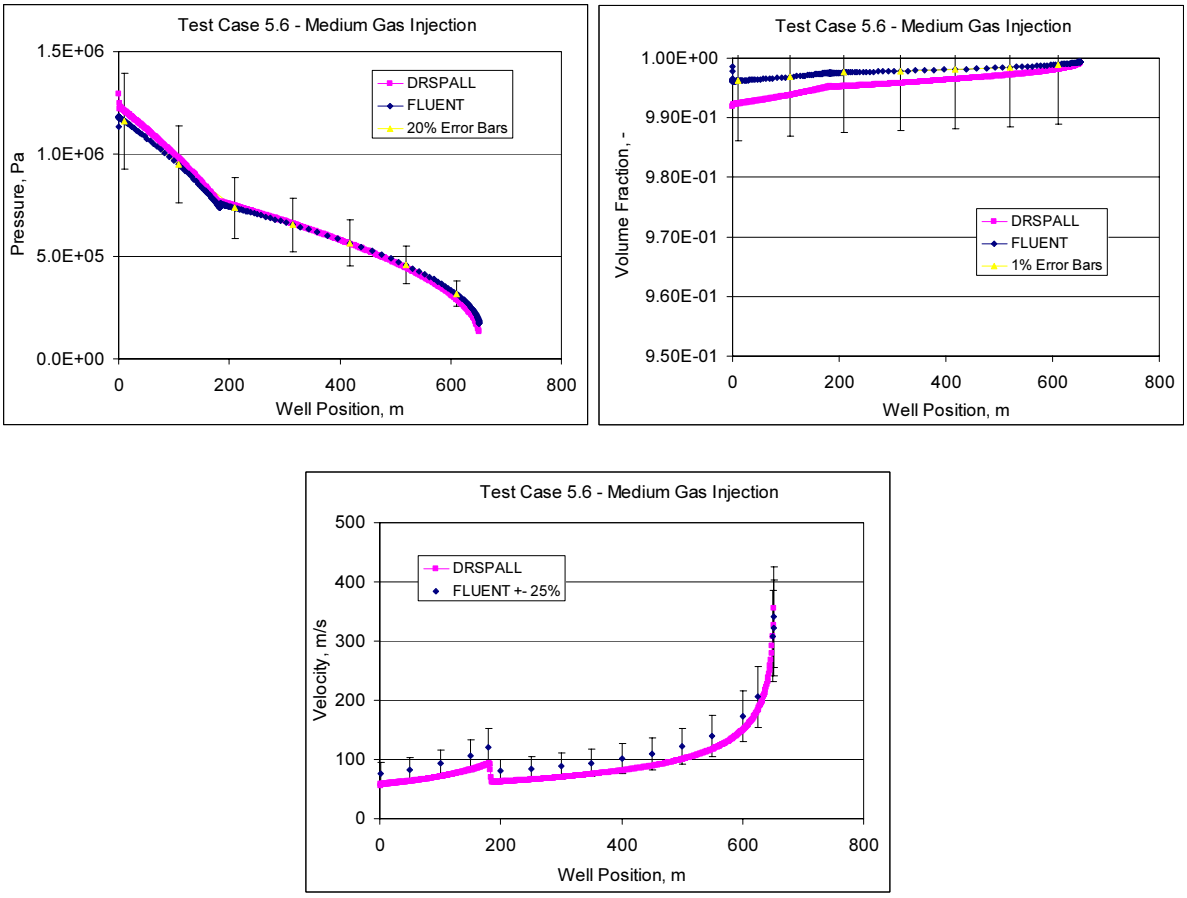

Figure 6.2-7. Pressure, Gas Volume Fraction and Velocity Profiles for Steady State, Nominal Mud Density and Medium Gas Injection Rate, Case 5.6.

6.2.5.6 Case 5.7 – Medium Gas and Low Solid Injection

The results for Case 5.7 (constant mud pumping rate = 0.02018 m^3/s; mud density = 1210 kg/m^3; gas injection rate = 2.5 kg/s; and low solid injection rate = 2.5kg/s) are summarized by the pressure, fluid velocity and gas and solid volume fraction profiles at 450 s shown in Figure 6.2-8. The gas injection rate is the same as in Case 5.6, section 6.2.5.5. The pressure profiles essentially overlay with an increase in bottomhole pressure relative to Case 5.6 due to the presence of solids in the wellbore. Gas volume fractions are near 99% but are lower than Case 5.6 because of the solids. Solid volume fractions are very small, near 5×10^{-4}. The fluid velocity profiles are very similar to Case 5.6 because of the dominance of the gas.

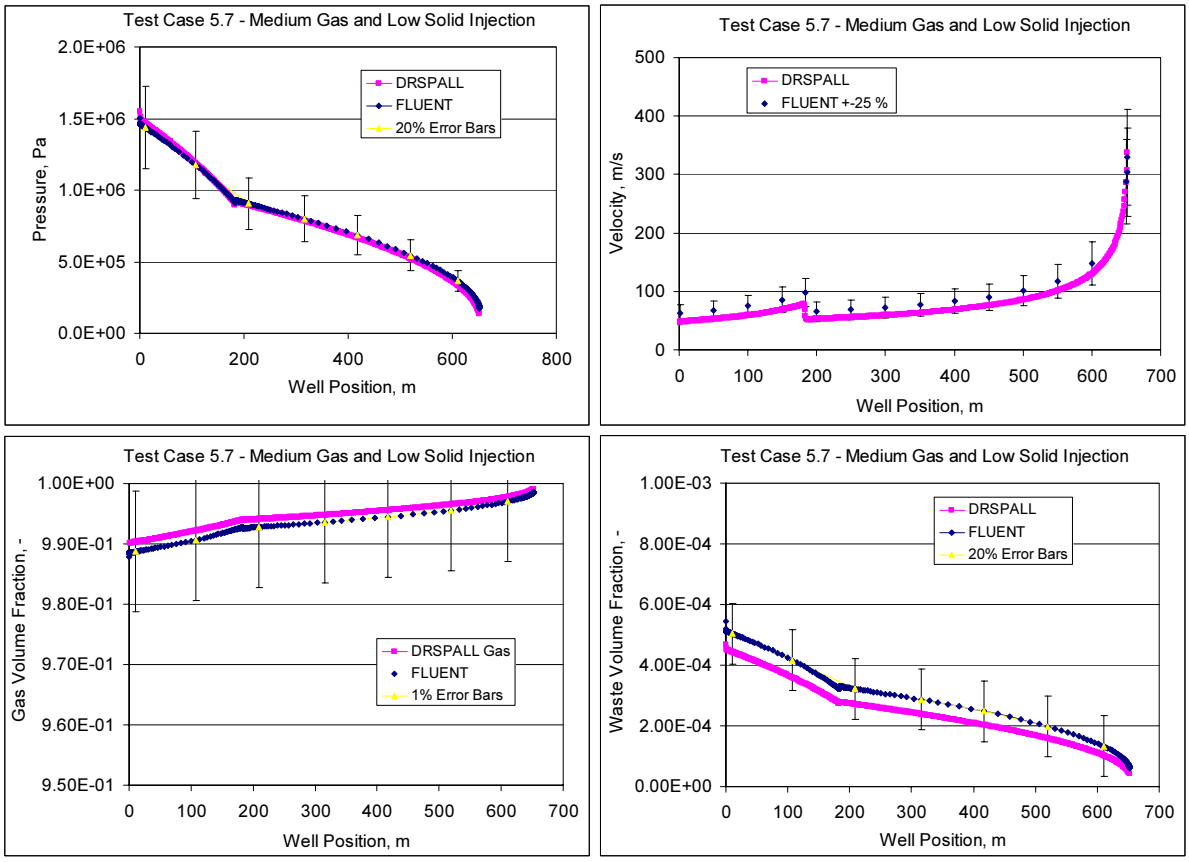

Figure 6.2-8. Pressure, Velocity and Volume Fraction Profiles for Steady State, Nominal Mud Density, Medium Gas and Low Solid Injection Rate, Case 5.7.

6.2.6 Conclusions

Comparisons of the FLUENT and DRSPALL results for both the static (Case 5.1) and steady state, mud-only (Cases 5.2, 5.3) calculations show very close agreement. All steady state cases with mud and gas injection (Cases 5.5, 5.6) or mud, gas and solid injection (Case 5.7) are also in good agreement. Much of the differences are probably due to the way friction loss is handled in the two models. DRSPALL uses an empirical friction factor that is a function of wall roughness and Reynolds number. FLUENT calculates shear forces in its two-dimensional cylindrical flow domain and assumed smooth walls for this analysis.

The Wellbore Flow Verification confirms that DRSPALL is properly calculating the multi-component mixture flow in the wellbore.

6.3 Internal Logic Checks

6.3.1 Test Objective

This test case demonstrates that DRSPALL accurately calculates:

1. Coupling of flows in the wellbore and the repository
2. Tensile failure of homogenous waste material using effective stress and seepage laws
3. Fluidized bed transport of disaggregated waste material
4. Expulsion of disaggregated waste material at the land surface.

This test case was referred to as "Test Case #4" in the DRSPALL VVP/VD (WIPP PA, 2003g).

6.3.2 Problem Description

The evolution of the WIPP underground over the 10,000-year regulatory period could result in a gas-filled repository at near-lithostatic pressure. DRSPALL is designed to estimate the mass of WIPP waste subject to tensile failure (spalling) and transport to the surface, if a drilling intrusion penetrates such a high-pressure repository. The problem domain here is a WIPP repository at a high, initial repository pressure in which a drilling intrusion results in a significant well blowout at the land surface. The repository domain is cast in spherical geometry.

This test case differs from the other DRSPALL test cases in that DRSPALL output are not compared against an independent model or experimental data. Rather, the selected intermediate and standard output variables are reported in tabular and graphical format to facilitate tests of (1) the program logic, and (2) verification or proper implementation of the mathematics outlined in the sections 3 and 4 of this report.

6.3.2.1 Boundary Conditions

The boundary conditions are set by the default conditions in DRSPALL. This includes a constant mud injection rate into the cavity at the well bottom, a constant pressure (1 atm) boundary condition at the outlet from the wellbore, and a no-flow gas boundary at the outer edge of the repository domain.

6.3.2.2 Input Parameters

In order to assure a spalling event, the repository initial pressure is near lithostatic pressure at 14.8 MPa, and the tensile strength is set to a low value in its range, 1.2E+05 Pa (17.4 psi). The remaining parameters are generally WIPP defaults and can be found in WIPP PA (2003g).

6.3.3 Analysis Methods

6.3.3.1 Coupling of the Wellbore and the Repository Flow Models

The coupling of the wellbore and repository flow models in DRSPALL is handled differently before and after bit penetration into the repository. Before penetration, a cylinder of altered-permeability salt material (called the drilling-damaged zone, or DDZ) with diameter equal to the drillbit moves ahead of the drillbit and is assumed to carry limited porous gas flow from the repository to the wellbore. Gas flow is driven by the difference between the gas pressure at the face of the waste and the gas pressure in the bottom of the approaching wellbore. Once the repository is penetrated, these two pressures equalize and gas flow from the repository is added directly to the wellbore.

Coupling of the wellbore and repository flow models will be tested by reporting intermediate variables near the time of bit penetration. The variables include:

- Run time (sec)
- Bit above repository (m) – Distance between bit and top of repository
- Repository penetrated (true/false)
- Cavity pressure (Pa) – Gas pressure in the preliminary cavity created at the point where the repository domain meets the DDZ
- Wellbore bottomhole pressure (Pa)
- Total gas in well (kg) – Spatial integral of gas mass over entire wellbore domain
- Total gas injected (kg) – Time integral of gas mass injected at bottom of well
- Gas mass in repository (kg) – Spatial integral over entire pore space in repository
- Gas mass from repository (kg) – Difference between starting gas mass in repository and current gas mass in repository
- Gas in storage[3] (kg) – Gas removed from repository by removal of repository zones is added to "storage" before it is released to the cavity (Section 3.5.5)
- Mass balance error (-) – Error in the mass of gas in the entire repository and wellbore system relative to time 0.

While distance of the bit above the repository is greater than zero, the logical variable, repository penetrated, should be false. In addition, the cavity pressure at the face of the repository and wellbore bottomhole pressure should converge as gas bleeds from the repository to the wellbore through the drilling-damaged zone. Once the height of the bit

[3] Both gas and solids removed from the repository by drilling are moved into "storage" before being released to the wellbore domain. Mass in storage is then released to the wellbore over a mixing time = (radius/superficial gas velocity) where the radius is the center of the cell that forms the cavity wall, the first intact repository zone. This is done because instantaneously adding the entire contents of one computational zone to the cavity causes numerical noise, and the controlled release from store dampens the numerical shock.

above the repository reaches zero, repository penetrated should be true. The cavity pressure and well bottomhole pressure should then be the same. Also, the spatial integral of total gas in the well should be equivalent to the time integral of gas injected into the bottom of the well until gas is ejected at the annulus outlet at the land surface. The 'gas mass from repository' should be similar to but not necessarily the same as the 'total gas injected.' Recall that pressure is the dependent variable in the repository model and gas density and flux are found by post processing using the equation-of-state and Darcy's law, respectively (Eqs. 3.5.1a and 3.5.1c). 'Gas mass from repository' includes all mass sources and sinks in the repository model including the wellbore boundary, far-field boundary and local mass balance errors due to errors in the pressure solution. The wellbore boundary should dominate the term and therefore be similar in value to total gas injected. The 'total gas injected' is calculated using Darcy's law applied at the interior boundary of repository domain and requires an approximation of the pressure gradient at the boundary, which is discontinuous.

6.3.3.2 Tensile Failure of Waste Material

In DRSPALL, the radial effective stress at any radius *r* is calculated as the sum of the radial seepage and elastic stress, minus the pore pressure:

$$\sigma_r(r) = \sigma_{sr}(r) + \sigma_{er}(r) - \beta P(r) \tag{6.3.1}$$

where the radial seepage stress is evaluated with the integral shown previously in Eq. (3.5.18), and the total radial elastic stress is evaluated as:

$$\sigma_{er}(r) = \sigma_{ff}\left[1 - \left(\frac{r_{cav}}{r}\right)^m\right] + P(r_{cav})\left(\frac{r_{cav}}{r}\right)^m \tag{6.3.2}$$

and the pore pressure, *P(r)*, is obtained from the transient solution to porous flow. The terms for the above equations were defined in section 3.5.2.

Tensile failure of the solid waste material is determined by comparing the mean radial effective stress ($\sigma_r'(r)$) over the characteristic length to the tensile strength T_s of the solid, shown graphically in drawing in Figure 6.3-1. DRSPALL uses the convention that a positive stress denotes compression, while a negative stress denotes tension. The maximum effective radial stress in tension (where $\sigma_r'(r) < 0$) will typically appear near the cavity wall and transition to compression ($\sigma_r'(r) > 0$) as *r* increases to the far-field. As such, tensile failure in the solid starts near the cavity wall and moves outward.

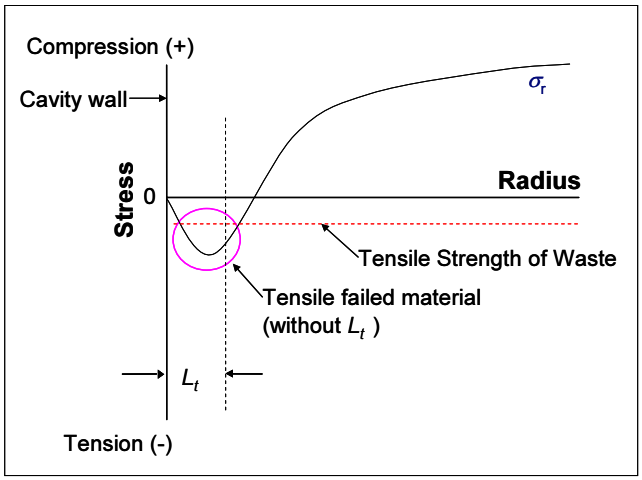

Figure 6.3-1. Drawing of a Theoretical Radial Effective Stress Curve.
Material is subject to tensile failure where $\sigma_r'(r)$ <Ts.

In the DRSPALL discretized repository domain, the failure criterion is tested according to the following expression:

$$\text{if } \frac{\sum_{i=1}^{n} \sigma_{r,i}}{n} < T_s \text{, then failure is initiated over } L_t \qquad (6.3.3)$$

where the sum is evaluated over n repository zones (of constant size) over a characteristic length L_t. Note that since T_s is represented by a negative constant in the current calculations, a tensile stress exceeding T_s would actually be less than T_s, hence the "less than" symbol in Eq. (6.3.3). Failure in DRSPALL thus occurs only when the mean radial effective stress (in tension) over a characteristic length, L_t, exceeds the tensile strength. L_t in this analysis was 2 cm. The characteristic length concept is introduced because without it, the stress formulations in Eqs. (6.3.1), (3.5.13), and 6.3.2 preclude tensile failure in zones near the wall at small zone size. Close examination of these equations will reveal that the radial effective stress is exactly zero at the cavity wall, implying that a zone size can always be found in which the very first zone next to the cavity wall has an effective stress insufficient to fail the solids. This is also illustrated in Figure 6.3-1. .

Tensile failure of waste material is tested by reporting the following output variables for selected times:

- Run time (sec)
- Cavity pressure (Pa)
- Cavity radius (m)
- Drilled radius (m)
- Cavity volume (m^3)

For computational cells in the repository in the vicinity of the wellbore, the following will be reported as a function of selected times:

- Repository cell index (-)
- Radius of cell center (m)
- Pore pressure in cell (Pa)
- Radial elastic stress in cell (Pa)
- Radial seepage stress in cell (Pa)
- Radial effective stress in cell (Pa)
- Tensile failure started (true/false)
- Fraction of cell fluidized (-)

In addition, elastic stress, seepage stress and effective stress will be calculated from Eqs. (3.5.16) through (3.5.19) in an independent spreadsheet analysis using a pore pressure profile, *P(r)*, generated by DRSPALL at one selected time. The spreadsheet values will be compared to those output from DRSPALL to verify that the stress calculations in DRSPALL are implemented correctly.

6.3.3.3 Fluidized Bed Transport of Disaggregated Waste Material

Once tensile failure occurs, material is moved from the repository to the wellbore by fluidized bed transport. In DRSPALL, the Ergun (1952) equation (3.5.20):

$$\frac{1.75}{a\phi^3}\left(\frac{d_p U_f \rho_g}{\eta_g}\right)^2 + 150\left(\frac{1-\phi}{a^2\phi^3}\right)\left(\frac{d_p U_f \rho_g}{\eta_g}\right) = \frac{{d_p}^3 \rho_g \left(\rho_w - \rho_g\right) g}{{\eta_g}^2}$$

is solved for fluidization velocity and compared with the superficial gas velocity perpendicular to the cavity wall. The superficial gas velocity is defined as the volume flow rate divided by the area perpendicular to flow direction. If the superficial gas velocity exceeds the fluidization velocity, the failed solids are assumed fluidized and added to the wellbore.

In DRSPALL, the fluidization velocity is nearly constant for a given set of input parameters, though it does change slightly as pressure near the cavity decreases and gas density decreases as a result.

Fluidization of a given zone requires a finite period of time, defined by the fluidization time t_f:

$$t_f = \frac{r_{c1}}{u_{repos}} \tag{6.3.4}$$

where r_{c1} is the center of the cell that forms the cavity wall and u_{repos} is the superficial gas velocity.

Fluidized bed transport will be tested by reporting the following output variables as a function of time:

- Runtime (sec)
- Cavity pressure (Pa)
- Cavity radius (m)
- Fluidization velocity (m/s)
- Superficial gas velocity at the cell center (m/s)
- Total waste in well (kg)

For computational cells in the repository in the vicinity of the wellbore, the following will be reported as a function of time:

- Cell index (-)
- Radius of cell center (m)
- Tensile failure completed (true/false)
- Fluidization started (true/false)
- Fluidization completed (true/false)
- Fraction fluidized (-)

Also, the fluidization velocity and fluidization time will be calculated given specific input variables using Equations (3.5.20) and (6.3.4), independent of DRSPALL. These values will be compared to output from DRSPALL to verify that DRSPALL computed the values correctly.

Finally, the volume and mass of material removed from the repository due to drilling (cuttings) and/or failure and fluidization will be verified by spreadsheet calculations based on the repository computational grid and zone removal tracking variables stored on the CAMDAT output file. The CAMDAT variables to be verified are:

- CUTMASS – mass of material removed by drilling (kg)
- TOTMASS – total mass of material remove due to either drilling or spall (kg)
- SPLMASS – difference between TOTMASS and CUTMASS (kg)
- SPLMAS2 – incrementally summed mass of material removed due to failure and fluidization (spall) (kg)
- CUTVOLEQ – equivalent uncompacted volume of material removed by drilling (m^3)
- TOTVOLEQ – equivalent uncompacted total volume of material remove due to either drilling or spall (m^3)
- SPLVOLEQ – difference between TOTVOLEQ and CUTVOLEQ (m^3)

- SPLVOL2 – incrementally summed equivalent uncompacted volume of material removed due to spall (m^3)

6.3.3.4 Expulsion of Disaggregated Waste Material

Upon transport of the waste material from the cavity at the bottom of the wellbore to the land surface, DRSPALL expels the waste from the problem domain and calculates the total mass of waste expelled as a function of time.

Expulsion of disaggregated waste material at the land surface will be tested by displaying the following output variables at selected times:

- Run time (sec)
- Repository penetrated (true/false)
- Zones removed from repository domain (-) – Actual number of computational cells removed from the inner wall of the repository domain due to cutting action of the drillbit or spalling
- Mass of waste removed (kg) – Mass of waste solids removed from repository domain
- Waste in store (kg) – Mass of waste in "store" after fluidization of a zone has completed but before it is released to the cavity
- Total waste in well (kg) – Spatial integral of waste mass in wellbore domain
- Waste mass ejected (kg) – Time integral of waste mass ejected at annulus outlet to land surface
- Waste position in well (m) – Position of waste front in well, where ~ -655 m is the well bottom, and 0 m is the land surface
- Mass balance error (-) – Relative difference between mass removed from repository domain and mass ejected to the surface.

Once the bit penetrates the repository, waste cuttings and potentially spallings will be transported up the wellbore to the surface. Monitoring the position of the waste front in the well will indicate how close it is to the land surface. Once the front reaches the surface, the quantity ejected will increase from zero. The mass of waste removed from the repository should balance with the sum of the waste in the well and the waste ejected.

6.3.4 Results

The presentation of results starts with a general description of the run behavior and then breaks out into discussions of specific functionality.

Key history variables for this run are shown in Figure 6.3-2 and Figure 6.3-3. Note that the code was executed for 450 seconds DRSPALL time. This was sufficient time to allow for the cavity pressure to stabilize (Figure 6.3-2), drilling to complete and failure of repository

material to stop and cavity radius to stabilize (Figure 6.3-3). Output variable names shown in the figures represent the CAMDAT variable names. The names are described in the User's Manual (WIPP PA, 2003f) and also in Appendix VG.

Understanding DRSPALL output typically begins with studying the pressure and cavity radius history plots. The pressure history plot in Figure 6.3-2 shows the fluid pressure at the bottom of the well (BOTPRS) and the repository pressure at the point of impending intrusion (CAVPRS). At the start of the simulation, BOTPRS is near hydrostatic (~8 MPa), and CAVPRS is at the initial repository pressure, 14.8 MPa. The well pressure is a little noisy at startup because the initial pressure distribution is chosen arbitrarily, and stable, dynamic flowing solution must be found, which takes a few seconds of DRSPALL time. The important issue here is for the wellbore pressure to settle down before bit penetration of the repository, which it does in all DRSPALL runs. As the bit nears the repository, gas bleed between the repository and wellbore causes BOTPRS and CAVPRS to converge and reach a common value near 9.5 MPa at the time of intrusion. After intrusion, direct coupling between the high-pressure repository and wellbore causes the drilling mud column to blow out, resulting in a drop in BOTPRS to near 3.5 MPa where it stays for the remainder of the run. The pressure spikes observed between 150 and 200 seconds are caused by tensile failure of repository solids and subsequent entrainment into the wellbore flow stream.

Also instructive is the radius history plot, shown here in Figure 6.3-3. Recall that the repository geometry is hemispherical in this study. Note that the initial cavity radius (CAVRAD) is small but not zero, representing the radius of the pseudo-cavity (section) created prior to bit penetration. The cavity then grows upon penetration of the repository, starting at 34 seconds. Until 150 seconds, all radial variables grow due to drilling. After 150 seconds, tensile failure occurs, and tensile radius (TENSRAD) and cavity radius (CAVRAD) grow accordingly. Drilled radius (DRILLRAD) continues along its path independent of the growing cavity in front of it, and stops only when the drillbit would have hit the bottom of the repository in the real system. In this case, the drilled radius is 0.48 m. The cavity radius and tensile-failed radius settle to a constant value near 0.59 m. The difference between these radii represents the material considered to be "spalled" in this conceptual model.

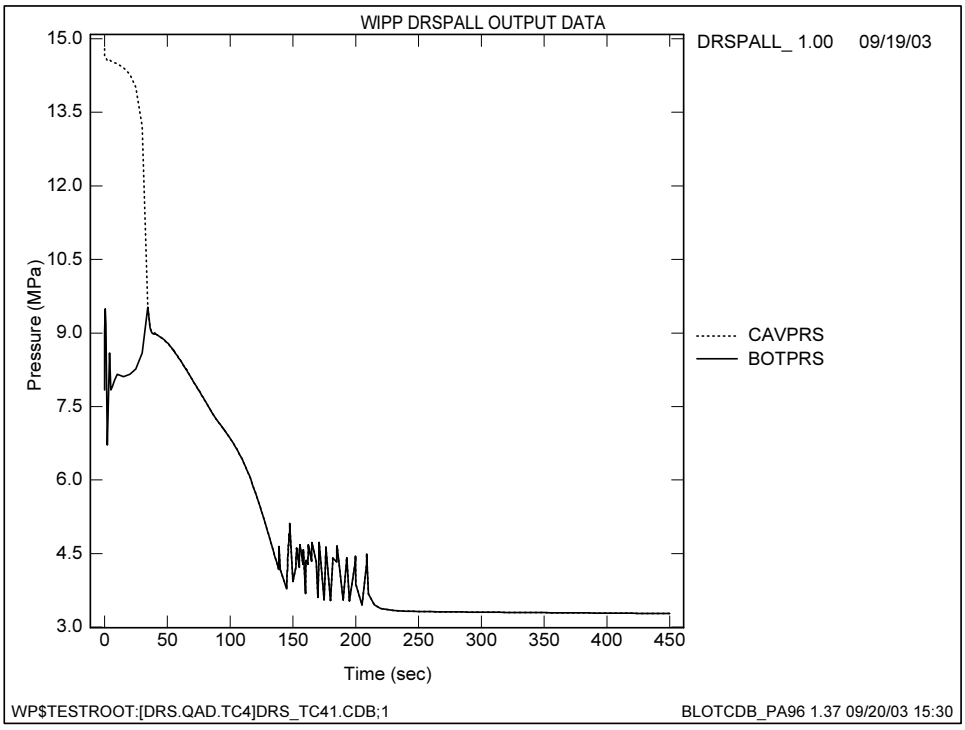

Figure 6.3-2. Pressure History Plot.

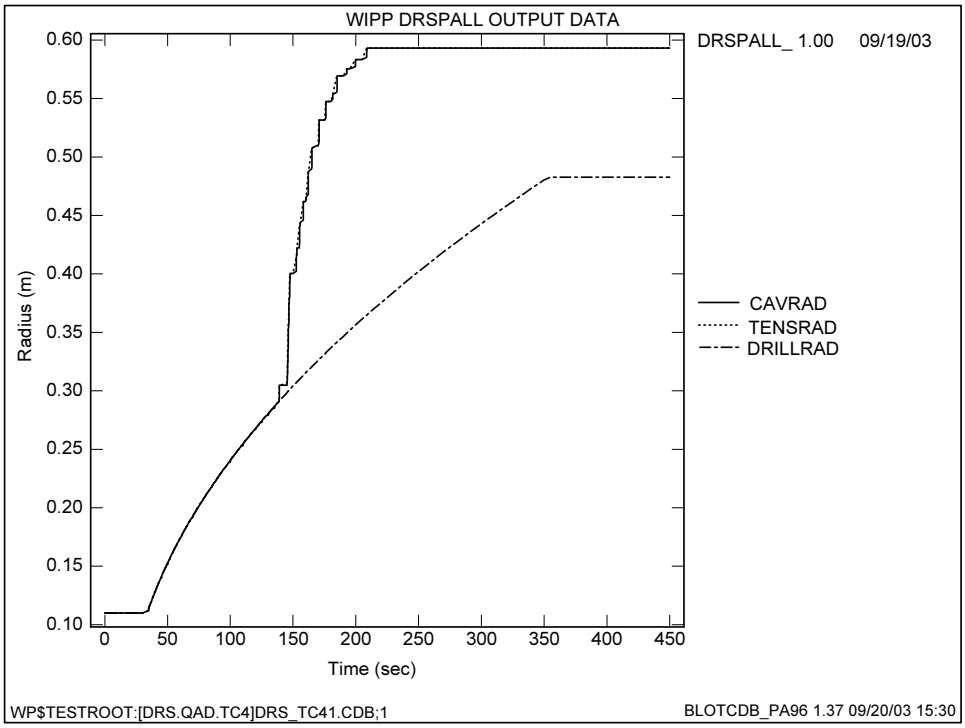

Figure 6.3-3. Radius History Plot.

6.3.4.1 Coupling of the Wellbore and Repository Flow Models

A coupling output file that contains coupling data at selected times is produced for this validation run only. An excerpt from the coupling output file is shown in Table 6.3-1. The information shown in this table relates to gas transport from the repository domain to the wellbore domain. Displayed output variables include run time, height of bit above repository, logical flag repository penetrated, cavity pressure, well bottom pressure, total gas in well, total gas injected, gas mass remaining in repository, gas mass from repository, gas in storage, and mass balance error. These variables are defined in section 6.3.3.1. Also shown for this discussion is graphical output in a pressure versus time plot shown in Figure 6.3-4.

6.3.4.1.1 Coupling Logic

Reporting in Table 6.3-1 starts at run time = 28.28596 seconds. The bit is 0.02427 m above the top of the repository at this point, and the Repository Penetrated logical is "F" (false). Gas pressure in the repository (Cavity Pressure = 13.61 MPa) is greater than Well Bottom Pressure at 8.43 MPa. This causes some gas to bleed from the repository to the well bottom through the drilling-damaged zone (DDZ), resulting in a nonzero and growing Total Gas in Well = 1.90 kg. As the bit proceeds downward with time, Cavity Pressure and Well Bottom Pressure converge to a common value of 9.52 MPa at ~33.79 seconds when the repository is penetrated. A horizontal line is drawn in the table at the time of penetration. The pressure behavior is also illustrated graphically in Figure 6.3-4, where data from Figure 6.3-2 were plotted on a time scale from 0 to 100 seconds to zoom in on events around the time of intrusion.

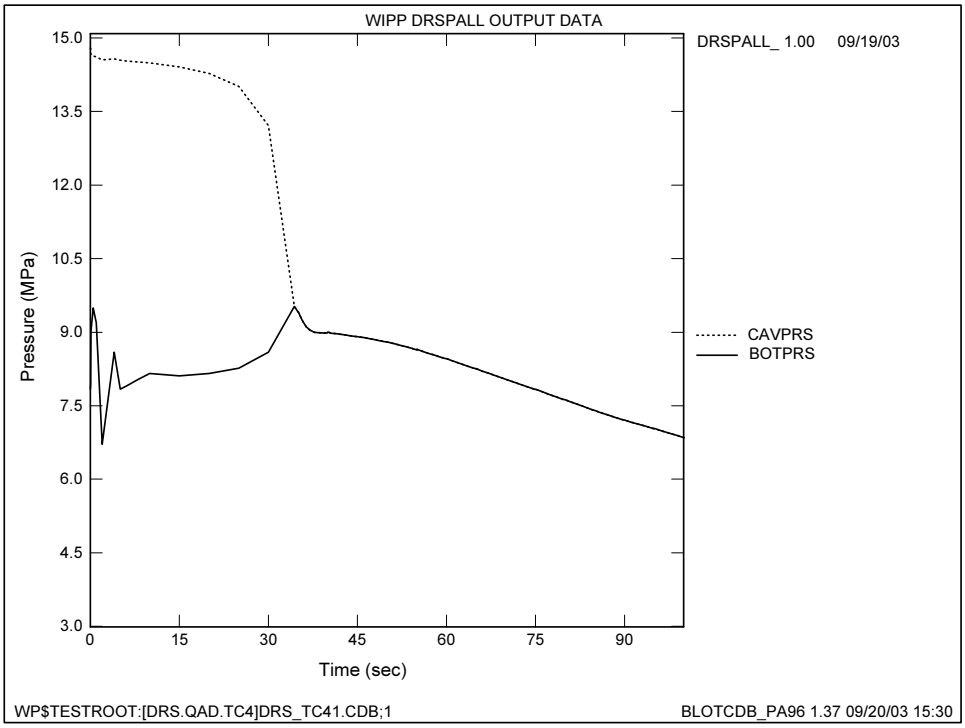

Figure 6.3-4. Pressure History Plot for Time = 0 to 100 Seconds.

In Table 6.3-1, the spatial integral Total Gas In Well agrees closely with the time integral Total Gas Injected until gas transports all the way to the top of the wellbore at the land surface (run time ~105 seconds) at which point gas is ejected to the atmosphere and out of the problem domain. Mass of gas injected and gas mass from repository are similar as expected and explained in section 6.3.3.1. The global mass balance error remains on the order of 1E-04 to 1E-06 for all reported times in Table 6.3-1.

Table 6.3-1. Excerpt from the Coupling Output File.

```
Program DR_SPALL - WIPP PA 2003
ASCII Output file for Test Case #4
          Verification of coupling between Repository and Wellbore

   Initial Repos Pressure (Pa)         1.4800000000000000E+07
   Initial Gas in Repos (kg)           1.025939986444641E+05
```

Runtime (sec)	Bit Above Repository(m)	Repository Penetrated(T/F)	Cavity Pressure(Pa)	Well Bottom Pressure (Pa)	Total Gas In Well(kg)	Total Gas Injected(kg)	Gas Mass In Repos(kg)	Gas Mass From Repos(kg)	Gas storage(kg)	Mass Bal Error(-)
28.28596	0.02427	F	1.3614296E+07	8.4290427E+06	1.9026425E+00	1.9026425E+00	1.0259199E+05	2.0087165E+00	0.0000000E+00	1.0339199E-06
28.45051	0.02354	F	1.3584261E+07	8.4412189E+06	1.9296418E+00	1.9296418E+00	1.0259196E+05	2.0386324E+00	0.0000000E+00	1.0623486E-06
28.61514	0.02281	F	1.3552717E+07	8.4540321E+06	1.9572490E+00	1.9572490E+00	1.0259193E+05	2.0692826E+00	0.0000000E+00	1.0920098E-06
28.77983	0.02207	F	1.3519543E+07	8.4674679E+06	1.9854912E+00	1.9854912E+00	1.0259190E+05	2.1007026E+00	0.0000000E+00	1.1229838E-06
28.94460	0.02134	F	1.3484610E+07	8.4815729E+06	2.0143977E+00	2.0143977E+00	1.0259187E+05	2.1329305E+00	0.0000000E+00	1.1553582E-06
29.10945	0.02061	F	1.3447785E+07	8.4964394E+06	2.0439997E+00	2.0439997E+00	1.0259183E+05	2.1660074E+00	0.0000000E+00	1.1892283E-06
29.27438	0.01988	F	1.3408915E+07	8.5121158E+06	2.0743305E+00	2.0743305E+00	1.0259180E+05	2.1999771E+00	0.0000000E+00	1.2246980E-06
29.43940	0.01914	F	1.3367821E+07	8.5285948E+06	2.1054257E+00	2.1054257E+00	1.0259176E+05	2.2348871E+00	0.0000000E+00	1.2618808E-06
29.60450	0.01841	F	1.3324301E+07	8.5458984E+06	2.1373241E+00	2.1373241E+00	1.0259173E+05	2.2707888E+00	0.0000000E+00	1.3009016E-06
29.76971	0.01767	F	1.3278144E+07	8.5641080E+06	2.1700673E+00	2.1700673E+00	1.0259169E+05	2.3077379E+00	0.0000000E+00	1.3418977E-06
29.93501	0.01694	F	1.3229113E+07	8.5833006E+06	2.2036999E+00	2.2036999E+00	1.0259165E+05	2.3457946E+00	0.0000000E+00	1.3850199E-06
30.10042	0.01620	F	1.3176929E+07	8.6035047E+06	2.2382704E+00	2.2382704E+00	1.0259161E+05	2.3850244E+00	0.0000000E+00	1.4304344E-06
30.26595	0.01547	F	1.3121275E+07	8.6247389E+06	2.2738312E+00	2.2738312E+00	1.0259157E+05	2.4254985E+00	0.0000000E+00	1.4783256E-06
30.43159	0.01473	F	1.3061799E+07	8.6470638E+06	2.3104396E+00	2.3104396E+00	1.0259153E+05	2.4672953E+00	0.0000000E+00	1.5288980E-06
30.59736	0.01399	F	1.2998104E+07	8.6705764E+06	2.3481576E+00	2.3481576E+00	1.0259149E+05	2.5105002E+00	0.0000000E+00	1.5823791E-06
30.76326	0.01326	F	1.2929741E+07	8.6953643E+06	2.3870529E+00	2.3870529E+00	1.0259144E+05	2.5552067E+00	0.0000000E+00	1.6390221E-06
30.92930	0.01252	F	1.2856184E+07	8.7214919E+06	2.4271994E+00	2.4271994E+00	1.0259140E+05	2.6015179E+00	0.0000000E+00	1.6991099E-06
31.09549	0.01178	F	1.2776827E+07	8.7490379E+06	2.4686782E+00	2.4686782E+00	1.0259135E+05	2.6495472E+00	0.0000000E+00	1.7629598E-06
31.26185	0.01104	F	1.2690982E+07	8.7781269E+06	2.5115782E+00	2.5115782E+00	1.0259130E+05	2.6994205E+00	0.0000000E+00	1.8309287E-06
31.42837	0.01030	F	1.2597853E+07	8.8089074E+06	2.5559975E+00	2.5559975E+00	1.0259125E+05	2.7512768E+00	0.0000000E+00	1.9034185E-06
31.59508	0.00956	F	1.2496504E+07	8.8415178E+06	2.6020439E+00	2.6020439E+00	1.0259119E+05	2.8052707E+00	0.0000000E+00	1.9808831E-06
31.76199	0.00882	F	1.2385833E+07	8.8760952E+06	2.6498371E+00	2.6498371E+00	1.0259114E+05	2.8615744E+00	0.0000000E+00	2.0638375E-06
31.92911	0.00808	F	1.2264538E+07	8.9128137E+06	2.6995097E+00	2.6995097E+00	1.0259108E+05	2.9203811E+00	0.0000000E+00	2.1528679E-06
32.09645	0.00733	F	1.2131084E+07	8.9518927E+06	2.7512098E+00	2.7512098E+00	1.0259102E+05	2.9819071E+00	0.0000000E+00	2.2486434E-06
32.26405	0.00659	F	1.1983633E+07	8.9935722E+06	2.8051023E+00	2.8051023E+00	1.0259095E+05	3.0463962E+00	0.0000000E+00	2.3519299E-06
32.43191	0.00584	F	1.1819954E+07	9.0380998E+06	2.8613725E+00	2.8613725E+00	1.0259088E+05	3.1141238E+00	0.0000000E+00	2.4636075E-06
32.60006	0.00509	F	1.1637326E+07	9.0857528E+06	2.9202288E+00	2.9202288E+00	1.0259081E+05	3.1854026E+00	0.0000000E+00	2.5846915E-06
32.76853	0.00434	F	1.1432402E+07	9.1368625E+06	2.9819072E+00	2.9819072E+00	1.0259074E+05	3.2605891E+00	0.0000000E+00	2.7163569E-06
32.93735	0.00359	F	1.1201016E+07	9.1918137E+06	3.0466756E+00	3.0466756E+00	1.0259066E+05	3.3400912E+00	0.0000000E+00	2.8599679E-06
33.10655	0.00284	F	1.0937890E+07	9.2510341E+06	3.1148401E+00	3.1148401E+00	1.0259057E+05	3.4243777E+00	0.0000000E+00	3.0171123E-06
33.27617	0.00209	F	1.0636221E+07	9.3150067E+06	3.1867526E+00	3.1867526E+00	1.0259048E+05	3.5139909E+00	0.0000000E+00	3.1896439E-06
33.44625	0.00133	F	1.0287064E+07	9.3843065E+06	3.2628209E+00	3.2628209E+00	1.0259039E+05	3.6095609E+00	0.0000000E+00	3.3797297E-06
33.61685	0.00057	F	9.8783325E+06	9.4596432E+06	3.3435224E+00	3.3435224E+00	1.0259029E+05	3.7118247E+00	0.0000000E+00	3.5899015E-06
33.78802	**-0.00019**	**T**	**9.5223525E+06**	**9.5223525E+06**	**3.4287849E+00**	**3.4287849E+00**	**1.0259018E+05**	**3.8211285E+00**	**0.0000000E+00**	**3.8242352E-06**
33.95975	-0.00095	T	9.5319626E+06	9.5319626E+06	3.5140628E+00	3.5140628E+00	1.0259007E+05	3.9313310E+00	0.0000000E+00	4.0671792E-06
34.13179	-0.00172	T	9.5368221E+06	9.5368221E+06	3.5989067E+00	3.5989067E+00	1.0258996E+05	4.0409391E+00	0.0000000E+00	4.3085596E-06
34.30404	-0.00248	T	9.5331246E+06	9.5331246E+06	3.6835667E+00	3.6835667E+00	1.0258985E+05	4.1502840E+00	0.0000000E+00	4.5491680E-06
34.47643	-0.00325	T	9.5430641E+06	9.5430641E+06	3.7698590E+00	3.7698590E+00	1.0258974E+05	4.2617995E+00	3.6244251E-04	4.7914893E-06
34.64902	-0.00401	T	9.5039778E+06	9.5039778E+06	3.8569497E+00	3.8569497E+00	1.0258962E+05	4.3736670E+00	1.0789983E-04	5.0354743E-06
34.82177	-0.00478	T	9.4630241E+06	9.4630241E+06	3.9442086E+00	3.9442086E+00	1.0258951E+05	4.4860611E+00	3.1809226E-05	5.2812122E-06
34.99467	-0.00555	T	9.4218308E+06	9.4218308E+06	4.0317753E+00	4.0317753E+00	1.0258940E+05	4.5989994E+00	9.2843924E-06	5.5287332E-06
35.16771	-0.00632	T	9.4045946E+06	9.4045946E+06	4.1219710E+00	4.1219710E+00	1.0258928E+05	4.7153013E+00	2.8177944E-04	5.7805381E-06
35.34095	-0.00709	T	9.3558123E+06	9.3558123E+06	4.2125073E+00	4.2125073E+00	1.0258917E+05	4.8316869E+00	8.3710512E-05	6.0344256E-06
35.51435	-0.00786	T	9.2987700E+06	9.2987700E+06	4.3034330E+00	4.3034330E+00	1.0258905E+05	4.9488625E+00	2.4532530E-05	6.2908650E-06
35.68790	-0.00863	T	9.2422980E+06	9.2422980E+06	4.3948841E+00	4.3948841E+00	1.0258893E+05	5.0668873E+00	7.0849135E-06	6.5500526E-06
35.86161	-0.00940	T	9.2137128E+06	9.2137128E+06	4.4896482E+00	4.4896482E+00	1.0258881E+05	5.1890449E+00	2.2624075E-04	6.8149255E-06
36.03552	-0.01018	T	9.1759153E+06	9.1759153E+06	4.5842244E+00	4.5842244E+00	1.0258869E+05	5.3107994E+00	6.6250169E-05	7.0813965E-06
36.20958	-0.01095	T	9.1409044E+06	9.1409044E+06	4.6789777E+00	4.6789777E+00	1.0258857E+05	5.4330003E+00	1.9240644E-05	7.3493912E-06

6.3.4.2 Tensile Failure of Waste Material

A stress output file that contains pore pressure and stress profiles is written for this validation test only. An excerpt from the stress output file (as formatted by EXCEL) is shown in Table 6.3-2. The header to this table gives information such as run time, cavity pressure, cavity radius, drilled radius, cavity volume, far-field pressure at the no-flow outer boundary (R = 19.2 m), and first intact zone. The first intact zone is defined as the repository computational cell corresponding to the intact cavity wall. Zones that are failed and fluidizing are considered intact until the fluidization process is complete. Below the header is a listing of repository cells in the vicinity of the cavity wall showing selected properties related to stress and material failure. Shown are the cell index, radius of the cell center relative to the origin of the repository domain, pore (gas) pressure, radial elastic stress, radial seepage stress, radial effective stress, logical flag for tensile failure, fraction of the zone fluidized and the radial effective stress calculated by the spreadsheet. Tensile strength for this test case is 0.12 MPa and is specified as input to DRSPALL and reported in the header to the stress output file.

6.3.4.2.1 Stress and Failure Logic

Reviewing Table 6.3-2 allows for an examination of the logic that controls waste material failure due to stresses in the solid. Starting with the first intact zone 103, if radial effective stress is less than tensile strength (T_s = -0.12 MPa), the material is subject to failure. Recall from section 6.3.3.2 and Eq. (6.3.4) that failure is allowed only if the mean radial effective stress in the cells that cover the specified characteristic length, L_t, exceeds the tensile strength. For this problem, L_t = 2 cm or 11 zones for the region where zone size is constant at slightly less than 0.2 cm. Examination of the radial effective stress "EffStre" for zones 103-113 reveals that the mean stress = -1.55932E+05 Pa, which is less than T_s = -0.12 MPa, and the logical variable "Failed" is thus True for zones within the characteristic length. Zones beyond the characteristic length are not allowed to fail until all the zones within the characteristic length have fluidized.

6.3.4.2.2 Verification of Stress Calculations

The data from Table 6.3-2 were imported into an EXCEL spreadsheet (Table 6.3-3) in order to verify the stress calculations. Note that the Effective Stress formulation (Eqs. 6.3.1, 6.3.2, and 3.5.13) requires only material properties, geometry, and the correct pore pressure profile to determine the stress state in the solid. As such, this verification will proceed by using the pore pressure profile shown in Table 6.3-2 to calculate a stress profile, which will be compared back to the stress profile calculated by DRSPALL. Table 6.3-3 displays the new stress profile calculations.

The header in Table 6.3-3 contains global properties such as Far-Field Stress, Tensile Strength, Poisson's Ratio, Geometry Index (2 = cylindrical, 3 = spherical), Far-Field Pressure, Biot's Beta, and the prefactor which is a convenient coupling of terms to create an intermediate variable as follows:

$$prefactor = (m-1)\beta\left(\frac{1-2\upsilon}{1-\upsilon}\right) \tag{6.3.5}$$

The calculations start at the first intact zone 103 and are carried through to zone 123. The following notes apply:

- r_c/r denotes the ratio cavity radius to zone center radius
- The Radial Elastic Stress is calculated per Eq. (6.3.2)
- The Integral Over *dr* represents the integral in Eq. (3.5.18) over one zone
- The sum is the integral over all zones from First Intact Zone to the given zone
- The Radial Seepage Stress is calculated by Eq. (3.5.18)
- The Radial Effective Stress is calculated by Eq. (3.5.16)

The spreadsheet results for the stress values are compared to DRSPALL values in the summary Table 6.3-4. The relative difference is calculated as follows:

$$\text{relative DIFF} = \left|(\text{DRSPALL stress} - \text{spreadsheet stress})\right| \div \text{DRSPALL stress} \tag{6.3.6}$$

Relative differences for the Radial Elastic Stress were all less than 1E-12, while relative differences for Radial Seepage Stress were less than 1E-12, and for Radial Effective Stress less than 1E-10. These calculations verify that the stress formulation given in section 6.3.3.2 was implemented in DRSPALL as intended.

Table 6.3-2. Excerpt from the Stress Output File, Run Time = 158.7951 Seconds.

```
Runtime(sec)   =     1.454425E+02
CavPres(Pa)    =     4.146353E+06
CavRadius(m)   =     3.128393E-01
DrilledRad(m)  =     2.989038E-01
CavityVol(m^3)=      1.136522E-01
Pff(Pa)        =     1.479203E+07
FirstIntactZone=     103
```

zone index	Radius(m)	PorePres(Pa)	ElastStr(Pa)	SeepStr(Pa)	EffStre(Pa)	Failed(T/F)	Fluidized(-)	Spreadsheet EffStre(Pa)
93	2.939482E-01	4.661860E+06	4.757951E+06	-1.571180E-01	9.609117E+04	T	1	9.609117E+04
94	2.959367E-01	4.686087E+06	4.779872E+06	-1.353646E+00	9.378394E+04	T	1	9.378394E+04
95	2.979252E-01	4.709829E+06	4.801601E+06	-3.319853E+00	9.176842E+04	T	1	9.176842E+04
96	2.999138E-01	4.733570E+06	4.823510E+06	-1.972065E+00	8.993815E+04	T	1	8.993815E+04
97	3.019023E-01	4.756543E+06	4.844462E+06	-2.779430E-01	8.791859E+04	T	1	8.791859E+04
98	3.038909E-01	4.767929E+06	4.850089E+06	-2.456990E+00	8.215786E+04	T	1	8.215786E+04
99	3.058794E-01	4.161419E+06	4.242081E+06	-4.044156E+00	8.065736E+04	T	1	8.065736E+04
100	3.078679E-01	4.217049E+06	4.305268E+06	-2.508475E+00	8.821718E+04	T	1	8.821718E+04
101	3.098565E-01	4.253661E+06	4.338075E+06	-3.641354E+00	8.441047E+04	T	1	8.441047E+04
102	3.118450E-01	4.273342E+06	4.350736E+06	-2.401319E+00	7.739207E+04	T	1	7.739207E+04
103	3.138336E-01	4.408686E+06	4.349476E+06	-5.124927E+04	-1.104600E+05	T	0	-1.104600E+05
104	3.158221E-01	4.597200E+06	4.547514E+06	-1.001251E+05	-1.498110E+05	T	0	-1.498110E+05
105	3.178107E-01	4.759872E+06	4.740627E+06	-1.469404E+05	-1.661846E+05	T	0	-1.661846E+05
106	3.197992E-01	4.910351E+06	4.928967E+06	-1.918497E+05	-1.732335E+05	T	0	-1.732335E+05
107	3.217877E-01	5.052969E+06	5.112680E+06	-2.349590E+05	-1.752475E+05	T	0	-1.752475E+05
108	3.237763E-01	5.189360E+06	5.291908E+06	-2.763567E+05	-1.738092E+05	T	0	-1.738092E+05
109	3.257648E-01	5.320327E+06	5.466786E+06	-3.161218E+05	-1.696637E+05	T	0	-1.696637E+05

110	3.277534E-01	5.446384E+06	5.637445E+06	-3.543279E+05	-1.632669E+05	T	0	-1.632669E+05
111	3.297419E-01	5.567924E+06	5.804013E+06	-3.910434E+05	-1.549543E+05	T	0	-1.549543E+05
112	3.317304E-01	5.685275E+06	5.966610E+06	-4.263329E+05	-1.449976E+05	T	0	-1.449976E+05
113	3.337190E-01	5.798725E+06	6.125356E+06	-4.602571E+05	-1.336264E+05	T	0	-1.336264E+05
114	3.357075E-01	5.908527E+06	6.280362E+06	-4.928735E+05	-1.210386E+05	F	0	-1.21039E+05
115	3.376961E-01	6.014908E+06	6.431739E+06	-5.242363E+05	-1.074060E+05	F	0	-1.07406E+05
116	3.396846E-01	6.118073E+06	6.579591E+06	-5.543969E+05	-9.287909E+04	F	0	-9.28791E+04
117	3.416731E-01	6.218207E+06	6.724022E+06	-5.834042E+05	-7.758968E+04	F	0	-7.75897E+04
118	3.436617E-01	6.315479E+06	6.865129E+06	-6.113045E+05	-6.165392E+04	F	0	-6.16539E+04
119	3.456502E-01	6.410040E+06	7.003008E+06	-6.381416E+05	-4.517429E+04	F	0	-4.51743E+04
120	3.476388E-01	6.502034E+06	7.137750E+06	-6.639575E+05	-2.824140E+04	F	0	-2.82414E+04
121	3.496273E-01	6.591587E+06	7.269444E+06	-6.887921E+05	-1.093553E+04	F	0	-1.09355E+04
122	3.516158E-01	6.678820E+06	7.398175E+06	-7.126832E+05	6.672114E+03	F	0	6.67211E+03
123	3.536044E-01	6.763842E+06	7.524027E+06	-7.356671E+05	2.451825E+04	F	0	2.45182E+04

Table 6.3-3. EXCEL Spreadsheet Showing Independent Calculations of Stress Profiles from Pore Pressure Data Obtained from Table 6.3-2.

Far-field stress	1.4900E+07
Tensile strength	1.2000E+05
Poisson's ratio	3.8000E-01
Geometry index	3
Far-field pressure	1.4792E+07
Biot Beta	1.0000E+00
Prefactor	3.8710E-01

RADIAL S

		Seepage stress				
Zone Index	r_c/r	Rad El Stress	Integral over dr	Sum	RadSeepStr	Radial Effective Stress
				0		
103	9.936637E-01	4.349476E+06	-2.046144E+03	-2.046144E+03	-5.124927E+04	-1.104600E+05
104	9.874072E-01	4.547514E+06	-2.027855E+03	-4.074000E+03	-1.001251E+05	-1.498110E+05
105	9.812290E-01	4.740627E+06	-2.018522E+03	-6.092522E+03	-1.469404E+05	-1.661846E+05
106	9.751276E-01	4.928967E+06	-2.012303E+03	-8.104825E+03	-1.918497E+05	-1.732335E+05
107	9.691017E-01	5.112680E+06	-2.007501E+03	-1.011233E+04	-2.349590E+05	-1.752475E+05
108	9.631497E-01	5.291908E+06	-2.003567E+03	-1.211589E+04	-2.763567E+05	-1.738092E+05
109	9.572704E-01	5.466786E+06	-2.000295E+03	-1.411619E+04	-3.161218E+05	-1.696637E+05
110	9.514625E-01	5.637445E+06	-1.997583E+03	-1.611377E+04	-3.543279E+05	-1.632669E+05
111	9.457246E-01	5.804013E+06	-1.995367E+03	-1.810914E+04	-3.910434E+05	-1.549543E+05
112	9.400555E-01	5.966610E+06	-1.993601E+03	-2.010274E+04	-4.263329E+05	-1.449976E+05
113	9.344540E-01	6.125356E+06	-1.992244E+03	-2.209498E+04	-4.602571E+05	-1.336264E+05

114	9.289188E-01	6.280362E+06	-1.991262E+03	-2.408625E+04	-4.928735E+05	-1.210386E+05
115	9.234488E-01	6.431739E+06	-1.990627E+03	-2.607687E+04	-5.242363E+05	-1.074060E+05
116	9.180429E-01	6.579591E+06	-1.990312E+03	-2.806719E+04	-5.543969E+05	-9.287909E+04
117	9.126999E-01	6.724022E+06	-1.990294E+03	-3.005748E+04	-5.834042E+05	-7.758968E+04
118	9.074187E-01	6.865129E+06	-1.990552E+03	-3.204803E+04	-6.113045E+05	-6.165392E+04
119	9.021983E-01	7.003008E+06	-1.991067E+03	-3.403910E+04	-6.381416E+05	-4.517429E+04
120	8.970376E-01	7.137750E+06	-1.991822E+03	-3.603092E+04	-6.639575E+05	-2.824140E+04
121	8.919356E-01	7.269444E+06	-1.992802E+03	-3.802372E+04	-6.887921E+05	-1.093553E+04
122	8.868913E-01	7.398175E+06	-1.993993E+03	-4.001772E+04	-7.126832E+05	6.672114E+03
123	8.819037E-01	7.524027E+06	-1.995382E+03	-4.201310E+04	-7.356671E+05	2.451825E+04

Table 6.3-4. Summary of Differences Between DRSPALL and Spreadsheet Calculations for Stress Verification.

	Absolute DIFF			Relative DIFF		
	Rad El Stress	*Rad Seep Stress*	*Rad Eff Stress*	*Rad El Stress*	*Rad Seep Stress*	*Rad Eff Stress*
103	7.90693E-07	2.01580E-07	6.11835E-07	1.81790E-13	3.93333E-12	5.53898E-12
104	6.05360E-07	1.45184E-07	4.30213E-07	1.33119E-13	1.45003E-12	2.87170E-12
105	3.94881E-07	9.11823E-08	2.72732E-07	8.32972E-14	6.20539E-13	1.64114E-12
106	1.41561E-07	4.94183E-08	1.32335E-07	2.87202E-14	2.57589E-13	7.63912E-13
107	6.51926E-08	3.87081E-09	9.97388E-08	1.27512E-14	1.64744E-14	5.69131E-13
108	6.72415E-07	1.61584E-07	4.50411E-07	1.27065E-13	5.84695E-13	2.59141E-12
109	3.87430E-07	1.16357E-07	2.91184E-07	7.08698E-14	3.68077E-13	1.71624E-12
110	2.30968E-07	7.17700E-08	1.18191E-07	4.09703E-14	2.02553E-13	7.23911E-13
111	6.79865E-08	3.38769E-08	3.35567E-08	1.17137E-14	8.66320E-14	2.16559E-13
112	7.54371E-08	2.56114E-09	1.12836E-07	1.26432E-14	6.00736E-15	7.78189E-13
113	4.61005E-07	1.28988E-07	3.92058E-07	7.52617E-14	2.80252E-13	2.93398E-12
114	3.34345E-07	9.74978E-08	2.56216E-07	5.32366E-14	1.97815E-13	2.11681E-12
115	2.03960E-07	6.23404E-08	1.21334E-07	3.17114E-14	1.18917E-13	1.12967E-12
116	7.45058E-09	2.73576E-08	5.26779E-09	1.13238E-15	4.93466E-14	5.67167E-14
117	5.05708E-07	1.46101E-07	4.28394E-07	7.52092E-14	2.50429E-13	5.52127E-12
118	4.36790E-07	1.10245E-07	2.97128E-07	6.36245E-14	1.80344E-13	4.81929E-12
119	2.76603E-07	7.68341E-08	1.56950E-07	3.94977E-14	1.20403E-13	3.47431E-12
120	1.22935E-07	5.28526E-08	2.70993E-08	1.72232E-14	7.96023E-14	9.59559E-13
121	4.09782E-08	2.66591E-08	1.07364E-07	5.63705E-15	3.87041E-14	9.81791E-12
122	4.55417E-07	1.24564E-07	2.98014E-07	6.15580E-14	1.74782E-13	4.46656E-11
123	3.11993E-07	9.25502E-08	2.32299E-07	4.14662E-14	1.25804E-13	9.47455E-12

6.3.4.3 Fluidized Bed Transport of Disaggregated Waste Material

A fluidization output file that contains fluidization data at selected times is produced for this validation run only. An excerpt from the fluidization output file is shown in Table 6.3-5. The header to this table gives information such as run time, cavity pressure, cavity radius, gas density in the cavity, minimum fluidization velocity, superficial gas velocity at the cavity wall, mass of waste in well, and the first intact zone. The first intact zone is defined as the repository computational cell corresponding to the intact cavity wall. Zones that are failed and fluidizing are considered intact until the fluidization process is complete. Below the header is a listing of repository cells in the vicinity of the cavity wall showing selected properties related to fluidization. Shown are the cell index, radius of the cell center relative to the origin of the repository domain, logical flags for failure of the cell completed, fluidization started, and fluidization completed, and the fraction of the cell fluidized. A -1.0 in the Fraction Fluidized column indicates that the cell was removed by drilling, while a 1.0 indicates that the zone was removed by tensile failure and fluidized bed transport.

Table 6.3-5. Excerpt from the Fluidization Output File at Time = 145.8678 Seconds.

```
Runtime (sec)              =  1.4586779704775E+02
Cavity Pressure(Pa)        =  4.3556358551769E+06
Cavity Radius(m)           =  3.3471325039864E-01
Gas Density (kg/m^3)       =  3.6760607574864E+00
Fluidization Velocity(m)   =  5.7394912081331E-01
Superficial Gas Velocity(m)
        (First Intact Zone)=  1.1524586428985E+00
Waste In Well (kg)         =  4.1079099663678E+01
      FirstIntactZone         114
```

Cell index	Radius(m)	Failure Completed(T/F)	Fluidization Start(T/F)	Fluidization Complete(T/F)	Fraction Fluidized
104	3.1582211225086E-01	T	T	T	1.0000
105	3.1781065306987E-01	T	T	T	1.0000
106	3.1979919388888E-01	T	T	T	1.0000
107	3.2178773470789E-01	T	T	T	1.0000
108	3.2377627552691E-01	T	T	T	1.0000
109	3.2576481634592E-01	T	T	T	1.0000
110	3.2775335716493E-01	T	T	T	1.0000
111	3.2974189798394E-01	T	T	T	1.0000
112	3.3173043880295E-01	T	T	T	1.0000
113	3.3371897962197E-01	T	T	T	1.0000
114	3.3570752044098E-01	T	T	F	0.0002
115	3.3769606125999E-01	T	T	F	0.0002
116	3.3968460207900E-01	T	T	F	0.0001
117	3.4167314289802E-01	T	T	F	0.0001
118	3.4366168371703E-01	F	F	F	0.0000
119	3.4565022453604E-01	F	F	F	0.0000
120	3.4763876535505E-01	F	F	F	0.0000
121	3.4962730617406E-01	F	F	F	0.0000
122	3.5161584699308E-01	F	F	F	0.0000
123	3.5360438781209E-01	F	F	F	0.0000
124	3.5559292863110E-01	F	F	F	0.0000
125	3.5758146945011E-01	F	F	F	0.0000
126	3.5957001026913E-01	F	F	F	0.0000
127	3.6155855108814E-01	F	F	F	0.0000
128	3.6354709190715E-01	F	F	F	0.0000
129	3.6553563272616E-01	F	F	F	0.0000
130	3.6752417354517E-01	F	F	F	0.0000
131	3.6951271436419E-01	F	F	F	0.0000

6.3.4.3.1 Fluidization Logic

At the point in the code execution shown in Table 6.3-5, 113 computational cells in the repository have been removed and transported into the cavity and wellbore by a combination of

drilling and tensile failure/fluidization. The first intact zone that forms the cavity wall is cell 114. Zones 104-113 were completely removed by tensile failure and fluidization (Fraction Fluidized = 1.0). Zones 114-117 have failed in tension (Failure Completed = T), and zones 114-117 are currently fluidizing (Fraction Fluidized > 0). In order for zones to fluidize, the superficial gas velocity at the cavity wall must exceed the minimum fluidization velocity. This condition can be confirmed by examining the header in Table 6.3-5. The Superficial Gas Velocity at the first intact zone (114) = 1.152 m/s, while the Fluidization Velocity = 0.5738 m/s. As such, the failed zone 114 is subject to fluidization, and fluidization is currently in process. Zones must complete fluidization in sequence such that zone 115 cannot completely fluidize until after zone 114 has completely fluidized. Also, zones require a finite time to fluidize. The progress of a particular zone through the fluidization process is given by the fraction fluidized, which varies from 0 (not fluidized) to 1.0 (fully fluidized). Notice that zones 114-117 are just starting to fluidize in Table 6.3-5. Eventual fluidization of failed zones 115 and 116 were confirmed by looking at the subsequent data snapshots in the fluidization output file for run times > 145 seconds.

6.3.4.3.2 Verification of Fluidization Velocity

Data from Table 6.3-5 were imported into an EXCEL spreadsheet (Table 6.3-6) in order to verify proper calculation of Ergun's minimum fluidization velocity (Eq. 3.5.20). The dependent variable in Ergun's formula is U_f, which can be solved for by the quadratic formula:

$$AU_f^2 + BU_f + C = 0 \tag{6.3.7}$$

$$U_f = \frac{-B \pm \sqrt{B^2 - 4AC}}{2A} \tag{6.3.8}$$

Eq. (3.5.20). was rearranged to form the constants A, B, and C, defined in Eq. (6.3.7), which are evaluated in Table 6.3-6. The two lines preceding the last in Table 6.3-6 compare the fluidization velocity calculated by the spreadsheet to that calculated by DRSPALL for the given input conditions. The relative difference [(DRSPALL U_f – spreadsheet U_f)/DRSPALL U_f] evaluated to 5.417E-15.

Table 6.3-6. Spreadsheet Solution for Minimum Fluidization Velocity, U_f.

Parameters	*Value*	*Units*
run time	1.4586777E+02	sec
gas density	3.6766585E+00	kg/m3
porosity	5.7500000E-01	-
waste density	2.6500000E+03	kg/m3
gas viscosity	8.9339000E-06	Pa*sec
particle diameter	1.0000000E-03	m
shape factor	5.5000000E-01	-
gravity	9.8067000E+00	m/sec2
a	2.8346290E+06	
b	4.5620861E+05	
c	-1.1954651E+06	
b^2-4ac	1.3762927E+13	
spreadsheet fluidization vel	5.7390813E-01	m/s
DRSPALL fluidization vel	5.7390813E-01	m/s
Relative difference	5.4165890E-15	

6.3.4.3.3 Verification of Fluidization Time

The spreadsheet calculation of the fluidization time is shown in Table 6.3-7. For the given conditions, the fluidization time calculated by Eq. (6.3.4) using r_{c1} and u_{repos} from runtime = 1.58797E+02 sec was t_f = 0.292 seconds. For comparison, t_f (FLUIDTIM) was extracted from the CAMDAT output file for several runtimes near 145.87 seconds, and are shown in Table 6.3-7, showing values of t_f = 0.245 to 0.292 sec.

Confirmation of proper implementation of t_f in DRSPALL is possible by examining the amount of time required to completely fluidize zone 114 that started to fluidize near runtime = 1.4587E+02 sec. The reporting frequency in the fluidization output file is not sufficient to capture both the beginning and ending of fluidization for zone 114, but the report of fraction fluidized at two times may be used to extrapolate an approximate fluidization time. This strategy is shown in the lower half of Table 6.3-7, with runtime #1 and runtime #2 representing the two selected runtime reports from which the fluidization time is extrapolated. The projected fluidization time from this coarse method is 0.307 sec. This compares favorably with the values calculated by spreadsheet (t_f = 0.291 sec) and extracted from the CAMDAT file using GROPECDB (WIPP PA, 1996b), Table 6.3-8 (step 208, t_f = 0.291).

Table 6.3-7. Spreadsheet Solution for Fluidization Time, T_f.

Fluidization Time, t_f

Parameter	*Value*	*Units*
run time	1.4586777E+02	sec
radius to cell center first intact zone	3.3471325E-01	m
superficial gas velocity	1.1519070E+00	m/sec
fluidization time	2.9057316E-01	sec
From Fluidization Output File		
runtime #1	1.4586777E+02	sec
fraction fluidized #1	0.0001	-
runtime #2	1.4586790E+02	sec
fraction fluidized #2	0.0005	-
projected fluidization time	3.07E-01	sec

Table 6.3-8. Fluidization Time Values Extracted from CAMDAT File.

CDB Step Index	Time (Sec)	Fluidization Time (sec)
207	1.45866E+02	4.21058E-01
208	1.46159E+02	2.91436E-01
209	1.46159E+02	2.91436E-01
210	1.46177E+02	3.09156E-01
211	1.46177E+02	3.09156E-01

Note: Consecutive times can appear to be equal because times listed by the GROPECDB utility do not have enough precision to capture the DRSPALL timestep. Fluidization Times on the CAMDAT file are for the first intact zone minus 1 or the last zone fluidized. Therefore, step 207 gives Fluidization Time for zone 113; steps 208 and 209 for zone 114.

6.3.4.3.4 Verification of Drilling and Spall Volumes And Masses

The spreadsheet calculations of waste volumes and masses removed from the repository due to drilling and spall (failure and fluidization) are shown in Table 6.3-9. The table also gives the values that were extracted from the diagnostic output file and the CAMDAT output file. The difference in CAVRAD0 between the diagnostic file and the CAMDAT file is due the precision in the displayed number not the actual value. The maximum relative difference [ABS(DRSPALL – spreadsheet)/DRSPALL] evaluated to 4.28E-05 for SPLVOLEQ.

Table 6.3-9. Drilling and Spall Volumes and Masses from CAMDAT File

CAMDAT Variable Name	Description	Value from Diagnostic Output File	Value from CAMDAT Output File	Spreadsheet Calculation	Relative Difference
CAVRAD0	Initial pseudo-cavity radius	0.1100	1.10008E-01	1.10008E-01	1.25E-06
CUTMASS	Cuttings mass	2.6078E+02	2.60779E+02	2.60779E+02	4.52E-07
TOTMASS	Total mass	4.8930E+02	4.89296E+02	4.89285E+02	2.15E-05
SPLMASS	Spall mass	2.2852E+02	2.28516E+02	2.28507E+02	4.11E-05
SPLMAS2	Incremental spall mass	4.3433E+02	4.34330E+02	4.34329E+02	2.54E-06
CUTVOLEQ	Equivalent uncompacted cuttings volume	6.56050E-01	6.56049E-01	6.56048E-01	2.28E-06
TOTVOLEQ	Equivalent uncompacted total volume	1.23090E+00	1.23093E+00	1.23091E+00	1.88E-05
SPLVOLEQ	Equivalent uncompacted spall volume	5.74880E-01	5.74884E-01	5.74859E-01	4.28E-05
SPLVOL2EQ	Equivalent uncompacted incremental spall volume	1.09270E+00	1.09266E+00	1.09265E+00	7.95E-06

6.3.4.4 Expulsion of Disaggregated Waste Material

An expulsion output file that contains solids transport data is produced for this validation run only. Excerpts from the expulsion output file are shown in Table 6.3-10, Table 6.3-11 and Table 6.3-12. Shown are:

a) data near the time of penetration (run time = 33.5 to 35.2 sec)

b) data exhibiting early waste expulsion (run time = 113.1 to 115.4 sec)

c) late time waste expulsion data approaching steady conditions (400 to 407 sec)

6.3.4.4.1 Near Bit Penetration

Table 6.3-10 shows the expulsion output file (as formatted by EXCEL) at several times near bit penetration at 33.8 sec. Prior to bit penetration, the logical variable Repository Penetrated = False, and no zones have been removed from the repository. Also, all of the waste mass accounting variables (i.e., total waste in well) are zero, and the waste position in the well is -653 m, representing the well bottom. After bit penetration, the number of zones removed increases monotonically due to drilling. The drillbit must completely penetrate a zone before that zone is removed from the repository, so there is a time lag between bit penetration (33.8 sec) and the removal of the first zone (34.4 sec). The Mass Waste Removed reflects the sum: Waste in Store + Total Waste In Well. An explanation of the Waste in Store variable is given in section 6.3.3.1. Waste Ejected is still zero since it has not had time to transport 653 m to the land surface, and Waste Position In Well shows that the location of the waste front moves upward with time.

6.3.4.4.2 Early Waste Expulsion at Surface

Table 6.3-11 shows the expulsion data near the time of the first arrival of waste solids at the land surface. Note that the position of the waste front in the well approaches z = 0 with time, and waste is first expelled at the surface at about 114.8 seconds. The Waste Mass Ejected variable reflects a time integral at the wellbore outlet, and the leading "tail" of the waste causes this variable to compute small but nonzero releases prior to the arrival of the "front" defined by Waste Position in Well. The mass balance error in this table is defined as [Mass Waste Removed – (Waste in Store + Waste In Well + Waste Ejected)]/ Mass Waste Removed.

6.3.4.4.3 Late Time Waste Expulsion

Data shown in Table 6.3-12 at late time (run time > 400 sec) show steady state behavior with a total of 243 zones removed, corresponding to 489.3 kg of waste removed from the repository and an identical 489.3 kg of waste expelled to the surface. The mass balance error is reported as 4.666e-7 kg.

6.3.5 Conclusions

The test of high-pressure WIPP intrusion with internal logic checks demonstrates the correct, expected behavior from DRSPALL for the functionality examined. Coupling data shows that the gas transported from the repository is successfully accounted for in the wellbore and ejected at the land surface. An analysis of the stress data indicates proper implementation of the stress equations and failure logic. A similar analysis of the fluidization data reveals proper calculation of the fluidization velocity and mobilization of solids by fluidized bed theory. The waste expulsion analysis demonstrates proper accounting for waste solids drilled or spalled from the repository, transported up the wellbore, and ejected at the land surface.

Table 6.3-10. Excerpt from the Expulsion Output File Near the Time of Penetration.

Runtime (sec)	Repository Penetrated(T/F)	Zones Removed(-)	Mass Waste Removed(kg)	Waste in Store (kg)	Total Waste In Well (kg)	Waste Mass Ejected (kg)	Waste Position In Well (m)	Mass Balance Error (-)
33.53346	F	0	0.00000000	0.00000000	0.00000000	0.00000000	-653.0	0.0000E+00
33.70435	F	0	0.00000000	0.00000000	0.00000000	0.00000000	-653.0	0.0000E+00
33.87582	T	0	0.00000000	0.00000000	0.00000000	0.00000000	-653.0	0.0000E+00
34.04774	T	0	0.00000000	0.00000000	0.00000000	0.00000000	-653.0	0.0000E+00
34.21989	T	0	0.00000000	0.00000000	0.00000000	0.00000000	-653.0	0.0000E+00
34.39221	T	1	0.17339133	0.16359581	0.00979530	0.00000000	-652.0	1.2450E-06
34.5647	T	1	0.17339133	0.04880662	0.12458449	0.00000000	-650.0	1.2450E-06
34.73738	T	1	0.17339133	0.01445852	0.15893259	0.00000000	-647.9	1.2450E-06
34.91021	T	1	0.17339133	0.00424100	0.16915011	0.00000000	-646.9	1.2450E-06
35.08317	T	2	0.35304977	0.12847249	0.22457760	0.00000000	-644.8	9.0138E-07
35.25632	T	2	0.35304977	0.03836360	0.31468649	0.00000000	-643.7	9.0138E-07

Table 6.3-11. Excerpt from The Expulsion Output File Near the Time of Early Waste Expulsion at Land Surface.

Runtime (sec)	Repository Penetrated(T/F)	Zones Removed(-)	Mass Waste Removed(kg)	Waste in Store (kg)	Total Waste In Well (kg)	Waste Mass Ejected (kg)	Waste Position In Well (m)	Mass Balance error (-)
113.0545	T	74	36.974594	0.02251904	36.925244	0.02685049	-37.9	5.4274E-07
113.2676	T	74	36.974594	0.01143368	36.930135	0.03304494	-33.8	5.4274E-07
113.4807	T	75	37.912394	0.64644939	37.225537	0.04043085	-29.8	5.9635E-07
113.6942	T	75	37.912394	0.32907453	37.534149	0.04919306	-24.7	5.9635E-07
113.9079	T	75	37.912394	0.16726158	37.685637	0.059518681	-19.8	5.9635E-07
114.1216	T	75	37.912394	0.08486001	37.755945	0.07161157	-13.9	5.9635E-07
114.3354	T	75	37.912394	0.04296723	37.783760	0.08569012	-7.3	5.9635E-07
114.5494	T	75	37.912394	0.02170973	37.788722	0.10198504	-2.0	5.9635E-07
114.7634	T	75	37.912394	0.01094530	37.780734	0.12073749	0.0	5.9635E-07
114.9775	T	76	38.864707	0.65317080	38.069350	0.14220226	0.0	4.1577E-07
115.1920	T	76	38.864707	0.33004099	38.368021	0.16666177	0.0	4.1577E-07
115.4066	T	76	38.864707	0.16648808	38.503872	0.19436304	0.0	4.1577E-07

Table 6.3-12. Excerpt from the Expulsion Output File at Late Time Nearing Steady Conditions.

Runtime (sec)	*Repository Penetrated(T/F)*	*Zones Removed(-)*	*Mass Waste Removed(kg)*	*Waste in Store (kg)*	*Total Waste In Well (kg)*	*Waste Mass Ejected (kg)*	*Waste Position In Well (m)*	*Mass Balance error (m)*
400.49056	T	243	489.29551	8.7577036-119	2.2632195E-12	489.29574	-653.0	4.6660E-07
401.10618	T	243	489.29551	3.6294466-119	2.2632195E-12	489.29574	-653.0	4.6660E-07
401.72180	T	243	489.29551	1.5041855-119	2.2632195E-12	489.29574	-653.0	4.6660E-07
402.33742	T	243	489.29551	6.2340912-120	2.2632195E-12	489.29574	-653.0	4.6660E-07
402.95304	T	243	489.29551	2.5837810-120	2.2632195E-12	489.29574	-653.0	4.6660E-07
403.56866	T	243	489.29551	1.0709003-120	2.2632195E-12	489.29574	-653.0	4.6660E-07
404.18428	T	243	489.29551	4.4386733-121	2.2632195E-12	489.29574	-653.0	4.6660E-07
404.79990	T	243	489.29551	1.8397893-121	2.2632195E-12	489.29574	-653.0	4.6660E-07
405.41551	T	243	489.29551	7.6259470-122	2.2632195E-12	489.29574	-653.0	4.6660E-07
406.03113	T	243	489.29551	3.1610419-122	2.2632195E-12	489.29574	-653.0	4.6660E-07
406.64675	T	243	489.29551	1.3103204-122	2.2632195E-12	489.29574	-653.0	4.6660E-07

6.4 Coalbed Methane Validation

6.4.1 Test Objective

The purpose of this test case is to demonstrate that DRSPALL can simulate the results of a field-scale coalbed cavitation completion experiment. Since this process of completing a coalbed methane well involves injecting high-pressure air and allowing a controlled blowout to occur which fails the coal and transports coal particles to the surface, it would appear to be an acceptable analog of the repository drilling intrusion spall phenomenon. The coalbed data chosen for comparison are reported by Khodaverdian et al. (1996).

This test case demonstrates the applicability of DRSPALL to simulating a drilling intrusion into the WIPP repository by modeling a field scale experiment that has similar characteristics.

This test case was referred to as "Test Case #2" in the DRSPALL VVP/VD (WIPP PA, 2003g).

6.4.2 Problem Description

6.4.2.1 Coalbed Cavitation

Coal is a naturally fractured organic material. The fractures, usually orthogonal and closely-spaced, are called "cleats." In-situ, the cleats are normally saturated with water and methane. Cleat porosity is usually a few percent. Coal, however, is different than most other geologic materials in that its matrix can hold abundant methane in an adsorbed state. When a coal reservoir is de-watered, this adsorbed methane can flow to the cleats and then to a well. As a result, the methane associated with the actual porosity of several tens of percent is producible from some coal reservoirs rather than just the few percent associated with the cleats. Because of this, these coal reservoirs are often drilled and produced as a methane source.

Wells in parts of certain coal reservoirs are most successfully completed using the "cavitation" process. The well is first drilled and cased to the top of the coal seam. Drilling then continues through the coal seam, which is left as an open hole. The completion process then takes several days to more than a week. The well is cyclically open to atmosphere and allowed to blow down, and then shut in and allowed to build up. When this is done (rarely) without any surface pumping, it is called "natural" cavitation. More often, air is introduced by high-pressure pumping at the surface to downhole pressures somewhere between reservoir pressure and lithostatic. This is "induced" cavitation. Anywhere from a few to many tens of cycles may be used, with possible bit runs between cycles to clean out the hole. When a cavitated well is blowing, a strongly flowing mixture of air, coal fines, methane, and some water comes to the surface. This is, in effect, an induced but controlled blowout. If

successful, the cavitation process produces a cavity of a few meters in diameter in the coal and leads to greatly enhanced water and ultimately, methane production.

6.4.2.2 An Acceptable Analog

Coalbed cavity completion would appear to be an analog to the WIPP drilling intrusion. This is because cavitated coal seams may be:

- in the same depth regime
- in the same thickness regime
- in the same mechanical property regime
- gas-pressurized during cavitation to the same pressure regime
- blown down in the same time regime as possible drilling intrusion occurrences

Possible shortcomings of coalbed cavitation as an analog are that peak coal cavitation pressures are somewhat lower than peak possible WIPP pressures and the strength of coal may be outside the WIPP tensile strength range, with particulate properties that may be different than degraded WIPP waste.

6.4.3 Analysis Method

6.4.3.1 Selected Field Test for Comparison

The cavitation experiments on the GRI COAL Site Well I#2 (Khodaverdian et al., 1996) have been selected for numerical simulation using DRSPALL. This selection was made based on the availability and quality of data. The well is in the Fruitland coals located in the San Juan Basin of New Mexico, and shown in Figure 6.4-1. The well was cavitated in July of 1991.

The key parameters, as reported by Khodaverdian et al. (1996), of the selected coal well are given in Table 6.4-1.

After all cavitation procedures were finished, the final cavity diameter was determined by sonar logging and is shown in Figure 6.4-2.

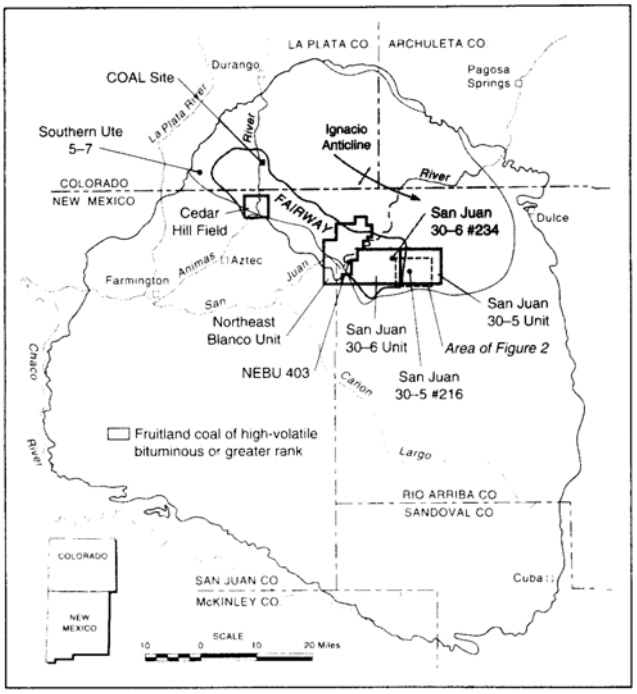

Reprinted with permission from GTI.

Figure 6.4-1. Location of Cavitated Coalbed Well (Khodaverdian et al., 1996).

Table 6.4-1. Key Coal Well Parameters

Parameter	Value (US)	Value (SI)
Depth	3150 ft	960 m
Thickness	45 ft	13.7 m
Bit Radius	0.5 ft	0.15 m
Post-Drilling (washout) Radius	1.0 ft	0.3 m
Horizontal Stress	2220 psi	15.3 MPa
Pore Pressure	1020 psi	7.0 MPa
Permeability	25 md	2.5×10^{-14} m^2

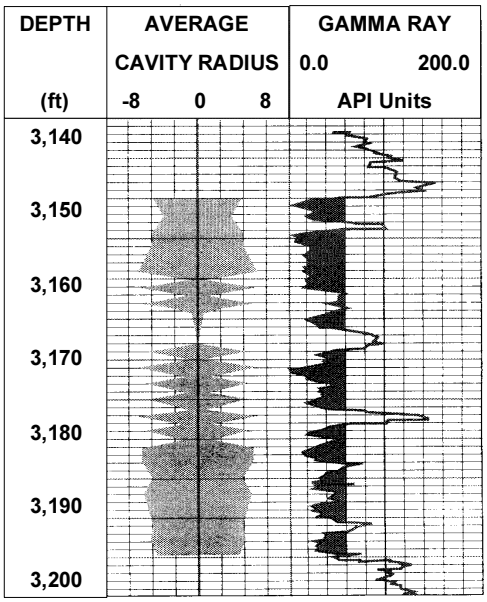

Adapted with permission from GTI.

Figure 6.4-2. Cavity Radius (Khodaverdian et al., 1996).

6.4.3.2 Approach

The authors (Khodaverdian et al., 1996) used observed surface injection pressures to estimate bottomhole pressures over time for the various cavitation cycles, as shown for the first day of cavitation activities, in Figure 6.4-3.

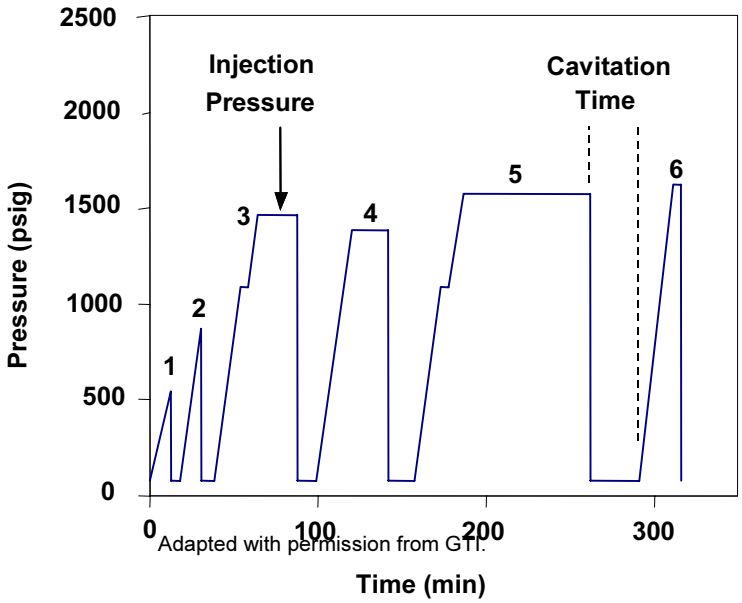

Adapted with permission from GTI.

Figure 6.4-3. Cavitation Times and Inferred Bottomhole Pressures (Khodaverdian et al., 1996).

The first day saw 6 cavitation cycles. Khodaverdian et al felt most cavity growth was completed in that time and have assumed so for their analysis. As can be seen from Figure 6.4-3, they assumed an instantaneous drawdown to 80 psi (0.55 MPa) downhole upon the start of each cavitation blowdown. In actuality, the drawdown rate would depend on pipe flow to surface and take some time (a minute or so) to develop. DRSPALL simulates the drawdown time and rates, since it includes viscous pipe flow. The relevant values in the figure are thus the peak injection pressures and the cavitation time intervals. These pressures and times are simulated in DRSPALL. The duration of the last blowdown interval is not reported, but is assumed by us to be the same as #5.

Khodaverdian et al used a numerical model (without accounting for wellbore flow) to reproduce their interpretation of the final cavity diameter (after 6 cycles) from Figure 6.4-2. Their model used the tensile failure radius as the cavity radius. Their calculations for earlier cycles thus were used to infer the cavity diameters vs. time. They used a number of permeability values (2.5, 25 and 250 md or $2.5x10^{-15}$, $2.5x10^{-14}$, $2.5x10^{-13}$ m^2) in an attempt to match the measured results, and found that a 25 md ($2.5x10^{-14}$ m^2) permeability gave the best match. This was accepted for their primary interpretation, supported also by rough laboratory measurements and other observations. Considerable uncertainty is added by having to interpret an average cavity size from the irregular data shown in Figure 6.4-2. Their final matching interpretations are shown in Figure 6.4-4. The input pressures and times, and results to compare with DRSPALL, as obtained from the author's figures, are shown in Table 6.4-2.

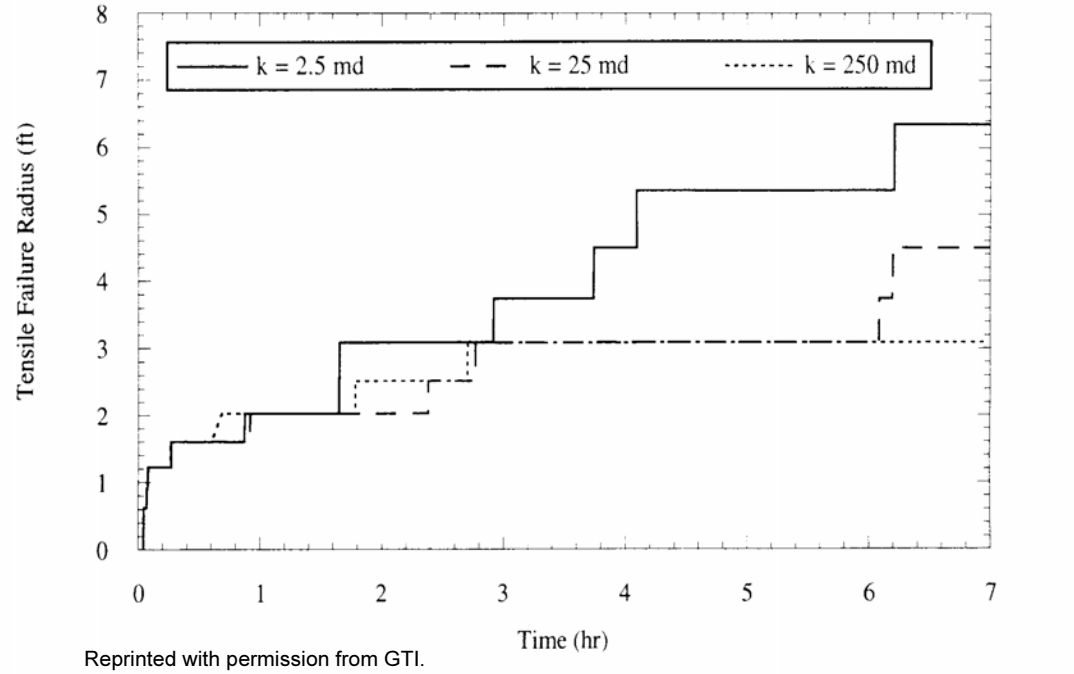

Reprinted with permission from GTI.

Figure 6.4-4. Interpreted Cavity Radii (Based on Tensile Failure Radii) from Khodaverdian et al. (1996).

Table 6.4-2. Input Values and Experimental Results to be Used and Compared with DRSPALL Results.

Cycle	Pressure, MPa	Duration, s	Cavity Radius, m Best Estimate	Cavity Radius, m Range
1	3.8	300	0.31	.31 – .31
2	6.2	360	0.49	.49 – .61
3	10.1	660	0.61	.61 – .91
4	9.6	900	0.73	.61 – .91
5	11.0	1680	0.91	.91 – 1.65
6	11.4	1680	1.37	.91 – 1.8

6.4.3.3 Input Parameters

DRSPALL was set up for these runs to only model the wellbore from the cavity to the surface, with flow allowed in the annulus. Also, only gas (air) and coal particles were allowed to flow. The code was run in cylindrical symmetry to best match the observed cavity geometry. For each of the six runs required, an initial formation (repository) gas pressure was set to match the corresponding value in Table 6.4-2, and an initial cavity size was set to match the previous run results. The first cavity size is 0.31 m. Each run continued for the reported time. Recall that the duration of the last cavitation cycle is unknown, which adds additional uncertainty to the results for the last cavitation cycle.

DRSPALL results depend on the tensile strength and permeability assumed in DRSPALL. It is unclear as to the exact tensile strength Khodaverdian et al assumed. They discuss cohesion in detail as it pertains to shear failure, but not tensile strength explicitly. A tensile strength of 0.25 MPa (36 psi) and a permeability of 3.0E-15 m^2 (3.0 md) were used for these runs. The input file for Run 6 is referenced in WIPP PA (2003g). All other runs were the same, except for initial pressure, initial cavity size, and run time.

6.4.4 Results

The DRSPALL results for each of the six runs are in a CAMDAT file and are summarized in the diagnostic text file. The output data were imported to a Microsoft EXCEL spreadsheet for post-processing and graphing. Table 6.4-3 and Figure 6.4-5 show the results of the DRSPALL runs and the comparison with field results. The DRSPALL results are for tensile failed and fluidized radii. The shape and scale of the cavity radius as a function of cavitation time show reasonable agreement as demonstrated in Figure 6.4-5.

Table 6.4-3. Results Comparison.

Cycle	Cavity Radius, m	
	Field Inferred	DRSPALL Calculated
1	0.31	0.30
2	0.49	0.30
3	0.61	0.58
4	0.73	0.79
5	0.91	1.01
6	1.37	1.20

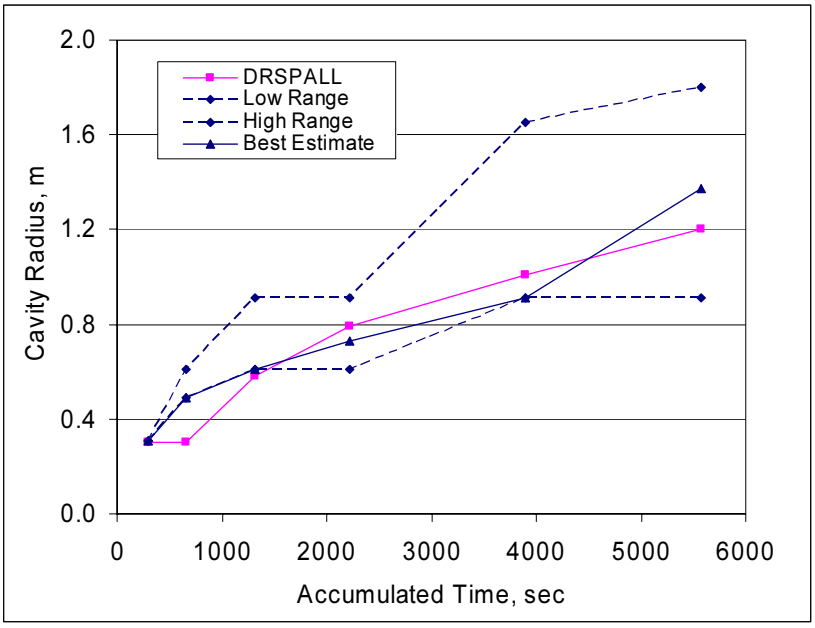

Note: Low, high and best estimates were derived from Figure 6.4-4 for k=250, 2.5 and 25 md (2.5e-13, 2.5e-15, 2.5e-14 m^2), respectively

Figure 6.4-5. Reported Field Results and DRSPALL Results Compared.

6.4.5 Conclusions

As discussed in section 6.4.2.2, the coalbed methane cavitation process is an acceptable analog to the WIPP drilling intrusion-created spalling process. The analog is good because of the similarities between the DRSPALL conceptual model and the coalbed cavitation process, both in behavior and scale. The coalbed methane test case demonstrates that DRSPALL reasonably simulates the coalbed methane cavitation process within the ranges of uncertainties of known data and values of parameters.

6.5 Summary of Verification/Validation Tests

The porous flow and wellbore flow tests verified that the two major flow models in DRSPALL were operating properly by successfully comparing output from DRSPALL and alternative computational tools for well-defined test problems. Moreover, the internal logic checks test problem verified that selected sub-models such as stress/failure and fluidization were also operating correctly by comparison to spreadsheet calculations. Finally, the coalbed methane test problem demonstrated that DRSPALL reasonably simulates the coalbed methane cavitation process within the ranges of uncertainties of known data and values of parameters. Taken as a whole, these tests give sufficient assurance that the model is operating within design requirements that it may be considered qualified for use in WIPP compliance calculations according to NP19-1 (Chavez, 2003) standards.

7 Sensitivity Study 1

This chapter documents sensitivity studies on the DRSPALL code. The objectives of this analysis are twofold:

1. To test the DRSPALL code stability over the entire parameter space possible in the WIPP Performance Assessment
2. To identify uncertain parameters that have the most impact on code output

Successful completion of this sensitivity analysis provides reassurance that the model will behave appropriately and stably when run in the broad parameter space encountered in the WIPP PA. Moreover, this analysis allows close inspection for proper implementation of the conceptual model by illustrating the relationships between key inputs such as pressure and tensile strength and outputs such as tensile failure radius and total spall release.

7.1 Problem Setup

This analysis focuses on the relationship between uncertain input parameters and code output, addressing what is referred to as *subjective* uncertainty in the WIPP PA context. Uncertainties related to time of intrusion, number of previous intrusions, etc., referred to as *stochastic* uncertainty in WIPP PA, are not addressed here. Rather, these are handled when results from this code are passed to the WIPP PA code CCDFGF (WIPP PA, 2003h) that generates comprehensive cumulative distribution functions (CCDFs).

7.1.1 Parameter Sampling

Latin Hypercube Sampling (LHS) (Helton and Davis, 2002) was used to generate the sampled input parameters sets. LHS is a Monte Carlo technique that is frequently used in uncertainty and sensitivity analyses of complex models. The technique was chosen here due to (a) conceptual simplicity and ease of implementation, (b) robust sampling over the full range of variability of each sampled variable, and (c) it is the current standard for sampling uncertain parameters used in WIPP PA.

DRSPALL requires more than 60 input parameters in order to execute, with a complete list given for vector 1 in Appendix INPUTS. Within this list, fifteen parameters were deemed sufficiently uncertain and potentially important to code output that they were sampled in the sensitivity analysis described here. Two parameter samplings were run, with the only difference being that the repository gas pressure range was varied from 8-15 MPa in the first sampling, and 12-15 MPa in the second sampling. Table 7.1-1 shows the parameter names, ranges, and distribution types used for the first sampling. Note that the second sampling is identical except for constraining the pressure range to 12-15 MPa. The reason for running the second sampling was that most of the spall failure and thus interesting model behavior occurs only at pressures above 12 MPa, and the second sampling allowed for more output resolution in the parameter space that leads to spalling. The rationale for the endpoints of the sampled parameters is presented in the Parameter Justification Report for DRSPALL

(Hansen et al., 2003). The distributions take two forms, either uniform or loguniform. In the event that the endpoints range over more than one order of magnitude, the distribution is loguniform. Relative to a uniform distribution, loguniform biases the sampling toward the low end of the range, deemed a conservative assumption in all four cases because low values of waste permeability, tensile strength, wellbore wall roughness, and drilling damaged zone (DDZ) permeability are understood to lead to higher or more likely spallings releases.

Table 7.1-1. Summary of Sampled DRSPALL Input Variables Including Range and Distribution.

Variable Name	Description	Units	Distribution	Low	High
REPIPRES	Repository gas pressure	Pa	UNIFORM	8.00E+06	1.50E+07
REPIPOR	Porosity of waste	-	UNIFORM	0.35	0.66
REPIPERM	Permeability of waste	m^2	LOGUNIFORM	2.40E-14	2.40E-12
POISRAT	Poisson's ratio of waste	-	UNIFORM	0.35	0.43
TENSLSTR	Tensile strength of waste	Pa	LOGUNIFORM	1.20E+05	1.70E+05
DNSFLUID	Initial mud density	kg/m^3	UNIFORM	1140	1380
VISCO	Initial mud viscosity	Pa s	UNIFORM	5.00E-03	3.00E-02
MUDSOLMX	Max solids volume fraction in mud	-	UNIFORM	0.59	0.64
MUDSOLVE	Solids viscosity exponent	-	UNIFORM	-1.8	-1.2
DRILRATE	Drill penetration rate	m/s	UNIFORM	2.96E-03	5.93E-03
MUDPRATE	Mud pump rate	m^2/s	UNIFORM	1.61E-02	2.42E-02
DDZPERM	DDZ permeability	m^2	LOGUNIFORM	1.00E-15	1.00E-13
ANNUROUG	Wall roughness	m	LOGUNIFORM	5.00E-05	3.10E-03
SHAPEFAC	Particle shape factor	-	UNIFORM	0.1	1.0
PARTDIAM	Particle diameter	m	UNIFORM	1.00E-03	1.00E-02

7.1.2 Code Flow for Sensitivity Study

The sensitivity study requires that a series of codes be run in order to create the input files, execute DRSPALL, and view the output. Input files are created by pre-processors, while output data are read and displayed by post-processors. The general code flow is shown in Figure 7.1-1 and Figure 7.1-2.

The first step requires running GENMESH (WIPP PA, 1996e) to create a binary CAMDAT[4] (Rechard, et al., 1993) file with a simple computational grid. Next, MATSET (WIPP PA, 2001) is run to create materials and properties and assign parameter values to the properties

[4] A CAMDAT is a special binary file that uses a self-describing structure to store Finite Element data such as the grid, boundary conditions and material properties. It is used extensively in WIPP PA analyses for input and output data and as a data link between analysis software and graphics packages.

in the CAMDAT file. The input file to MATSET specifies all material names and default property values. The output from MATSET is a template CAMDAT file that is read directly by LHS (WIPP PA, 1996f).

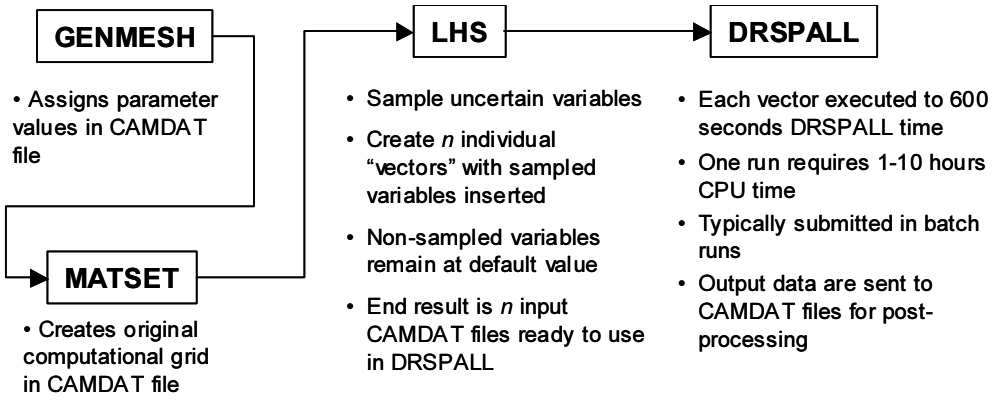

Figure 7.1-1. Code Flow Diagram for DRSPALL Pre-Processors.

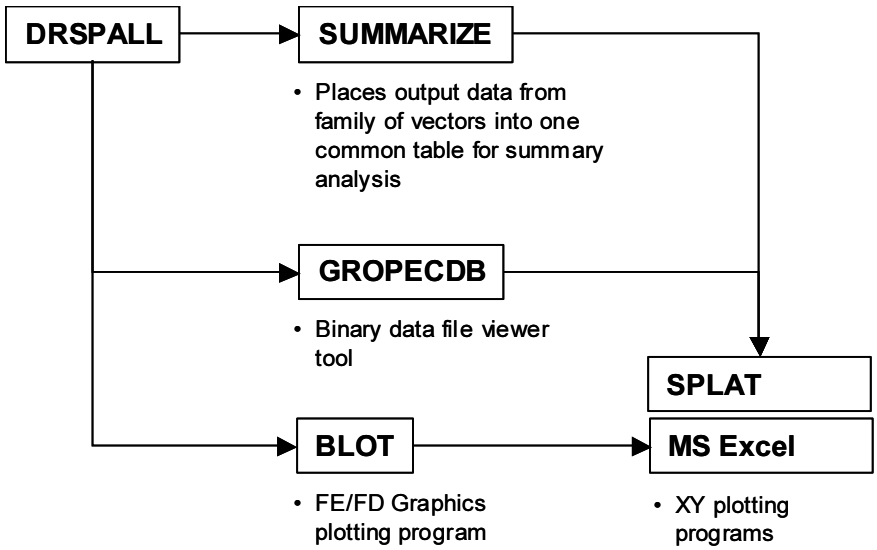

Figure 7.1-2. Code Flow Diagram for DRSPALL Post-Processors.

The third step requires running LHS to create *n* individual output vectors containing unique sets of input variables, where $n = 50$ in this case. The input to LHS includes the CAMDAT file created by MATSET and a text input file that gives the ranges and distribution types for sampled variables. Output from LHS appears in both ASCII and binary format. The ASCII file is in tabular format, with an example given in Appendix S1_LO_TRN. The binary output appear as *n* individual CAMDAT files (1 per vector) that serve as input to DRSPALL.

The next step requires submitting one DRSPALL run per vector. DRSPALL requires two input files to run: an input control file (*.DRS) and a CAMDAT file (*.CDB). An example input control file is given in Appendix DRS. Runs are typically submitted in batch mode. This analysis ran 4 samples (2 pressure ranges × 2 geometries) of 50 vectors each, requiring a total of 200 DRSPALL runs. All runs were executed to 600 seconds in DRSPALL time. This run time was determined by repeated trial and error in the model development process. Inspection of the output will reveal that drilling, tensile failure, fluidization, and spall releases to the surface all settle to steady values by 600 seconds. As such, there is no new information gained from running the code out longer.

Post-processing DRSPALL output takes two primary paths. The binary data from 50 runs can be summarized into one aggregate ASCII table for querying and analysis in a database or spreadsheet. Alternatively, the binary data may be read directly into a plotting program like BLOT (WIPP PA, 1996a), or preprocessed for input to SPLAT (WIPP PA, 1996c) for direct observation of history or spatial variables.

7.1.3 System Specifications

This analysis was run on the Open VMS 7.3-1 operating system at Sandia National Laboratories, Carlsbad, NM. Runs were submitted to Compaq Alpha ES40, ES45, and 8400 machines, with a total of 20 processors available for computations.

7.2 Output Variable Definitions

A comprehensive list of variable definitions is given in Appendix VG. Of interest in this sensitivity study are:

- Radial variables
  - Cuttings radius (DRILLRAD)
  - Cavity radius (CAVRAD)
  - Tensile failure radius (TENSRAD)
- Pressure variables
  - Cavity pressure in repository (CAVPRS)
  - Flowing bottomhole pressure in wellbore (BOTPRS)
- Equivalent uncompacted volume
  - Cuttings volume (CUTVOLEQ)
  - Spallings (SPLVOL2)
- Velocity variables
  - Waste boundary superficial velocity (WBSUPVEL)
  - Minimum fluidization velocity (FLUIDVEL)
- Spatial Variables
  - Pore pressure (POREPRS)
  - Radial elastic stress (RADELSTR)
  - Radial seepage stress (RADSPSTR)
  - Radial effective stress (RADEFSTR)

7.2.1 Radial Variables

The radius is a key variable to understand in the DRSPALL model because spatial variables in the 1-D cylindrical and spherical geometries are all expressed as a function of radius. The origin for the cylindrical geometry is a line down the center of the borehole denoting the axis of symmetry (Figure 7.2-1). The origin for the spherical repository domain is a point where the axis of the drillbit first touches the top of the repository. The three primary radial variables in DRSPALL output are the drill cuttings radius, cavity radius, and the tensile-failed radius. The relationship among these three is demonstrated in Figure 7.2-1. The easiest place to start is with the cutting radius. This represents the position of the drillbit face in the repository. In most cases run here, drilling is the only mechanism that expands the cavity radius, so the drill radius and cavity radius will overlay. In the event of spallings, however, the cavity radius may actually grow larger than the drilled radius. This implies that in the assumed 1D geometry the spallings mechanism has removed material ahead of the drill bit. This could represent spall occurring either in front the drill bit or circumferentially, but, the two mechanisms can not be distinguished in the 1D DRSPALL geometry. A third radial variable, tensile-failed radius, is also important to monitor because this variable identifies solid material that has failed due to the stress state, but has not mobilized into the flow stream. This may or may not be larger than the cavity radius, but it can never be smaller. Figure 7.2-1 shows a situation in which material has failed out ahead of the bit, but has not fluidized and therefore forms a bed of disaggregated material subject to fluidization as the gas velocity reaches a sufficiently high value.

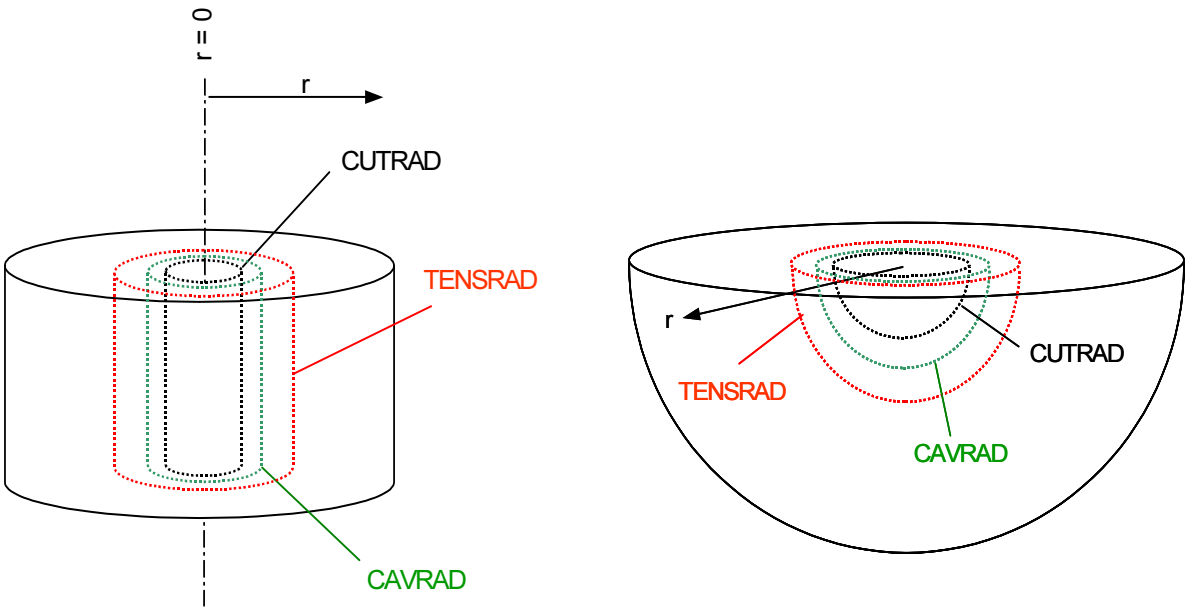

Figure 7.2-1. Radial Variables in Cylindrical Geometry and Spherical Geometry.

7.2.1.1 Mapping the Cuttings Radius in DRSPALL Geometry

Drill cuttings in the real 3-D system are mapped to an equivalent 1-D cuttings radius by conserving the surface area of the expanding cavity. For the cylindrical geometry, this involves starting with a narrow cylinder that extends through the entire repository height along the drilling axis, and expanding the radius as the real bit penetrates downward. For the spherical geometry, this requires defining a small hemisphere that has its origin at the point where the drillbit would first intersect the repository, and expanding this hemisphere radially as the bit proceeds. Drilling continues in both geometries for the amount of time required for a real bit to penetrate the entire depth of the repository. This implies that the rate of areal expansion of the drilled cavity is the same in all systems. A schematic of the mapping is given in Figure 7.2-2 for the spherical geometry at the point when drilling is complete for a repository of height = 1.23 m. The length scale on the figures is equivalent. The equivalent cavity radius in DRSPALL in this case is 0.45 m, which is nearly 1.5× the wellbore diameter, and about 1/3 of the repository height.

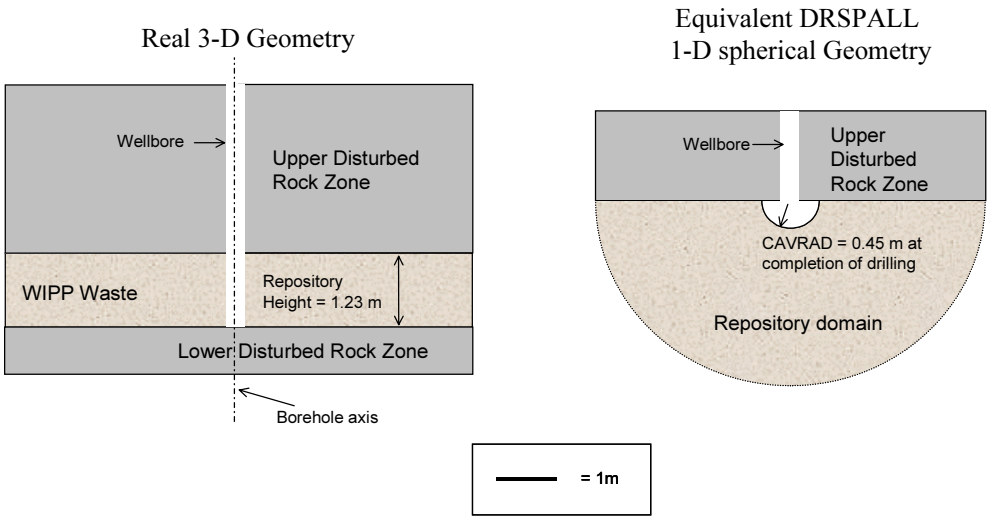

Figure 7.2-2. Schematic Mapping the Cavity Dimensions in the Real 3-D System to the 1-D Radially Symmetric Geometry in DRSPALL at Completion of Drilling.

7.2.2 Pressure Variables

The two pressure variables of interest prior to bit penetration are the pseudo-cavity pressure in the repository and the flowing bottomhole pressure in the wellbore. The pseudo-cavity is a small volume created in the repository in order to avoid forcing the gas to flow to a single point (spherical geometry) or line (cylindrical geometry) at the origin of the domain (see section 3.5.1.1). Upon bit penetration, the cavity and well bottom define the same region in the model domain and thus evaluate to the same pressure.

7.2.3 Equivalent Uncompacted Volumes

DRSPALL calculates the mass of repository solids ejected to the land surface. For the purpose of comparing these release masses to releases from CCA and PAVT (MacKinnon and Freeze, 1997) analyses, the DRSPALL expelled masses are converted to "equivalent uncompacted volume" units:

$$V_{eq} = \frac{m_s}{\rho_s(1-\phi_o)} \tag{7.2.1}$$

where V_{eq} is the equivalent volume prior to compaction, m_s is the solids mass ejected at the surface, ρ_s is the solids density, and ϕ_o is the porosity of a waste-filled room prior to closure. Values of ρ_s = 2650 kg/m^3 and ϕ_o = 0.85 (DOE, 1996: Appendix PAR, Table PAR-38) are used in this analysis.

7.2.3.1 Cuttings Volume - CUTVOLEQ

The equivalent cuttings volume is the repository volume removed by drilling action, related directly to the output variable DRILLRAD, converted to equivalent uncompacted volume units through Eq. (7.2.1).

7.2.3.2 Spallings Volume - SPLVOL2

The spallings volume reported here is the equivalent uncompacted volume of all repository zones removed by the spallings mechanism.

In DRSPALL the total volume removed is not necessarily equal to the sum of the cuttings volume (CUTVOLEQ) and the spallings volume (SPLVOL2) due to the equivalent one-dimensional geometry assumption and because total volume (TOTVOLEQ), CUTVOLEQ, SPLVOL2 are accumulated independently. In some cases spalling occurs out in front of the drilling process. The cuttings volume is the borehole volume that would be removed independent of spallings. The volume of material actually removed by drilling is the difference between total volume and spallings volume.

7.2.4 Velocity Variables

The minimum fluidization velocity (FLUIDVEL) and the waste boundary superficial velocity (WBSUPVEL) describe conditions at the cavity wall that either allow or prevent fluidized bed transport of disaggregated (failed) waste from the cavity to the wellbore. The minimum fluidization velocity derives from the fluidized bed theory developed by Ergun (1952), described in section 3.5.3. In the event that superficial gas velocity moving through a packed bed of particulate solids exceeds the minimum fluidization velocity, the bedded material will become fluidized and entrained in the flow stream. The waste boundary superficial velocity in DRSPALL is defined as the volume flow rate divided by the cavity surface area.

7.2.5 Spatial Variables

Stress and pore pressure profiles are given at selected times to illustrate the conditions leading to or preventing material failure. These variables were introduced in the Zone Size Sensitivity Study, section 5.3.

7.3 Results and Discussion: Spherical Geometry

The results of the sensitivity analysis are organized as follows:

- Summary of LHS-generated input pressures and final spall volumes on a vector-by-vector basis (spherical geometry)
- History plots for selected variables
- Scatter plots for correlating input and output data
- Cylindrical geometry – Full analysis and comparison with spherical geometry

7.3.1 LHS Samplings

LHS (WIPP PA, 1996f) was executed twice for this study (see section 7.1.1). Each sampling created 50 vectors, with the full results given in Appendices S1_LO_TRN and S1_HI_TRN. The 8-character variable names are defined in Appendix VG. The first sampling (LO) used a repository pressure range from 8-15 MPa, while the second sampling (HI) used a repository pressure range from 12-15 MPa. Provided that the same random seed is given to LHS in input, LHS produces the same values in both samplings for all variables other than pressure.

7.3.2 DRSPALL Final Spallings Volumes

While there are many output variables of potential interest in the spallings model, the item of most concern from a regulatory perspective is the volume of spalled solids that is released to the surface. This volume is ultimately multiplied by radionuclide concentration to yield a radionuclide release value that is weighed against regulatory standards (see section 9). Shown in Table 7.3-1 is the summary of spallings releases (SPLVOL2) for both the 8-15 MPa and 12-15 MPa runs. While the pressure ranges differ between samplings, the relative ranking of pressures is the same, so the largest releases resulting from high pressure in either sample set should fall among a common set of vectors. The median release volume of the 8-15 MPa observations was $\tilde{x} = 0$ m^3, and the mean release volume was $\bar{x} = 0.044$ m^3. The median release volume of the 12-15 MPa observations was also $\tilde{x} = 0$ m^3, but the mean release volume was expectedly higher at $\bar{x} = 0.092$ m^3. Median release volumes were zero in both cases because of the large number of vectors with no release.

Table 7.3-1. Summary of Equivalent Uncompacted Spall Volumes for Nonzero Release Vectors, Sorted by Descending Spallings Volume in the 12-15 MPa Runs.

	LO: 8-15 MPa		HI: 12-15 MPa	
Vector	REPIPRES (MPa)	SPLVOL2 (m^3)	REPIPRES (MPa)	SPLVOL2 (m^3)
5	14.2	0.832	14.7	1.454
46	13.3	0.341	14.3	0.509
22	13.7	0.266	14.4	0.487
1	13.5	0.297	14.4	0.393
23	14.8	0.339	14.9	0.368
44	12.8	0.000	14.1	0.358
26	10.0	0.000	12.8	0.258
24	13.2	0.043	14.2	0.199
29	13.0	0.052	14.1	0.187
47	11.6	0.000	13.6	0.129
12	14.0	0.006	14.6	0.061
9	11.2	0.000	13.4	0.054
18	14.6	0.028	14.8	0.038
21	12.4	0.000	13.9	0.038
14	9.8	0.000	12.8	0.028
33	14.4	0.000	14.7	0.028
28	11.9	0.000	13.7	0.005

7.3.3 Analysis of History Variables

In addition to looking at the summary output across a collection of vectors as presented above, it is instructive to review the progress of selected individual vectors in order to better understand the mechanisms controlling the release volumes. Vector 026 is chosen for examination here because for the first sampling with REPIPRES = 9.96 MPa it gave no spall release, but for the second sampling with REPIPRES = 12.8 MPa, it yielded a release of SPLVOL2 = 0.258 m^3.

7.3.3.1 Pressure History

Figure 7.3-1 and Figure 7.3-2 display the history variables well bottomhole pressure (BOTPRS) and cavity pressure (CAVPRS) for vector 026. Labeled for reference on these plots is the hydrostatic pressure at the well bottom. Notice that at time = 0, the well bottomhole pressure starts near hydrostatic pressure, while the cavity pressure representing the face of the repository starts at 10.0 MPa in Figure 7.3-1 and 12.8 MPa in Figure 7.3-2. As time progresses and the drillbit approaches the repository, the pressures converge due to gas bleed through the DDZ and become equivalent when the drill actually penetrates the

repository around 40 seconds. The bottomhole pressure continues to drop as the mud column is displaced by gas and blown out of the borehole. In an actual drilling operation in the field, the driller would recognize this as an increasing mud return rate, at which time he would likely close the blowout preventer. For the purpose of the WIPP PA, driller intervention is precluded and therefore no preventative steps are taken by the hypothetical driller. Once the mud is displaced by the repository gas and ejected to the surface, the bottomhole pressure stabilizes to less than 2 MPa as gas blowdown continues. Several spikes in pressure appear in the 12.8 MPa case (Figure 7.3-2) between 200 and 300 seconds. These correspond to failure and entrainment of repository solids into the flow stream. Combined factors such as increases in mixture density and viscosity, and numerical noise upon addition of discrete quantities of solids to the largely gas flow stream cause the spikes. Notice that the pressure history is smooth in the same time window in the 10 MPa case (Figure 7.3-1) where no spalling is observed.

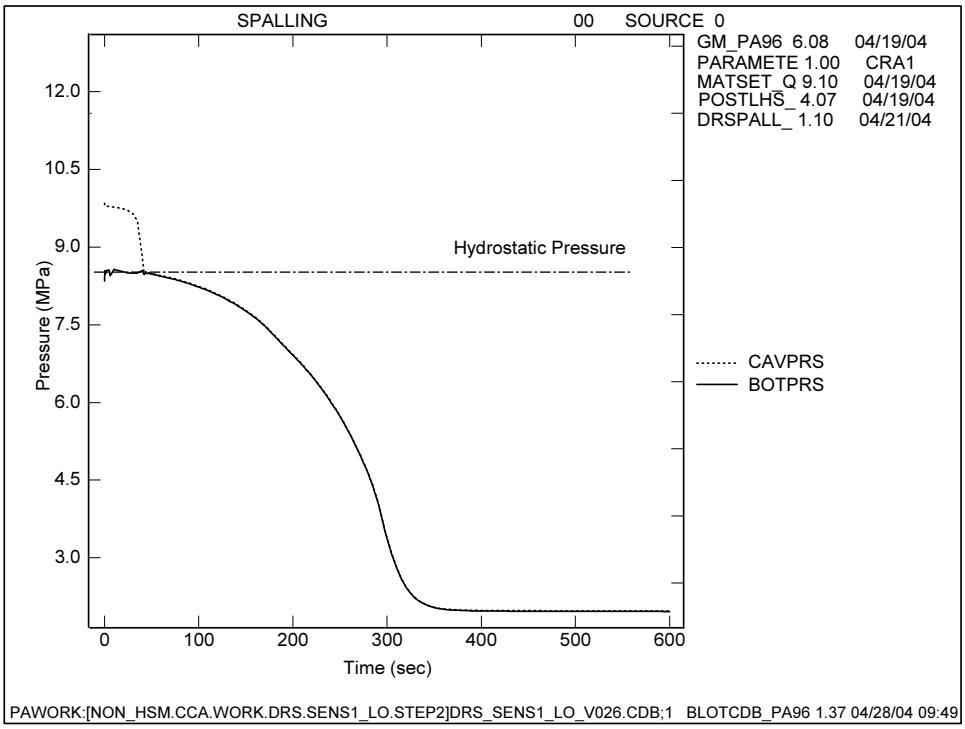

Figure 7.3-1. Pressure History Plot for V026, 10 MPa Initial Pressure.

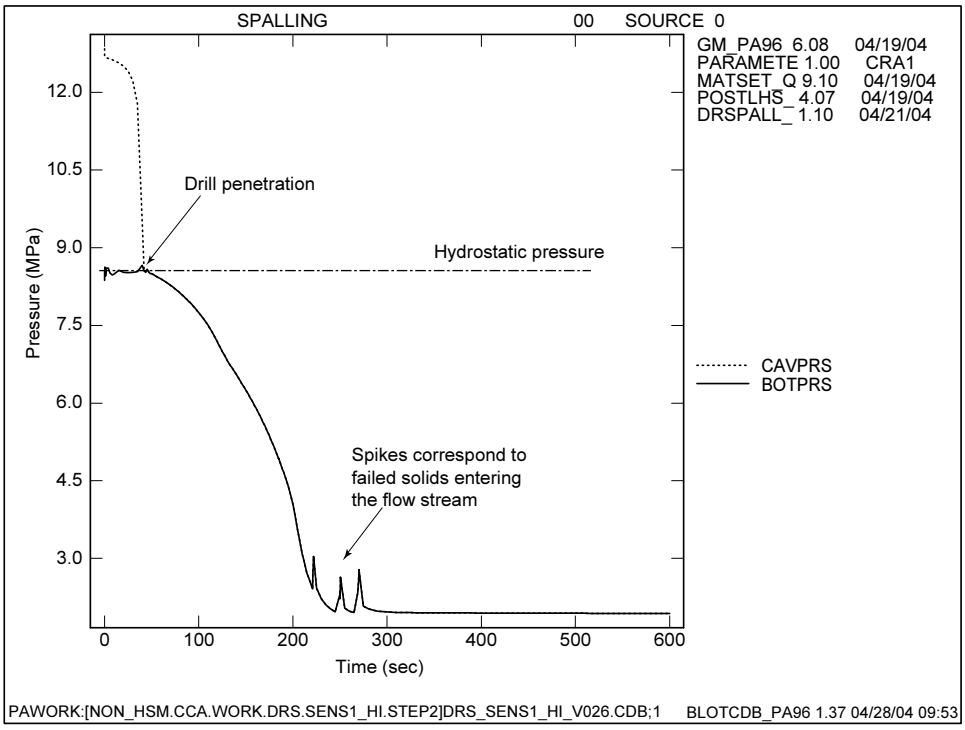

Figure 7.3-2. Pressure History Plot for V026, 12.8 MPa Initial Pressure.

7.3.3.2 Radius Variables

Figure 7.3-3 and Figure 7.3-4 display three radii that describe the progress of drilling (DRILLRAD), material failure (TENSRAD), and cavity growth (CAVRAD) in the hemispherical repository domain. All radii start at the small pseudo-cavity radius and remain there until the bit intersects the repository at about 40 seconds. The drillbit proceeds through the repository domain until drilling stops at about 300 seconds. The endpoint for drilling is set by the simple formula:

$$\text{drilling time} = \text{repository height}/\text{drill penetration rate} \tag{7.3.1}$$

Repository height varies directly with porosity (Eq. (3.5.23)), and porosity is a sampled variable (0.35 to 0.66), making repository height an indirectly sampled variable with values ranging from 0.9 to 1.7 m in this study. It is important to distinguish that the repository height is not a feature of the DRSPALL hemispherical domain, but rather a feature of the conceptual models for repository geometry and creep closure. The repository height concept is used in DRSPALL to yield a reasonable estimate for drilling time. In Figure 7.3-3 and Figure 7.3-4, the resulting final drilled radius in the spherical domain is about 0.41 m. The slight difference in final radii seen in Figure 7.3-3 is due to the different techniques used to calculate the variables. CAVRAD and TENSRAD are accumulated discretely in increments equal to the zone size as zone are removed due to drilling or tensile failure and fluidization. DRILLRAD is calculated algebraically using the bit radius and penetration velocity.

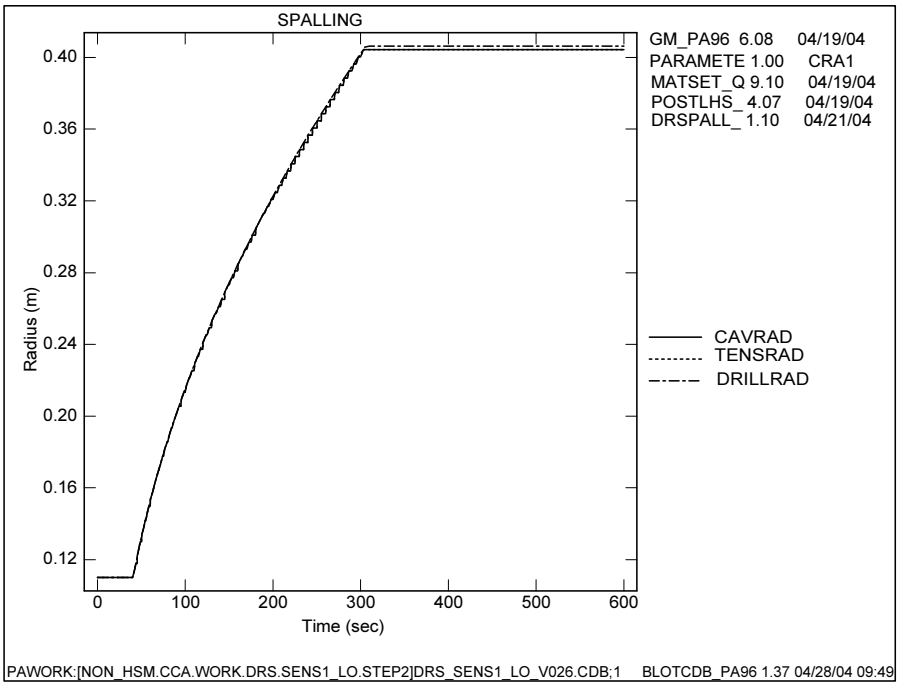

Figure 7.3-3. Radius Variables History Plot for V026, 10 MPa Initial Pressure.

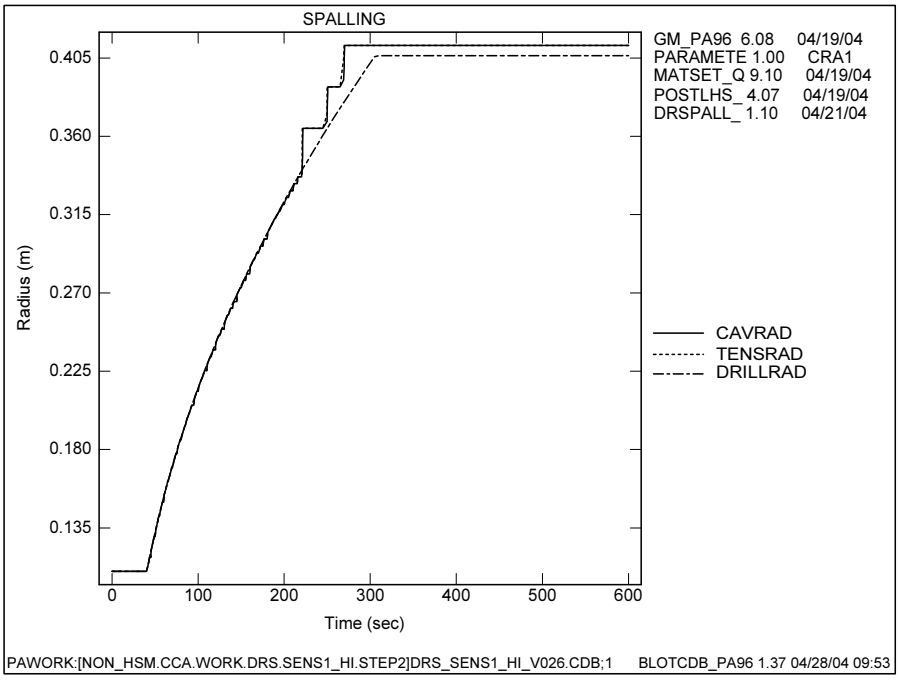

Figure 7.3-4. Radius Variables History Plot for V026, 12.8 MPa Initial Pressure.

The overlay of CAVRAD, TENSRAD, and DRILLRAD throughout the entire simulation in the 10 MPa case indicates that cavity growth is caused directly by drilling and there is no mechanical failure of repository material or cavity growth by the spalling mechanism. In contrast, TENSRAD and CAVRAD grow ahead of DRILLRAD starting at about 200 seconds in the 12.8 MPa run. The CAVRAD ultimately grows to a value of 0.412 m where it stabilizes. TENSRAD growth leads CAVRAD by a few seconds, but they generally stay together, indicating that the failed material readily fluidizes and transports into the wellbore domain.

7.3.3.3 Velocity History

Fluidization behavior can be confirmed by examining the velocity history for the 12.8 MPa run in Figure 7.3-5. When WBSUPVEL exceeds FLUIDVEL, failed solids are subject to fluidization. This condition is generally satisfied at times beyond 100 seconds in v026. The spikes in WBSUPVEL result from discrete zones in the repository domain dropping into the wellbore, and are largely numerical. The small regularly-sized and spaced spikes from 50 to 200 seconds represent zones dropped due to drilling. The large spikes from 200 to 300 seconds are the result of fluidization of failed material. The spalling/fluidization spikes are larger than the drilling spikes because the spalled material fails in 10-zone increments and the zones tend to fluidize in rapid succession, whereas the drilling liberates one zone at a time in a slow, steady fashion.

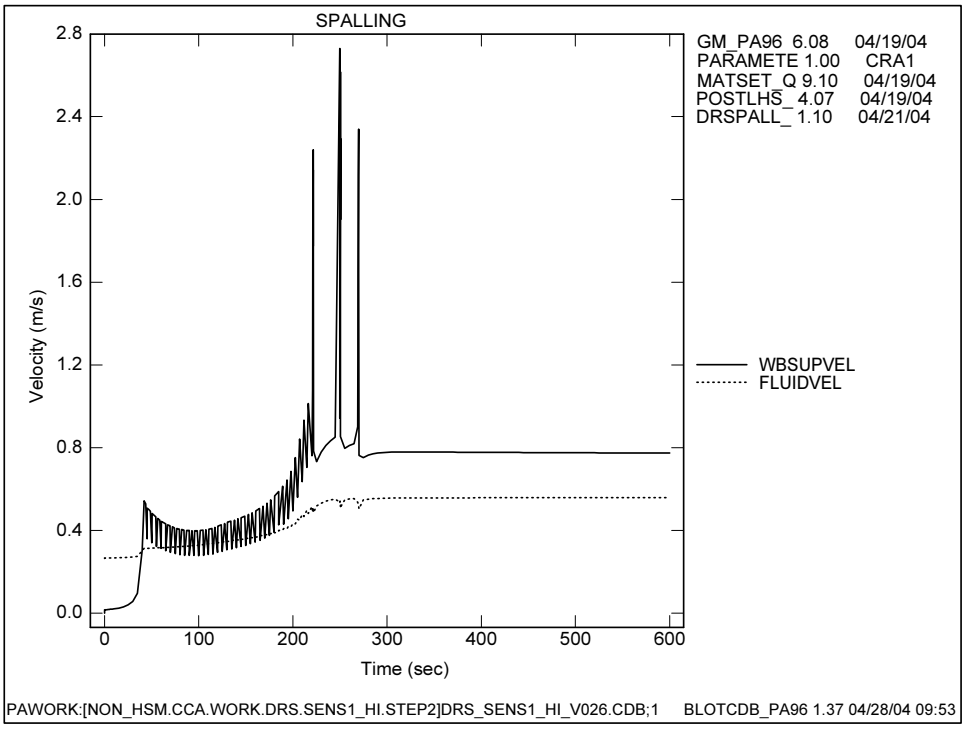

Figure 7.3-5. Velocity History Variables for V026, 12.8 MPa Initial Pressure.

7.3.3.4 Volume History

The volume history plots (uncompacted equivalent volume units) are shown in Figure 7.3-6 and Figure 7.3-7. For the 10 MPa run, all removed volume results from drilling with a final volume of CUTVOLEQ = 0.54 m^3 while SPLVOL2 remains at zero. In contrast, the 12.8 MPa run exhibits spalling starting at 200 seconds where the cavity volume expands rapidly until about 300 seconds where it stabilizes through the end of the simulation. The final SPLVOL2 for the 12.8 MPa run is 0.258 m^3 (see also Table 7.3-1).

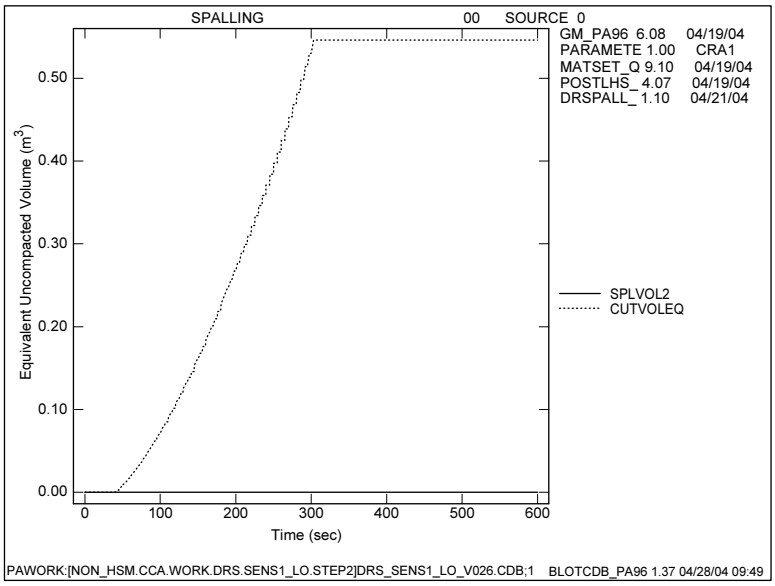

Figure 7.3-6. Volume History Variables for V026, 10 MPa Initial Pressure.

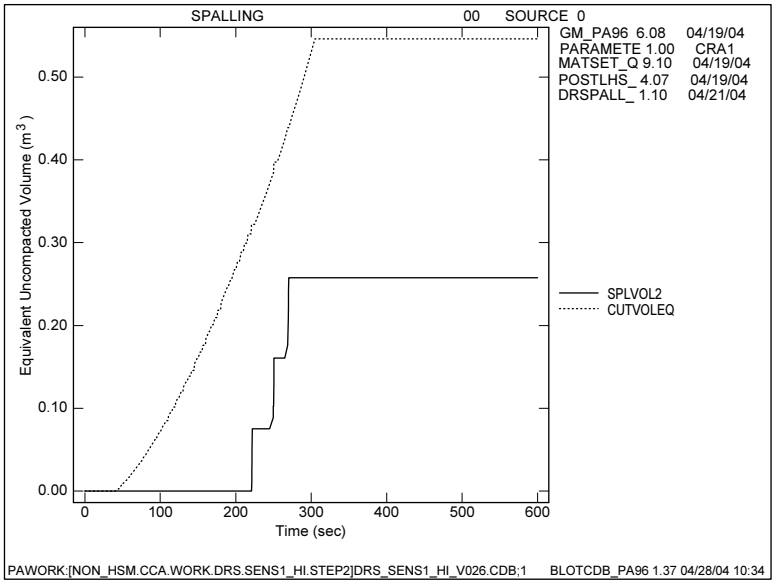

Figure 7.3-7. Volume History Variables for V026, 12.8 MPa Initial Pressure.

7.3.3.5 Summary of History Variables for V026

Since repository initial pressure is the only differing input between the v026 runs shown here, then it is logically the only factor causing a larger spallings release in the 12.8 MPa case. The larger pressure gradient local to the borehole in the 12.8 MPa case led to greater tensile stresses, more tensile failure, and more cavity growth (compare Figure 7.3-3 and Figure 7.3-4). The 12.8 MPa pressure also drove sufficiently high superficial gas velocity to fluidize failed waste (Figure 7.3-5), with a resulting higher volume of spalled material (compare Figure 7.3-6 and Figure 7.3-7).

7.3.4 Scatter Plots

In addition to reviewing tables of output data such as those presented above, model sensitivity may also be explored with scatter plots. A selected dependent variable such as equivalent uncompacted spall volume (SPLVOL2) at a late time in the run, typically 600 seconds, is plotted as a function of an independent variable such as initial repository pressure (REPIPRES). In this format, possible correlations are explored between the input and output variable by visually inspecting the results of all vectors on one set of axes. For the data shown here, the following dependent variables were explored:

- Equivalent uncompacted spall volume (SPLVOL2)
- Tensile radius – cutting radius (TENSRAD–DRILLRAD)

…as a function of the following independent variables:

- Repository initial pressure (REPIPRES)
- Repository permeability (REPIPERM)
- Waste tensile strength (TENSLSTR)
- Particle diameter × shape factor (PARTDIAM × SHAPEFAC)

For this analysis a new dependent variable is defined by computing the difference between the tensile-failed radius and the drilled or cuttings radius (TENSRAD-DRILLRAD). This new variable is depicted schematically in Figure 7.3-8. While not of particular interest to overall WIPP PA results, the difference between these two variables indicates the extent to which the repository material failed ahead of the ultimate drilled radius. This gives an indication of the potential for spallings, independent of how much material was fluidized and actually moved up the borehole. Tensile failure is a necessary precursor to spall release. In this sensitivity sample where the spall releases are typically small, this new intermediate variable helps to visualize the coupled mechanisms that control spall releases, and provides more resolution to the output.

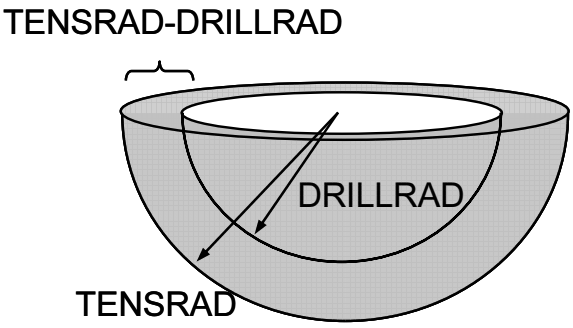

Figure 7.3-8. Schematic of Definition of TENSRAD-DRILLRAD Output Variable.

7.3.4.1 Repository Initial Pressure

Figure 7.3-9 shows SPLVOL2 and TENSRAD−DRILLRAD at 600 seconds plotted as a function of the initial repository pressure (REPIPRES). Each symbol corresponds to one vector, so for the two samplings shown, there are $2 \times 50 = 100$ vectors plotted on these axes. It is apparent from this figure that no vectors with REPIPRES < 12.5 MPa exhibited spallings. However, failure can occur down to about 11.0 MPa, as evidenced by the nonzero values for TENSRAD−DRILLRAD that occur between 11 and 15 MPa. Vectors that spall are thus a subset of the vectors that exhibit material failure.

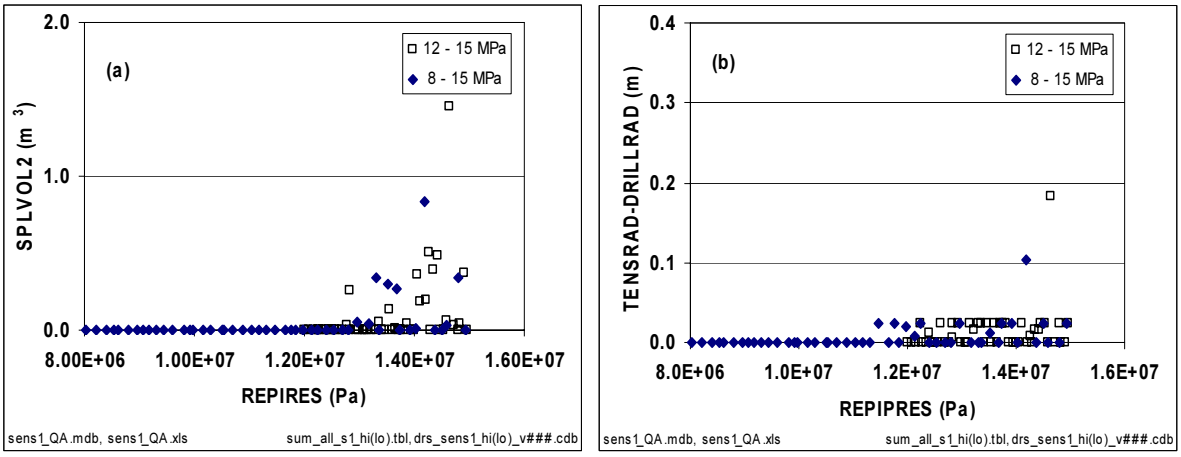

Figure 7.3-9. Scatter Plots of SPLVOL2 and TENSRAD-DRILLRAD vs. REPIPRES.

Repository pressure is a critical variable in the spallings model for several reasons. First, the stress state in the porous solid is a direct function of the pore pressure gradient formed between the far field and the wellbore. A larger pore pressure gradient leads to stresses of higher magnitude and more potential failure. Second, mobilization of tensile-failed solids requires a sufficient gas velocity for the loose particles to mobilize into the flow stream by fluidized bed theory. A minimum fluidization velocity defined by the Ergun model must be exceeded in order to mobilize waste. The gas velocity at the cavity face that causes fluidization is directly proportional to the pressure gradient at the cavity wall. Therefore, the

repository pressure relative to the wellbore pressure is a critical variable impacting the equivalent uncompacted spall volume releases. Put simply, higher repository pressure will fail, fluidize, and ultimately release more solids to the surface.

7.3.4.2 Waste Tensile Strength

Also potentially important in determining SPLVOL2 is the tensile strength of waste (TENSLTR). Figure 7.3-10 shows scatter plots with TENSLSTR as the independent variable. The spallings release (Figure 7.3-10(a)) exhibits reasonably uniform behavior throughout the sampled range of tensile strength. Though the sampling range is narrow, it represents the assumption that the waste form is a completely degraded granular material that is lightly cemented with a tensile strength from 0.12 to 0.17 MPa. Given that many of the materials in the WIPP waste stream begin much larger than the cm length scale and have much higher tensile strength than 0.17 MPa, the tensile strength range exercised in the DRSPALL model is exceedingly conservative and neglects the high end of the likely tensile strength distribution. See Hansen et al. (2003) for a continued discussion on the degraded waste assumptions.

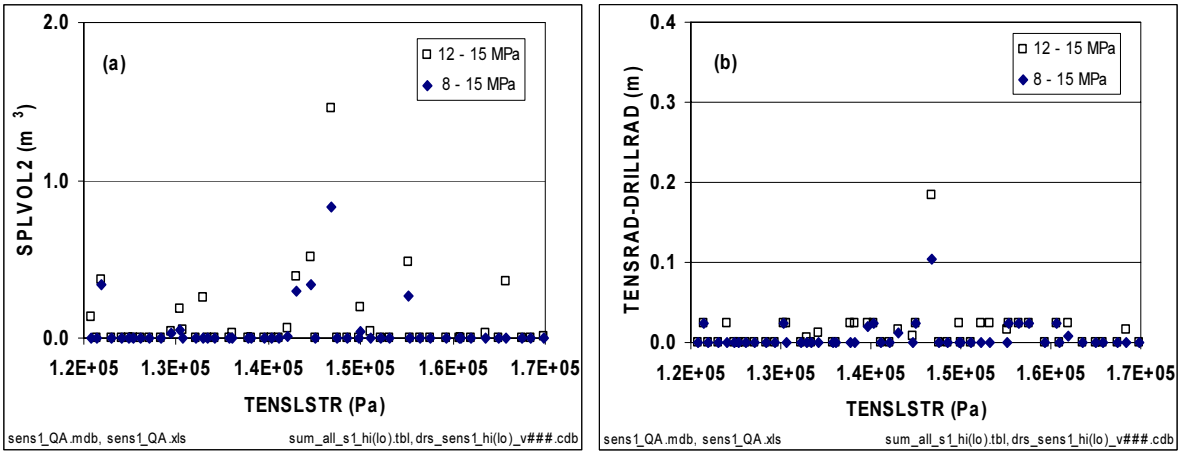

Figure 7.3-10. Scatter Plots of SPLVOL2 and TENSRAD-DRILLRAD vs. TENSLSTR.

The sensitivity of TENSRAD–DRILLRAD to TENSLTR is illustrated in Figure 7.3-10(b). No particular correlation is observed, with failure apparently just as likely over the range of tensile strength (0.12-0.17 MPa) examined. However, it can be seen that for a given tensile strength (or vector) higher pressure (12-15 MPa sample set) leads to more tensile failure.

7.3.4.3 Repository Permeability

Figure 7.3-11a shows SPLVOL2 plotted against the repository (waste) permeability (REPIPERM). Very little spalling release is observed for waste material with permeability above 7E–13 m^2 or below 8E–14 m^2. This is consistent with the design of the conceptual model that would suggest more failure with higher pressure gradients in less permeable media, but bounded at low permeability due to limited mobilization. For low values of

permeability, the fluid flow velocity is less likely to exceed the critical fluidization velocity. This is addressed in more detail in a subsequent section on the role of fluidization.

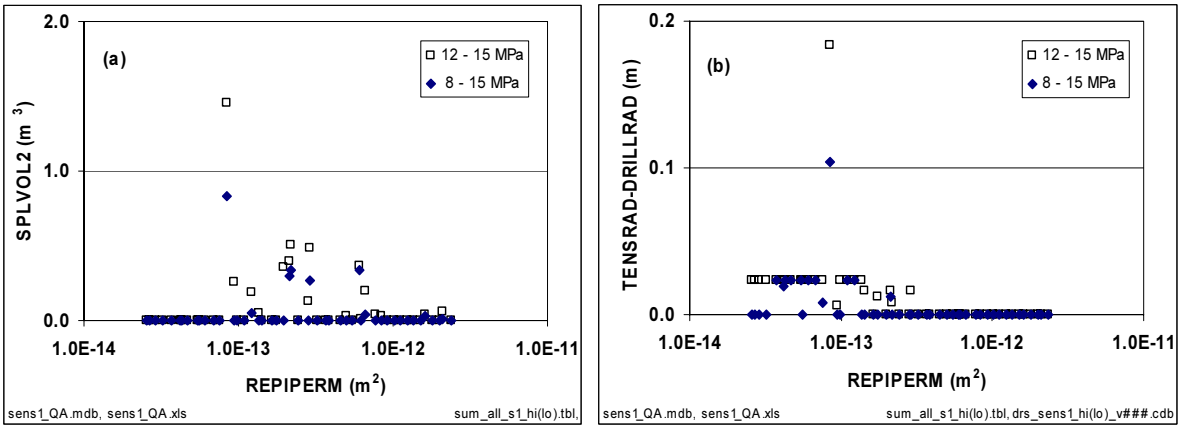

Figure 7.3-11. Scatter Plot of SPLVOL2 vs. REPIPERM.

Plotting the TENSRAD–DRILLRAD against repository permeability, shown in Figure 7.3-11b illustrates another important relationship. No failure beyond the drilled radius is observed for waste material with permeability above 3E–13 m^2. Alternatively, many failures are observed at permeability below 1E–13 m^2. For the high pressure set (12-15 MPa) all vectors with permeability below 1E–13 m^2 exhibited failure but none exhibited spallings below 8E–14 m^2. The frequently occurring TENSRAD-DRILLRAD value of 0.02 m at low REPIPERM is a result of failure over one characteristic failure length.

The several nonzero, but small, spallings volumes that occur in Figure 7.3-11 for permeability above 1E–12 m^2 are a result of spallings releases that start and stop during the drilling process. In these cases, drilling cavity growth subsequently catches up with and overtakes the spalled cavity radius. This is an inherent feature of the one-dimensional geometry in which material can only be removed from the domain by growing the radius.

7.3.4.4 Particle Diameter and Shape Factor

Particle diameter (PARTDIAM) and shape factor (SHAPEFAC) can become important to spall release volumes through their impact on the minimum fluidization velocity (Ergun, 1952, Hansen et al., 2003). These two factors appear as a product in Ergun's model and have the general effect of lowering the minimum fluidization velocity as their product is lowered. In physical terms, small or non-spherical particles in a packed bed are more likely to fluidize than large, spherical particles. The scatter plot shown in Figure 7.3-12(a) shows the relationship between the product SHAPEFAC×PARTDIAM and SPLVOL2. There is a tendency for larger spall release to occur with smaller independent variable and most of the activity occurs below a product of 3.0E–3 m. Recall that particle diameter is varied from 1 mm to 1 cm, while shape factor is varied from 0.1 to 1.0. TENSRAD–DRILLRAD shows failure across the whole range of the independent variable.

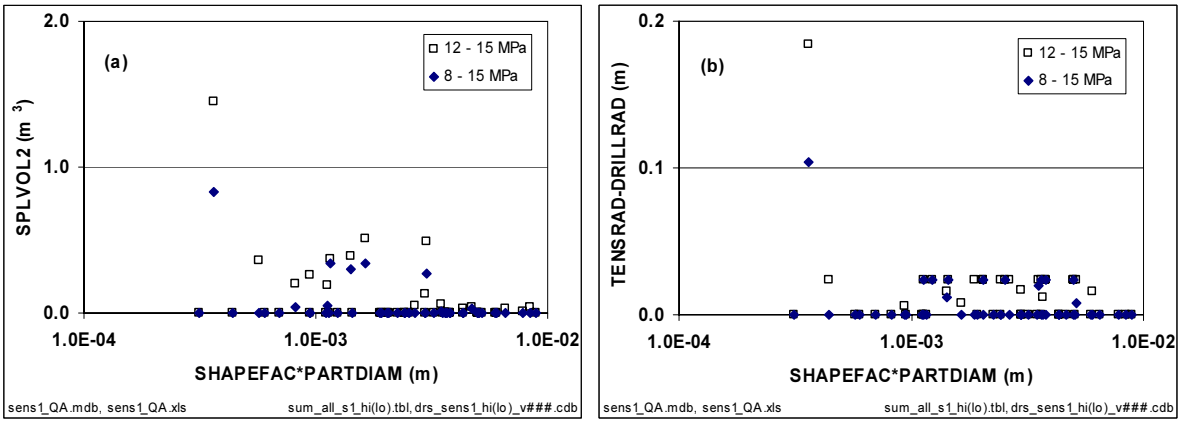

Figure 7.3-12. Scatter Plots of SPLVOL2 and TENSRAD-DRILLRAD vs. SHAPEFAC×PARTDIAM.

7.3.4.5 Role of Fluidization

Repository material that is released to the surface may be removed from the repository domain by either drilling or failure and fluidization (spalling). Sensitivity analysis on DRSPALL output must include some discussion of the role of fluidization because it is mechanistically important, though potentially overlooked in favor of stress and failure mechanisms. Failed material is not "released" unless it is also fluidized. The solution to the Ergun equation (Eq. 3.5.20) yields a minimum fluidization velocity (FLUIDVEL) that is compared to the superficial gas velocity at the cavity face (WBSUPVEL) to determine if failed material will fluidize. Thus, if WBSUPVEL > FLUIDVEL, then fluidization is active. Otherwise, failed material will remain bedded. To visualize the frequency with which fluidization is active, a scatter plot was created in Figure 7.3-13 in which FLUIDVEL and WBSUPVEL were plotted versus REPIPERM at 400 seconds, a time shortly after the end of drilling in most vectors. WBSUPVEL correlates strongly with REPIPERM with higher permeability allowing higher gas velocity. Where WBSUPVEL exceeds FLUIDVEL for a particular vector, any failed, bedded material will be swept into the wellbore flow stream. Note that the occurrence of WBSUPVEL > FLUIDVEL is non-existent at REPIPERM< 8.0E−14 m^2. Thus, it is difficult to mobilize failed waste when permeability is low. The implication of this in spall volumes is apparent in Figure 7.3-11 where SPLVOL2 is zero for REPIPERM< 8.5E−14 m^2. Vectors that exhibit terminally bedded material are called fluidization-limited.

While high superficial gas velocity is one way to promote fluidization, another possibility is low minimum fluidization velocity. The Ergun (1952) equation is quite sensitive to the product of particle shape factor and particle diameter (SHAPEFAC×PARTDIAM). Low values of both of these input variables drive FLUIDVEL similarly low as shown in Figure 7.3-14 (see Hansen et al, 2003 for more discussion). Their impact on SPLVOL2 was shown in Figure 7.3-12. Here, spallings release is observed most frequently when SHAPEFAC×PARTDIAM < 3E−3 m. This is a manifestation of the fact that 1mm, tabular particles (SHAPEFAC → 0.1) are easier to fluidize than 10mm spherical (SHAPEFAC → 1.0) particles.

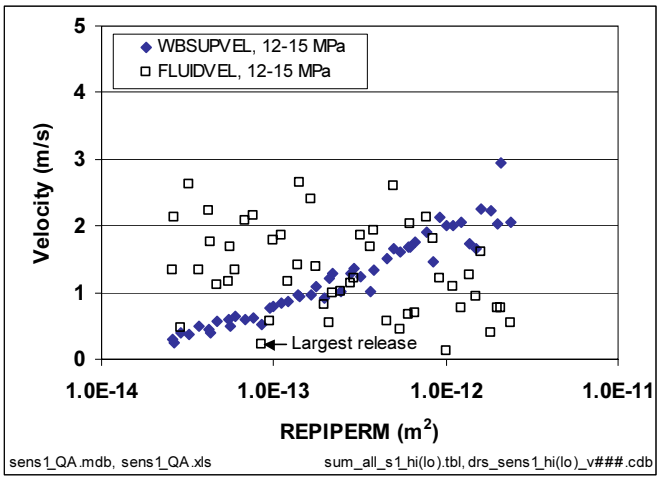

Figure 7.3-13. Scatter Plot of Velocity vs. REPIPERM.

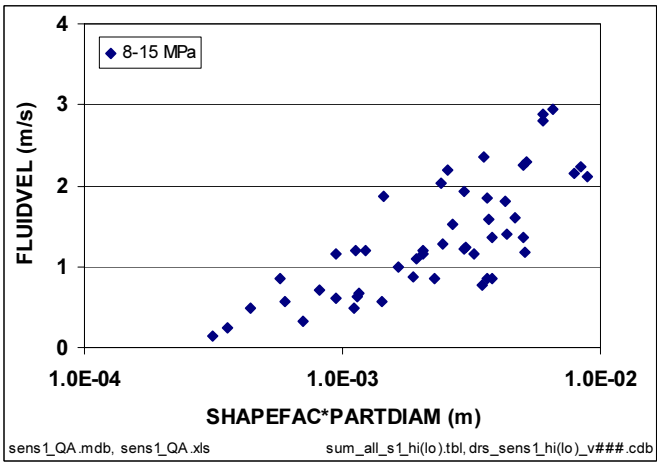

Figure 7.3-14. Scatter Plot of FLUIDVEL vs. SHAPEFAC×PARTDIAM.

7.3.4.6 Other Variables

The preceding discussion addresses the sensitivity of DRSPALL output to five of the fifteen uncertain variables that were sampled by LHS. The remaining ten sampled variables were analyzed in a similar manner and found to have no apparent systematic impact on SPLVOL2 or TENSRAD-CUTRAD. These scatter plots are presented in Appendix S1_LO_SCATTER and S1_HI_SCATTER.

An exception is the drilling rate (DRILRATE) for which spalling releases occur more frequently over the lower half of the range. A constant value of DRILRATE= 4.445e-3 m/s was selected for use in subsequent analyses. This value is the median of the distribution (range 2.96e-3 to 5.93e-3 m/s) and is at the high end of the range where spalling occurs. The largest spallings release occurs very near this value.

7.4 Results and Discussion: Cylindrical Geometry

The purpose of this discussion is to compare the results of cylindrical versus spherical repository model geometry for the same set of input parameters. For the discussions in the remainder of this section, the high pressure set of 50 runs used in the original sensitivity study presented in section 7.3 were repeated with only the geometry input flag switched from hemispherical to cylindrical. All other sampled and numerical modeling parameters remained the same. The result was that zero spall release was calculated for all 50 vectors when using cylindrical geometry as compared to 17 vectors that had nonzero spall release when using spherical geometry (see Table 7.3-1).

In this section, histories (variable versus time) and profiles (variable versus repository radius) of intermediate results for vector 005 from the high-pressure sampled set are compared to demonstrate the effect of the one-dimensional model geometries. Vector 005 had the largest spall release in the original spherical sensitivity study. Profiles were taken at 240 seconds during tensile failure with spherical geometry. Note these profiles will have almost the same cavity surface area but different repository inner radii and drilled volumes because of the equivalent geometry assumption that conserves surface area.

7.4.1 History Variables

Figure 7.4-1 shows bottomhole (BOTPRS) and cavity (CAVPRS) pressure histories for the spherical geometry (a), and the cylindrical geometry (b). Small differences first appear at runtime ~30 sec, or near bit penetration. In the spherical geometry, cavity pressure at the face of the waste decreases from 14.6 to 8.1 MPa right before penetration, in cylindrical geometry, the cavity pressure decreases to 9.1 MPa right before penetration. Eventually, bottomhole pressure stabilizes at a lower value with the cylindrical repository geometry around 200 seconds. The spikes in pressure between 170 and 270 sec for the spherical case are a result of spalled waste entering the wellbore.

Figure 7.4-2 shows equivalent uncompacted spall (SPLVOL2) and cuttings (CUTVOLEQ) volume histories and clearly reveals the spall releases in the spherical case (1.5 m^3 at 600 seconds). In contrast, volume removal in the cylindrical geometry is due strictly to cuttings, and SPLVOL2 remains at zero. Also evident is the difference in cuttings volume (final spherical CUTVOLEQ = 0.55 m^3, cylindrical CUTVOLEQ = 0.33 m^3) because the equivalent geometries do not conserve volume. Similar results are shown for cavity radius (CAVRAD), tensile failure radius (TENSRAD) and equivalent drilling radius (DRILLRAD) in Figure 7.4-3. The fact that CAVRAD and TENSRAD overlay in Figure 7.4-3(a) after 250 seconds indicates that any solid material that failed in tension was also fluidized. With no failure or spalling in the cylindrical geometry, all of the shown radii overlay for the entire simulation.

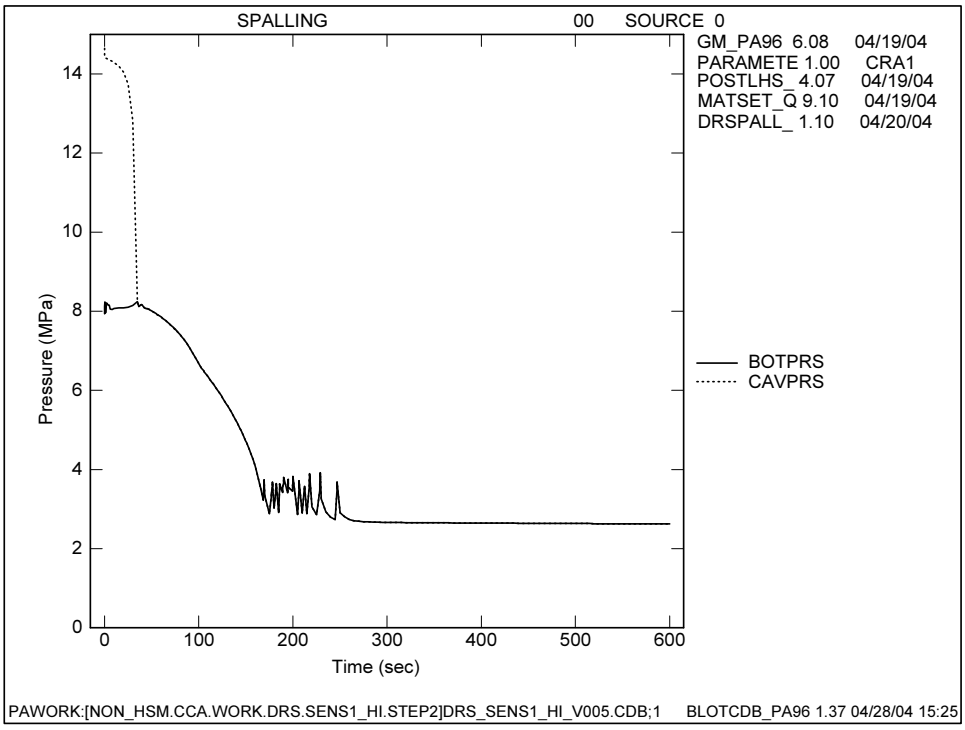

(a) Spherical

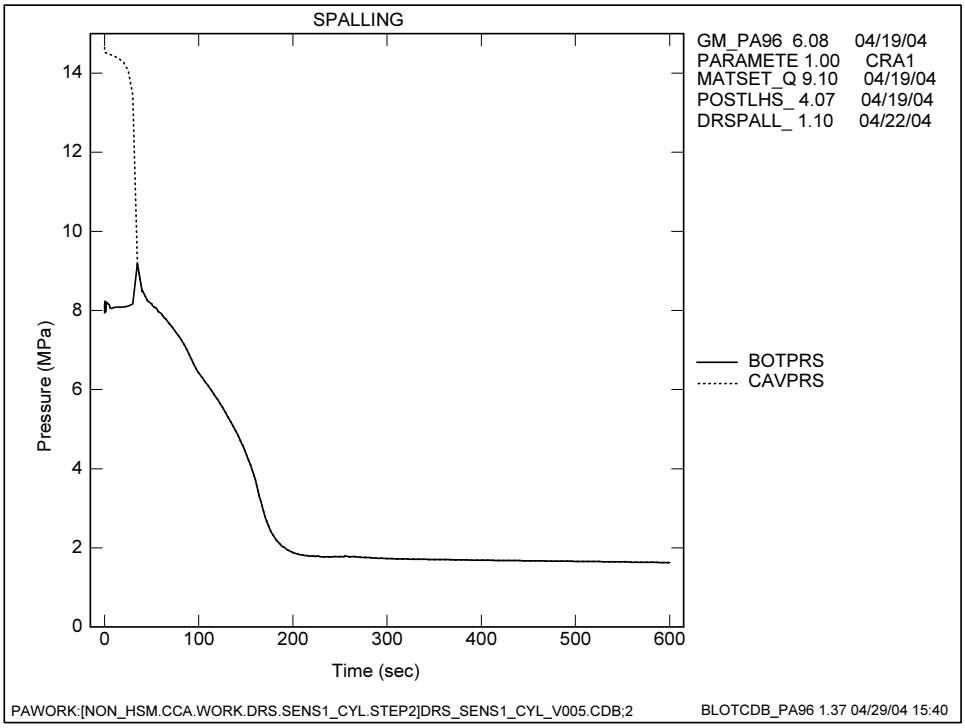

(b) Cylindrical

Figure 7.4-1. Bottom Hole and Cavity Pressure Histories.

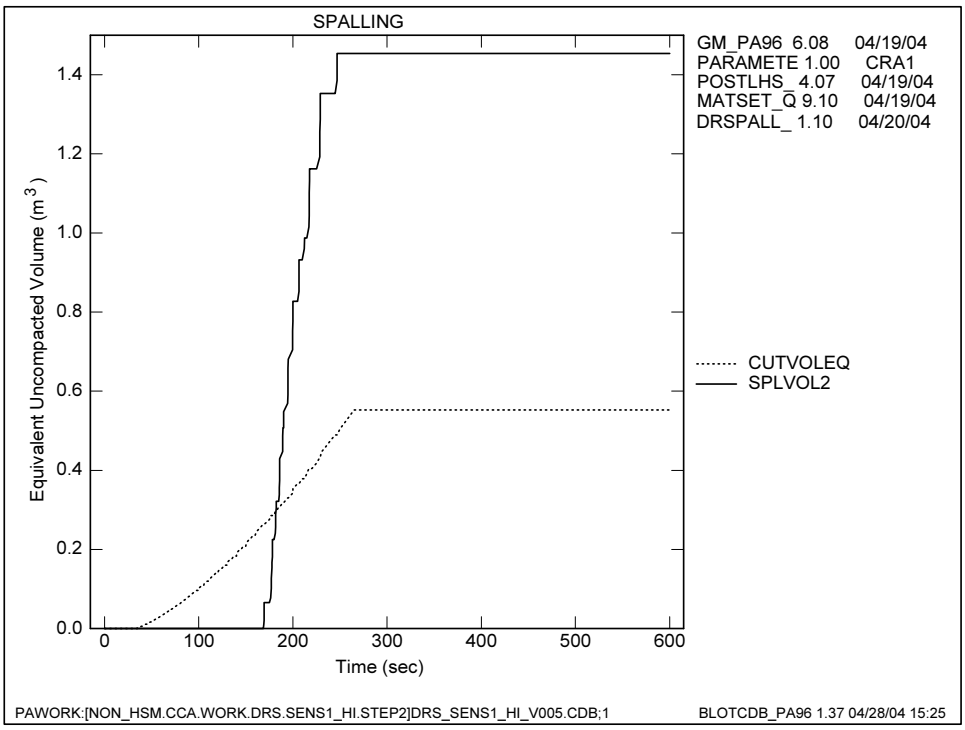

(a) Spherical

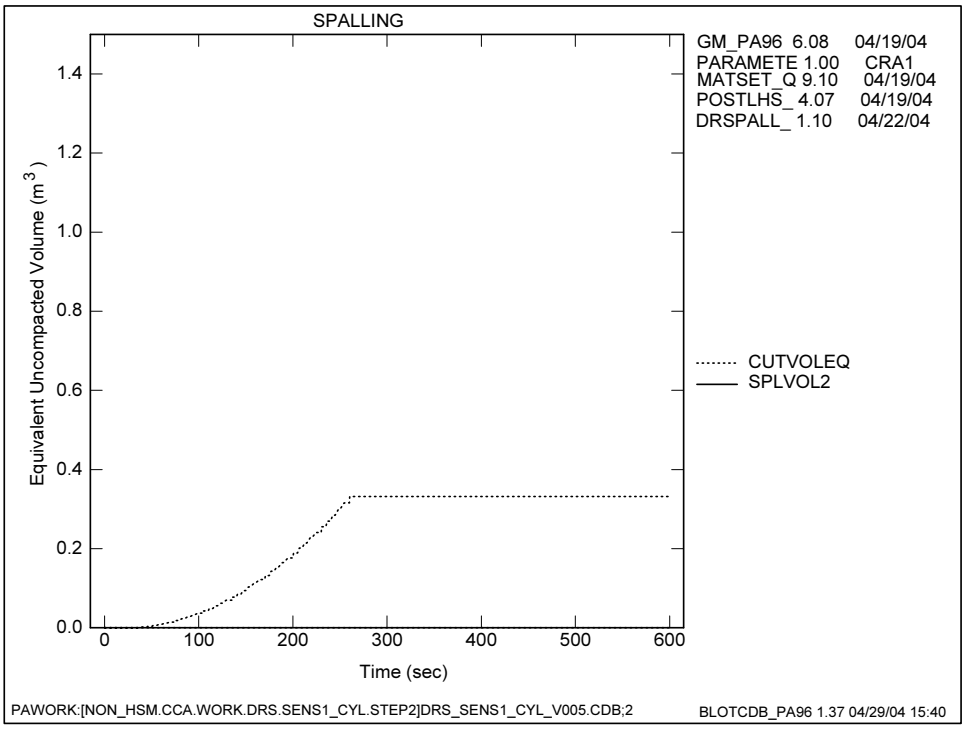

(b) Cylindrical

Figure 7.4-2. Cuttings and Spallings Volume Histories.

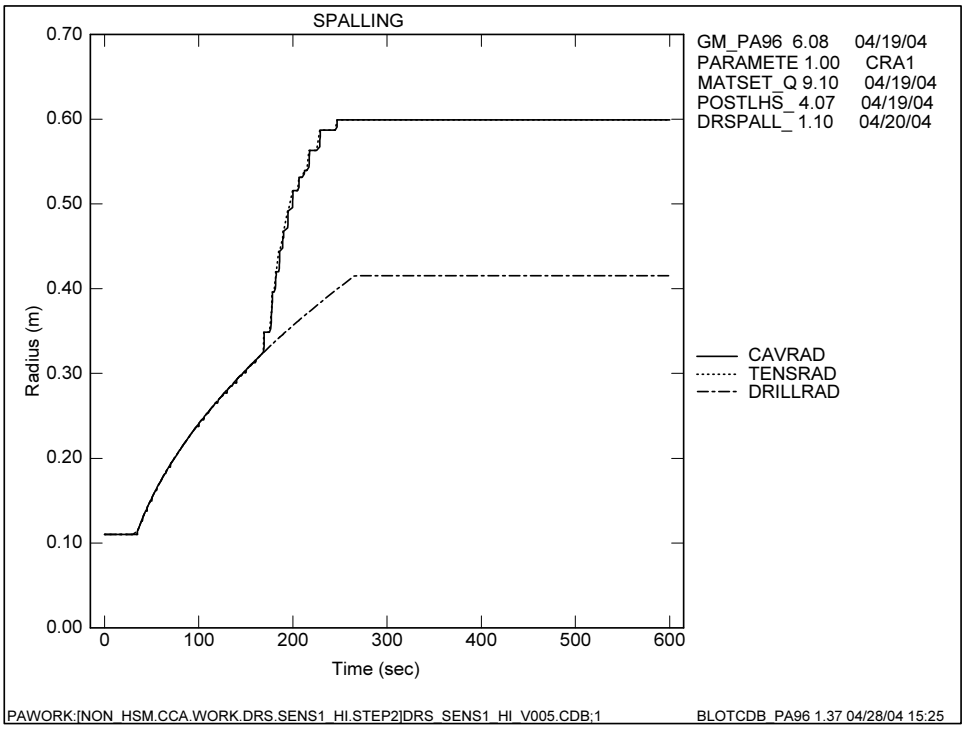

(a) Spherical

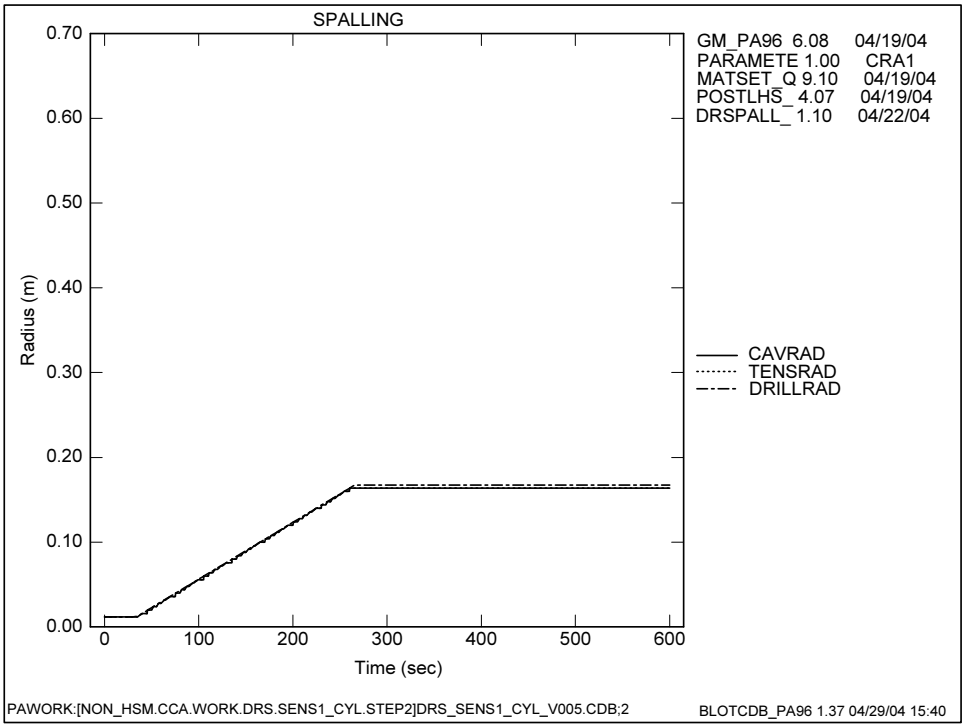

(b) Cylindrical

Figure 7.4-3. Cavity, Tensile and Equivalent Drilling Radii Histories.

Figure 7.4-4 shows fluidization velocity threshold (FLUIDVEL) and superficial velocity (WBSUPVEL) histories for the cell next to the wellbore. The cell comprising the cavity wall varies as material is drilled or fails and fluidizes. The superficial velocities are very similar until the time of spalling in the spherical geometry. Late time superficial velocity is higher in the cylindrical case because the wellbore interface is at a smaller radius (smaller flux area) due to no spall. In both geometries superficial gas velocity near the cavity face exceeded the fluidization threshold, indicating that spall release was limited by cessation of failure rather than by the fluidization mechanism.

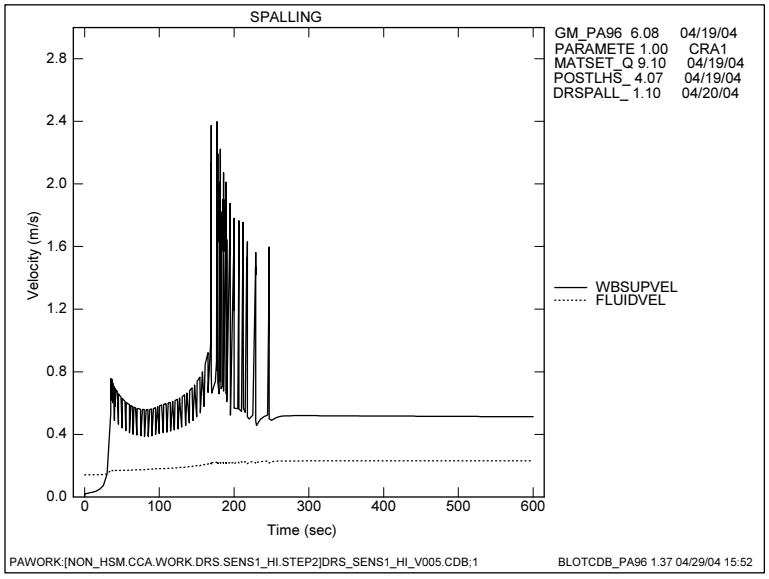

(a) Spherical

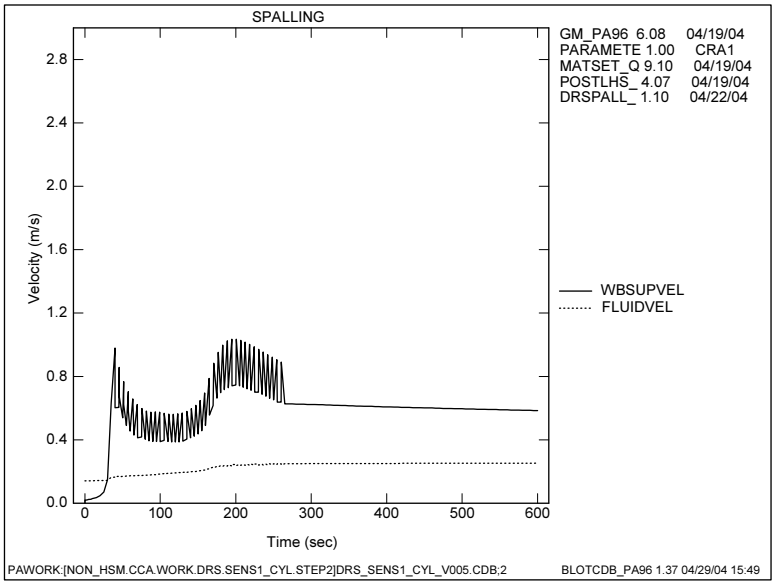

(b) Cylindrical

Figure 7.4-4. Fluidization Threshold and Superficial Pore Velocity Histories.

7.4.2 Spatial Variables

Figure 7.4-5 shows pore pressure (POREPRS), radial elastic stress (RADELSTR), and radial seepage stress (RADSPSTR) profiles at 240 sec during tensile failure. The effect of the geometry on gradients is apparent in pore pressure profiles, with the spherical case showing steeper gradients near the wellbore. This would also be expected in the elastic stress profile, however, the very small effective radius in the cylindrical geometry is strongly influencing the behavior near the well as was demonstrated earlier (section 3.6).

Figure 7.4-6 shows radial effective stress (RADEFSTR) profiles over the entire repository domain at 240s. Figure 7.4-7 zooms in on radial effective stress in the region near the cavity wall where the tensile phase develops. Note that on this figure the abscissa is relative to the wall rather than the center axis of the wellbore. Also, recall that radial effective stress is calculated from the elastic stress minus the pore pressure (Figure 7.4-5) plus the seepage stress and that its average value over a characteristic length (2.0 cm for this study) is compared to the tensile cutoff value to determine material failure. Therefore, its behavior is important in determining the effect of geometry on spall release. The seepage stress component is very similar for both geometries, indicating that the combined effects of geometry and differential pressure are similar in the two geometries. The peak compressive radial effective stress, however, is more than twice as large in the cylindrical case indicating the pore pressure has dropped more in the interior of the repository relative to the elastic stress. This is also evident in Figure 7.4-6. Close examination of the region near the cavity interface shows that radial effective stress does not go into tension in cylindrical geometry. In contrast, in the spherical geometry the phasing and relative gradients of the stress components develops a tensile phase right at the cavity interface that covers 5 cm and 12 zones. It is in this region that the average tensile stress may eventually exceed the tensile limit and cause failure.

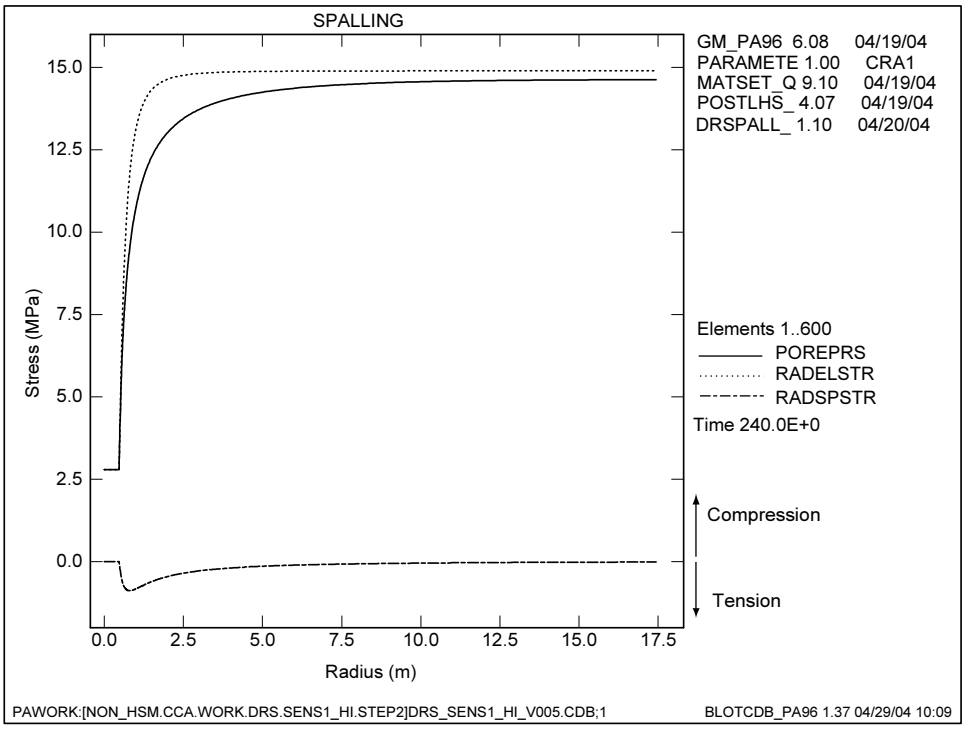

(a) Spherical

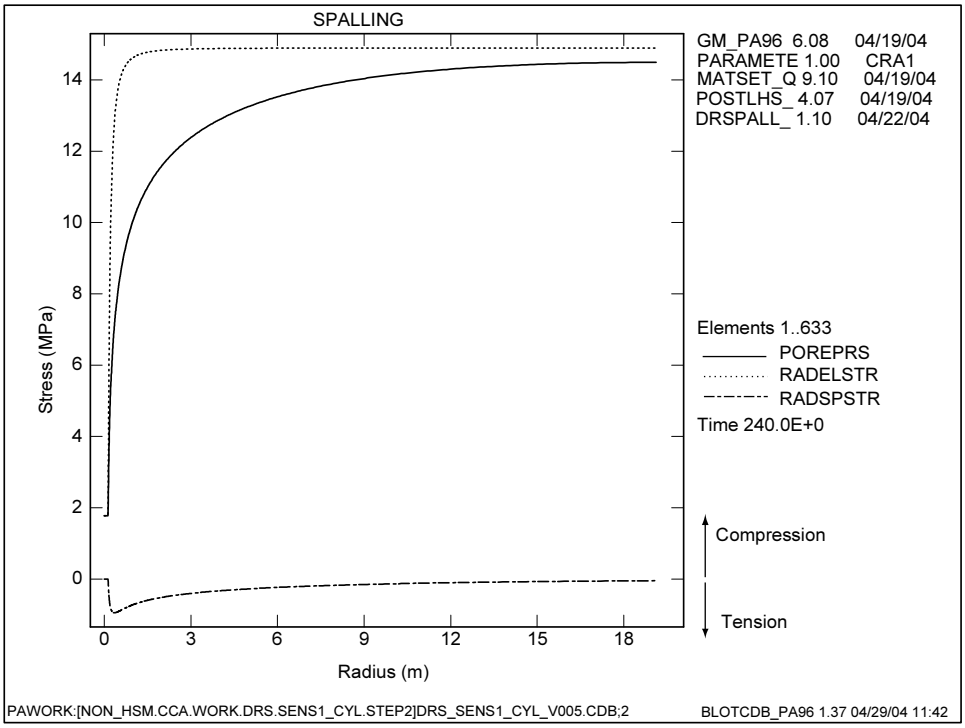

(b) Cylindrical

Note: Compressive stress is positive, and tensile stress is negative.

Figure 7.4-5. Pore Pressure, Radial Elastic Stress, and Seepage Stress Profiles for Entire Repository Domain.

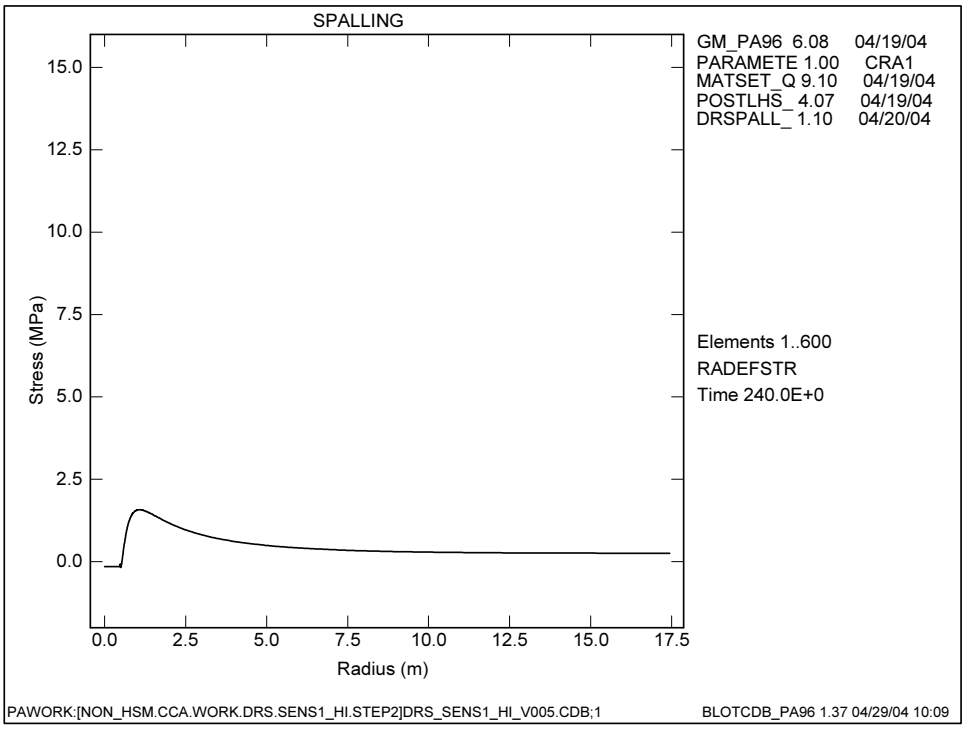

(a) Spherical

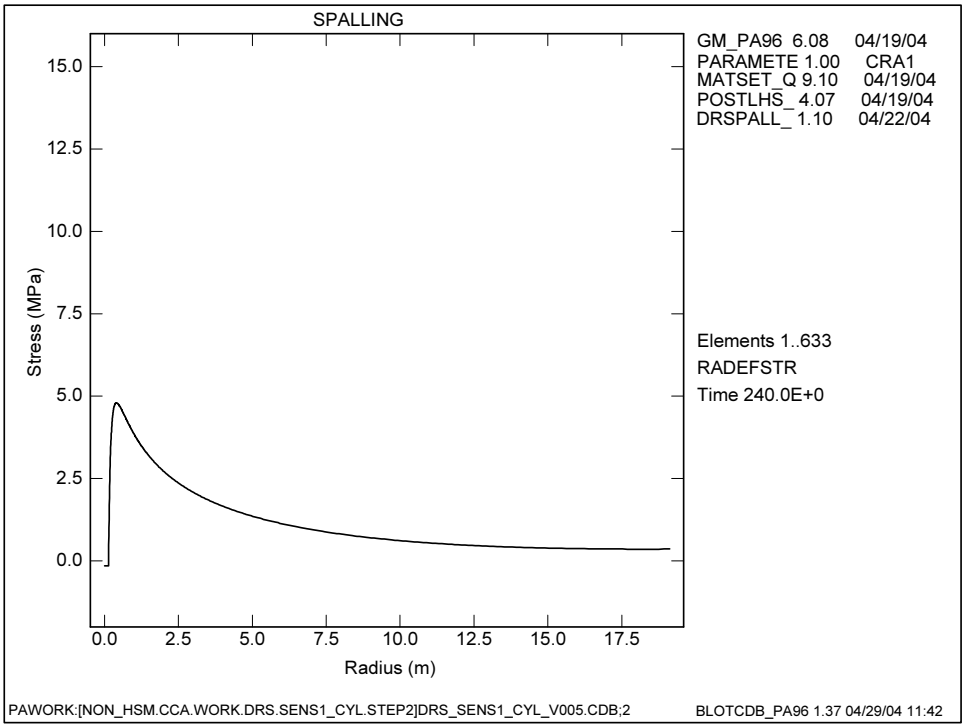

(b) Cylindrical

Figure 7.4-6. Radial Effective Stress Profiles for Entire Repository Domain.

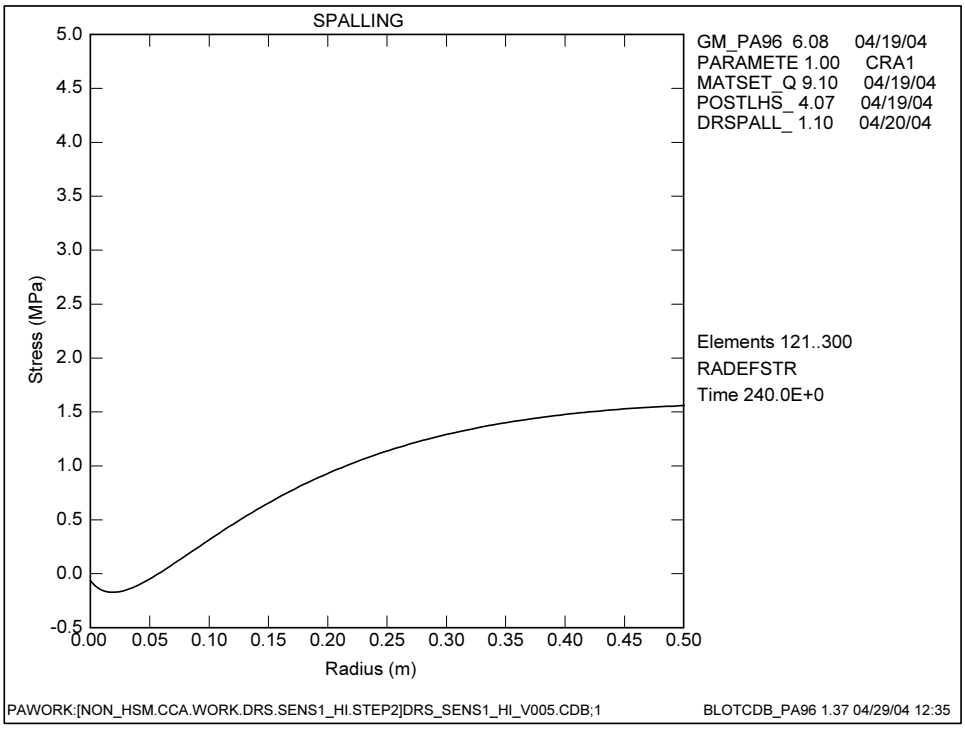

(a) Spherical

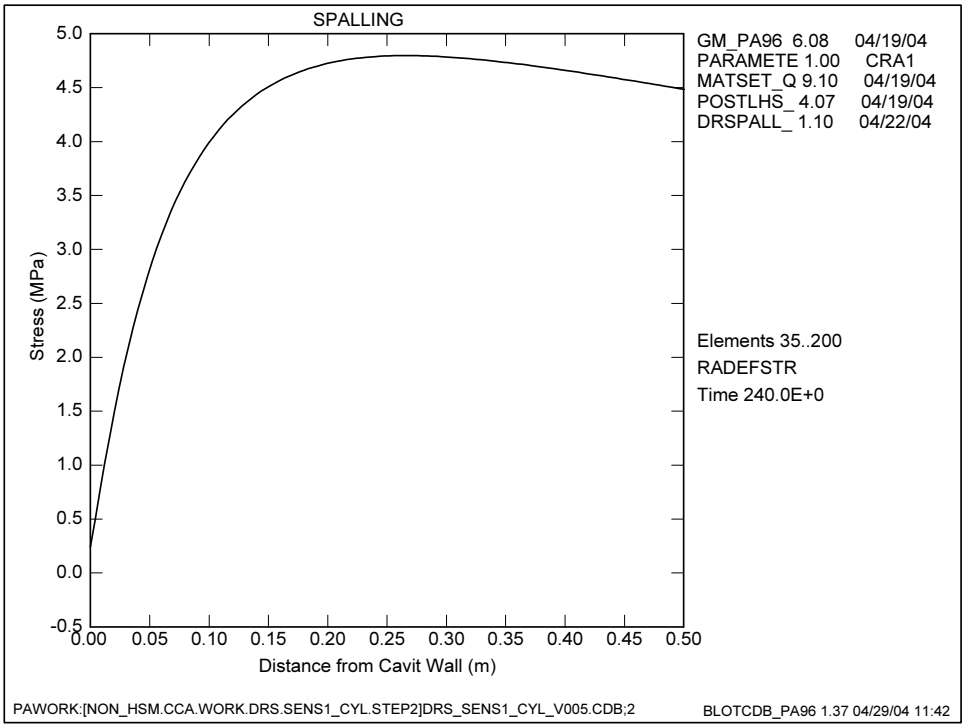

(b) Cylindrical

Figure 7.4-7. Radial Effective Stress Profile, Magnified

7.5 Summary

The sensitivity analysis presented here indicates that the DRSPALL model shows a sensitivity to input parameters that is consistent with the conceptual model. Key parameters include repository pressure and repository permeability. Both of these factors are expected to directly affect the magnitude of tensile stresses and fluidization capacity of the system, which will, in turn, affect spall release volumes. Larger spall volumes were associated with small shape factor×particle diameter. No particular correlation was observed between spall release volumes and waste tensile strength. Most of the release volumes were actually zero (see Table 7.3-1). This implies that spall releases are expected only in a small parameter space and are thus very unlikely for any given intrusion.

The results of this sensitivity analysis allow for the following specific conclusions.

- Spall volumes resulting from the sampled input parameters given in Table 7.1-1 ranged from 0 to 1.5 m^3 equivalent uncompacted volume.
- No tensile failure beyond maximum drilling radius was observed for

  REPIPRES < 11 MPa

  REPIPERM> 3E−13 m^2
- No spall releases were observed for

  REPIPRES < 12.5 MPa

  Cylindrical geometry
- Larger spall volumes were associated with small values of SHAPEFAC×PARTDIAM
- No correlation of SPLVOL2 or TENSRAD−DRILLRAD was observed for

  TENSLSTR over the range 0.12 to 0.17 MPa
- No correlations of SPLVOL2 or TENSRAD−DRILLRAD were identified with the following sampled variables: POISRAT, INITMDEN, MUDVISCO, MUDSOLMX, MUDSOLVE, DRILRATE, MUDPRATE, DDZPERM, ANNUROUG.
- The selected one-dimensional geometry (spherical versus cylindrical) has a significant effect on the calculation of spall release due its affect on pressure and stress gradients.
- Spherical geometry is more likely to result in spall release, and is thus conservative relative to cylindrical geometry releases for the study shown here.

8 Sensitivity Study 2

This chapter documents the second in a series of sensitivity studies on the DRSPALL code. The objective of this analysis is to further refine the previous analysis by focusing on a subset of uncertain parameters and ranges that were identified in Sensitivity Study 1 (section 7) as significant in leading to waste failure, disaggregation and spallings release. Sensitivity study 2 was guided, in part, by the requests of the spallings conceptual model peer review panel (Yew et al., 2003) that convened in July 2003. In particular, the range of the tensile failure strength (TENSLTR) has been expanded to verify that very low tensile strengths will not lead to runaway failure, and also to possibly identify an upper bound above which failure is not expected.

8.1 Problem Setup

DRSPALL was run in spherical geometry for sensitivity study 2.

8.1.1 Parameter Sampling

Latin Hypercube Sampling (LHS) (Helton and Davis, 2002) was used to generate the sampled input parameters sets. Among the more than sixty input parameters required to run DRSPALL, fifteen were deemed sufficiently uncertain and potentially important to code output that they were sampled in the sensitivity analysis in section 7. As a result of that analysis, the list of sampled parameters was narrowed to five, as shown in Table 8.1-1. The sampling ranges here are identical to those in sensitivity study 1 except for the waste tensile strength. The range of tensile strength was expanded to 1.0E+4 to 1.0E+6 Pa at the request of the conceptual model peer review panel in July 2003. The rationale was that expanding the sampled range would identify whether any extreme model sensitivities to tensile strength lie just outside the range 0.12-0.17 MPa originally sampled. Also, shape factor (SHAPEFAC) was set to a constant value of 0.1 and particle diameter (PARTDIAM) was sampled over a range such that the range of SHAPEFAC×PARTDIAM was same as in the first sensitivity study. 100 parameter sets were generated for this study.

Table 8.1-1. Summary of Sampled DRSPALL Input Variables, Including Range and Distribution.

Variable name	Units	Distribution	Low	High
Repository Gas Pressure	Pa	UNIFORM	8.00E+06	1.50E+07
Porosity of Waste	-	UNIFORM	0.35	0.66
Permeability of Waste	m^2	LOGUNIFORM	2.40E-14	2.40E-12
Tensile Strength of Waste	Pa	LOGUNIFORM	1.00E+04	1.00E+06
Particle Diameter	m	LOGUNIFORM	0.001	0.1

Ten parameters from sensitivity study 1 were held constant for sensitivity study 2. These parameters and their values are listed in Table 8.1-2. These parameters were screened from the sampling scheme because the results of the sensitivity study 1 indicated that DRSPALL was not sufficiently sensitive to justify continued sampling. Instead, the values were set to default constants that are specified in the WIPP PA parameter database that is used in compliance calculations. The remaining input parameters are listed in Appendix INPUTS.

Table 8.1-2. Summary of DRSPALL Input Variables Sampled in Study 1 but Held Constant in Study 2.

CAMDAT Name	Parameter Name	Units	Value
POISRAT	Poisson's ratio of waste	-	0.38
INITMDEN	Initial mud density	kg/m^3	1210
MUDVISCO	Initial mud viscosity	Pa*s	9.17E-03
MUDSOLMX	Max solids vol fraction in mud	-	0.615
MUDSOLVE	Solids viscosity exponent	-	-1.50
DRILRATE	Drill penetration rate	m/s	4.445E-03
MUDPRATE	Mud pump rate	m^3/s	2.0181E-02
DDZPERM	DDZ permeability	m^2	1.00E-14
ANNUROUG	Wall roughness	m	5.00E-05
SHAPEFAC	Particle shape factor	-	0.10

8.2 Results and Discussion

The results of the sensitivity analysis are organized as follows:

- Summary of LHS-generated input variable sets and final spall volumes on a vector-by-vector basis (spherical geometry)
- History plots for selected variables
- Scatter plots for correlating input and output data

8.2.1 Summary Results

8.2.1.1 LHS Sampling Results

The results of the sampling are summarized in and listed in full in Appendix S2_TRN. Recall that there are 100 vectors (rows) with 5 sampled variables (columns). Units are given in Table 8.1-2.

The summary of spallings releases at 600 seconds is given in Table 8.2-2. SPLVOL2 was non-zero for the 23 vectors shown and zero for the 77 vectors not shown. Only two of the 23 release vectors exceeded 1 m^3 equivalent uncompacted release volume. The median release volume of the 100 observations was $\tilde{x} = 0$ m^3, and the mean release volume was $\bar{x} = 0.150$ m^3.

Table 8.2-1. Results of 8-15 MPa LHS Sampling.

Vector	REPIPRES	REPIPOR	REPIPERM	TENSLSTR	PARTDIAM	Vector	REPIPRES	REPIPOR	REPIPERM	TENSLSTR	PARTDIAM
1	9.96E+06	0.533	1.41E-12	4.96E+04	1.50E-03	51	8.69E+06	0.412	4.51E-14	1.26E+05	3.31E-03
2	9.43E+06	0.424	4.81E-14	6.24E+05	9.49E-02	52	1.14E+07	0.375	1.08E-12	1.92E+04	1.99E-03
3	1.03E+07	0.456	8.10E-13	1.06E+04	1.86E-03	53	1.13E+07	0.554	7.64E-14	2.42E+04	2.69E-03
4	1.35E+07	0.611	1.91E-13	3.18E+05	1.82E-03	54	1.04E+07	0.578	1.25E-13	8.54E+05	6.45E-03
5	1.39E+07	0.402	3.84E-13	1.53E+05	2.54E-03	55	1.37E+07	0.603	1.13E-12	7.48E+05	1.72E-03
6	1.07E+07	0.431	8.49E-14	1.20E+05	4.22E-02	56	1.10E+07	0.548	8.62E-13	3.57E+05	2.76E-02
7	1.09E+07	0.615	3.53E-13	2.28E+04	1.57E-03	57	9.79E+06	0.540	6.98E-13	6.99E+04	4.10E-03
8	1.44E+07	0.529	1.24E-12	3.92E+05	6.59E-02	58	1.24E+07	0.394	2.97E-14	5.57E+05	2.05E-03
9	9.32E+06	0.470	6.59E-13	5.31E+04	5.45E-02	59	1.21E+07	0.380	3.21E-13	3.95E+04	9.56E-02
10	8.02E+06	0.607	4.78E-13	7.62E+05	4.70E-03	60	1.47E+07	0.545	3.35E-14	8.23E+05	2.29E-02
11	1.33E+07	0.411	5.93E-14	2.82E+05	1.18E-02	61	1.31E+07	0.580	8.26E-14	4.75E+05	1.23E-03
12	1.25E+07	0.511	1.39E-13	6.43E+04	2.80E-03	62	1.41E+07	0.513	6.88E-14	1.98E+05	7.08E-03
13	8.42E+06	0.625	1.14E-13	8.51E+04	3.07E-02	63	1.46E+07	0.658	9.35E-14	2.58E+05	8.98E-02
14	9.82E+06	0.397	1.18E-12	1.11E+05	1.08E-02	64	1.13E+07	0.638	6.56E-14	4.01E+05	1.37E-03
15	1.27E+07	0.626	1.74E-13	1.04E+05	8.81E-03	65	1.33E+07	0.601	5.99E-13	5.77E+04	3.59E-03
16	1.30E+07	0.356	1.57E-12	1.72E+05	6.04E-03	66	1.39E+07	0.655	1.29E-13	7.95E+04	2.32E-02
17	9.95E+06	0.478	1.04E-12	1.81E+04	1.60E-03	67	1.28E+07	0.561	2.16E-12	4.19E+05	3.38E-02
18	1.18E+07	0.504	5.66E-13	1.82E+04	3.01E-02	68	1.30E+07	0.486	4.35E-14	1.31E+05	8.69E-02
19	9.60E+06	0.526	5.08E-14	1.83E+05	7.97E-03	69	1.28E+07	0.426	3.77E-14	6.97E+05	1.16E-03
20	1.48E+07	0.557	1.00E-12	2.28E+05	4.83E-02	70	1.01E+07	0.439	2.44E-14	2.68E+05	5.09E-02
21	8.59E+06	0.640	4.91E-13	7.35E+04	3.12E-03	71	1.07E+07	0.364	3.46E-13	2.99E+05	2.19E-03
22	1.20E+07	0.360	1.34E-12	2.08E+05	8.17E-02	72	1.26E+07	0.549	1.47E-13	2.53E+04	3.97E-03
23	1.36E+07	0.620	4.02E-13	2.31E+04	1.11E-03	73	9.69E+06	0.608	6.88E-13	1.40E+04	4.43E-02
24	1.12E+07	0.593	2.89E-13	1.30E+04	5.19E-03	74	8.24E+06	0.649	1.91E-12	1.32E+05	1.74E-02
25	1.41E+07	0.494	7.93E-13	2.16E+04	1.05E-03	75	1.22E+07	0.646	6.10E-13	6.17E+04	2.06E-02
26	1.23E+07	0.445	3.14E-14	3.02E+04	2.12E-03	76	1.02E+07	0.631	1.08E-13	1.63E+05	2.74E-02
27	8.90E+06	0.566	5.06E-13	3.76E+04	1.63E-02	77	1.25E+07	0.393	2.06E-12	6.55E+05	2.44E-03
28	8.19E+06	0.644	1.78E-12	4.37E+04	1.78E-02	78	1.47E+07	0.633	5.41E-14	1.24E+04	3.51E-02
29	8.36E+06	0.498	9.40E-13	9.85E+04	7.62E-02	79	1.50E+07	0.523	1.32E-13	5.59E+04	1.29E-02
30	9.09E+06	0.428	5.74E-14	4.25E+04	4.11E-02	80	1.19E+07	0.461	7.32E-13	3.40E+05	1.55E-02
31	8.10E+06	0.467	6.98E-14	3.78E+05	1.98E-02	81	1.45E+07	0.463	1.47E-12	1.74E+05	5.25E-03
32	1.05E+07	0.366	5.29E-13	6.76E+05	8.61E-03	82	1.49E+07	0.574	1.68E-12	2.08E+04	9.74E-03
33	9.00E+06	0.440	4.38E-13	1.04E+04	7.31E-03	83	1.38E+07	0.437	2.15E-13	8.99E+04	5.99E-03
34	8.55E+06	0.586	2.20E-13	1.17E+04	6.05E-02	84	1.32E+07	0.538	1.19E-13	2.67E+04	3.82E-02
35	1.29E+07	0.483	3.60E-14	2.93E+04	9.47E-03	85	1.19E+07	0.558	1.31E-12	1.47E+04	3.73E-02
36	1.17E+07	0.499	1.61E-12	5.02E+05	1.22E-02	86	9.25E+06	0.455	2.76E-14	4.49E+05	4.20E-03
37	1.36E+07	0.419	6.19E-14	7.61E+04	1.10E-02	87	1.11E+07	0.507	1.87E-12	2.46E+05	1.33E-02
38	1.40E+07	0.515	2.08E-13	3.23E+04	6.80E-02	88	1.23E+07	0.408	2.24E-12	3.04E+05	7.92E-03
39	1.16E+07	0.486	1.53E-13	1.39E+05	3.40E-03	89	1.09E+07	0.373	8.84E-13	1.46E+05	1.03E-02
40	1.14E+07	0.450	3.05E-13	2.18E+05	5.50E-02	90	1.17E+07	0.652	2.31E-13	4.81E+05	2.32E-03
41	8.72E+06	0.387	2.56E-13	5.08E+04	2.45E-02	91	1.06E+07	0.591	1.83E-13	4.77E+04	6.99E-02
42	1.46E+07	0.568	2.81E-14	1.37E+04	2.09E-02	92	9.49E+06	0.448	2.65E-13	1.71E+04	3.18E-02
43	1.10E+07	0.619	2.53E-14	8.82E+05	4.90E-03	93	1.44E+07	0.585	2.48E-13	3.60E+04	4.37E-03
44	1.43E+07	0.383	4.16E-14	1.64E+04	1.41E-02	94	1.03E+07	0.519	4.66E-14	4.13E+04	6.63E-03
45	1.32E+07	0.358	4.26E-13	1.12E+04	3.66E-03	95	1.01E+07	0.536	2.84E-13	1.07E+05	1.84E-02
46	1.34E+07	0.475	2.38E-12	9.73E+05	2.60E-02	96	1.06E+07	0.596	7.52E-14	9.24E+05	1.42E-03
47	9.66E+06	0.491	3.69E-13	5.88E+05	7.43E-02	97	8.31E+06	0.371	9.67E-14	2.87E+04	1.04E-03
48	1.42E+07	0.350	8.80E-14	6.61E+04	6.00E-02	98	9.35E+06	0.404	1.79E-13	3.40E+04	1.28E-03
49	8.77E+06	0.571	3.85E-14	1.56E+04	5.69E-03	99	1.15E+07	0.387	1.64E-13	5.35E+05	2.92E-03
50	8.94E+06	0.417	1.02E-13	9.30E+04	1.45E-02	100	9.19E+06	0.472	3.27E-14	2.33E+05	4.67E-02

Note: A glossary of variable names is given in Appendix VG.

Table 8.2-2. Summary of Nonzero Spallings Releases from Spherical Geometry at 600 Seconds.

Vector	REPIPRES	SPLVOL2
	(Pa)	(m3)
26	1.23E+07	6.97
93	1.44E+07	1.44
83	1.38E+07	0.90
72	1.26E+07	0.67
79	1.50E+07	0.61
23	1.36E+07	0.51
12	1.25E+07	0.46
45	1.32E+07	0.44
25	1.41E+07	0.42
5	1.39E+07	0.40
62	1.41E+07	0.34
15	1.27E+07	0.32
82	1.49E+07	0.26
53	1.13E+07	0.25
65	1.33E+07	0.16
37	1.36E+07	0.16
4	1.35E+07	0.15
59	1.21E+07	0.14
20	1.48E+07	0.13
81	1.45E+07	0.11
61	1.31E+07	0.08
11	1.33E+07	0.08
39	1.16E+07	0.01

8.2.2 Analysis of History Variables

The history data for cavity radius is shown in Figure 8.2-1. This figure includes all 100 vectors overlaid in a "horsetail" plot. CAVRAD represents the actual cavity radius and thus requires drilling action or failure plus fluidization to remove material for this value to increase. The "drilling curve" common to all vectors is evident as the dark line that starts at time = 0 and fades between 200 and 400 seconds as individual vectors diverge due to the end of drilling or the start of spalling. Repository penetration occurs at about 30 seconds for all vectors, and is marked by the upward turn in CAVRAD. Spalling events correspond to upward deviations from the drilled history. For example, the second largest spallings release vector, v093, with a final cavity radius of 0.64m, begins to spall around 120 seconds, and stabilizes at about 180 seconds.

The horsetail plot for SPLVOL2, which incrementally sums the equivalent volume corresponding to the deviations from DRILLRAD, is shown in Figure 8.2-2. Note that the

curves are monotonically increasing and reflect the equivalent uncompacted volume of waste that was removed strictly due to failure and fluidization. Spalling activity in most vectors occurs between approximately 100 and 250 seconds, except for v026, which is still spalling at 600 seconds. V026 was rerun with a stop time of 1200 seconds. SPLVOL2 stabilized at 11.02 m^3 (CAVRAD=1.14 m) at about 1100 s.

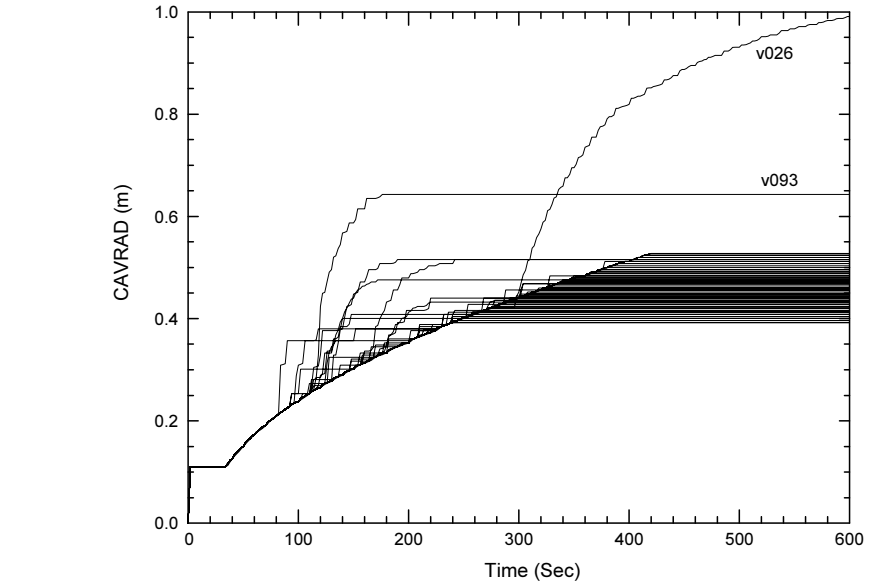

Figure 8.2-1. Horsetail Plot of CAVRAD vs. Time for All 100 Vectors in Spherical Geometry.

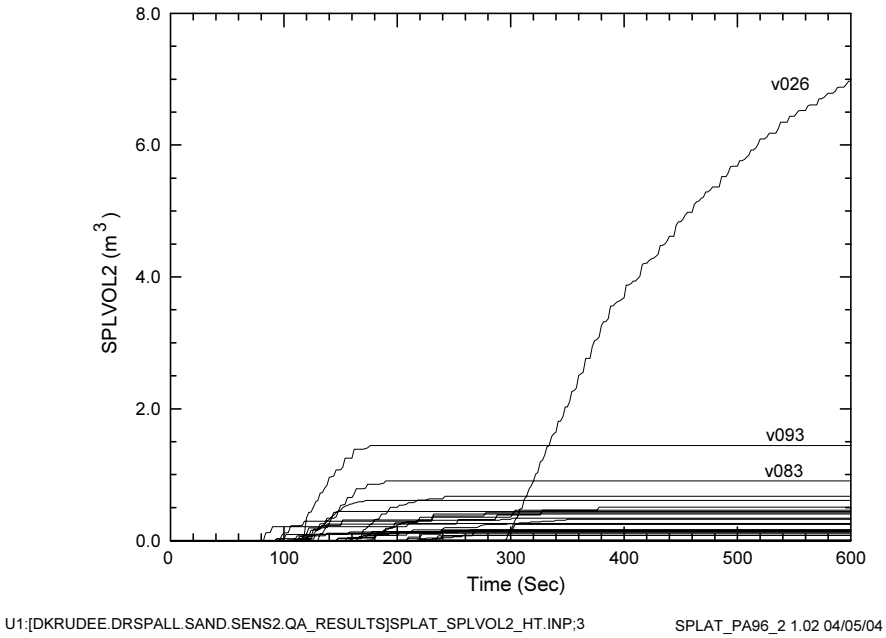

Figure 8.2-2. Horsetail Plot of SPLVOL2 vs. Time for All 100 Vectors in Spherical Geometry.

8.2.3 Scatter Plots

The values of selected output variables at 600 sec, the end of the simulation, are plotted against sampled independent variables in scatter plots below. Each point represents the result from one vector, so every data series contains 100 points. For the data shown here, the following dependent variables were explored:

- Tensile radius – cuttings radius
- Spall volume
- Fluidization velocity
- Superficial gas velocity

as a function of the following independent variables:

- Repository initial pressure
- Repository permeability
- waste tensile strength
- Shape factor × particle diameter

8.2.3.1 Repository Initial Pressure

Repository initial pressure is a primary variable controlling the spallings process, driving tensile failure and fluidization with high pressure gradients and gas velocities near the cavity face. The impact of REPIPRES on SPLVOL2 and TENSRAD-DRILLRAD is shown in Figure 8.2-3. TENSRAD-DRILLRAD appears to be categorically zero at pressure below 12 MPa. This is largely because the resulting pressure gradients are not high enough to cause tensile failure. Above 12 MPa, failure is observed in some vectors, though not universally because other input variables such as permeability and tensile strength impact failure as well. Most of the vectors above 12 MPa show failure. Recall that the growth of tensile radius is limited to one characteristic length (0.02m) until the material within that characteristic length is fluidized, so many of the vectors that exhibit failure only show a 0.02 m value TENSRAD-DRILLRAD.

The spallings volume (SPLVOL2) exhibits sensitivity to repository initial pressure (REPIPRES) illustrated in Figure 8.2-3b. Note that the spallings release in most vectors is zero. The lowest pressure that led to a spall release was 11.3 MPa in v053, with SPLVOL2 = 0.246 m^3. Though pressure above 12.3 MPa is sufficient to cause tensile failure as indicated by the many nonzero TENSRAD-CAVRAD vectors, the fluidization mechanism that moves the failed material into the wellbore requires even higher pressure, and more importantly, high gas velocity at the cavity face. Therefore, only a subset of the failed vectors exhibits spall release.

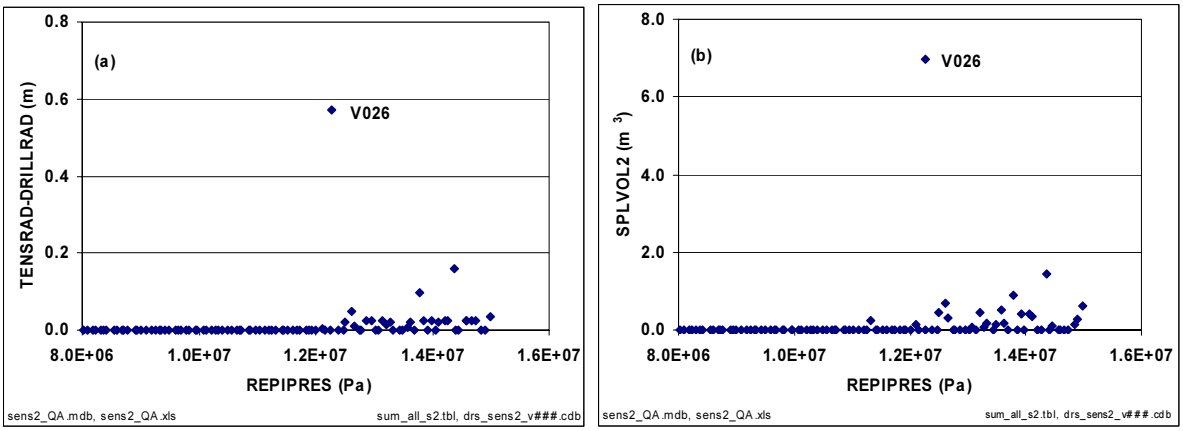

Figure 8.2-3. Scatter Plots of SPLVOL2 and TENSRAD-DRILLRAD vs. REPIPRES.

8.2.3.2 Repository Permeability

Repository permeability is recognized as another variable of primary importance controlling the spallings process. The relationship between REPIPERM and TENSRAD–DRILLRAD is plotted in Figure 8.2-4a. Note the higher frequency of nonzero TENSRAD-DRILLRAD for REPIPERM< 2.5E–13 m^2. Here, lower values of REPIPERM tend to promote more failure due to higher pressure gradients in the waste.

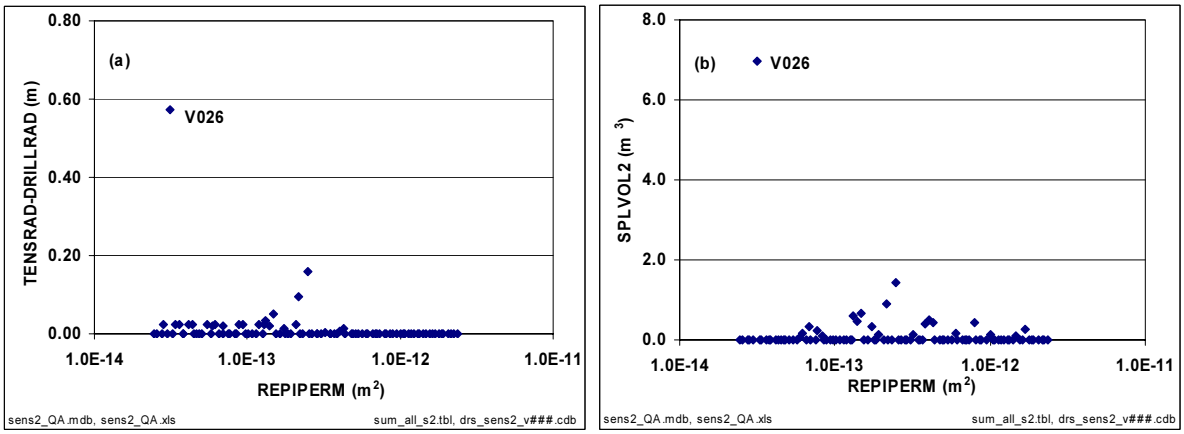

Figure 8.2-4. Scatter Plots of SPLVOL2 and TENSRAD-DRILLRAD vs. REPIPERM.

Shown in Figure 8.2-4b is SPLVOL2 as a function of REPIPERM. The highest frequency of nonzero spall vectors occurs in the middle range of REPIPERM. While low REPIPERM may lead to more failure, it also limits gas velocity, which limits fluidization of failed solids. Alternatively, high REPIPERM promotes high gas velocity near the wellbore to drive fluidization of any failed material, but does not develop the pressure gradients that are observed in low REPIPERM. The result of these coupled processes appears to define a range near the middle of the sampled distribution of REPIPERM where spall releases exceeding 0.1 m^3 are most likely. Above 1.3E-13 m^2 there are cases where SPLVOL2 is greater than zero,

but TENSRAD-CAVRAD is equal to zero. For these vectors spall started and stop during drilling the final cuttings radius exceeded the early time spall radius.

8.2.3.3 Waste Tensile Strength

The sensitivity of TENSRAD−DRILLRAD to waste tensile strength is shown in Figure 8.2-5a. The parallel vertical bars on the figure denote the parameter range used in the first sensitivity test (section 7) and declared in Hansen et al. (2003). The range used here is from 1E+04 to 1E+06 Pa. A higher frequency of failure (nonzero values) is evident at low tensile strengths according to the plot, though failures are observed throughout the entire sampled range of TENSLSTR. Also, the larger failed radii tend to appear at lower TENSLSTR, which is consistent with expectations.

SPLVOL2 shown in Figure 8.2-5b exhibits a similar pattern to TENSRAD−DRILLRAD as a function of TENSLSTR, with more and larger releases at smaller TENSLSTR. The largest SPLVOL2 value (6.97 m^3) was observed at TENSLSTR = 3.02E+04 Pa. This vector (v026) had a sampled permeability, tensile strength, and particle diameter that ranked in the lowest quarter of sampled vectors, and had a repository initial pressure of P = 12.3 MPa. This combination of parameter values has consistently demonstrated a higher likelihood of failure, fluidization, and ultimately spalling release throughout the sensitivity studies shown in this report. Expanding the range of the TENSLSTR sampling from that in Sensitivity Study 1 to two orders of magnitude here demonstrated model behavior that is consistent with expectations, with larger releases occurring at lower tensile strength values. Moreover, there were no "runaway" failures that demonstrate extreme model sensitivity or instability in a parameter space just outside the already very conservative TENSLSTR range recommended in Hansen et al. (2003).

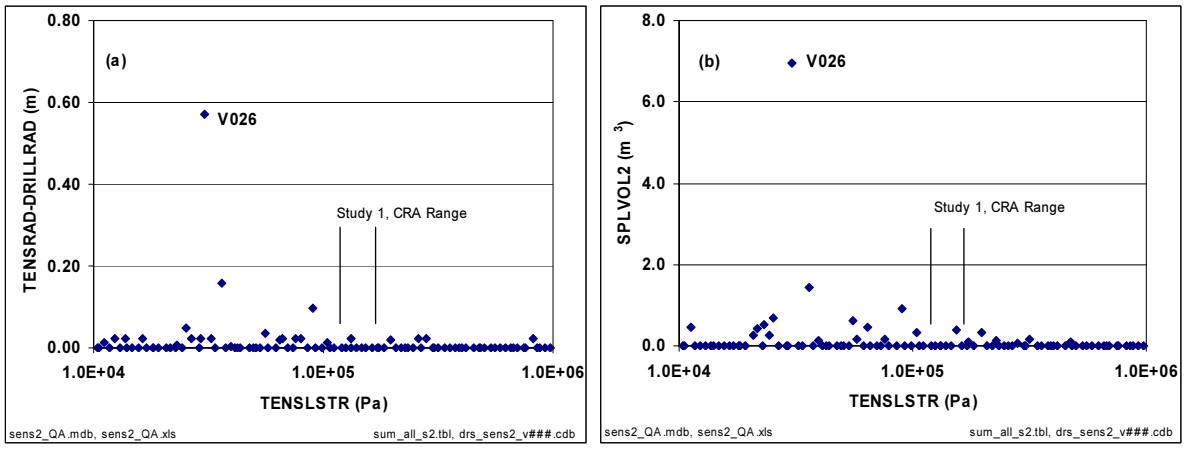

Figure 8.2-5. Scatter Plots of SPLVOL2 and TENSRAD-DRILLRAD vs. TENSLSTR.

8.2.3.4 Role of Fluidization

Recall that the solution to the Ergun equation (Eq. 3.5.20) yields a minimum fluidization velocity (FLUIDVEL) that is compared to the superficial gas velocity at the cavity face (WBSUPVEL) to determine if failed material will fluidize. Thus, if WBSUPVEL > FLUIDVEL, then fluidization is active. Otherwise, failed material will remain bedded. To visualize the frequency with which fluidization is active, a scatter plot was created in Figure 8.2-6 in which FLUIDVEL and WBSUPVEL were plotted versus REPIPERM at 450 seconds, a time shortly after the end of drilling in most vectors. The superficial gas velocity correlates strongly with permeability. Where WBSUPVEL exceeds FLUIDVEL for a particular vector, any failed, bedded material will be swept into the wellbore flow stream. Note that the occurrence of WBSUPVEL > FLUIDVEL becomes less likely as REPIPERM decreases. The implication of this in spall volumes is that most vectors with REPIPERM< 1.3E-13 m^2 do not spall. Such vectors that exhibit terminally bedded material are called fluidization-limited. On the other end of the REPIPERM scale, failed material will always fluidize and spall, but the failure mechanism is limited due to the lower pressure gradients in high-permeability media.

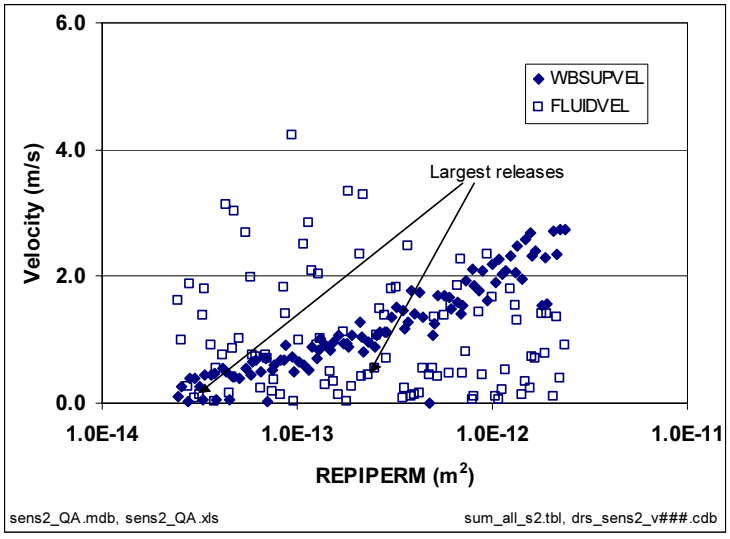

Figure 8.2-6. Scatter Plot of Velocity vs. REPIPERM for Spherical Geometry.

While high superficial gas velocity is one way to promote fluidization, another possibility is low minimum fluidization velocity. For example, the highest release vector (v026) exhibits a very low fluidization velocity (0.12 m/s), nearly assuring fluidization for any failed material. Ergun's equation is quite sensitive to the product of particle shape factor and particle diameter. Low values of both of these input variables drive FLUIDVEL similarly low (see Hansen et al, 2003 for more discussion). However, for this study shape factor was held constant at 0.1 and particle diameter was sampled over the range 0.001 to 0.1 m, which covers the same range as SHAPEFAC×PARTDIAM used in section 7. The impact of particle diameter on SPLVOL2 is shown in Figure 8.2-7. Here, spall release tends to be larger for smaller values of PARTDIAM. This is a manifestation of the fact that small,

tabular particles (PARTDIAM→1mm; SHAPEFAC → 0.1) are easier to fluidize than large, round particles (PARTDIAM→10mm; SHAPEFAC → 1.0).

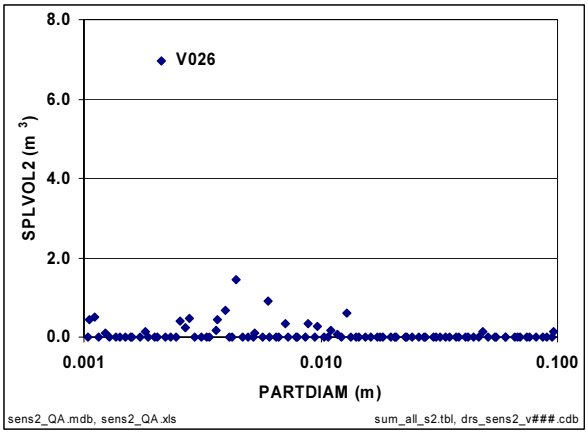

Figure 8.2-7. Scatter Plot of SPLVOL2 vs. PARTDIAM×SHAPEFAC for Spherical Geometry.

8.2.3.5 Other Sampled Variables

There was no identifiable sensitivity of results to the remaining sampled parameter, repository initial porosity (REPIPOR). Figure 8.2-8.shows a fairly uniform distribution of SPLVOL2 and TENSRAD-DRILLRAD across the full range of the independent variable.

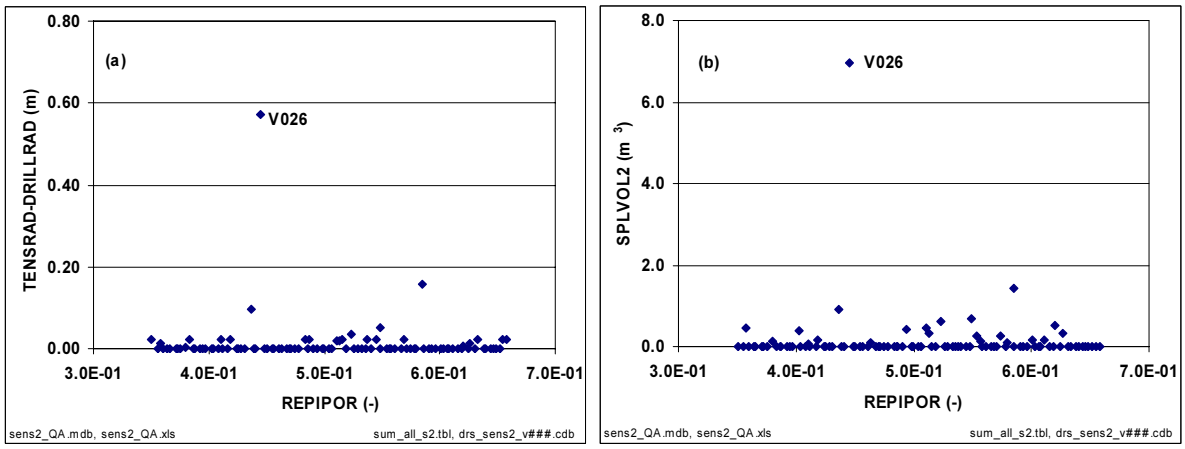

Figure 8.2-8. Scatter Plots of SPLVOL2 and TENSRAD-DRILLRAD vs. REPIPOR.

8.3 Response Surface

The effects of four primary independent variables: REPIPRES, REPIPERM, TENSLSTR, and PARTDIAM are examined together here in an effort to create a spallings "response surface." While the scatter plots presented earlier in this section analyze model sensitivity to one variable, it is understood that the model is actually sensitive to several variables simultaneously. Figure 8.3-1 attempts to elucidate this more complex relationship by presenting the SPLVOL2 output as a function of two key independent variables. The magnitude of spallings release volume is expressed in symbol area where the largest symbol corresponds to a 6.97 m^3 uncompacted volume release. Zero releases have zero area, and thus do not appear on these plots. Six independent variable pairings are presented in Figure 8.3-1.

TENSLSTR vs. REPIPRES: Releases are more likely where TENSLSTR < 1E+05 Pa and REPIPRES > 12 MPa. Thus, the lower right quadrant of the plot is the most heavily-populated region of the parameter space.

TENSLSTR vs. REPIPERM: Low TENSLSTR and moderate to low values of REPIPERM tend to affect the largest releases, and thus the lower left quadrant of the parameter space exhibits the most releases.

PARTDIAM vs. REPIPRES: Among the six bubble plots displayed here, this one distinguishes most clearly the ranges of parameter space that do and do not promote spalling releases. 21 of the 23 release vectors from this study result from REPIPRES > 12 MPa, and PARTDIAM < 0.02m.

PARTDIAM vs. REPIPERM: Medium to low REPIPERM coupled with low PARTDIAM lead to the most frequent and largest releases.

PARTDIAM vs. TENSLSTR: The frequency of spall failures is similar across the entire TENSLSTR range, but the largest spall volumes are clearly concentrated at low TENSLSTR and low PARTDIAM quadrant.

REPIPERM vs. REPIPRES: Releases are most prevalent in the high range of pressure, and middle range of permeability. Releases at high permeability are constrained to a few high-pressure vectors, as tensile failure is unlikely in highly-permeable media in all but the highest-pressure vectors.

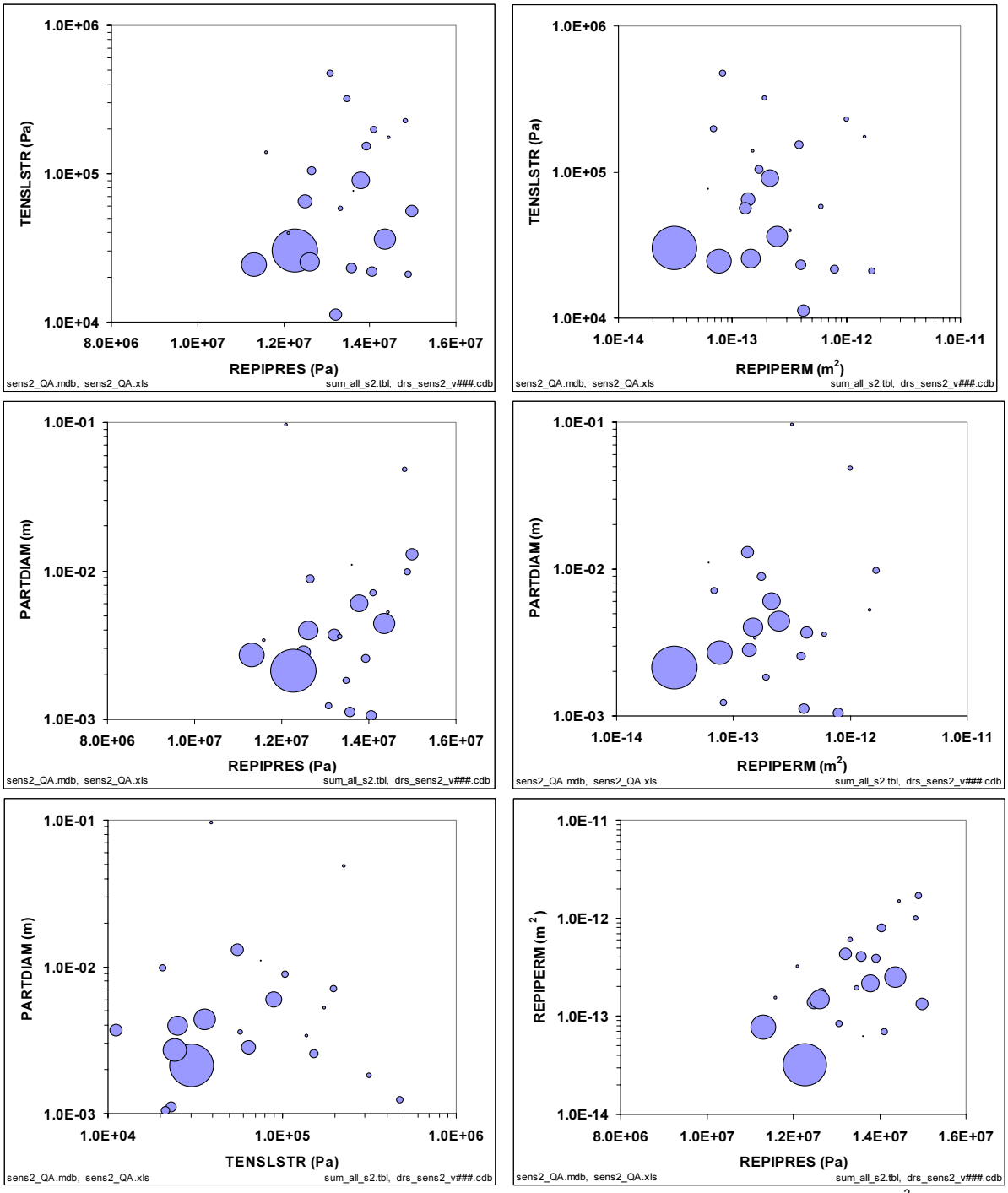

Note: SPLVOL2 magnitude correlates to symbol area, with largest symbol representing to 6.97 m^3 uncompacted volume release.

Figure 8.3-1. SPLVOL2 Response to Paired Independent Variables.

8.4 Summary

This analysis examines the sensitivity of DRSPALL output variables uncompacted equivalent spall volume (SPLVOL2) and depth of failed material (TENSRAD-DRILLRAD) to sampled input variables. Input parameters demonstrated to be of primary importance include repository pressure (REPIPRES), repository permeability (REPIPERM), and waste tensile strength (TENSLSTR). Also potentially important due to their influence on the fluidization mechanism are waste porosity (REPIPOR) and particle shape factor × diameter (SHAPEFAC×PARTDIAM). None of the other sampled parameters demonstrated any conspicuous influence on the spall output.

Spall release volumes greater than zero were observed in 23% of the sampled vectors, and releases exceeded 1 m^3 equivalent uncompacted volume in just 1%. For comparison, the 8-15 MPa run in Sensitivity Study 1 yielded nonzero release in 10% of the sampled vectors, with 2% (one observation) exceeding 1 m^3 equivalent uncompacted volume. The most likely cause for the higher frequency of nonzero releases in Sensitivity Study 2 is due to the extended waste tensile strength range, where the low-strength vectors tended to fail more readily. The maximum SPLVOL2 for the spherical geometry in Sensitivity Study 1 (section 7) for the high-pressure runs was 1.45 m^3, while the maximum SPLVOL2 in Sensitivity Study 2 was 6.97 m^3. The doubling of sample size in Sensitivity Study 2, coupled with the low tensile strengths, likely led to the larger maximum release volume. It is important to note that in a risk analysis, both frequency and consequence are considered. Simply doubling the LHS sample size increases the likelihood of obtaining parameter sets that will lead to higher and lower extreme spallings release values, though it should not affect the mean or median release values and results in a lower probability for a single given outcome.

9 Compliance Recertification Approach

This chapter describes the WIPP PA spallings release calculations for the 2004 Compliance Recertification Application (CRA) (DOE, 2004).

9.1 Methodology

The calculation of spallings releases for CRA required several steps. First, the uncertain parameters were sampled to create a matrix of input data sets. Next, DRSPALL was run once for each input data set to create a table of release values. This table was then imported into the WIPP PA code CUTTINGS_S (WIPP PA, 2003k), which was used to compute the spallings release volume as a function of time for each PA vector. The cumulative spallings releases were then estimated from the WIPP PA code CCDFGF (WIPP PA, 2003h). Finally, a sensitivity analysis was run on the CCDF results. Each step is described in more detail below.

9.1.1 Treatment of Uncertainty

Four uncertain parameters, initial waste porosity (REPIPOR), initial repository permeability (REPIPERM), failed material particle diameter (PARTDIAM) and waste material tensile strength (TENSLSTR) were sampled for the single intrusion spalling calculations performed with DRSPALL. A fifth parameter, repository pressure, was varied over four values (10, 12, 14 and 14.8 MPa) where each pressure value was termed a DRSPALL scenario. Table 9.1-1 lists the uncertain parameters in the DRSPALL calculations.

Table 9.1-1. Uncertain Parameters in the DRSPALL Calculations

Parameter	Variable	Implementation
Repository Pressure	REPIPRES	Initial repository pressure (Pa); spall calculated for values of 10, 12, 14 and 14.8 MPa.
Repository Permeability	REPIPERM	Permeability (m^2) of waste, implemented by parameter SPALLMOD/REPIPERM. Loguniform distribution from 2.4×10^{-14} to 2.4×10^{-12}.
Repository Porosity	REPIPOR	Porosity (dimensionless) of waste, implemented by parameter SPALLMOD/REPIPOR. Uniform distribution from 0.35 to 0.66.
Particle Diameter	PARTDIAM	Particle diameter of waste (m) after tensile failure, implemented by parameter SPALLMOD/PARTDIAM. Loguniform distribution from 0.001 to 0.1 (m).
Tensile Strength	TENSLSTR	Tensile strength of waste (Pa), implemented by parameter SPALLMOD/TENSLSTR. Uniform distribution from 0.12 MPa to 0.17 MPa.

Repository pressure in WIPP PA is a time-dependent value computed by the BRAGFLO model and can vary over a wide range (Stein and Zelinski, 2003). The computational requirements of DRSPALL prohibit calculation of spall volumes for all possible combinations of repository pressure and other parameter values. Consequently, DRSPALL calculations were performed for the small number of pressures listed in Table 9.1-1.

The remaining four parameters listed in Table 9.1-1 were treated as subjectively uncertain. The uncertainty represented by these parameters pertains to the future state of the waste, which is modeled in performance assessment as a homogeneous material with uncertain properties. In order to ensure that sampled values were independent and that the extremes of each parameter's range were represented in the results, the CRA PA used Latin hypercube sampling (LHS) to generate a sample of 50 parameter sets, or vectors, for the DRSPALL calculations. Spall volumes were computed for each combination of initial pressure and sample element, for a total of $4 \times 50 = 200$ model runs. Although repository porosity could be treated as an initial condition (using the time-dependent value computed by BRAGFLO), to reduce the number of computational cases, and to ensure that extreme porosity values were represented, repository porosity was included as a sampled parameter. The LHS sample for DRSPALL and the results of the DRSPALL single-intrusion calculations are presented in sections 9.2 and 9.3 of this report.

The general PA calculations included 64 other uncertain parameters, such as halite porosity and permeability that are not used in the DRSPALL model. These uncertain parameters were also treated as subjectively uncertain. LHS (WIPP PA, 1996f) was used to generate a total of 100 vectors for each replicate of the PA, independent of the LHS generated for the DRSPALL calculations. For each replicate, the LHS for PA included an uncertain parameter SPALLMOD/RNDSPALL, sampled from a uniform distribution on [0,1], that was used as an index to assign a DRSPALL vector to each PA vector. Thus, the intent was for each DRSPALL vector to be assigned to two PA vectors in each replicate. However, there were instances where LHS sampled values ended up exactly on the boundary between two bins which resulted in consecutive DRSPALL vectors being assigned to 1 and 3 PA vectors instead of 2 and 2. In replicate 1, vector 45 is used once and vector 46 three times. In replicate 2, vector 13 is used once and vector 14 three times. The mapping of DRSPALL vectors to PA vectors for each replicate is shown in Appendix MAP.

9.1.2 Calculation of Spall Volumes in CUTTINGS_S

The spallings submodel of the code CUTTINGS_S (WIPP PA, 2003k) was used to compute the spallings release volume as a function of time, for each PA vector. CUTTINGS_S obtains the time-varying repository pressure from the output of BRAGFLO. For each PA vector, and at each of a set of discrete times and locations within the repository (see WIPP PA (2003h) for details), CUTTINGS_S obtains a value for pressure, P. CUTTINGS_S then uses the DRSPALL results assigned to the PA vector to compute a spall volume by linear interpolation. If $P < 10$ MPa or $P > 14.8$ MPa, the spall volume is the value computed for REPIPRES = 10 MPa or REPIPRES = 14.8 MPa, respectively. If P falls between 10 and 14.8 MPa, the spall volume is constructed by linear interpolation between the DRSPALL results for pressures that bracket P.

9.1.3 Construction of Complementary Cumulative Distribution Function

The WIPP PA code CCDFGF version 5.01A (WIPP PA, 2003h) assembles results obtained from several other WIPP PA codes (e.g. BRAGFLO, PANEL, NUTS, CUTTINGS_S, etc.) to build complementary cumulative distribution functions (CCDFs) that are evaluated by the US Environmental Protection Agency (EPA) against regulatory standards designated in 40 CFR 191 (EPA, 1985). CCDFGF uses random sampling to assess the stochastic uncertainty about future states of the repository by calculating radionuclide releases for each of 10,000 randomly generated futures. For each future, CCDFGF computes a single radionuclide release. The distribution of releases computed for all futures of a single vector forms a single CCDF. The subjective uncertainty in WIPP PA parameter values is incorporated into CRA PA by creating multiple parameter sets, or vectors. The CRA analysis computed releases for three sets of 100 vectors (termed replicates R1, R2, and R3); thus, the CRA analysis computes a total of 300 CCDFs. The use of random sampling allows the code CCDFGF to generate a set of CCDFs for total releases as well as sets of CCDFs for other quantities, including spall releases and spall release volumes.

The code CCDFGF computes total releases by spallings for each future by first randomly determining a sequence of intrusion times and locations. CCDFGF then uses the average concentration of radioactivity in the CH waste and the spall volumes computed by CUTTINGS_S to compute a spall release for each intrusion (see WIPP PA (2003h) for details). The total spall release for each future is the sum of releases for each intrusion; the distribution of spall releases for all futures forms one CCDF. Total releases from the repository are computed by summing the releases by all mechanisms, including cuttings and cavings, spallings, direct brine releases, and transport releases.

The CCDF illustrates the probability versus consequence relationship, a classical risk assessment metric. The set of 300 CCDFs is often summarized statistically by computing a mean CCDF, representing the average probability that releases (or volumes) exceed each given amount. Figure 9.1-1 shows the mean CCDF curves for total releases and for individual release mechanisms (cuttings and cavings, spallings, and direct brine releases) for the 100 vectors in replicate 1 of the CRA (transport releases were too small to appear on the

scale of Figure 9.1-1). The horizontal axis represents normalized release in EPA units, and the vertical axis represents the probability of a release exceeding a given value. For example, there is a nearly 1.0 probability that the mean CCDF for total releases will exceed 10^{-4} EPA units (left extreme of the release axis shown), while the probability that the mean CCDF for spallings releases will exceed the same is about 0.3. At the other extreme, there is a 1 in 10,000 probability that the mean CCDF for total releases will exceed 10^{0} = 1 EPA unit. The bold dashed line in the upper right corner of the figure represents the regulatory standard enforced by the EPA. Predicted releases falling to the left and below this line indicate that repository performance is expected to remain within regulatory compliance.

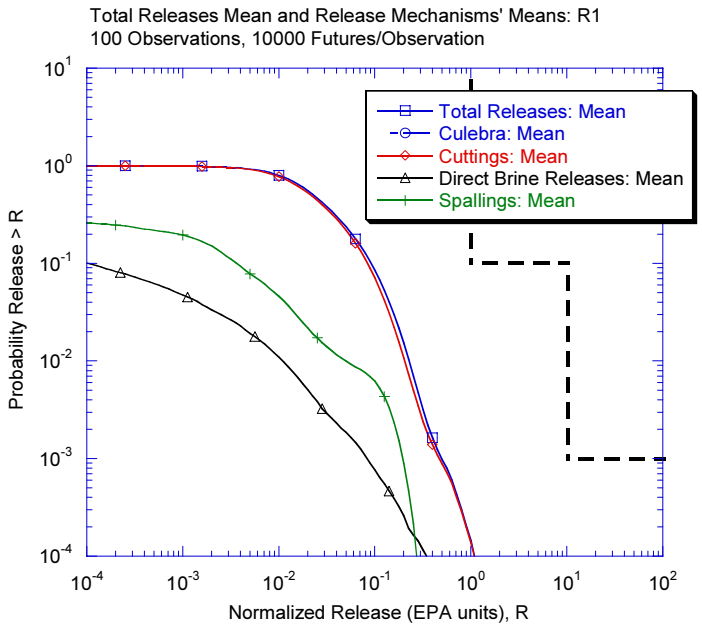

Note: Culebra mean releases were too low to plot on this scale.

Figure 9.1-1. Mean CCDFs of Total Releases and Releases by Individual Mechanisms for Replicate 1 of the CRA.

9.1.4 Uncertainty and Sensitivity Analysis

The uncertainty and sensitivity analysis aims to identify any key relationships between input variables and the output spallings volume in the CRA PA. The variation across vectors (i.e. individual curves in Figure 9.4-1 in section 9.4.1) represents the subjective parameter (material property) uncertainty. The variation along a single curve represents the stochastic uncertainty in future events for a given set of parameters.

For the sensitivity results presented below, the mean total spallings volume across the 10,000 sampled futures is used as a representative spallings value for a single CCDF. The spall volumes are reported as equivalent original uncompacted volumes to facilitate comparisons

of waste volumes at different states of compaction and hence different porosities and to simplify conversions of waste volume to EPA units.

9.1.5 Output Variable Definitions

In addition to the variables described in section 7.2, several new variables are defined here:

- Bed depth (BEDDEPTH)
- Normalized release (EPA units)

9.1.5.1 Bed Depth

The bed depth refers to the depth of failed, but not fluidized, material in the cavity. It is calculated from the difference TENSRAD – CAVRAD = BEDDEPTH. Increases in BEDDPETH indicate material failure from the cavity wall, while decreases in BEDDEPTH indicate fluidization.

9.1.5.2 Normalized Release (EPA units)

Normalized (spallings) release is calculated based on release limits for selected radionuclides as well as the total amount of curies of alpha-emitting transuranic radionuclides with half-lives of greater than 20 years to be emplaced in the repository (EPA, 1985). The concentration of radionuclides in the spallings release volume (defined in section 7.2) is computed as the average activity per m^3 in the rooms filled with CH waste at the time of intrusion. Activities in each waste stream are computed at a discrete set of times by the WIPP PA code EPAUNI (WIPP PA, 2003i,j), and determined at other times by linear interpolation.

9.2 LHS Sampling Results

The results of the LHS sampling are summarized in Table 9.2-1. Recall that there are 50 vectors (rows) with 4 sampled variables (columns). The porosity of the waste, the permeability of the waste, the tensile strength of the waste, and the particle diameter are denoted by REPIPOR, REPIPERM, TENSLSTR, and PARTDIAM, respectively. All other input variables are constants, with values given in Appendix INPUTS.

Table 9.2-1. Results of LHS Sampling.

Vector	REPIPOR (-)	REPIPERM (m^2)	TENSLSTR (Pa)	PARTDIAM (m)
1	5.17E-01	3.97E-13	1.38E+05	4.69E-02
2	3.77E-01	5.77E-14	1.25E+05	3.88E-03
3	6.24E-01	3.90E-14	1.47E+05	7.72E-02

Vector	REPIPOR (-)	REPIPERM (m^2)	TENSLSTR (Pa)	PARTDIAM (m)
4	6.41E-01	5.49E-14	1.39E+05	2.13E-03
5	4.91E-01	7.22E-14	1.52E+05	1.11E-02
6	6.32E-01	8.82E-13	1.66E+05	2.96E-03
7	5.69E-01	4.28E-14	1.64E+05	2.39E-02
8	6.04E-01	2.42E-14	1.55E+05	3.80E-02
9	5.33E-01	7.55E-13	1.30E+05	1.07E-02
10	6.12E-01	1.03E-13	1.60E+05	7.51E-02
11	4.85E-01	3.05E-13	1.23E+05	5.82E-02
12	5.38E-01	2.81E-13	1.31E+05	6.80E-02
13	4.52E-01	1.27E-12	1.50E+05	5.60E-02
14	4.70E-01	1.72E-12	1.65E+05	1.64E-02
15	4.96E-01	1.00E-12	1.37E+05	3.51E-03
16	3.59E-01	2.74E-14	1.54E+05	4.60E-03
17	4.61E-01	3.46E-14	1.44E+05	4.98E-03
18	3.51E-01	2.62E-13	1.63E+05	4.10E-02
19	4.46E-01	6.33E-14	1.26E+05	4.06E-03
20	5.85E-01	1.96E-13	1.44E+05	2.08E-02
21	4.36E-01	1.11E-13	1.21E+05	8.34E-02
22	6.02E-01	1.82E-12	1.29E+05	6.48E-03
23	3.73E-01	1.18E-13	1.67E+05	1.50E-02
24	4.62E-01	3.53E-13	1.50E+05	1.16E-03
25	5.88E-01	1.24E-12	1.33E+05	1.76E-03
26	3.97E-01	1.76E-13	1.48E+05	2.17E-02
27	6.18E-01	4.75E-14	1.53E+05	3.43E-02
28	4.37E-01	2.13E-13	1.42E+05	1.24E-03
29	4.77E-01	4.52E-13	1.47E+05	1.24E-02
30	4.02E-01	2.89E-14	1.39E+05	1.04E-03
31	5.21E-01	1.64E-13	1.55E+05	1.51E-03
32	6.51E-01	1.39E-12	1.62E+05	8.35E-03
33	6.38E-01	7.17E-13	1.35E+05	2.73E-03
34	3.68E-01	5.05E-13	1.58E+05	2.06E-03
35	3.85E-01	8.31E-13	1.29E+05	9.83E-02
36	5.11E-01	1.40E-13	1.59E+05	5.84E-03
37	5.45E-01	8.10E-14	1.27E+05	1.44E-02
38	4.21E-01	2.04E-12	1.34E+05	1.64E-03
39	5.94E-01	4.59E-13	1.70E+05	4.84E-02
40	5.63E-01	7.35E-14	1.22E+05	2.90E-02
41	5.26E-01	2.31E-12	1.43E+05	3.17E-02
42	4.30E-01	6.55E-13	1.26E+05	3.18E-03
43	3.93E-01	1.13E-12	1.35E+05	7.96E-03
44	4.08E-01	1.55E-12	1.69E+05	2.56E-02

Vector	REPIPOR (-)	REPIPERM (m^2)	TENSLSTR (Pa)	PARTDIAM (m)
45	5.51E-01	2.23E-13	1.45E+05	1.84E-02
46	5.79E-01	5.84E-13	1.21E+05	5.57E-03
47	5.03E-01	9.51E-14	1.61E+05	1.40E-03
48	4.14E-01	1.28E-13	1.68E+05	9.49E-03
49	5.58E-01	3.53E-14	1.41E+05	7.40E-03
50	6.57E-01	3.24E-13	1.56E+05	2.32E-03

9.3 DRSPALL Single-Intrusion Analyses

The final spallings volumes calculated by DRSPALL for the four scenarios and 50 vectors are listed in Table 9.3-1. These volumes are based on the 1D spherical flow geometry in the repository, except for four cases (2 vectors in scenarios S3 and S4) where cavity radius exceeded repository height. Analysis of individual scenarios and specific vectors are addressed in the discussion that follows.

Table 9.3-1. Summary of Spallings Releases for the 4 Scenarios and 50 Vectors

Vector	SPLVOL2 (m^3)			
	R1S1 P=10 MPa	R1S2 P=12 MPa	R1S3 P=14 MPa	R1S4 P=14.8 MPa
1	0.00	0.00	0.40	0.56
2	0.00	1.22	7.22	7.30
3	0.00	0.00	0.00	0.00
4	0.00	0.56	1.29	1.61
5	0.00	0.00	0.08	0.21
6	0.00	0.00	0.07	0.18
7	0.00	0.00	0.00	0.00
8	0.00	0.00	0.00	0.00
9	0.00	0.00	0.19	0.34
10	0.00	0.00	0.00	0.00
11	0.00	0.00	0.28	0.38
12	0.00	0.00	0.04	0.09
13	0.00	0.00	0.10	0.22
14	0.00	0.00	0.04	0.14
15	0.00	0.00	0.11	0.27
16	0.00	1.71	3.13	3.95
17	0.00	0.00	0.09	0.38
18	0.00	0.00	0.60	1.17
19	0.00	0.61	4.41	5.32
20	0.00	0.01	0.22	0.32
21	0.00	0.00	0.00	0.00

Vector	SPLVOL2 (m^3)			
	R1S1 P=10 MPa	R1S2 P=12 MPa	R1S3 P=14 MPa	R1S4 P=14.8 MPa
22	0.00	0.00	0.03	0.11
23	0.00	0.17	1.79	2.25
24	0.00	0.00	0.46	0.63
25	0.00	0.00	0.06	0.17
26	0.00	0.14	1.03	1.79
27	0.00	0.00	0.00	0.00
28	0.00	0.03	0.74	1.45
29	0.00	0.00	0.38	0.49
30	0.00	7.00	9.45	12.06
31	0.00	0.10	0.69	1.43
32	0.00	0.00	0.02	0.10
33	0.00	0.00	0.12	0.26
34	0.00	0.00	0.41	0.60
35	0.00	0.00	0.27	0.44
36	0.00	0.18	0.95	1.67
37	0.00	0.00	0.00	0.00
38	0.00	0.00	0.05	0.16
39	0.00	0.00	0.21	0.35
40	0.00	0.00	0.00	0.00
41	0.00	0.00	0.01	0.09
42	0.00	0.00	0.31	0.52
43	0.00	0.00	0.16	0.33
44	0.00	0.00	0.07	0.18
45	0.00	0.00	0.48	0.65
46	0.00	0.00	0.22	0.43
47	0.00	0.24	1.81	3.11
48	0.00	0.22	1.34	2.33
49	0.00	0.00	0.00	0.00
50	0.00	0.00	0.32	0.55

9.3.1 Scenario 1 (R1S1) Results

Initial repository pressure was set to 10 MPa for scenario 1. No spallings releases were observed for this scenario, primarily because the pressure difference between the repository (10 MPa) and the wellbore (hydrostatic pressure of about 8 MPa) is not sufficient to cause tensile failure and fluidization of the waste material.

Also instructive is the evolution of the cavity radius as a function of time. Since no failure is observed in scenario 1, cavity growth is caused by drilling alone. Figure 9.3-1 displays the cavity radius as a function of time for all 50 vectors. Drilling starts above the repository

domain in the overlying salt, and cavity radius is constant until the bit penetrates the repository at about 34 seconds. The initial cavity radius is set to 0.11 meters in all vectors. This initial radius represents the pseudo-cavity that is formed prior to bit penetration in order to prevent flow to a single point (spherical geometry) or line (cylindrical geometry) in the one-dimensional, radially symmetric domain. Once the bit contacts the repository, the cavity begins to grow due to material removal by the bit. Note that for a 1-D domain, the bit must expand radially to remove material, and the cavity radius will increase as drilling proceeds.

Termination of drilling occurs when the drill penetration rate × drilling time = repository height. The array of resultant drilling times and cavity radii seen in Figure 9.3-1 occur because current repository height is a direct function of current waste porosity and initial waste room height and initial porosity (Eq. 3.5.23) where current waste porosity is a sampled parameter, as shown in Table 9.2-1. The uniformly sampled current waste porosities ultimately cause the similarly-distributed final cavity radii in Figure 9.3-1.

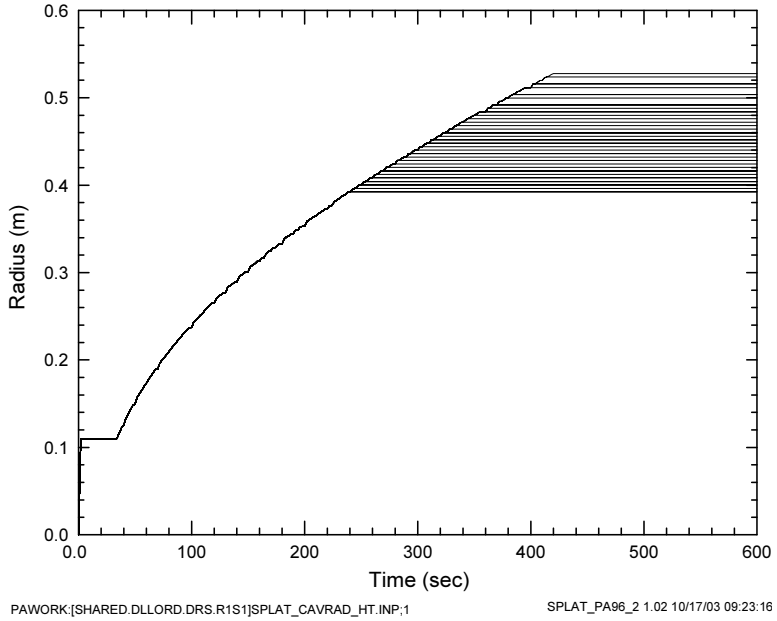

Figure 9.3-1. Horsetail Plot of CAVRAD for Scenario 1.

9.3.2 Scenario 2 (R1S2) Results

Initial repository pressure was set to 12 MPa for scenario 2. The summary data presented in Table 9.3-1 indicate that spallings releases range from 0 to 7 m^3 uncompacted volume. These same data are displayed graphically in the bar graph shown in Figure 9.3-2. The vectors are sorted in ascending order of release volume. Since each vector is equally probable (1 in 50), the figure also may be interpreted as a cumulative distribution function (CDF). For example, since 47 of the 50 vectors exhibit less than 1 m^3 release, there is a 94% probability that an intrusion at 12 MPa would release less than 1 m^3 of spalled material.

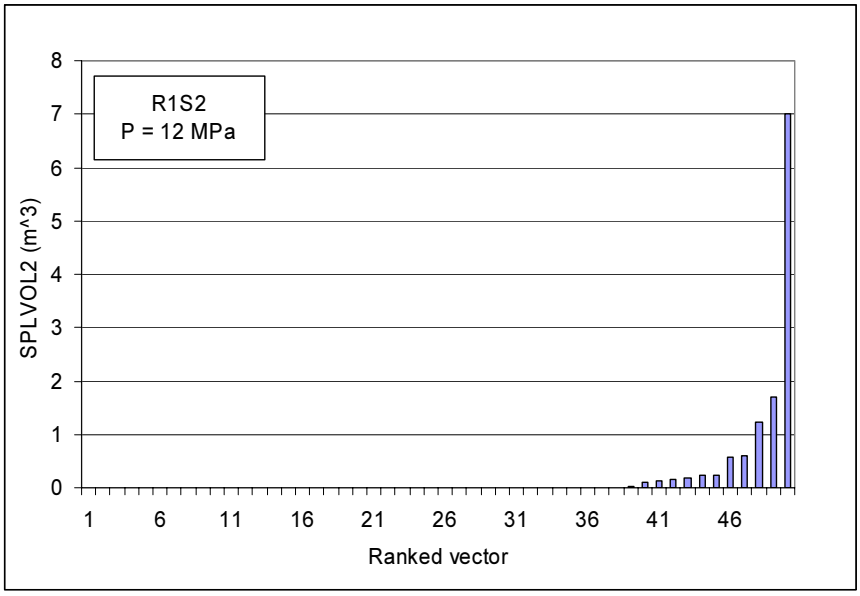

Figure 9.3-2. Bar Graph of SPLVOL2 Releases per Vector for Scenario 2, Ranked in Ascending Order.

9.3.2.1 R1S2 Cavity Radius

The SPLVOL2 values shown above in Figure 9.3-2 represent final values obtained after the system reached a steady state. In order to confirm that the system had stabilized, the cavity radius was examined as a function of time in the horsetail plot shown in Figure 9.3-3. While 49 of the 50 vectors exhibit a steady CAVRAD value by 600 seconds, one vector (v030) is still increasing. It was thus necessary to run v030 out beyond 600 seconds. Figure 9.3-4 shows the cavity radius, drilled radius, and tensile radius for v030 alone, run out to 1000 seconds, indicating that the cavity radius stabilizes to 0.97 m after 750 seconds. Hence the SPLVOL2 value obtained for v030 was captured at 1000 seconds rather than at 600 seconds for the 49 other vectors in this scenario.

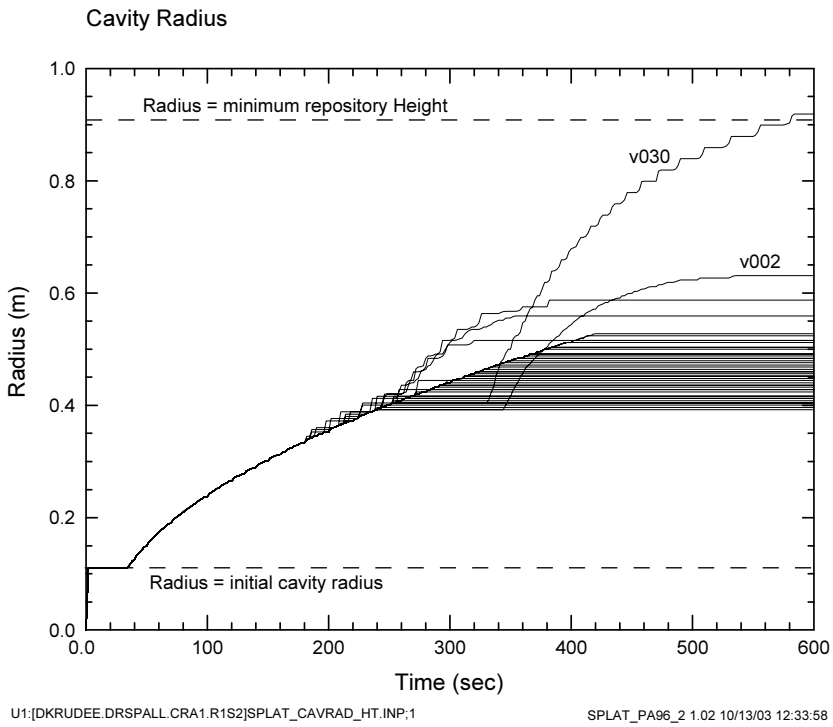

Figure 9.3-3. Horsetail Plot of CAVRAD for Scenario 2.

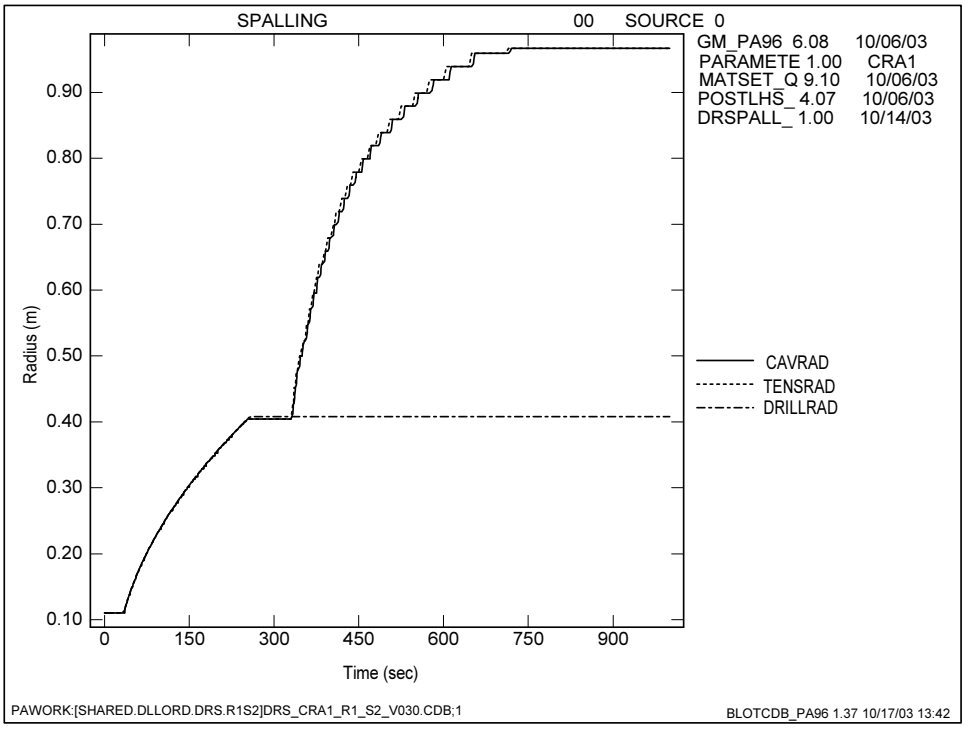

Figure 9.3-4. History Plot of CAVRAD, DRILLRAD, and TENSRAD for R1S2 V030 Run Out to 1000 Seconds.

An examination of the input parameters for vector 030 shows that this large release vector had relatively low waste porosity and permeability, as well as the lowest particle diameter in its sampled range. Once failed, the particulate solid waste was easily fluidized. This feature is confirmed by examining the plot of the waste boundary superficial velocity (WBSUPVEL) and the minimum fluidization velocity (FLUIDVEL) shown in Figure 9.3-5. When WBSUPVEL > FLUIDVEL, as it is for the entire duration plotted in Figure 9.3-5, failed waste will readily fluidize and transport up the borehole.

The individual spikes in the WBSUPVEL curve in Figure 9.3-5 occur when individual zones are removed from the repository domain via failure and fluidization. The small spikes that occur between 50 and 300 seconds are due to drilling in the repository. The spikes beyond 300 seconds result from fluidization of recently failed zones.

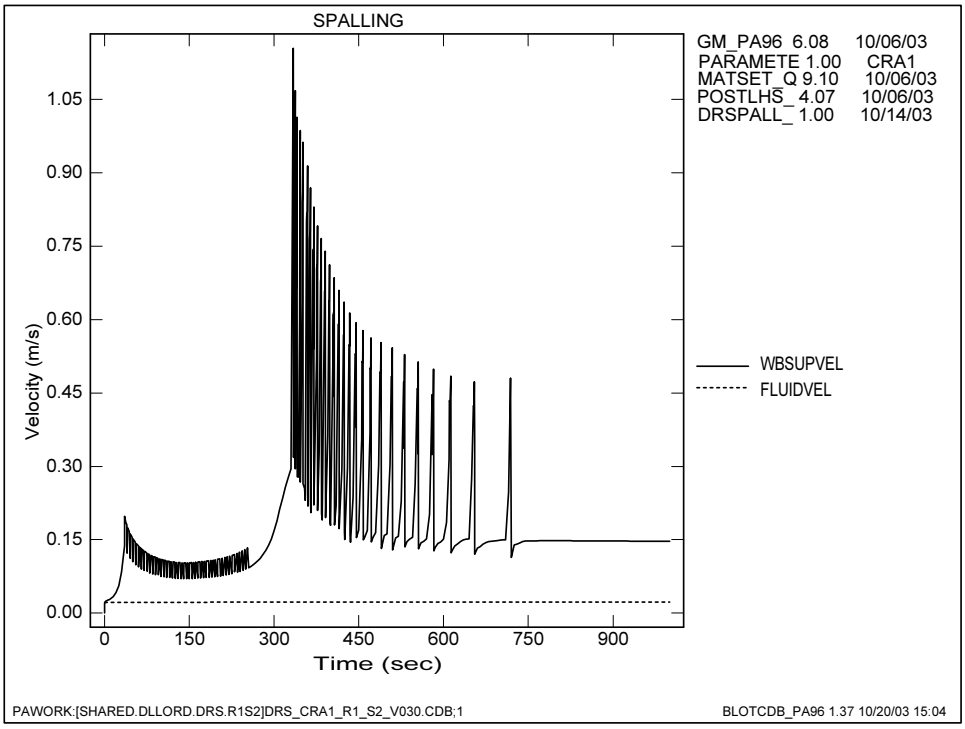

Figure 9.3-5. History Plot of Waste Boundary Superficial Velocity (WBSUPVEL) and Minimum Fluidization Velocity (FLUIDVEL) for Scenario 2, V030.

9.3.2.2 R1S2 V030 Radial Effective Stress

Since all bedded material will fluidize in v030, the cavity growth must be limited by tensile failure. In order to visualize the stress state in the solid that leads to stabilization of the cavity, the radial effective stress (RADEFSTR) is plotted at a selected time, 750 sec, in Figure 9.3-6. The x-axis "distance" in Figure 9.3-6 is given from a reference point in the cavity. The current cavity wall, marked in the figure, is located at 0.967 m from the origin. Negative stress values indicate tension, while positive stress values indicate compression. The horizontal line of constant stress from DISTANCE = 0 to the cavity wall indicates failed, fluidized material, and is arbitrarily set to the tensile strength (T_s = 1.39E+05 Pa) of the solid. The grid in DRSPALL is zone-centered, so the cavity wall falls halfway between the last grid point in the cavity and the first grid point in the waste. Radial effective stress at the cavity wall is zero by definition (Eq. 3.5.16). Since there is no grid point exactly at the cavity wall, however, the plot below does not show an exact zero value. The "line" in Figure 9.3-6 that connects discrete points is simply added by the plotting utility and is not used in DRSPALL calculations.

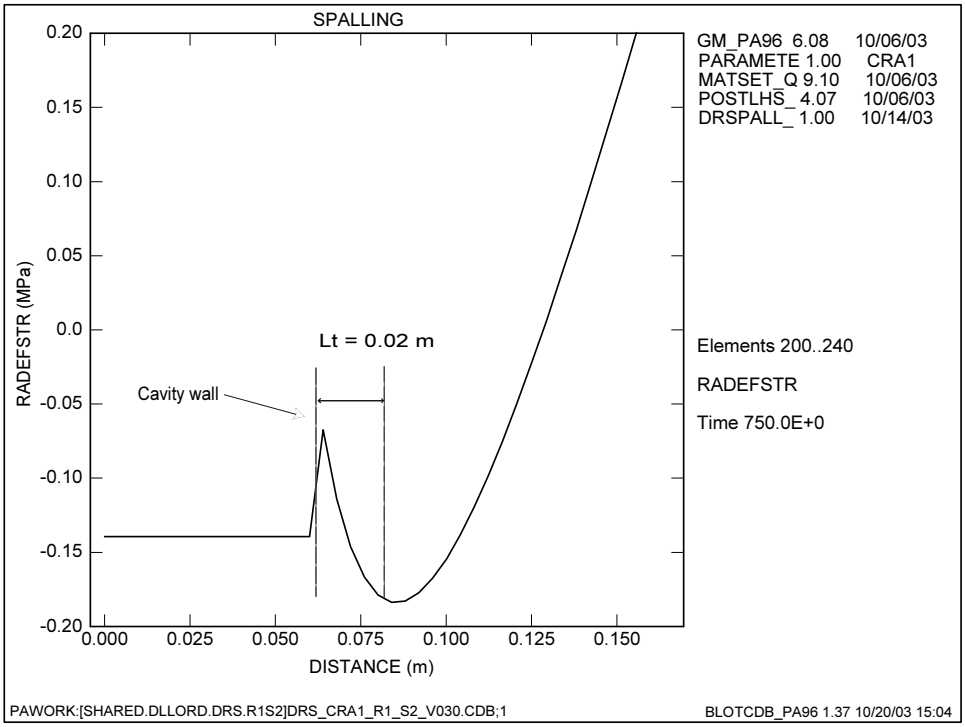

Figure 9.3-6. Spatial Plot of Radial Effective Stress (RADEFSTR) Near Cavity Wall for V030 at 750 Seconds.

From the cavity wall outward, the radial effective stress decreases to a minimum near −1.75E+05 Pa tension at about 0.02 m from the cavity wall. Moving further outward beyond the minimum, RADEFSTR climbs into a compressive state (>0). This plot demonstrates that tensile failure does not occur at the cavity wall at runtime = 750 seconds because the mean radial effective stress in tension over the characteristic length L_t does not exceed the tensile strength. Table 9.3-2 computes the average RADEFSTR over L_t explicitly. Reviewing the

calculation, the cavity wall starts with DRSPALL coordinate 0.9691m (plot coordinate 0.0640 m). One characteristic length includes five zones, identified by the bold border in the table. The mean RADEFSTR for these five zones is –1.3461E+05 Pa, which is not sufficient to fail the waste with T_s = 1.39E+05 Pa

Table 9.3-2. Calculation of Mean RADEFSTR Over L_t for S2, V030 at 750 Seconds.

DRSPALL COORD	Plot Coordinate	RADEFSTR	Average RADEFSTR over L_t
0.9611	0.0560	-1.3930E+05	
0.9651	0.0600	-1.3930E+05	
0.9691	0.0640	-6.7352E+04	
0.9731	0.0680	-1.1412E+05	
0.9771	0.0720	-1.4607E+05	-1.3461E+05
0.9811	0.0760	-1.6679E+05	
0.9851	0.0800	-1.7873E+05	
0.9891	0.0840	-1.8363E+05	
0.9931	0.0880	-1.8278E+05	

9.3.2.3 Scenario 2 Scatter Plots

Scatter plots are used here to examine model sensitivity to the sampled input variables waste porosity, waste permeability, waste tensile strength, and waste particle diameter. SPLVOL2 values are plotted against each input variable on a vector-by-vector basis to identify any important relationships. Shown in Figure 9.3-7 are four scatter plots for the scenario 2 runs. The independent variable values on the x-axes correspond to the values obtained in the LHS sampling listed in Table 9.2-1, while the SPLVOL2 values correspond to those listed in Table 9.3-1.

According to Figure 9.3-7, the majority of nonzero spallings releases appear to correlate with low waste porosity, low waste permeability, and small particle diameter. The relationship with tensile strength is less definitive. These correlations are reasonable. Low waste permeability will lead to larger tensile stresses and more tensile failure of the waste due to higher pressure gradients near the borehole, though low permeability also leads to low gas velocity which can prevent fluidization of failed wastes. Low waste porosity and particle diameter tend to promote fluidization of failed particles, so the higher frequency of nonzero SPLVOL2 releases when these values are low is consistent with expectations.

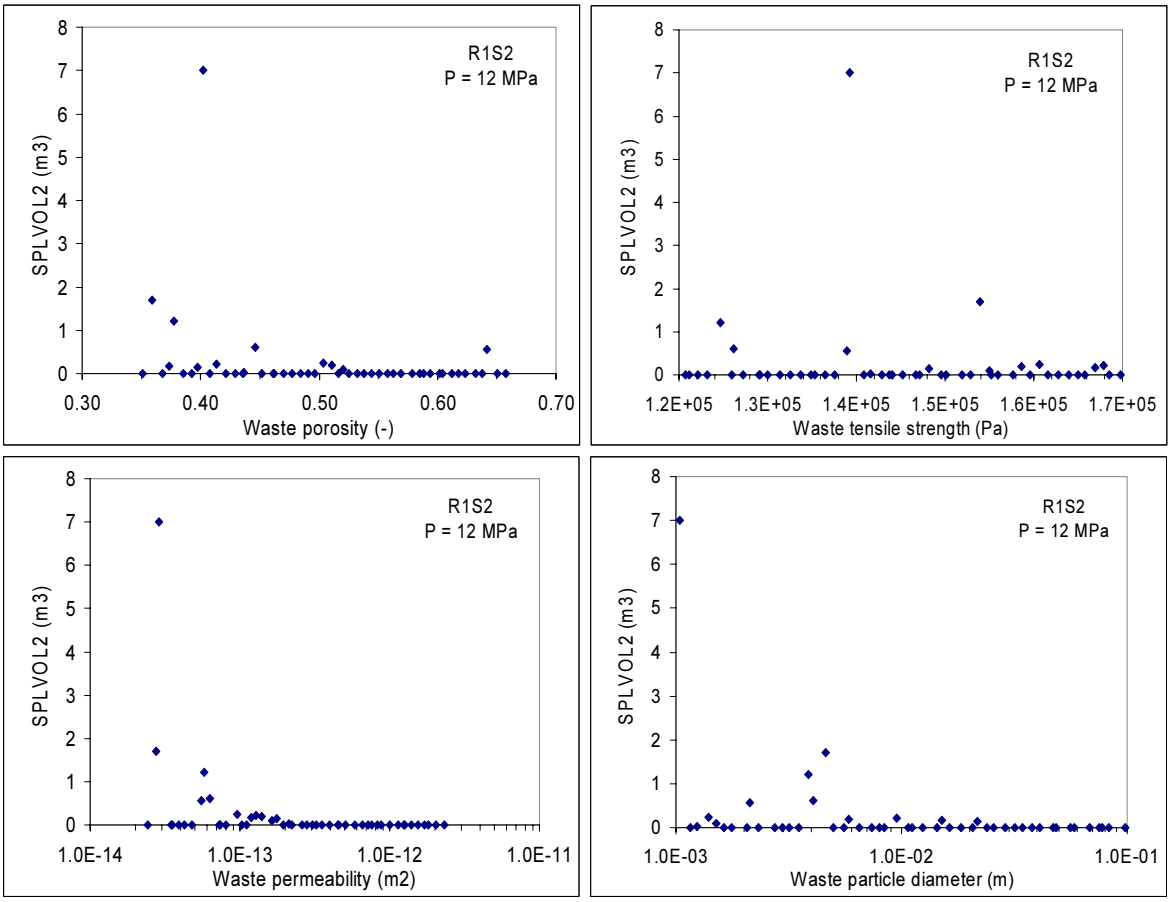

Figure 9.3-7. Scatter Plots of SPLVOL2 vs. the Sampled Waste Properties of Porosity, Tensile Strength, Permeability, and Particle Diameter for Scenario 2.

9.3.3 Scenario 3 (R1S3) Results

Initial repository pressure was set to 14 MPa for scenario 3. The summary data presented in Table 9.3-1 indicate that spallings releases range from 0 to 9.5 m^3 uncompacted volume. These same data are displayed graphically in the bar graph shown in Figure 9.3-8. Relative to scenario 2, these release volumes are larger; an expected result of higher initial repository pressure leading to higher tensile stresses and gas velocities.

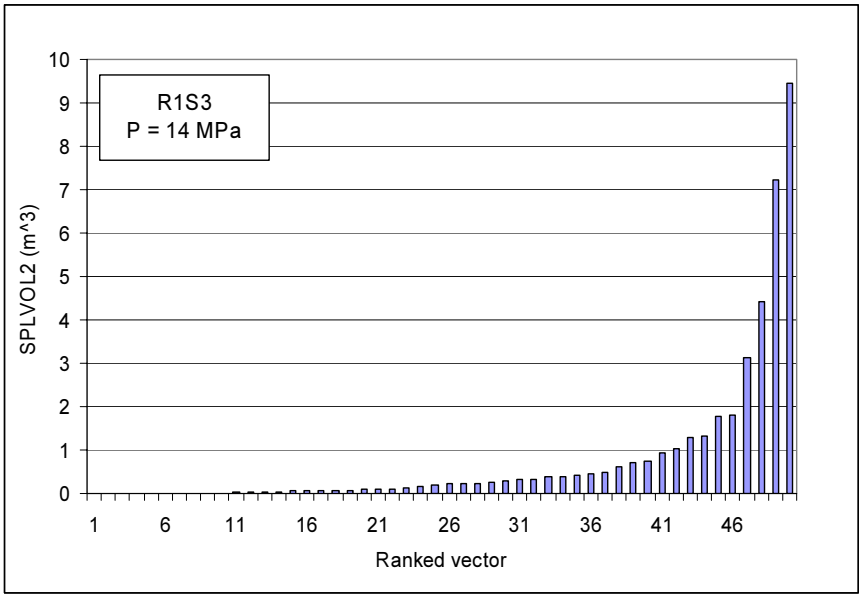

Figure 9.3-8. Bar Graph of SPLVOL2 Releases per Vector for Scenario 3, Ranked in Ascending Order.

9.3.3.1 Scenario 3 History Plots

Figure 9.3-9 shows the horsetail plot of CAVRAD for scenario 3. Cavity growth ahead of drilling begins between 100 and 150 seconds and stabilizes by 300 seconds in most vectors. The cavity radius of two vectors, v002 and v030, has not stabilized by 600 seconds, therefore requiring additional analysis.

The magnitude of the cavity radius in vectors 002 and 030 nears or exceeds the height[5] of the repository by 600 seconds. This implies that if the cavity formed by spallings is indeed a radially symmetric hemisphere, the cavity would intersect with the Disturbed Rock Zone (DRZ) below the repository, as depicted in the schematic shown in Figure 9.3-10. Important to note here is that the unsteady porous flow and stress equations that describe the repository in spherical geometry do not address the presence of the lower DRZ. Therefore, radial fluid flow, stress distributions, failure, and cavity growth will all proceed regardless of whether the cavity radius has intersected the lower DRZ. While this conservative assumption is useful in simplifying the calculations, and furthermore a fair representation of the relevant problem geometry early in penetration, its applicability breaks down as the cavity radius approaches the repository height. Release volumes are certainly overestimated when CAVRAD $\rightarrow H$ as some of the cavity volume originates from the DRZ, which has very different properties from the WIPP waste. To address this issue, DRSPALL is also exercised in cylindrical geometry for vectors 002 and 030 in order to better understand the flow, stress, and cavity growth properties, and form a defensible upper bound for the cavity size and release volumes.

[5] Heights of repository for v002 and v030 are H_{v002} = 0.954063 m, and H_{v030} = 0.993311 m.

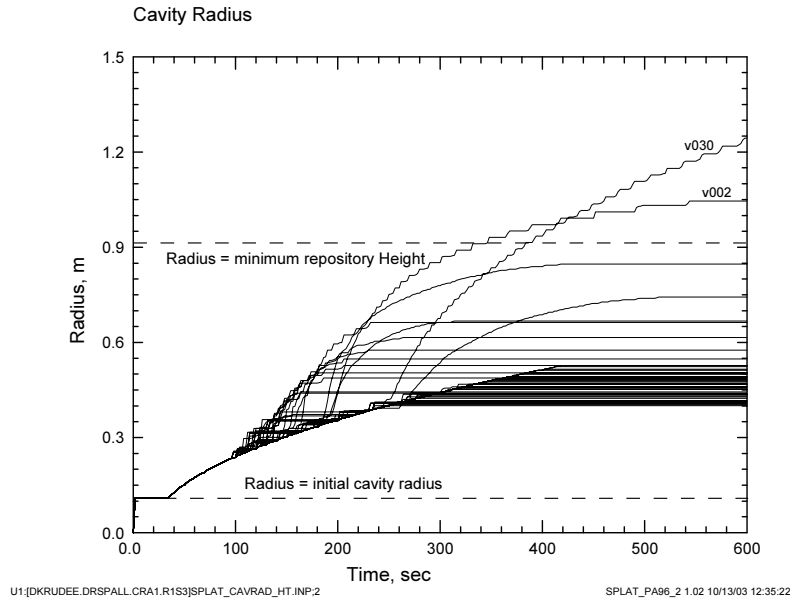

Figure 9.3-9. Horsetail Plot of CAVRAD for Scenario 3

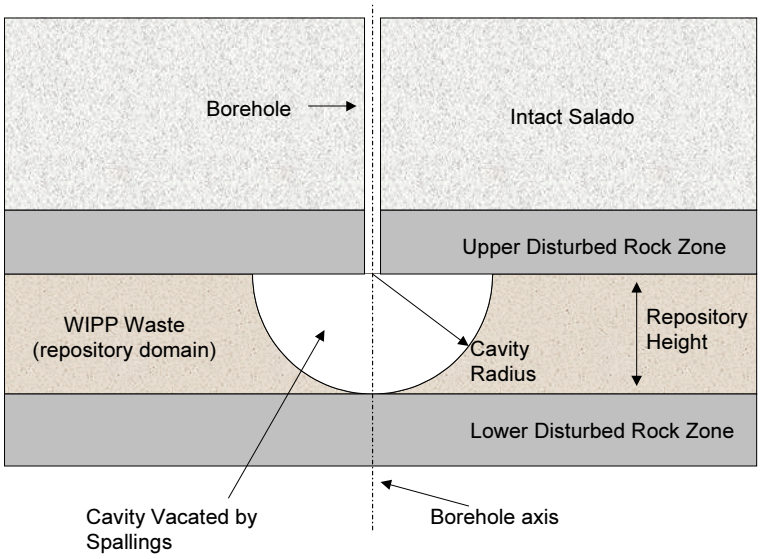

Figure 9.3-10. Schematic of Hemispherical Spallings Cavity Intersecting the Lower DRZ.

9.3.3.2 Special Cylindrical Runs, V002 and V030

Vectors v002 and v030 were re-run in cylindrical geometry, with the initial cavity radius set equal to their respective repository heights. DRSPALL is configured to start with an arbitrary cavity radius, though in normal runs the initial cavity radius is defined by the pseudo-cavity[6] assumption. The special cylindrical runs started with a large, gas-filled cylindrical cavity at REPIPRES = 14 MPa, connected to the surface by a mud-filled

[6] See section 3.3.2.

borehole. The DRSPALL code version 1.00 does not have the capability to start with an arbitrary pressure profile in the repository that resembles the profile observed as CAVRAD $\rightarrow H$ in the spherical runs. Therefore, a uniform pressure distribution and mud-filled column is used for the initial conditions that would be present at the end of the run in spherical geometry.

Figure 9.3-11 shows the history plot of CAVRAD for the v002 and v030 cylindrical runs. Cavity radius starts at the specified input values of 0.95 (v002) and 0.99 m (v030). For v002, no more cavity growth is observed. For v030, the cavity expands slightly to a stable value of 1.06 m

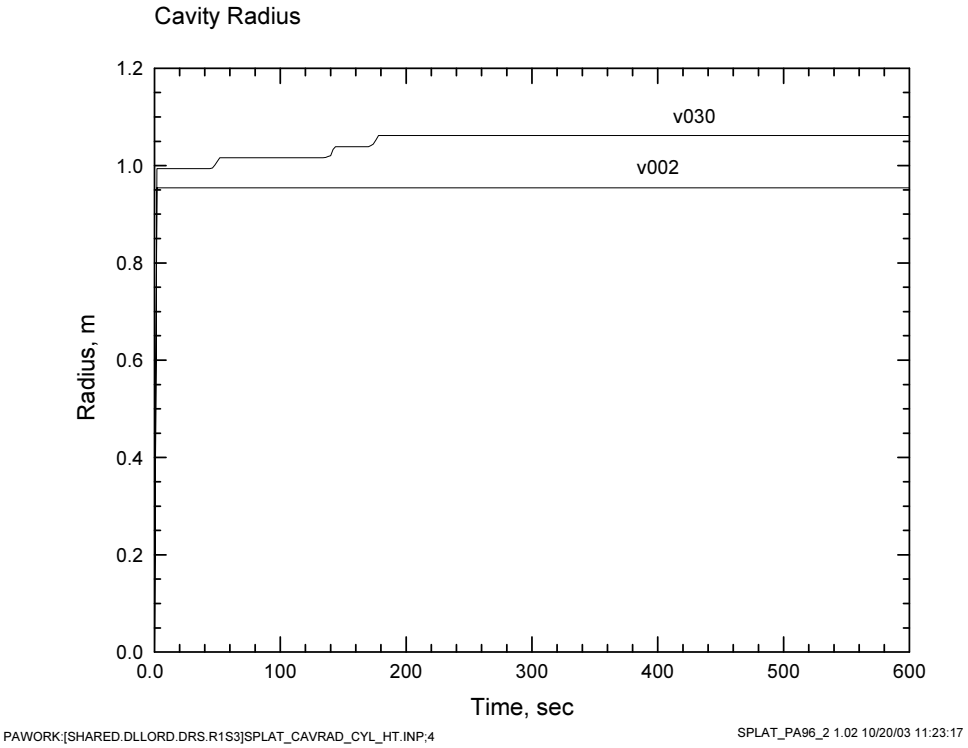

Figure 9.3-11. Horsetail Plot of CAVRAD for V002 and V030, Cylindrical Geometry, Scenario 3.

9.3.3.3 Scenario 3 Radial Effective Stress

A closer look at the stress and fluidization parameters is required to determine what mechanisms ultimately stabilize the cavity in v002 and v030. For v002, the radial effective stress profile is plotted at t = 140 seconds in Figure 9.3-12. Recall that the tensile strength for v002 is T_s = 0.125 MPa, which falls well below (more tensile) the given RADEFSTR profile. Similar profiles at earlier and later times were examined (not shown) and t = 140 second represents the largest tensile stresses observed. Thus, the stresses in this configuration are not sufficient to cause more failure and the system is failure-limited.

For v030, a similar strategy was used, and the largest tensile stresses near the cavity wall were observed near t = 200 seconds (see Figure 9.3-13). In this case, stresses 1 to 11 cm

interior to the cavity wall exceed the tensile strength (T_s = 0.139 MPa), but fall beyond the characteristic length, and thus do not fail the solid. Again, this vector is failure-limited. The mean RADEFSTR over L_t is computed explicitly in Table 9.3-3.

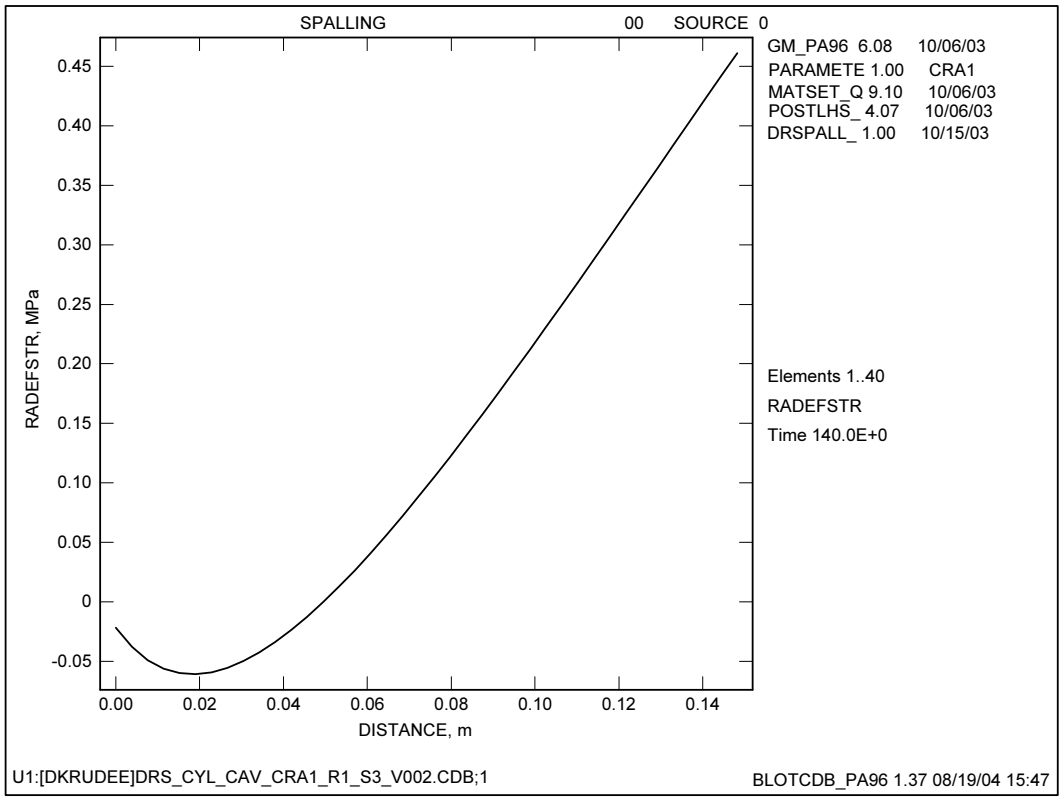

Figure 9.3-12. Spatial Plot of Radial Effective Stress (RADEFSTR) Near Cavity Wall for V002 in Cylindrical Geometry, T_S = 0.125 MPa.

Table 9.3-3. Calculation of Mean RADEFSTR Over L_t for S3, V030 at Runtime = 200 Seconds in Cylindrical Geometry.

DRSPALL COORD	Plot Coordinate	RADEFSTR	Average RADEFSTR over L_t
1.0559	0.0266	-1.3930E+05	
1.0597	0.0303	-1.3930E+05	
1.0635	0.0341	-4.9744E+04	
1.0673	0.0379	-8.9325E+04	
1.0711	0.0417	-1.2101E+05	-1.1460E+05
1.0749	0.0455	-1.4637E+05	
1.0787	0.0493	-1.6654E+05	
1.0825	0.0531	-1.8237E+05	
1.0862	0.0569	-1.9453E+05	

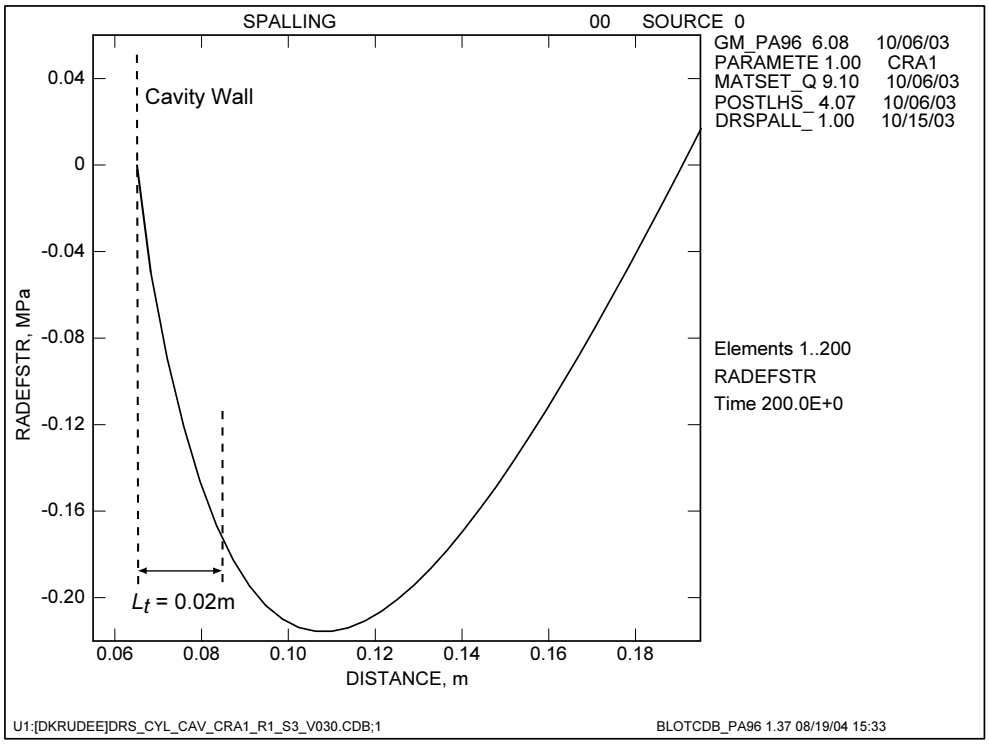

Figure 9.3-13. Spatial Plot of Radial Effective Stress (RADEFSTR) Near Cavity Wall for V030 at 200 Seconds in Cylindrical Geometry, T_S = 0.139 MPa.

9.3.3.4 Final SPLVOL2 Volumes for R1S3

Constructing the table of final releases (Table 9.3-1) for scenario 3 required merging the SPLVOL2 data from the spherical runs and the two special cylindrical runs. For the 48 vectors that stabilized in spherical geometry, the final SPLVOL2 value was simply extracted from the corresponding CDB output file at a runtime of 600 seconds. For v002 and v030, the final release was the sum of SPLVOL2 from the spherical geometry when CAVRAD = H (repository height), and SPLVOL2 calculated from the cylindrical run at runtime = 600 seconds. The procedure is demonstrated below.

9.3.3.5 Example Calculation of SPLVOL2, V002 and V030

The GROPECDB utility (WIPP PA, 1996b) is used to find the SPLVOL2 value that corresponds to the point when CAVRAD = H. First, the value for repository height H is retrieved from the CDB (variable name REPOSTCK), with H = 9.93311E-01 m for v030. Second, a listing of the data line number, runtime, SPLVOL2, and CAVRAD values is produced in order to find the point at which CAVRAD ≥ H. An excerpt from the ASCII output listing for v030 is given below in Table 9.3-4. The point where CAVRAD ≥ 9.93311E-01 gives SPLVOL2 = 7.70755E+00 (highlighted in table). A similar procedure for v002 yields SPLVOL2 = 7.21800E+00. Recall that SPLVOL2 is equivalent uncompacted volume and is much greater than the volume enclosed by the cavity radius, CAVRAD. Also, the enclosed volume includes cuttings volume, where as SPLVOL2 does not.

Table 9.3-4. Excerpt from GROPECDB Output File Analyzing R1S3, V030 for the Point When CAVRAD ≥ H (Highlighted).

STEP	TIME (sec)	CAVRAD (m)	SPLVOL2 (m^3)
315	4.23E+02	9.79097E-01	7.31703E+00
316	4.23E+02	9.83097E-01	7.41347E+00
317	4.24E+02	9.87098E-01	7.51070E+00
318	4.24E+02	9.91098E-01	7.60873E+00
319	4.25E+02	9.95098E-01	7.70755E+00
320	4.25E+02	9.95098E-01	7.70755E+00
321	4.30E+02	9.95098E-01	7.70755E+00
322	4.34E+02	9.99098E-01	7.80716E+00
323	4.35E+02	1.00310E+00	7.90758E+00

SPLVOL2 values are then retrieved from the cylindrical run CDB output using the standard WIPP PA SUMMARIZE (WIPP PA, 1996d) utility, with the results given in Table 9.3-5.

Table 9.3-5. SPLVOL2 Values at 600 Seconds for the Special Cylindrical Runs.

VECTOR	TIME	SPLVOL2
v002	6.00E+02	0.00000E+00
v030	6.00E+02	1.74541E+00

The final SPLVOL2 values are then taken as the sum of the spherical and cylindrical releases (across a row) as shown in Table 9.3-6. The WIPP utility SUMMARIZE is used to build the draft version of the ASCII table of final spallings volumes that is passed to CUTTINGS_S (WIPP PA, 2003k), though this draft does not have the updated final volumes from Table 9.3-6 for v002 and v030. These values are substituted manually to create a final version ready for transfer to CUTTINGS_S. A listing of this file is given in Appendix SPALL_TABLE.

Table 9.3-6. Summary of Final Releases for V002 and V030, R1S3 and R1S4. Units are m^3 Uncompacted Spall Volume.

Scenario	Vector	SPLVOL2 (SPH)	SPLVOL2 (CYL)	SPLVOL2 (FINAL)
R1S3	v002	7.21800E+00	0.00000E+00	7.21800E+00
	v030	7.70755E+00	1.74541E+00	9.45296E+00
R1S4	v002	7.29747E+00	0.00000E+00	7.29747E+00
	v030	7.80900E+00	4.25304E+00	1.20620E+01

9.3.4 Scenario 4 (R1S4) Results

Initial repository pressure was set to 14.8 MPa for scenario 4. The summary data presented in Figure 9.3-14 indicate that spallings releases range from 0 to 12.1 m^3 uncompacted volume. These same data are displayed graphically in the bar graph shown in Figure 9.3-14. Relative to the other three scenarios, these releases are larger; an expected result of higher initial repository pressure leading to higher tensile stresses and gas velocities.

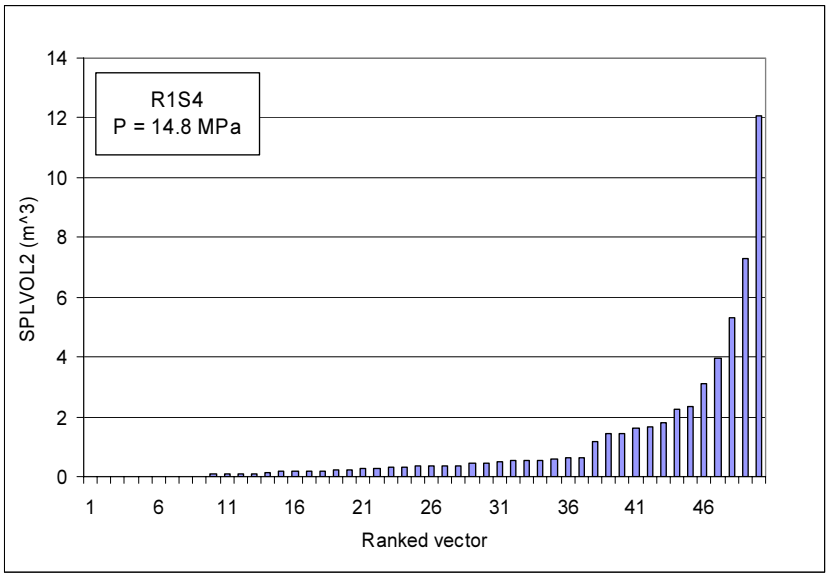

Figure 9.3-14. Bar Graph of SPLVOL2 Releases per Vector for Scenario 4, Ranked in Ascending Order.

9.3.4.1 Scenario 4 History Plots

Figure 9.3-15 shows the horsetail plot of CAVRAD for scenario 4. Cavity growth ahead of drilling begins between 100 and 150 seconds and stabilizes by 500 seconds in most vectors. The cavity radius of two vectors, v002 and 030, has not stabilized by 600 seconds, therefore requiring additional analysis.

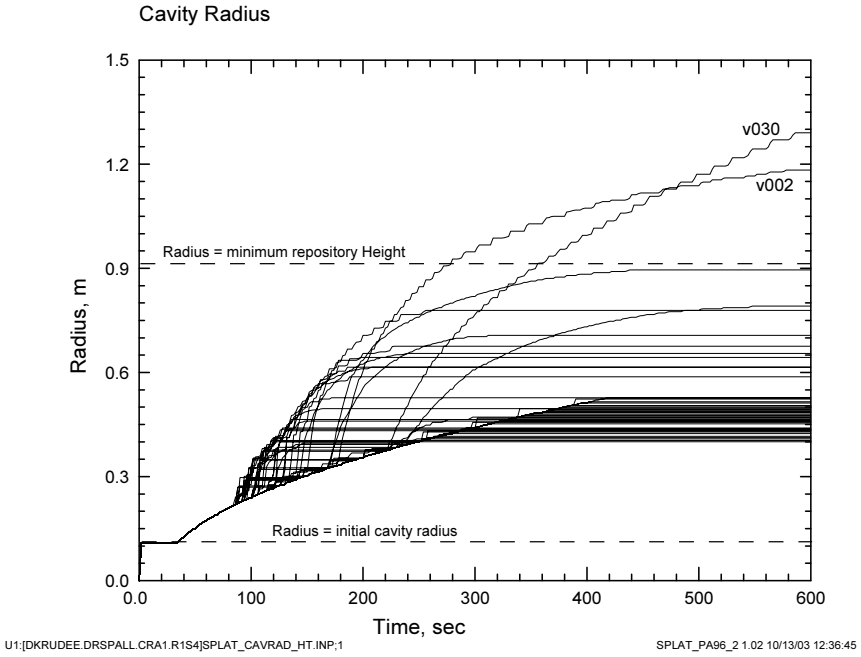

Figure 9.3-15. Horsetail Plot of CAVRAD for Scenario 4.

9.3.4.2 Special Cylindrical Runs, V002 and V030

Using the same procedure as described for scenario 3, v002 and 030 were re-run using the cylindrical geometry and a starting CAVRAD = *H*. Histories for the cylindrical runs are shown in Figure 9.3-16. V002 did not fail any further, while v030 failed out to CAVRAD = 1.15m where it then stabilized.

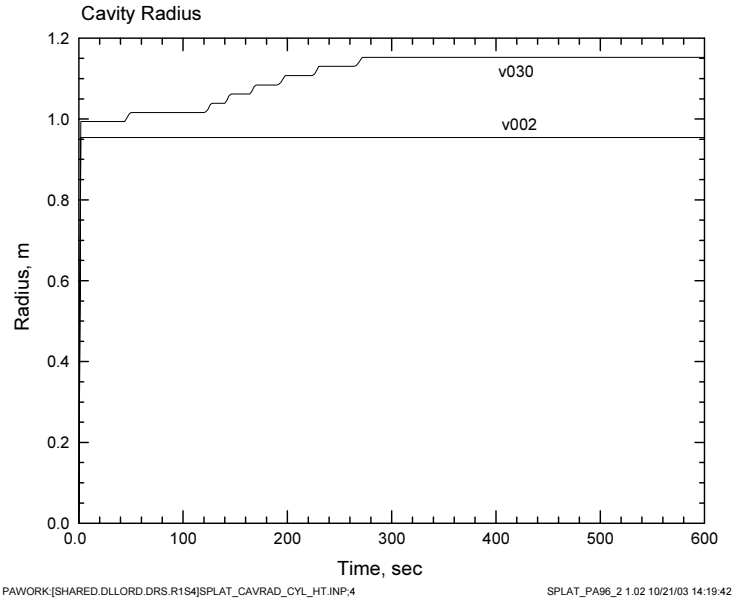

Figure 9.3-16. History Plot of CAVRAD for V002 and V030, Cylindrical Geometry, Scenario 4.

9.3.5 Scenario 4 Scatter Plots

Scatter plots for scenario 4 are shown in Figure 9.3-17, illustrating final SPLVOL2 values as a function of the four sampled input variables. Larger releases appear to correlate with low waste porosity, low waste permeability, and small particle diameter. No particular correlation is evident with tensile strength, though the sampling range is smaller for this variable than any of the other three. These observations are consistent with those from scenario 2, discussed in section 9.3.2.3.

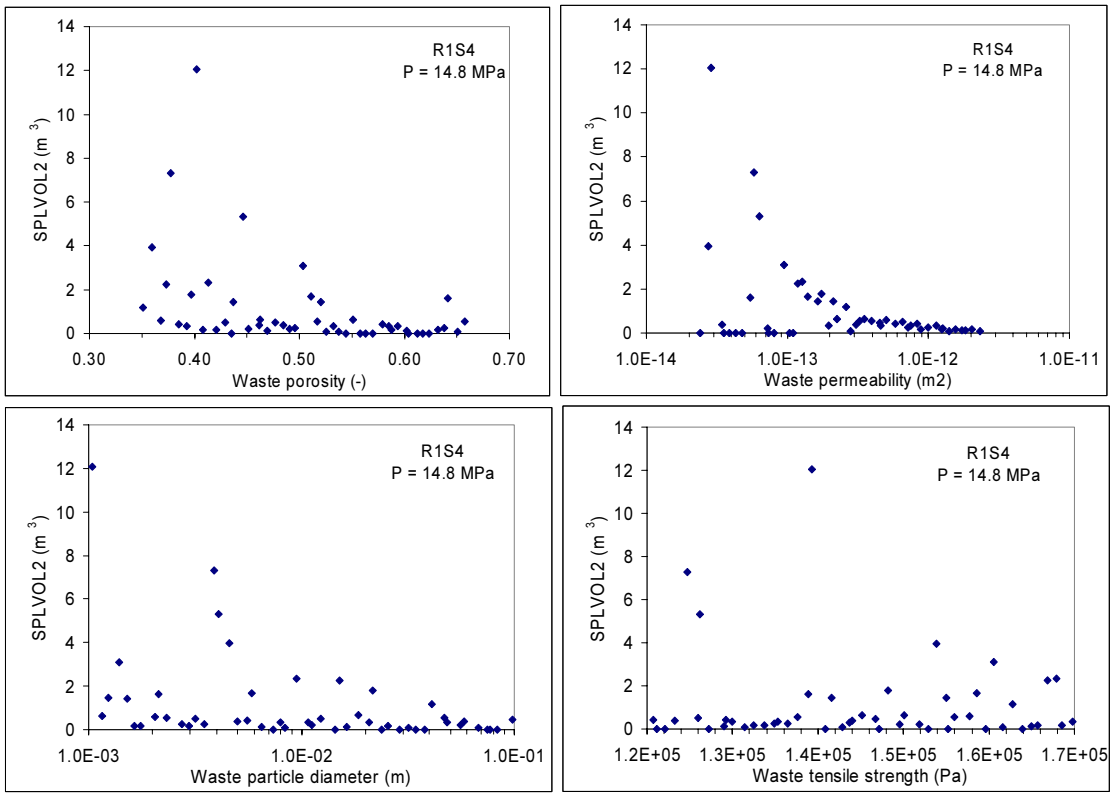

Figure 9.3-17. Scatter Plots of SPLVOL2 vs. Sampled Waste Properties for Porosity, Permeability, Tensile Strength and Particle Diameter for Scenario 4.

9.4 Multiple Intrusion Analyses by CCDFGF

Single-intrusion spall volumes presented in section 9.3 are ultimately wrapped into the WIPP PA through execution of the CCDFGF code (WIPP PA, 2003h) to produce the complimentary cumulative distribution functions. These data are compared directly against regulatory standards developed by EPA (EPA, 1985), and thus provide a measure of compliance with federal environmental law.

9.4.1 Spallings CCDFs

The 100 CCDFs for CRA replicate 1 spallings volumes are assembled in Figure 9.4-1. Each curve corresponds to a single PA vector. 59 of the 100 curves fall off-scale with values too low to plot. Figure 9.4-2 displays the mean and percentile curves for each replicate and the overall mean CCDF obtained by pooling replicates R1, R2, and R3. These summary curves are constructed by analyzing the distribution of probability values at selected points along the x-axis of Figure 9.4-1, computing the mean, 90th, 50th(median), and 10th quantile values, and plotting them as a function of 'volume removed.' This amounts to taking vertical slices through Figure 9.4-1, statistically analyzing the points where the slice intersects the horsetails, and connecting these statistical values (i.e., mean) with a smooth curve. While the 90th quantile for each replicate is plotted in Figure 9.4-2, the 50th (median) and 10th quantile curves are too low to appear on this plot scale. This reflects the large number of very low release vectors (off-scale in Figure 9.4-1), and relatively small number of large release vectors that yield a mean value much larger than the median value.

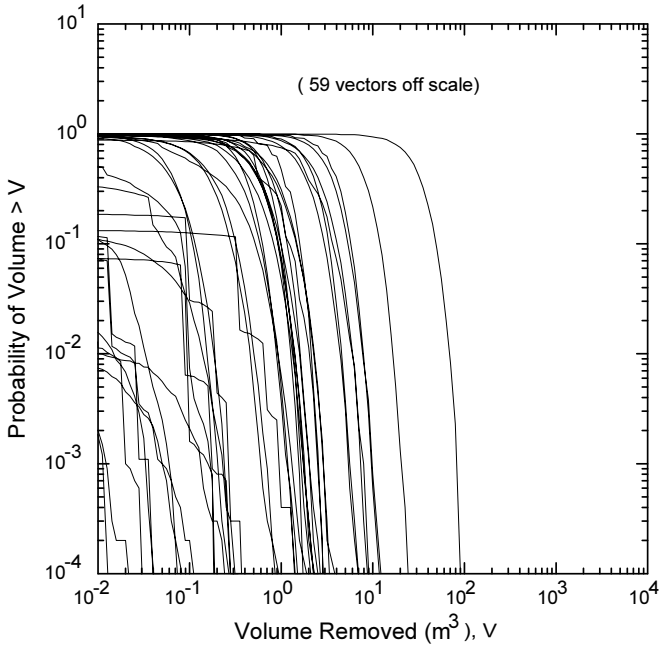

Figure 9.4-1. Distribution of CCDFs for Spallings Release Volume Over 10,000 Years, CRA Replicate 1.

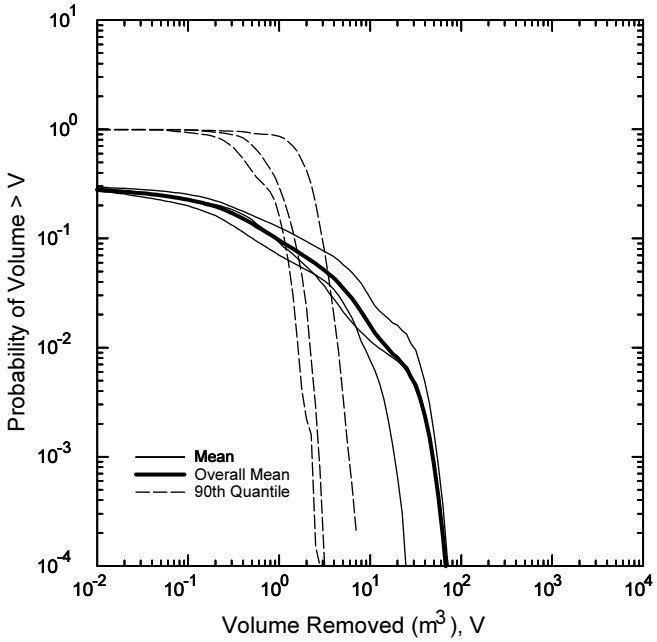

Figure 9.4-2. Mean and Percentile CCDF Curves for Spallings Release Volume Over 10,000 Years, CRA Replicates 1, 2, 3, and Pooled.

Shown next are the normalized spallings releases in EPA units with the regulatory limits overlaid for perspective. Figure 9.4-3 displays releases (in EPA units) for the 100 observations in CRA replicate 1. Here, 57 observations fall too low on the scale to appear on the figure. Shown for comparison in Figure 9.4-4 is the same plot (Helton et al., 1998) from the 1996 CCA. The CRA results are generally lower than the CCA, and distributed over several more orders of magnitude on the low end of the 'normalized release' axis. This is due largely to the implementation of the new spallings model DRSPALL that predicts mostly zero or small releases unless an appropriate combination of waste property values and high repository pressure is encountered.

Figure 9.4-5 shows the mean CCDFs for R1, R2, and R3, as well as the overall mean CCDF and percentile curves for the pooled 300 observations in the CRA. Again, the 50^{th} and 10^{th} quantile curves are too low to appear on this plot scale. Relative to the EPA limit, the overall mean spallings CCDF is about 33 times lower, and over most of the relevant domain, is several orders of magnitude lower. This indicates that the spallings releases alone are predicted to fall well within regulatory limits.

The effect of the new spallings model on mean spallings CCDFs relative to the 1996 CCA (Figure 9.4-6) is a slight shift down the probability axis for all release levels. For example, in the CCA, the probability of the mean spallings release exceeding 10^{-5} through 10^{-3} EPA units is about 0.5. In the current CRA analysis, the probability of exceeding the same is shown in Figure 9.4-5 at about 0.3 and 0.2, respectively.

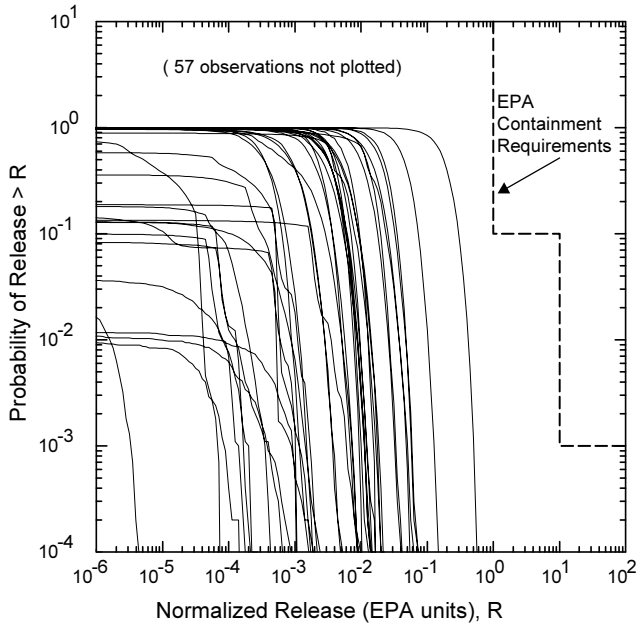

CCDFSUM_CRA1_ALL.AI_2

Figure 9.4-3. Distribution of CCDFs for Spallings Normalized Release Over 10,000 Years, CRA Replicate 1.

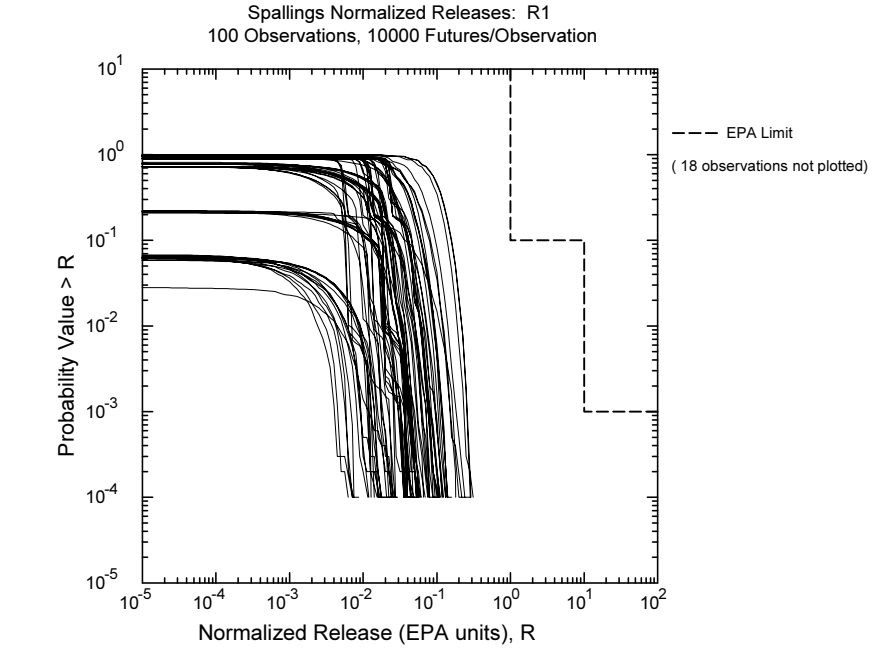

CCGF_CCDFSUM_POSTCCA_VERBOSE_1.PI_3

Figure 9.4-4. Distribution of CCDFs for Spallings Normalized Release Over 10,000 Years, CCA Replicate 1.

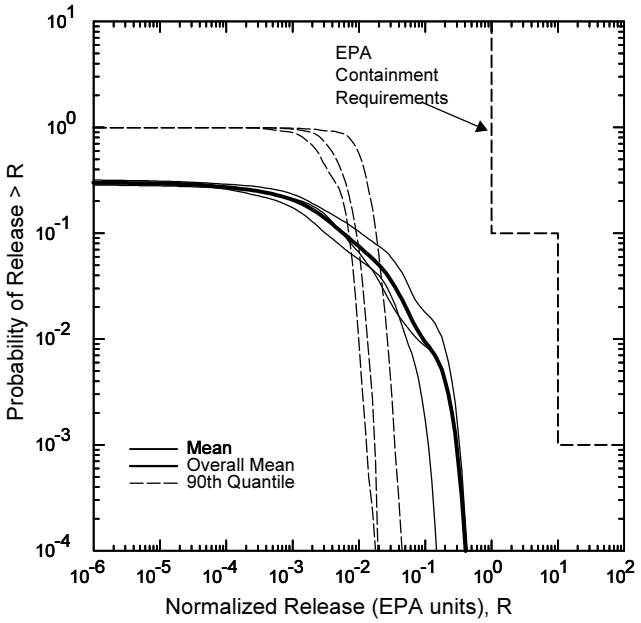

CCDFSUM_CRA1_ALL.AI_218

Figure 9.4-5. Mean and Percentile CCDF Curves for Spallings Normalized Release Over 10,000 Years, CRA Replicates 1, 2, 3, and Pooled.

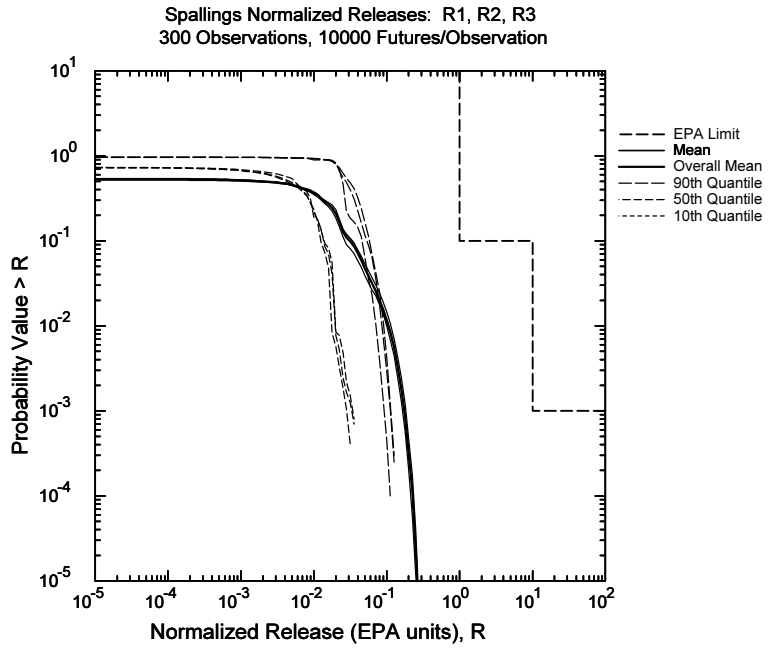

CCGF_CCDFSUM_POSTCCA_VERBOSE_1.PI_75

Figure 9.4-6. Mean and Percentile CCDF Curves for Spallings Normalized Release Over 10,000 Years, CCA Replicates 1,2,3, and Pooled.

9.5 Uncertainty and Sensitivity Analysis

9.5.1 Subjective Uncertainty

The range of uncertainty in the mean total spallings volumes (0 to 32.8 m^3) for all observations is shown in Figure 9.5-1. Vectors are listed in ascending order of spall volume. Each point on the plot represents the mean over 10,000 futures for a single set of uncertain parameters. At least 51 of 100 vectors from each replicate have 0 spallings release resulting in a median value of 0 for each replicate. The maximum mean total spallings volumes are 30.2, 32.8 and 11.7 m^3 for replicates R1 to R2 and R3, respectively.

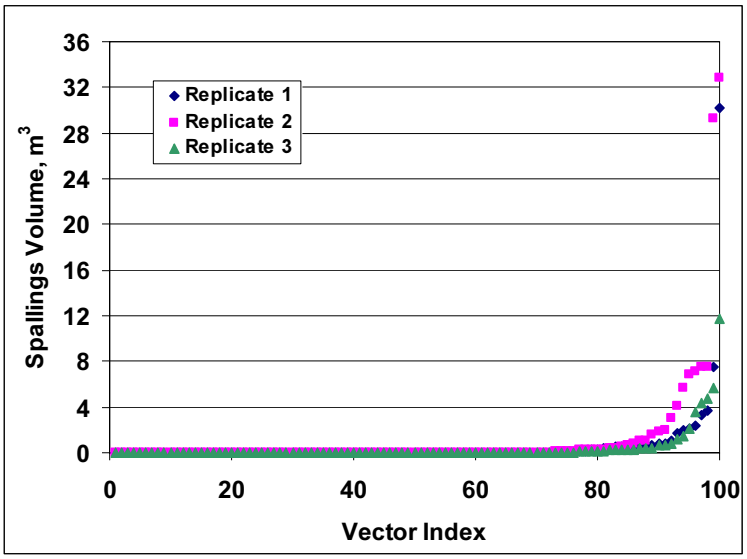

Figure 9.5-1. Mean Total Spallings Release Volume Ranked by Increasing Volume.

9.5.2 Sensitivity of Mean Total Spall Volumes to Waste Properties

Sensitivity of the multi-intrusion spalling volumes to the four sampled DRSPALL parameters (REPIPOR, PARTDIAM, REPIPERM and TENSLSTR) are shown as scatter plots in Figure 9.5-2 to Figure 9.5-5, respectively.

Larger mean spall volumes occur with smaller values of porosity, particle diameter, and permeability, where smaller refers to the lower third to half of the range of the independent parameter. These results are consistent with previous sensitivity studies (Section 7 and 8). Spall volumes generally occur uniformly over the rather narrow range of tensile strengths as in section 7, but with the 3 largest releases occurring in the lower half of the range due to higher resolution from using four pressure scenarios of 100 vectors each. However, the results do not provide conclusive support for a trend across the range. Scatter occurs, in part, due to the sensitivity of the spallings releases to repository pressures influenced by the vector-mapping technique described in Appendix MAP. Spalling occurs only for vectors that combine generally high pressures with waste material properties likely to allow spalling.

Observations that lead to generally low pressures will not spall, even if the waste material properties are subject to spalling. In addition, vectors may have zero spall releases even for high pressures, because many sets of DRSPALL parameters do not allow spall (section 9.3).

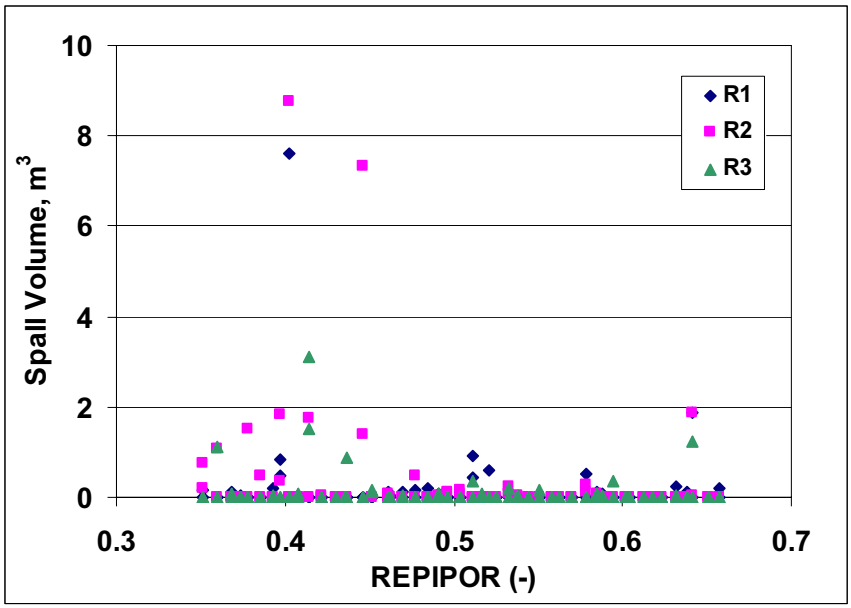

Figure 9.5-2. Scatter Plot of Mean Total Spallings Release Volume vs. Initial Repository Porosity (REPIPOR).

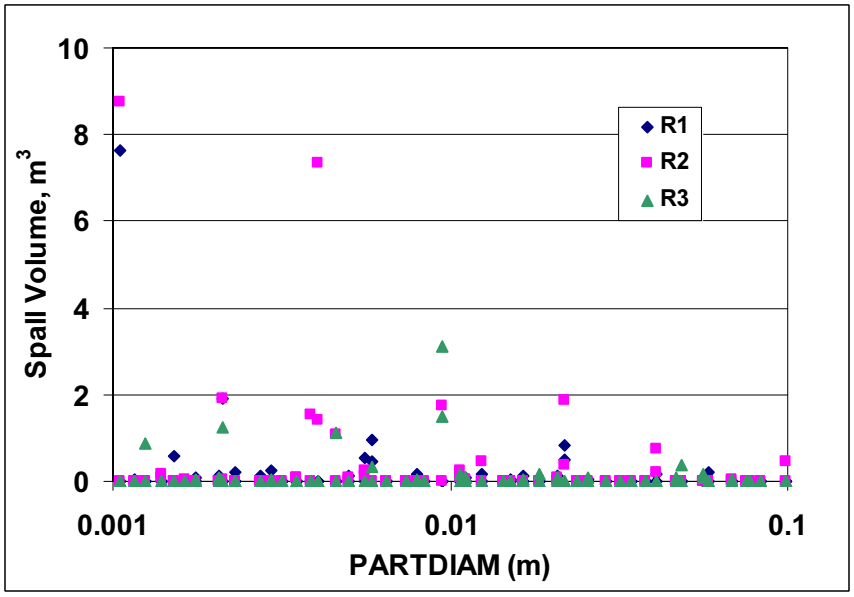

Figure 9.5-3. Scatter Plot of Mean Total Spallings Release Volume vs. Failed Waste Material Particle Diameter (PARTDIAM).

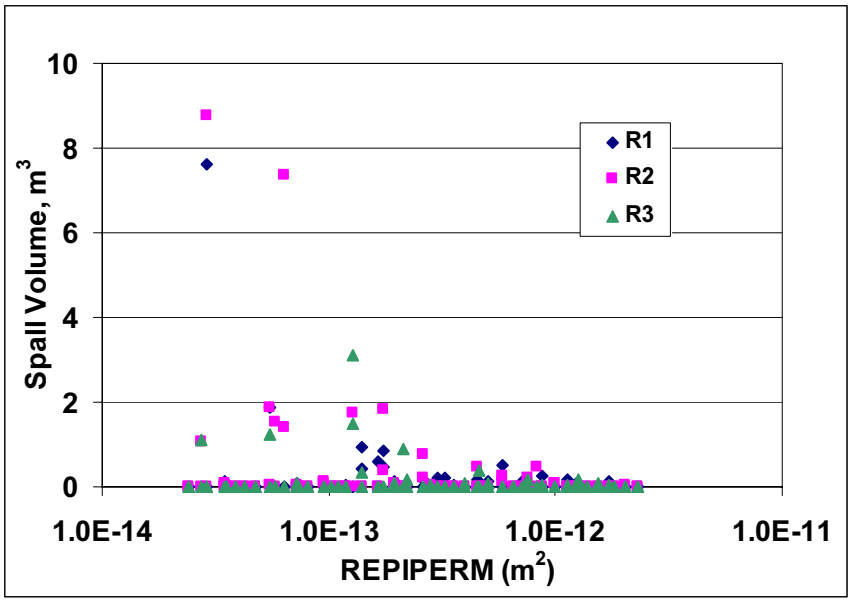

Figure 9.5-4. Scatter Plot of Mean Total Spallings Release Volume vs. Initial Repository Permeability (REPIPERM).

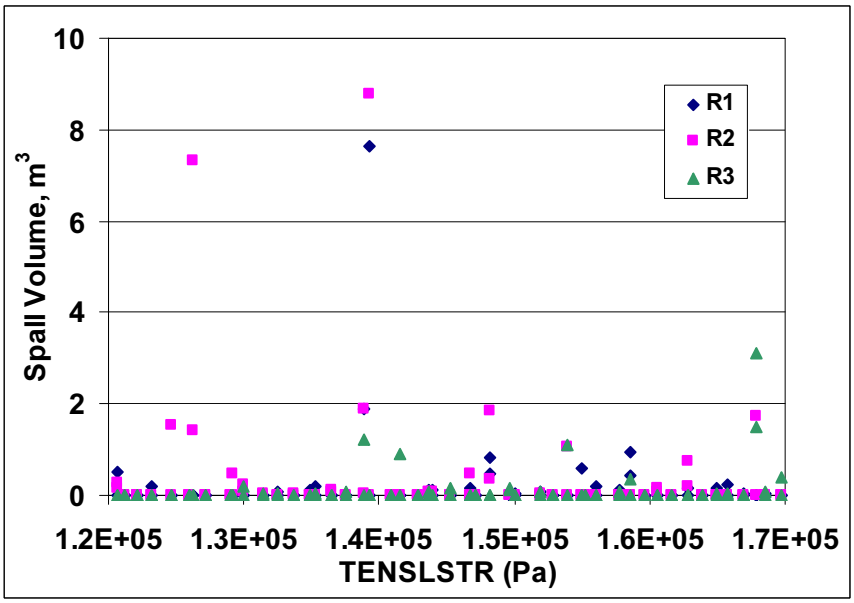

Figure 9.5-5. Scatter Plot of Mean Total Spallings Release Volume vs. Waste Material Tensile Strength (TENSLSTR).

9.5.3 Sensitivity of Mean Releases to Pressure

Single intrusion spall volume is clearly sensitive to repository pressure at the time of intrusion (section 9.3). It is therefore reasonable to assume that the mean spall volume over many intrusions would reflect this sensitivity, though selecting a representative pressure for a CCDF observation to demonstrate this hypothesis is not straightforward. The mean spallings volume used as the dependent variable in this analysis is the mean over 10,000 futures, where each future has a unique drilling sequence (number and timing of intrusions) and therefore unique history of repository pressures. In lieu of the actual pressures used to compute spall releases in each vector, the pressure from the undisturbed scenario (S1) at 10,000 years was selected as the independent variable for the sensitivity plot in Figure 9.5-6. This pressure is assumed to be representative of the repository pressure for a given vector, independent of the intrusion time. Figure 9.5-6 shows behavior comparable to the response surface discussed in section 9.3- spalling only occurs at pressures greater than 12 MPa.

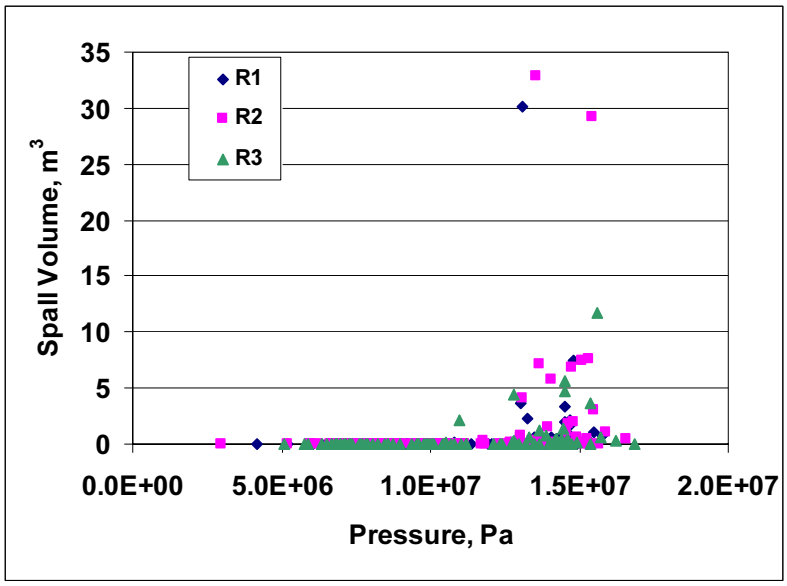

Figure 9.5-6. Scatter Plot of Mean Total Spallings Release Volume vs. Repository Pressure.

Important to determining the repository pressure is the uncertain parameter WMICDFLG (Stein and Zelinski, 2003), the indicator for microbial action in WIPP PA. Figure 9.5-7 displays the mean spall release over 10,000 futures against the single-intrusion spall release at 14.8 MPa. The values of WMICDFLG are keyed into the symbols on this plot, and partition the vectors into two sets of equal size: a set of vectors where microbial action occurs (WMICDFLG = 1 or 2) and a set where no microbial action is present (WMICDFLG = 0). Figure 9.5-7 indicates that spall releases occur only when microbial action is present to pressurize the repository beyond a threshold value (see Figure 9.5-6). For vectors that reside above the threshold pressure, the mean spallings volume appears to reflect the single-intrusion value, with larger mean releases resulting from larger single intrusion values.

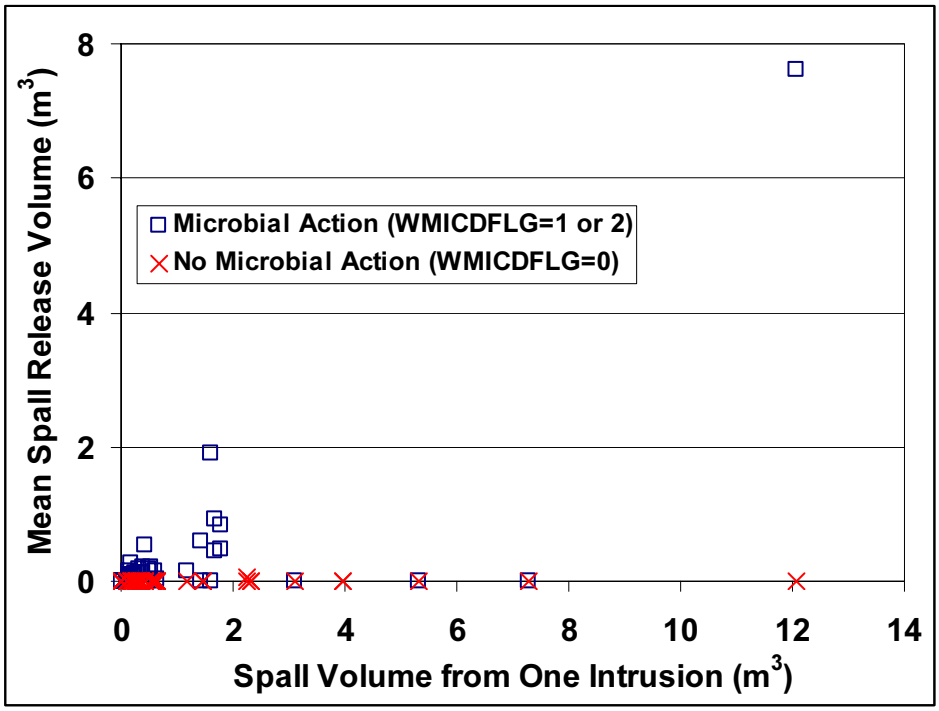

Figure 9.5-7. Sensitivity of Mean Total Spallings Release Volume to Microbial Action and Single Intrusion Spallings Volume, Replicate 1.

9.6 SUMMARY

The analysis of spallings release CCDFs and associated sensitivity studies for the WIPP PA conducted for the 2004 CRA indicates generally lower mean spallings releases with the new DRSPALL model than observed in past PA calculations for the 1996 CCA (compare Figure 9.4-3 and Figure 9.4-4). This stems largely from the generally lower single-intrusion spall values (section 9.3) relative to single-intrusion values from prior spall models. Most single intrusions with DRSPALL give zero spall release. These zeroes propagate through CCDFGF to result in lower overall mean CCDFs in spite of occasional, but very unlikely, single intrusion releases that exceed the maximum CCA single-intrusion values.

10 References

Aronson, D.G. 1986. "The Porous Medium Equation," *Nonlinear Diffusion Problems*. *Lecture Notes in Mathematics*, Vol. 1224. Eds. A. Fascano and M. Primucerio. New York, NY: Springer-Verlag.

ASME. 1990. *Quality Assurance Requirements for Nuclear Facility Applications*. NQA-2a-1990, Part 2.7. New York, NY: American Society of Mechanical Engineers.

Baker, R. 1998. *Practical Well Control, Fourth Edition*. Austin, TX: Petroleum Extension Service, University of Texas at Austin.

Barree, R.D., and M.W. Conway. 1995. "Experimental and Numerical Modeling of Convective Proppant Transport," *Journal of Petroleum Technology*. Vol. 47, no. 3, 216-222.

Belhaj, H.A., K.R. Agha, A.M. Nouri, S.D. Butt, H.F. Vaziri, and M.R. Islam. 2003. "Numerical Simulation of Non-Darcy Flow Utilizing the New Forchheimer's Diffusivity Equation," *MEOS 2003: Society of Petroleum Engineers 13th Middle East Oil and Gas Show and Conference, Technology Solution for the Oil & Gas Business: New Middle East Focus, Proceedings, 9-12 June, 2003, Bahrain International Exhibition Centre, Bahrain*. SPE 81499. *Richardson, TX: Society of Petroleum Engineers.*

Berglund, J.W. 1992. *Mechanisms Governing the Direct Removal of Wastes from the Waste Isolation Pilot Plant Repository Caused by Exploratory Drilling*. SAND92-7295. Albuquerque, NM: Sandia National Laboratories.

Chan, D.Y.C., B.D. Hughes, and L. Patterson. 1993. "Transient Gas Flow Around Boreholes," *Transport in Porous Media*. Vol. 10, 137-152.

Chavez, M.J. 2003. *Nuclear Waste Management Program Procedure NP19-1, Software Requirements, rev. 10.* Carlsbad, NM: Sandia National Laboratories.

Cherimisinoff, N.P., and P.N. Cherimisinoff. 1984. *Hydrodynamics of Gas-Solids Fluidization*. Houston, TX: Gulf Publishing Company.

Djordjevic, S., and M. Adams. 2003. "Utility Code for Spallings Model Porous Flow Validation." Memo to David Lord, June 5, 2003. Carlsbad, NM: Sandia National Laboratories. (Copy on file in the Sandia WIPP Records Center, Carlsbad, NM as ERMS# 531129.)

DOE (US Department of Energy). 1996. *Title 40 CFR Part 191 Compliance Certification Application for the Waste Isolation Pilot Plant*. DOE/CAO-1996-2184. Carlsbad, NM: US Dept. of Energy, Waste Isolation Pilot Plant, Carlsbad Area Office. Vols. I-XXI.

DOE (US Department of Energy). 2004. *Title 40 CFR Part 191 Subparts B and C Compliance Recertification Application for the Waste Isolation Pilot Plant*. DOE/WIPP 2004-3231. Carlsbad, NM: US Dept. of Energy, Waste Isolation Pilot Plant, Carlsbad Area Office.

EPA (US Environmental Protection Agency). 1985. "40 CFR Part 191: Environmental Standards for the Management and Disposal of Spent Nuclear Fuel, High-Level and Transuranic Radioactive Wastes; Final Rule," *Federal Register*. Vol. 50, no. 182, 38066-38089.

EPA (US Environmental Protection Agency). 1993. "40 CFR Part 191: Environmental Radiation Protection Standards for the Management and Disposal of Spent Nuclear Fuel, High-Level and Transuranic Radioactive Wastes; Final Rule," *Federal Register*. Vol. 58, no. 242, 66398-66416.

EPA (US Environmental Protection Agency). 1996. "40 CFR Part 194: Criteria for the Certification and Recertification of the Waste Isolation Pilot Plant's Compliance with the 40 CFR Part 191 Disposal Regulations; Final Rule," *Federal Register*. Vol. 61, no. 28, 5224-5245.

Ergun, S. 1952. "Fluid Flow Through Packed Columns," *Chemical Engineering Progress*. Vol. 48, no. 2, 89-94.

FLUENT 6.1 User's Guide. Lebanon, NH: Fluent, Inc., February 2003 **(11/22/04,** http://www.fluent.com/software/fluent/**)**.

Fox, R.W., and A.T. McDonald. 1985. *Introduction to Fluid Mechanics*, 3rd ed. New York, NY: John Wiley and Sons.

Gross, M.B., and T.W. Thompson. 1998. "Analysis Package for the Semi-Analytical Calculations Conducted In Support of Spalling Release Estimates for the 1998 Annual Sensitivity Study (ASA98)." Carlsbad, NM: CAO Technical Assistance Contract, Waste Isolation Pilot Plant (WIPP) Project. (On file in the Sandia WIPP Records Center, Carlsbad, NM as Analysis Package ERMS# 507629).

Hansen, F.D., M.K. Knowles, T.W. Thompson, M. Gross, J.D. McLennan, and J.F. Schatz. 1997. *Description and Evaluation of a Mechanistically Based Conceptual Model for Spall.* SAND97-1369. Albuquerque, NM: Sandia National Laboratories.

Hansen, F.D., T.W. Pfeifle, and D.L. Lord. 2003. *Parameter Justification Report for DRSPALL.* SAND2003-2930. Carlsbad, NM: Sandia National Laboratories.

Hassanizadeh, S.M., and W.G. Gray. 1987. "High Velocity Flow in Porous Media," *Transport in Porous Media*. Vol. 2, no. 6, 521-531.

Helton, J.C., and F.L. Davis. 2002. *Latin Hypercube Sampling and the Propagation of Uncertainty in Analyses of Complex Systems.* SAND2001-0417. Albuquerque, NM: Sandia National Laboratories.

Helton, J.C., J.E. Bean, J.W. Berglund, F.J. Davis, J.W. Garner, J.D. Johnson, R.J. MacKinnon, J. Miller, D.G. O'Brien, J.L. Ramsey, J.D. Schreiber, A. Shinta, L.N. Smith, D.M. Stoelzel, C. Stockman, and P. Vaughn. 1998. *Uncertainty and Sensitivity Analysis Results Obtained in the 1996 Performance Assessment for the Waste Isolation Pilot Plant*. SAND98-0365. Albuquerque, NM: Sandia National Laboratories.

Jaeger, J.C., and N.G.W. Cook. 1969. *Fundamentals of Rock Mechanics.* London, England: Chapman and Hall Ltd.

Khodaverdian, M.F., J.D. McLennan, I.D. Palmer, H.H. Vaziri, and X. Wang. 1996. *Cavity Completions for Enhanced Coalbed Methane Recovery*. GRI-95/0432. Chicago, IL: Gas Research Institute.

Lenke, L.R. 1996. *Blowout Experiments using Fine-Grained Silica Sands in an Axisymmetric Geometry.* NMERI Report 1996/7/32250. Albuquerque, NM: Sandia National Laboratories. (Copy on file in the Sandia WIPP Records Center, Carlsbad, NM as ERMS# 246953.)

Li, D., R.K. Svec, T.W. Engler, and R.B. Grigg, 2001. "Modeling and Simulation of the Wafer Non-Darcy Flow Experiments," *SPE Western Regional Meeting, Proceedings, 2001 SPE Odyssey, March 26-30, 2001, Bakersfield, California*. SPE 68822. Richardson, TX: Society of Petroleum Engineers. (Copy on file in the Sandia WIPP Records Center, Carlsbad, NM as ERMS# 535944.)

Lick, W.J. 1989. "Difference Equations from Differential Equations," *Lecture Notes in Engineering*. New York, NY: Springer-Verlag.

Lord, D.L., D.K. Rudeen, and C.W. Hansen. 2003. "Analysis Package for DRSPALL: Compliance Recertification Application, Part I – Calculation of Spall Values." Carlsbad, NM: Sandia National Laboratories. (Copy on file in the Sandia WIPP Records Center, Carlsbad, NM in Records Package ERMS# 530162.)

Lord, D.L., D.K. Rudeen, and C.W. Hansen. 2004. "Analysis Package for DRSPALL: Compliance Recertification Application, Part II (Rev 1)– CCDF Analysis." Carlsbad, NM: Sandia National Laboratories. (Copy on file in the Sandia WIPP Records Center, Carlsbad, NM as Records Package ERMS# 538467.)

MacKinnon, R., and G. Freeze. 1997. "Summary of EPA-Mandated Performance Assessment Verification Test (Replicate 1) and Comparison with the Compliance Certification Application Calculations." Albuquerque, NM: Sandia National Laboratories. (Copy on file in the Sandia WIPP Records Center, Carlsbad, NM as ERMS# 246674.)

Narayanaswamy, G., M.K. Sharma, and G.A. Pope. 1999. "Effect of Heterogeneity on the Non-Darcy Flow Coefficient," *Proceedings, 1998 SPE Gas Technology Symposium, March 15-18, 1998, Calgary, Canada*. SPE 39979. Richardson, TX: Society of Petroleum Engineers.

NAS/NRC (National Academy of Sciences/National Research Council). 1957. *The Disposal of Radioactive Waste on Land: Report of the Committee on Waste Disposal of the Division of Earth Sciences*. Publication 519. Washington, DC: National Academy of Sciences/National Research Council.

NRC (US Nuclear Regulatory Commission). 1988. *Peer Review for High-Level Nuclear Waste Repositories*. NUREG-1297. Washington, DC: US Nuclear Regulatory Commission, Division of High-Level Nuclear Waste Management.

Oran, E.S., and J.P. Boris. 1987. *Numerical Simulation of Reactive Flow*. New York, NY: Elsevier.

Podio, A.L., and A.P. Yang. 1986. "Well Control Simulator for IBM Personal Computer," *Proceedings, IADC/SPE Drilling Conference, February 10-12, 1986, Dallas, Texas*. IADC/SPE 14737. Richardson, TX: Society of Petroleum Engineers.

Press, W.H., B.P. Flannery, S.A. Teukolsky, and W.T. Vetterling. 1989. *Numerical Recipes in Pascal—The Art of Scientific Computing*. Cambridge, England: Cambridge University Press.

Public Law 102-579. 1992. *Waste Isolation Pilot Plant Land Withdrawal Act*. (106 Stat. 4777).

Rath, J.S. and A.L. Podio. 2000. "Advanced Transient Simulator for Studying Shallow Gas Blowouts," *Proceedings, IADC/SPE Drilling Conference, New Orleans, Louisiana,. February 23-25, 2000*. IADC/SPE 59178. Richardson, TX: Society of Petroleum Engineers.

Rechard, R.P., A.P. Gilkey, H.J. Iuzzolino, D.K. Rudeen, and K.A. Byle. 1993. *Programmer's Manual for CAMCON: Compliance Assessment Methodology Controller*. SAND90-1984. Albuquerque, NM: Sandia National Laboratories.

Ruth, D., and H. Ma. 1992. "On the Derivation of the Forchheimer Equation by Means of the Averaging Theorem," *Transport in Porous Media*. Vol. 7, no. 3, 255-264.

Serghides, T.K. 1984. "Estimate Friction Factor Accurately," *Chemical Engineering*. Vol. 91, no. 5, 63-64.

Stein, J., and W. Zelinski. 2003. "Analysis Package for BRAGFLO: Compliance Recertification Application." Carlsbad, NM: Sandia National Laboratories. (Copy on file in the Sandia WIPP Records Center, Carlsbad, NM as ERMS# 530142.)

Swift, P.N., and T.F. Corbet. 2000. "The Geologic and Hydrogeologic Setting of the Waste Isolation Pilot Plant," *Reliability Engineering and System Safety*. Vol. 69, no. 1-3, 47-58.

Timoshenko, S.P., and J.N. Goodier. 1970. *Theory of Elasticity*, 3rd ed. New York, NY: McGraw-Hill.

Webb, S. 2003. "FLUENT Code for Spallings Model Borehole Verification." Memo to Dave Lord, August 8, 2003. Carlsbad, NM: Sandia National Laboratories. (Copy on file in the Sandia WIPP Records Center, Carlsbad, NM as ERMS# 532255.)

Whitaker, S. 1996. "The Forchheimer Equation: A Theoretical Development," *Transport in Porous Media.* Vol. 25, no. 1, 27-61.

Wilson, C., D. Porter, J. Gibbons, E. Oswald, G. Sjoblom, and F. Caporuscio. 1997. *Conceptual Models Third Supplementary Peer Review Report.* Carlsbad, NM: US Dept. of Energy, Office of Regulatory Compliance, Carlsbad Area Office. (Copy on file in the Sandia WIPP Records Center, Carlsbad, NM as ERMS# 510788.)

WIPP PA (Performance Assessment). 1996a. "User's Manual for BLOTCDB, Version 1.37." Albuquerque, NM: Sandia National Laboratories. (Copy on file in the Sandia WIPP Records Center, Carlsbad, NM as ERMS# 237501.).

WIPP PA. 1996b. "User's Manual for GROPECDB (Version 2.12), Document Version 1.0." Albuquerque, NM: Sandia National Laboratories. (On file in the Sandia WIPP Records Center, Carlsbad, NM as ERMS# 237496.)

WIPP PA. 1996c. "User's Manual for SPLAT, Version 1.02." Albuquerque, NM: Sandia National Laboratories. (Copy on file in the Sandia WIPP Records Center, Carlsbad, NM as ERMS# 240960.)

WIPP PA. 1996d. "User's Manual for SUMMARIZE, Version 2.10." Albuquerque, NM: Sandia National Laboratories. (Copy on file in the Sandia WIPP Records Center, Carlsbad, NM as ERMS# 237460.)

WIPP PA. 1996e. "User's Manual for GENMESH, Version 6.07ZO." Albuquerque, NM: Sandia National Laboratories. (Copy on file in the Sandia WIPP Records Center, Carlsbad, NM as ERMS# 223291.)

WIPP PA. 1996f. "User's Manual for LHS, Version 2.41." Albuquerque, NM: Sandia National Laboratories. (Copy on file in the Sandia WIPP Records Center, Carlsbad, NM as ERMS# 230732.)

WIPP PA. 2001. "User's Manual for MATSET, Version 9.10." Carlsbad, NM: Sandia National Laboratories. (Copy on file in the Sandia WIPP Records Center, Carlsbad, NM as ERMS# 519736.)

WIPP PA. 2003. "Design Document for BRAGFLO, Version 5.0, Document Version 5.00." Carlsbad, NM: Sandia National Laboratories. (Copy on file in the Sandia WIPP Records Center, Carlsbad, NM as ERMS# 525702.)

WIPP PA. 2003a. "Design Document for DRSPALL Version 1.00, Document Version 1.10." Carlsbad, NM: Sandia National Laboratories. (Copy on file in the Sandia WIPP Records Center, Carlsbad, NM as ERMS# 529878.)

WIPP PA. 2003b. "Implementation Document for DRSPALL Version 1.00, Document Version 1.00." Carlsbad, NM: Sandia National Laboratories. (Copy on file in the Sandia WIPP Records Center, Carlsbad, NM as ERMS# 524781.)

WIPP PA. 2003c. "Installation and Checkout for DRSPALL Version 1.00, Document Version 1.00." Carlsbad, NM: Sandia National Laboratories. (Copy on file in the Sandia WIPP Records Center, Carlsbad, NM as ERMS# 524783.)

WIPP PA. 2003d. "Requirements Document for DRSPALL Version 1.00, Document Version 1.20." Carlsbad, NM: Sandia National Laboratories. (Copy on file in the Sandia WIPP Records Center, Carlsbad, NM as ERMS# 524777.)

WIPP PA. 2003e. "Software Quality Assurance Plan for DRSPALL Version 1.00, Document Version 1.10." Carlsbad, NM: Sandia National Laboratories. (Copy on file in the Sandia WIPP Records Center, Carlsbad, NM as ERMS# 529876.)

WIPP PA. 2003f. "User's Manual for DRSPALL, Version 1.00, Document Version 1.10." Carlsbad, NM: Sandia National Laboratories. (Copy on file in the Sandia WIPP Records Center, Carlsbad, NM as ERMS# 524780.)

WIPP PA. 2003g. "Verification and Validation Plan/Validation Document for DRSPALL, Version 1.00, Document Version 1.00." Carlsbad, NM: Sandia National Laboratories. (Copy on file in the Sandia WIPP Records Center, Carlsbad, NM as ERMS# 524782.)

WIPP PA. 2003h. "Design Document and User's Manual for CCDFGF (Version 5.00), Document Version 1.00." Carlsbad, NM: Sandia National Laboratories. (Copy on file in the Sandia WIPP Records Center, Carlsbad, NM as ERMS# 534071.)

WIPP PA. 2003i. "Design Document for EPAUNI (Version 1.15), Document Version 1.15." Carlsbad, NM: Sandia National Laboratories. (Copy on file in the Sandia WIPP Records Center, Carlsbad, NM as ERMS# 529567.)

WIPP PA. 2003j. "User's Manual for EPAUNI (Version 1.15), Document Version 1.15." Carlsbad, NM: Sandia National Laboratories. (Copy on file in the Sandia WIPP Records Center, Carlsbad, NM as ERMS# 529570.)

WIPP PA. 2003k. "User's Manual for CUTTING_S, Version 5.10." Carlsbad, NM: Sandia National Laboratories. (Copy on file in the Sandia WIPP Records CenterCarlsbad, NM as ERMS #532340.)

Yew, C., J. Hanson, and L. Teufel. 2003. "Waste Isolation Pilot Plant Spallings Conceptual Model Peer Review Report." Carlsbad, NM: Sandia National Laboratories. (Copy on file in the Sandia WIPP Records Center, Carlsbad, NM as ERMS# 532520.)

Appendix INPUTS

Shown below is a table of input parameter values for the two sensitivity studies using the input DRS file as a template. The LHS-sampled values are specific to vector 1, but the remaining values are common to all vectors. LHS-sampled parameters are highlighted. Column 3 lists either the parameter value or material and property name of the parameter on the CAMDAT binary file.

Parameter Description	Units	Material/Property Name or Value	S1_Lo	S1_Hi	S2	CRA
REPOSITORY						
Land Elevation	(m):	SPALLMOD SURFELEV	1037.3	1037.3	1037.3	1037.3
Repository top	(m):	SPALLMOD REPOSTOP	384.7	384.7	384.7	384.7
Total Thickness	(m):	0	0.93191	0.93191	1.2711	1.2288
DRZ Thickness	(m):	0.85	0.85	0.85	0.85	0.85
DRZ Permeability	(m^2):	SPALLMOD DRZPERM	1.00E-15	1.00E-15	1.00E-15	1.00E-15
Outer Radius	(m):	19.2	1.92	19.2	19.2	19.2
Initial Gas Pressure	(Pa):	SPALLMOD REPIPRES	1.351E+07	1.44E+07	9.96E+06	1.00E+07
Far-Field In-Situ Stress	(m):	SPALLMOD FFSTRESS	1.49E+07	1.49E+07	1.49E+07	1.49E+07
WASTE						
Porosity	(-):	SPALLMOD REPIPOR	0.3626	0.3626	0.5327	0.5166
Permeability	(m^2):	SPALLMOD REPIPERM	2.12E-13	2.12E-13	1.409E-12	3.97E-13
Forch Beta	(-):	1.156E-06	1.156E-06	1.15E-06	1.15E-06	1.15E-06
Biot Beta	(-):	SPALLMOD BIOTBETA	1	1	1	1
Poisson Ratio	(-):	SPALLMOD POISRAT	0.4085	0.4085	0.38	0.38
Cohesion	(Pa):	SPALLMOD COHESION	1.40E+05	1.40E+05	1.40E+05	1.40E+05
Friction Angle	(deg):	SPALLMOD FRICTANG	45.8	45.8	45.8	45.8
Tensile Strength	(Pa):	SPALLMOD TENSLSTR	1.431E+05	1.431E+05	4.961E+04	1.376E+05
Lt	(m):	0.02	0.02	0.02	0.02	0.02
Particle Diameter	(m):	SPALLMOD PARTDIAM	2.97E-03	2.97E-03	1.50E-03	4.69E-02
Gas Viscosity	(Pa-s):	H2 VISCO	8.934E-06	8.934E-06	8.934E-06	8.934E-06
MUD						
Density	(kg/m^3):	DRILLMUD DNSFLUID	1210	1210	1210	1210
Viscosity	(Pa-s):	DRILLMUD VISCO	9.17E-03	9.17E-03	9.17E-03	9.17E-03
Wall Roughness Pipe	(m):	SPALLMOD PIPEROUG	5.00E-05	5.00E-05	5.00E-05	5.00E-05
Wall Roughness Annulus	(m):	SPALLMOD ANNUROUG	2.96E-03	2.96E-03	5.00E-05	5.00E-05
Max Solids Vol. Frac.	(Pa-s):	SPALLMOD MUDSOLMX	0.613	0.613	0.615	6.15E-01
Solids Viscosity Exp.	(Pa-s):	SPALLMOD MUDSOLVE	-1.65	-1.65	-1.5	-1.5
WELLBORE/DRILLING						
Bit Diameter	(m):	BOREHOLE DIAMMOD	0.31115	0.31115	0.31115	0.31115
Pipe Diameter	(m):	BOREHOLE PIPED	0.1143	0.1143	0.1143	0.1143
Collar Diameter	(m):	BOREHOLE COLDIA	0.2032	0.2032	0.2032	0.2032
Pipe Inside Diameter	(m):	SPALLMOD PIPEID	0.09718	0.09718	0.09718	0.09718

Parameter Description	Units	Material/Property Name or Value	S1_Lo	S1_Hi	S2	CRA
Collar Length	(m):	BOREHOLE L1	182.88	182.88	182.88	182.88
Exit pipe Length	(m):	0	0	0	0	0
Exit Pipe Diameter	(m):	0.2032	0.2894	0.2894	0.2894	2.89E-01
Drilling Rate	(m/s):	SPALLMOD DRILRATE	3.99E-03	3.99E-03	4.45E-03	4.45E-03
Bit Above Repository	(m):	0.15	0.15	0.15	0.15	0.15
Mud Pump Rate	(m^3/s):	SPALLMOD MUDPRATE	0.01685	0.01685	0.020181	0.020181
Max Pump Pressure	(Pa):	27.5d6	2.75E+07	2.75E+07	2.75E+07	2.75E+07
DDZ Thickness	(m):	SPALLMOD DDZTHICK	0.16	0.16	0.16	0.16
DDZ Permeability	(m^2):	SPALLMOD DDZPERM	1.276E-14	1.276E-14	1E-14	1.00E-14
Stop Drill Exit Vol Rate	(m^3/s):	SPALLMOD STPDVOLR	1000	1000	1000	1000
Stop Pump Exit Vol Rate	(m^3/s):	SPALLMOD STPPVOLR	1000	1000	1000	1000
Stop Drilling Time	(s):	1.00E+03	1000	1000	1000	1000
COMPUTATIONAL						
Spherical/Cylindrical	(S/C):	S	S	S	S	S
Allow Fluidization	(Y/N):	Y	Y	Y	Y	Y
Max Run Time	(s):	600	600	600	600	600
Respository Cell Length	(m):	0.004	0.004	0.004	0.004	0.004
radius, Growth rate	(m,-):	0.5, 1.01	0.5, 1.01	0.5, 1.01	0.5, 1.01	0.5, 1.01
Wellbore Cell Length	(m):	2.0	2.00E+00	2.00E+00	2.00E+00	2.00E+00
wellbore Zone Growth Rate	(-):	1.0	1.00E+00	1.00E+00	1.00E+00	1.00E+00
First wellbore Zone	(-):	10	327	327	327	327
Well Stability factor	(-):	0.05	0.05	0.05	0.05	0.05
Repository Stability factor	(-):	5	5	5	5	5
Mass Diffusion factor	(-):	0	0	0	0	0.0001
Momentum Diffusion factor	(-):	0.01	0.01	0.01	0.01	0.01
PARAMETERS						
Pi	(-):	REFCON PI	3.1416	3.1416	3.1416	3.1416
Atmospheric Pressure	(Pa):	SPALLMOD REFPRS	1.02E+05	1.02E+05	1.02E+05	1.02E+05
gravity	(m/s^2):	REFCON GRAVACC	9.8067	9.8067	9.8067	9.8067
Gas Constant	(J/kg K):	BLOWOUT RGAS	4116	4116	4116	4116
Repository Temperature	(K):	BLOWOUT TREPO	300	300	300	300
Water Compressibility	(1/Pa):	BRINESAL COMPRES	3.1E-10	3.1E-10	3.1E-10	3.10E-10
Waste Density	(kg/m^3):	BLOWOUT RHOS	2650	2650	2650	2650
Salt Density	(kg/m^3):	SPALLMOD SALTDENS	2180	2180	2180	2180
Shape Factor	(-):	SPALLMOD SHAPEFAC	0.479	0.479	0.1	0.1
Tensile Velocity	(m/s):	1.00E+03	1000	1000	1000	1000
Bit Nozzle Number	(-):	3.00E+00	3	3	3	3
Bit Nozzle Diameter	(m):	1.1112E-02	0.011112	0.011112	0.011112	0.011112
Choke Efficiency	(-):	9.00E-01	0.9	0.9	0.9	0.9

Appendix DRS

The following is a listing of the file "DRS_SENS1_LO.DRS". This is a generic input file that, coupled with the CAMDAT file for a given vector, is required input to DRSPALL.

Parameter values retrieved from the WIPP PA Parameter Database appear in MATERIAL PROPERTY format below. Parameter values set by this file appear as a number.

```
REPOSITORY
Land Elevation                    (m):  SPALLMOD SURFELEV
Repository top                    (m):  SPALLMOD REPOSTOP
Total Thickness                   (m):  0.0
DRZ Thickness                     (m):  0.85     !SPALLMOD DRZTCK
DRZ Permeability                (m^2):  SPALLMOD DRZPERM
Outer Radius                      (m):  19.2
Initial Gas Pressure             (Pa):  SPALLMOD REPIPRES
Far-Field In-Situ Stress          (m):  SPALLMOD FFSTRESS

WASTE
Porosity                          (-):  SPALLMOD REPIPOR
Permeability                    (m^2):  SPALLMOD REPIPERM
Forch Beta                        (-):  1.15e-6
Biot Beta                         (-):  SPALLMOD BIOTBETA
Poisoson   Ratio                  (-):  SPALLMOD POISRAT
Cohesion                         (Pa):  SPALLMOD COHESION
Friction Angle                  (deg):  SPALLMOD FRICTANG
Tensile Strength                 (Pa):  SPALLMOD TENSLSTR
Lt                                (m):  0.02
Particle Diameter                 (m):  SPALLMOD PARTDIAM
Gas Viscosity                  (Pa-s):  H2       VISCO

MUD
Density                      (kg/m^3):  DRILLMUD DNSFLUID
Viscosity                      (Pa-s):  DRILLMUD VISCO
Wall Roughness Pipe               (m):  SPALLMOD PIPEROUG
Wall Roughness Annulus            (m):  SPALLMOD ANNUROUG
Max Solids Vol. Frac.          (Pa-s):  SPALLMOD MUDSOLMX
Solids Viscosity Exp.          (Pa-s):  SPALLMOD MUDSOLVE

WELLBORE/DRILLING
Bit Diameter                      (m):  BOREHOLE DIAMMOD
Pipe Diameter                     (m):  BOREHOLE PIPED
Collar Diameter                   (m):  BOREHOLE COLDIA
Pipe Inside Diameter              (m):  SPALLMOD PIPEID
Collar Length                     (m):  BOREHOLE L1
Exit pipe Length                  (m):  0.0
Exit Pipe Diameter                (m):  0.2032
Drilling Rate                   (m/s):  SPALLMOD DRILRATE
Bit Above Respository(init.)      (m):  0.15
Mud Pump Rate                 (m^3/s):  SPALLMOD MUDPRATE
Max Pump Pressure                (Pa):  27.5d6
DDZ Thickness                     (m):  SPALLMOD DDZTHICK
DDZ Permeability                (m^2):  SPALLMOD DDZPERM
```

Stop Drill Exit Vol Rate	(m^3/s):	SPALLMOD	STPDVOLR
Stop Pump Exit Vol Rate	(m^3/s):	SPALLMOD	STPPVOLR
Stop Drilling Time	(s):	1.0000E+03	

COMPUTATIONAL		
Spherical/Cylindrical	(S/C):	S
Allow Fluidization	(Y/N):	Y
Max Run Time	(s):	600.
Respository Cell Length	(m):	0.004
radius, Growth rate	(m,-):	0.5, 1.01
Wellbore Cell Length	(m):	2.0
wellbore Zone Growth Rate	(-):	1.0
First wellbore Zone	(-):	10
Well Stability factor	(-):	0.05
Repository Stability factor	(-):	5.0
Mass Diffusion factor	(-):	0.0
Momentum Diffusion factor	(-):	0.01

PARAMETERS			
Pi	(-):	REFCON	PI
Atmospheric Pressure	(Pa):	SPALLMOD	REFPRS
gravity	(m/s^2):	REFCON	GRAVACC
Gas Constant	(J/kg K):	BLOWOUT	RGAS
Repository Temperature	(K):	BLOWOUT	TREPO
Water Compressibility	(1/Pa):	BRINESAL	COMPRES
Waste Density	(kg/m^3):	BLOWOUT	RHOS
Salt Density	(kg/m^3):	SPALLMOD	SALTDENS
Shape Factor	(-):	SPALLMOD	SHAPEFAC
Tensile Velocity	(m/s):	1.0000E+03	
Bit Nozzle Number	(-):	3.0000E+00	
Bit Nozzle Diameter	(m):	1.1112E-02	
Choke Efficiency	(-):	9.0000E-01	

Appendix MAP

The following table lists the mapping of DRSPALL LHS sampled vectors (only one replicate of 50 vectors) to CCDF vectors (three replicates of 100 vectors). Each DRSPALL vector is used twice in each replicate. This table is used to pair up the DRSPALL vector with appropriate CCDF release vector or observation. Mapping is determined by sampled variable (material/property) SPALLMOD/RNDSPALL. RNDSPALL was uniformly sampled over the range 0 to 1 and is mapped to vector number (1 to 50) using the following equation:

$$n = \text{int}(\frac{r}{\Delta r} + 1)$$

$$\Delta r = \frac{1}{N}$$

where n is the DRSPALL vector number , r is the random variable (RNDSPALL), and N is the total number of DRSPALL vectors.

	DRSPALL Vector				DRSPALL Vector		
Vector	R1	R2	R3	Vector	R1	R2	R3
1	9	20	3	51	31	25	43
2	18	9	6	52	13	29	11
3	9	20	9	53	38	29	22
4	17	1	3	54	28	37	18
5	29	9	17	55	13	14	19
6	41	50	33	56	28	18	4
7	35	23	46	57	23	50	29
8	2	45	13	58	15	23	48
9	38	42	23	59	48	11	6
10	50	24	44	60	47	12	38
11	42	41	41	61	33	39	36
12	8	21	11	62	39	11	28
13	46	48	50	63	15	44	7
14	29	14	31	64	25	27	16
15	20	3	32	65	8	13	34
16	12	8	2	66	6	38	40
17	10	49	45	67	27	17	38
18	34	36	10	68	26	18	14
19	21	28	46	69	37	2	30
20	45	5	49	70	43	19	49
21	20	33	25	71	32	34	30
22	4	7	45	72	44	46	27
23	47	30	47	73	49	8	16
24	12	34	28	74	34	32	25
25	30	4	13	75	35	49	26

	DRSPALL Vector				DRSPALL Vector		
Vector	R1	R2	R3	Vector	R1	R2	R3
26	46	10	37	76	3	15	37
27	43	40	23	77	42	40	19
28	4	19	7	78	31	21	43
29	6	16	50	79	14	44	20
30	26	6	40	80	7	3	9
31	5	43	24	81	39	17	15
32	40	39	31	82	49	37	24
33	16	12	36	83	18	4	17
34	3	36	8	84	25	30	29
35	32	31	21	85	37	2	4
36	24	47	48	86	41	22	18
37	23	5	15	87	24	24	39
38	19	45	21	88	46	33	35
39	19	41	10	89	14	35	14
40	36	10	12	90	33	7	20
41	5	27	35	91	22	1	22
42	21	25	44	92	40	31	5
43	2	48	26	93	36	35	12
44	7	32	27	94	1	47	1
45	11	42	41	95	48	15	32
46	11	6	8	96	10	28	47
47	27	14	1	97	16	16	5
48	44	26	42	98	22	26	33
49	1	46	34	99	30	38	39
50	50	22	42	100	17	43	2

There are instances where LHS sampled values ended up exactly on the boundary between two bins which resulted in consecutive DRSPALL vectors being assigned to 1 and 3 PA vectors instead of 2 and 2. In replicate 1, vector 45 is used once and vector 46 three times. In replicate 2, vector 13 is used once and vector 14 three times.

Appendix S1_LO_SCATTER

The following scatter plots document the sensitivity of spallings releases (SPLVOL2) to the sampled input variables from the Sensitivity Study 1 over the pressure range 8-15 MPa.

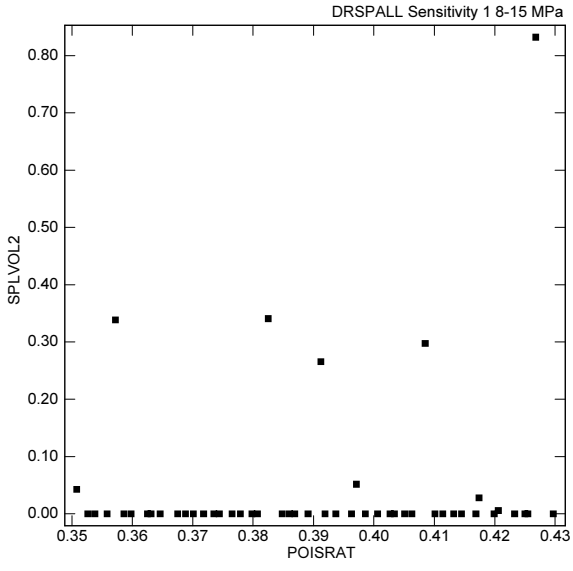

U1:[DKRUDEE.DRSPALL.SAND.SENS1.QA_RESULTS.CORRECTED_MUD.LO]STEP_S1_LO.INP;2
STEPWISE_PA9 2.21 05/05/04 08:21

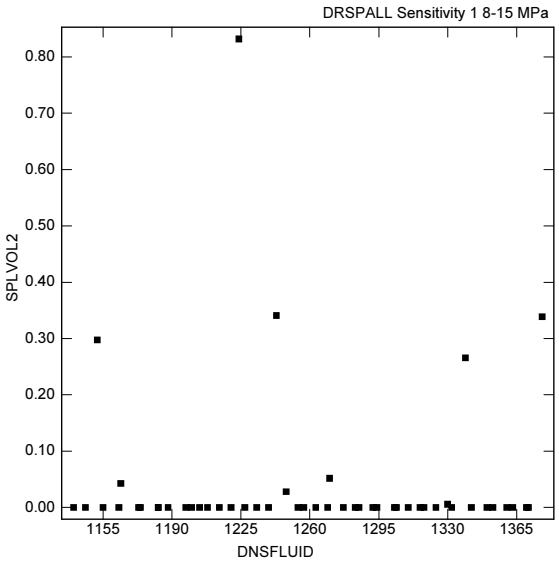

U1:[DKRUDEE.DRSPALL.SAND.SENS1.QA_RESULTS.CORRECTED_MUD.LO]STEP_S1_LO.INP;2
STEPWISE_PA9 2.21 05/05/04 08:21

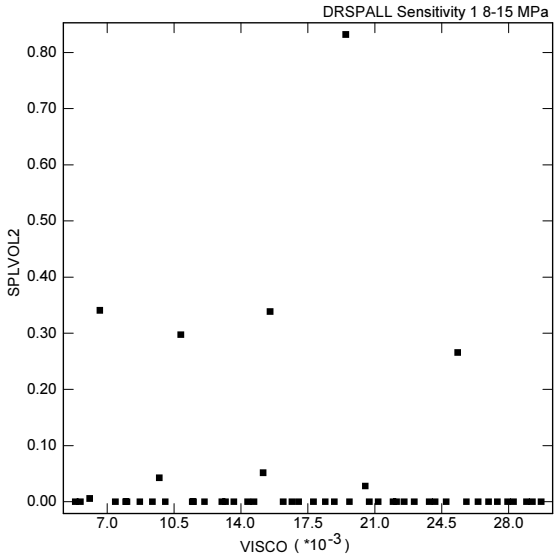

U1:[DKRUDEE.DRSPALL.SAND.SENS1.QA_RESULTS.CORRECTED_MUD.LO]STEP_S1_LO.INP;2
STEPWISE_PA9 2.21 05/05/04 08:21

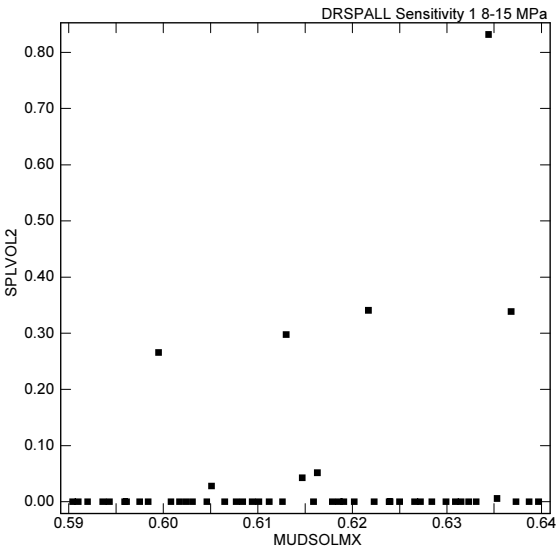

U1:[DKRUDEE.DRSPALL.SAND.SENS1.QA_RESULTS.CORRECTED_MUD.LO]STEP_S1_LO.INP;2
STEPWISE_PA9 2.21 05/05/04 08:21

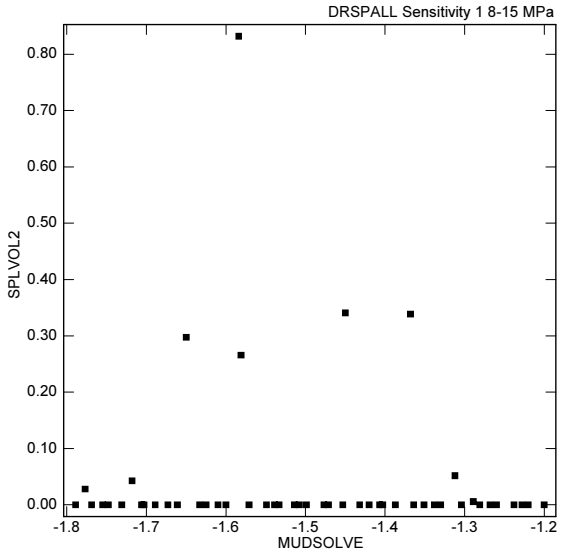

U1:[DKRUDEE.DRSPALL.SAND.SENS1.QA_RESULTS.CORRECTED_MUD.LO]STEP_S1_LO.INP;2
STEPWISE_PA9 2.21 05/05/04 08:21

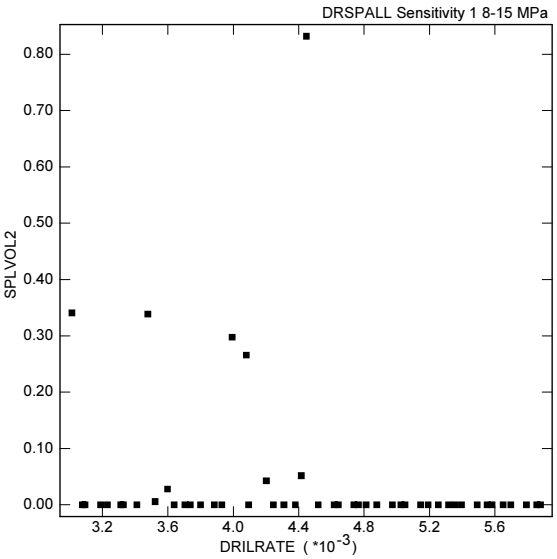

U1:[DKRUDEE.DRSPALL.SAND.SENS1.QA_RESULTS.CORRECTED_MUD.LO]STEP_S1_LO.INP;2
STEPWISE_PA9 2.21 05/05/04 08:21

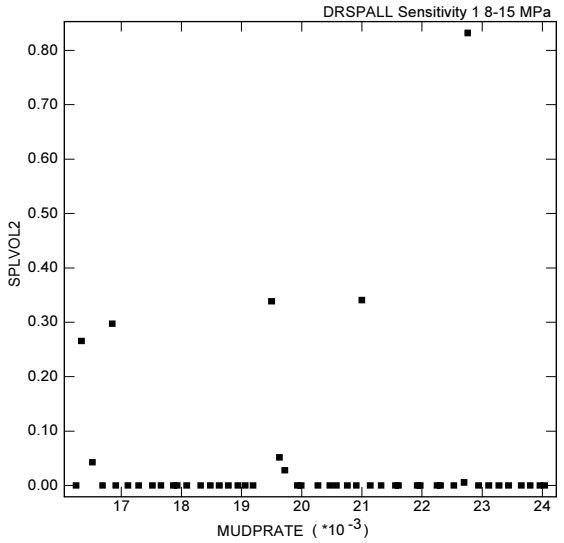

U1:[DKRUDEE.DRSPALL.SAND.SENS1.QA_RESULTS.CORRECTED_MUD.LO]STEP_S1_LO.INP;2
STEPWISE_PA9 2.21 05/05/04 08:21

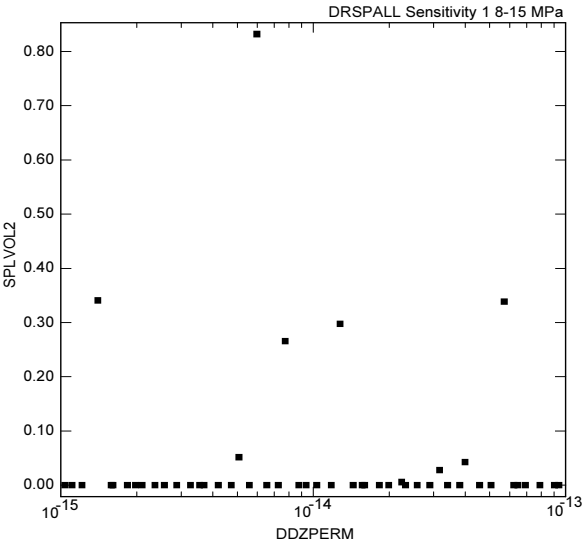

U1:[DKRUDEE.DRSPALL.SAND.SENS1.QA_RESULTS.CORRECTED_MUD.LO]STEP_S1_LO_LOG.INP;4
STEPWISE_PA9 2.21 05/05/04 08:21

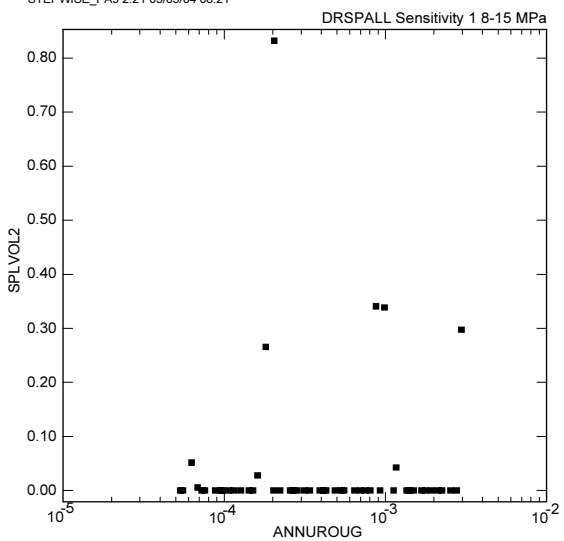

U1:[DKRUDEE.DRSPALL.SAND.SENS1.QA_RESULTS.CORRECTED_MUD.LO]STEP_S1_LO_LOG.INP;4
STEPWISE_PA9 2.21 05/05/04 08:21

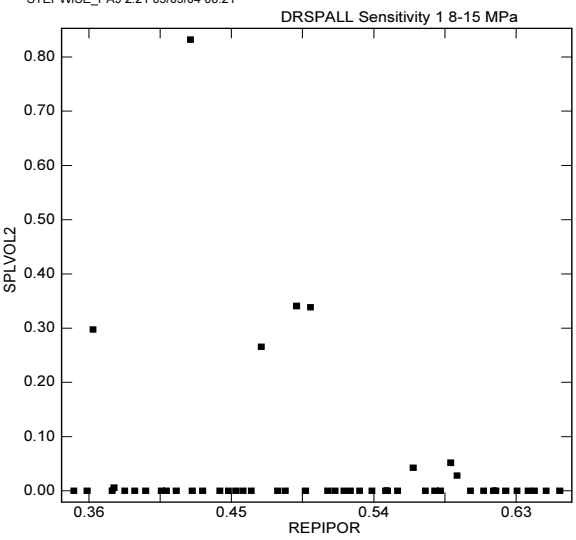

U1:[DKRUDEE.DRSPALL.SAND.SENS1.QA_RESULTS.CORRECTED_MUD.LO]STEP_S1_LO.INP;3
STEPWISE_PA9 2.21 10/01/04 14:34

Appendix S1_HI_SCATTER

The following scatter plots document the sensitivity of spallings releases (SPLVOL2) to the sampled input variables from the Sensitivity Study 1 for the pressure range 12-15 MPa.

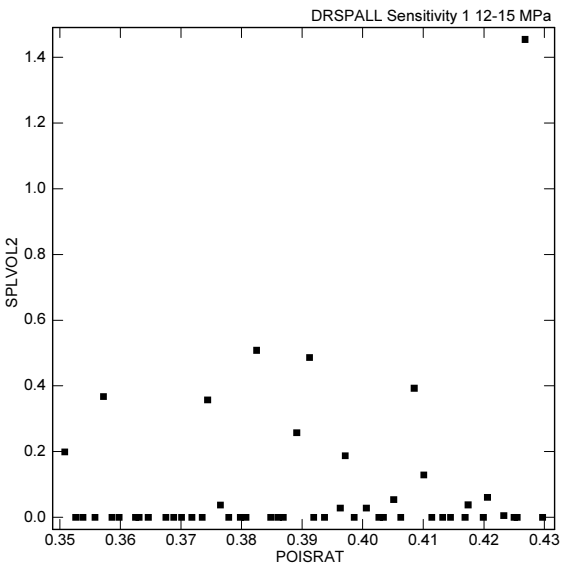

U1:[DKRUDEE.DRSPALL.SAND.SENS1.QA_RESULTS.CORRECTED_MUD.HI]STEP_S1_HI.INP;3
STEPWISE_PA9 2.21 05/05/04 10:01

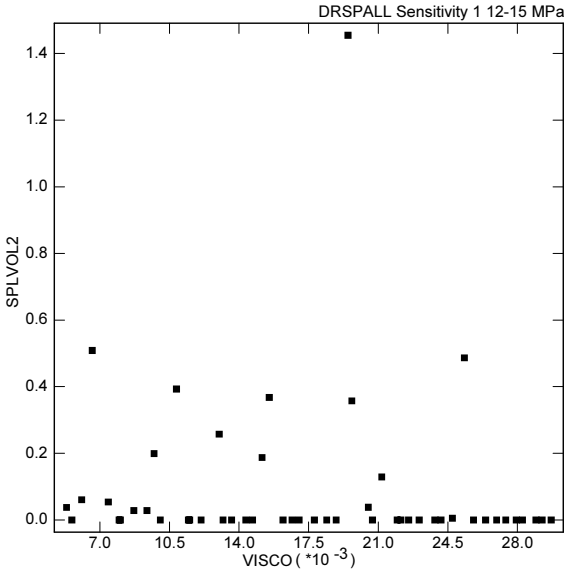

U1:[DKRUDEE.DRSPALL.SAND.SENS1.QA_RESULTS.CORRECTED_MUD.HI]STEP_S1_HI.INP;3
STEPWISE_PA9 2.21 05/05/04 10:01

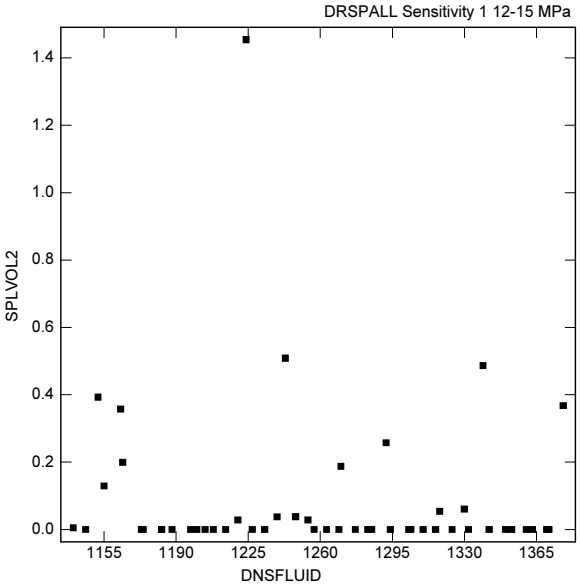

U1:[DKRUDEE.DRSPALL.SAND.SENS1.QA_RESULTS.CORRECTED_MUD.HI]STEP_S1_HI.INP;3
STEPWISE_PA9 2.21 05/05/04 10:01

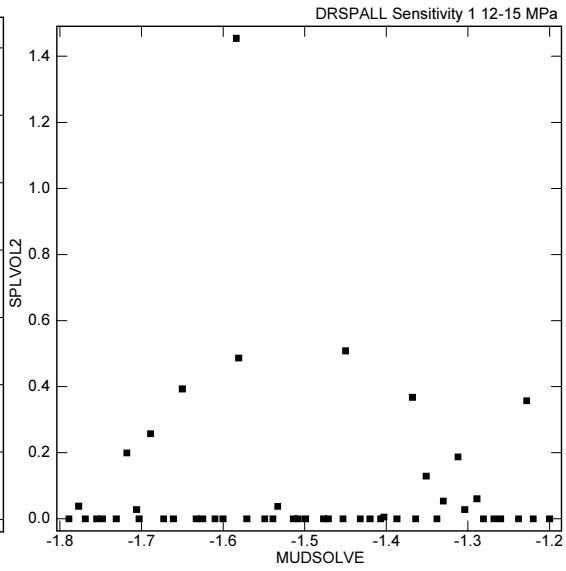

U1:[DKRUDEE.DRSPALL.SAND.SENS1.QA_RESULTS.CORRECTED_MUD.HI]STEP_S1_HI.INP;3
STEPWISE_PA9 2.21 05/05/04 10:01

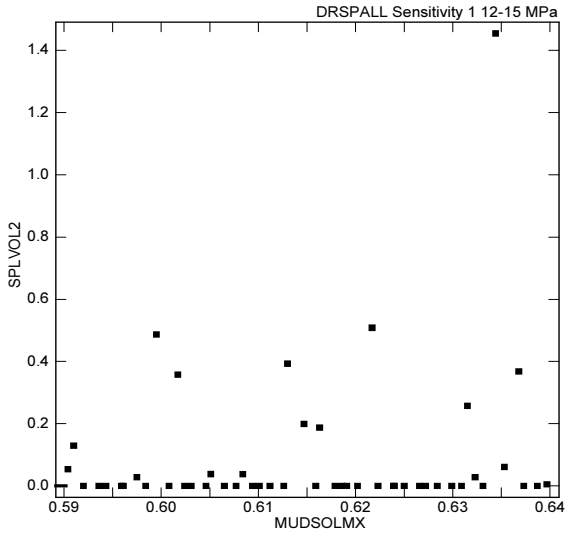

U1:[DKRUDEE.DRSPALL.SAND.SENS1.QA_RESULTS.CORRECTED_MUD.HI]STEP_S1_HI.INP;3
STEPWISE_PA9 2.21 05/05/04 10:01

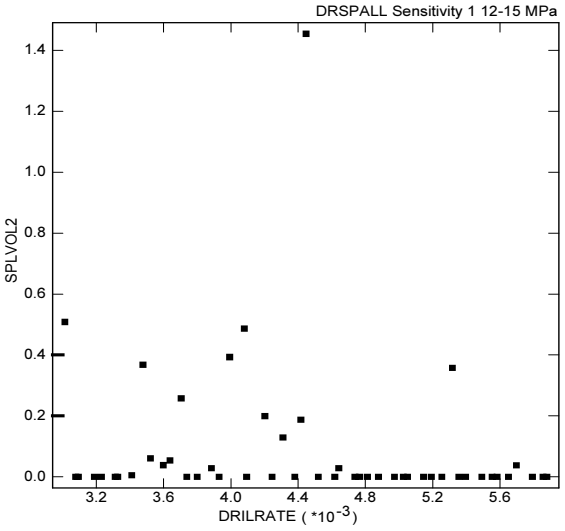

U1:[DKRUDEE.DRSPALL.SAND.SENS1.QA_RESULTS.CORRECTED_MUD.HI]STEP_S1_HI.INP;3
STEPWISE_PA9 2.21 05/05/04 10:01

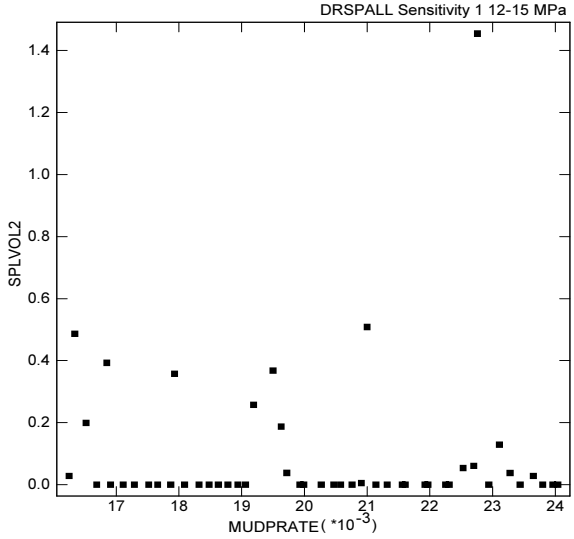

U1:[DKRUDEE.DRSPALL.SAND.SENS1.QA_RESULTS.CORRECTED_MUD.HI]STEP_S1_HI.INP;3
STEPWISE_PA9 2.21 05/05/04 10:01

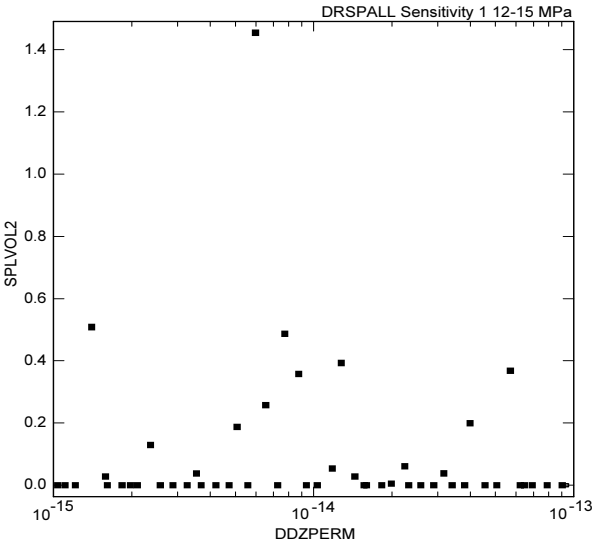

U1:[DKRUDEE.DRSPALL.SAND.SENS1.QA_RESULTS.CORRECTED_MUD.HI]STEP_S1_HI_LOG.INP;3
STEPWISE_PA9 2.21 05/05/04 10:03

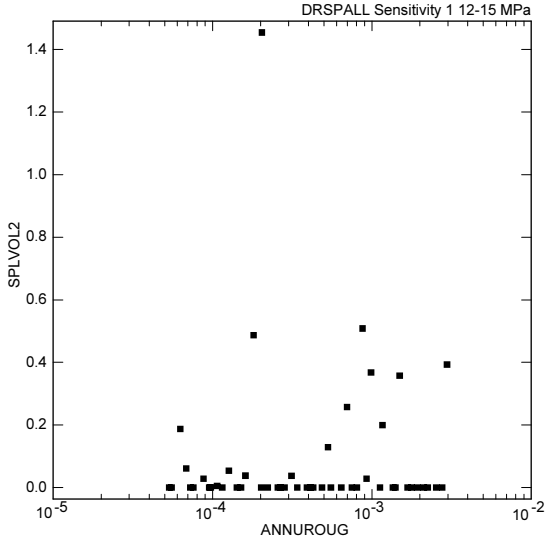

U1:[DKRUDEE.DRSPALL.SAND.SENS1.QA_RESULTS.CORRECTED_MUD.HI]STEP_S1_HI_LOG.INP;3
STEPWISE_PA9 2.21 05/05/04 10:03

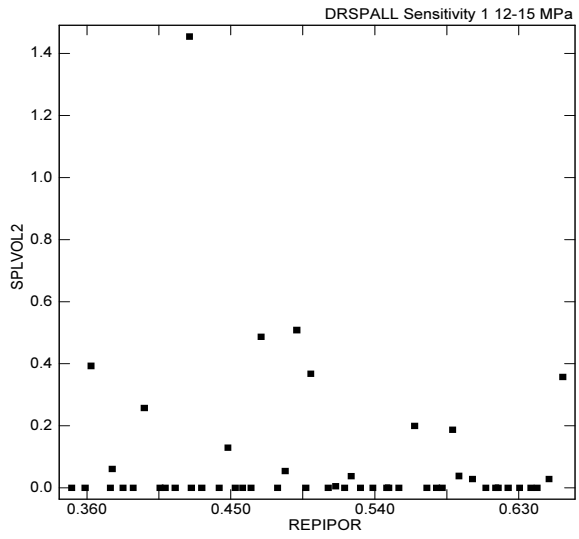

U1:[DKRUDEE.DRSPALL.SAND.SENS1.QA_RESULTS.CORRECTED_MUD.HI]STEP_S1_HI.INP;4
STEPWISE_PA9 2.21 10/01/04 14:38

Appendix S1_LO_TRN

The following is a listing of the LHS transfer file "LHS2_DRS_SENS1_LO.TRN" that gives tabular data regarding the LHS sampling for low-pressure runs in Sensitivity Study 1.

```
1

    TITLE SDB: PARAMETER_PROD     Calc: CRA1         Ver: 1.00     03/03/04 08:00:03

    RANDOM SEED =   921196800

    NUMBER OF VARIABLES =  15

    NUMBER OF OBSERVATIONS =   50
0   THE SAMPLE INPUT VECTORS WILL BE PRINTED ALONG WITH THEIR CORRESPONDING RANKS
0   HISTOGRAMS OF THE ACTUAL SAMPLE WILL BE PLOTTED FOR EACH INPUT VARIABLE
0   THE CORRELATION MATRICES (RAW DATA AND RANK CORRELATIONS) WILL BE PRINTED
1

    TITLE SDB: PARAMETER_PROD     Calc: CRA1         Ver: 1.00     03/03/04 08:00:03

    VARIABLE  DISTRIBUTION          RANGE           LABEL
0       1     UNIFORM            8.0000E+06 TO   1.5000E+07  SPALLMOD  REPIPRES
0       2     UNIFORM            0.3500     TO   0.6600      SPALLMOD  REPIPOR
0       3     LOGUNIFORM         2.4000E-14 TO   2.4000E-12  SPALLMOD  REPIPERM
0       4     UNIFORM            0.3500     TO   0.4300      SPALLMOD  POISRAT
0       5     LOGUNIFORM         1.2000E+05 TO   1.7000E+05  SPALLMOD  TENSLSTR
0       6     UNIFORM             1140.     TO    1380.      SPALLMOD  INITMDEN
0       7     UNIFORM            5.0000E-03 TO   3.0000E-02  SPALLMOD  MUDVISCO
0       8     UNIFORM            0.5900     TO   0.6400      SPALLMOD  MUDSOLMX
0       9     UNIFORM            -1.800     TO   -1.200      SPALLMOD  MUDSOLVE
0      10     UNIFORM            2.9600E-03 TO   5.9300E-03  SPALLMOD  DRILRATE
0      11     UNIFORM            1.6100E-02 TO   2.4200E-02  SPALLMOD  MUDPRATE
0      12     LOGUNIFORM         1.0000E-15 TO   1.0000E-13  SPALLMOD  DDZPERM
0      13     LOGUNIFORM         5.0000E-05 TO   3.1000E-03  SPALLMOD  ANNUROUG
0      14     UNIFORM            0.1000     TO    1.000      SPALLMOD  SHAPEFAC
0      15     UNIFORM            1.0000E-03 TO   1.0000E-02  SPALLMOD  PARTDIAM
1TITLE SDB: PARAMETER_PROD     Calc: CRA1         Ver: 1.00     03/03/04 08:00:03
0LATIN HYPERCUBE SAMPLE INPUT VECTORS

 RUN NO.  X(1)       X(2)       X(3)       X(4)       X(5)       X(6)       X(7)       X(8)       X(9)       X(10)
0    1  1.351E+07  3.626E-01  2.120E-13  4.085E-01  1.431E+05  1.152E+03  1.085E-02  6.130E-01 -1.650E+00  3.993E-03
0    2  8.016E+06  5.821E-01  3.215E-13  3.558E-01  1.358E+05  1.285E+03  8.024E-03  6.112E-01 -1.220E+00  4.380E-03
0    3  1.450E+07  4.090E-01  6.029E-14  3.526E-01  1.607E+05  1.208E+03  2.924E-02  6.094E-01 -1.477E+00  4.738E-03
0    4  8.529E+06  5.786E-01  5.621E-14  3.986E-01  1.522E+05  1.316E+03  1.004E-02  6.024E-01 -1.610E+00  3.093E-03
0    5  1.418E+07  4.242E-01  8.474E-14  4.268E-01  1.468E+05  1.224E+03  1.948E-02  6.344E-01 -1.584E+00  4.447E-03
0    6  1.494E+07  5.388E-01  1.100E-13  3.688E-01  1.214E+05  1.183E+03  1.209E-02  6.387E-01 -1.268E+00  5.051E-03
```

S1_LO_TRN-2

0	7	8.407E+06	5.475E-01	1.513E-12	4.145E-01	1.249E+05	1.188E+03	2.579E-02	6.186E-01	-1.407E+00	4.618E-03
0	8	9.436E+06	5.550E-01	9.834E-14	3.598E-01	1.382E+05	1.257E+03	1.145E-02	6.373E-01	-1.769E+00	3.312E-03
0	9	1.118E+07	4.840E-01	1.368E-13	4.051E-01	1.307E+05	1.318E+03	7.422E-03	5.904E-01	-1.330E+00	3.638E-03
0	10	1.130E+07	3.826E-01	5.473E-13	3.675E-01	1.485E+05	1.233E+03	7.958E-03	5.961E-01	-1.661E+00	3.930E-03
0	11	9.933E+06	6.375E-01	2.670E-14	4.255E-01	1.532E+05	1.353E+03	1.319E-02	6.240E-01	-1.625E+00	4.520E-03
0	12	1.404E+07	3.759E-01	2.099E-12	4.206E-01	1.421E+05	1.330E+03	6.080E-03	6.353E-01	-1.289E+00	3.522E-03
0	13	1.017E+07	3.747E-01	2.569E-14	3.586E-01	1.498E+05	1.204E+03	1.841E-02	6.266E-01	-1.453E+00	4.812E-03
0	14	9.801E+06	6.011E-01	4.977E-13	3.963E-01	1.361E+05	1.254E+03	8.709E-03	6.323E-01	-1.304E+00	3.884E-03
0	15	9.608E+06	3.589E-01	1.238E-12	3.701E-01	1.650E+05	1.370E+03	2.195E-02	5.936E-01	-1.600E+00	4.878E-03
0	16	1.253E+07	3.889E-01	1.012E-12	3.937E-01	1.475E+05	1.371E+03	1.779E-02	6.126E-01	-1.499E+00	5.025E-03
0	17	1.337E+07	6.305E-01	1.362E-12	3.807E-01	1.412E+05	1.310E+03	2.826E-02	6.008E-01	-1.789E+00	5.192E-03
0	18	1.458E+07	5.926E-01	1.615E-12	4.174E-01	1.294E+05	1.248E+03	2.050E-02	6.051E-01	-1.777E+00	3.598E-03
0	19	1.053E+07	4.057E-01	1.111E-12	4.027E-01	1.271E+05	1.183E+03	2.794E-02	6.077E-01	-1.200E+00	4.094E-03
0	20	9.066E+06	6.234E-01	2.448E-13	3.848E-01	1.334E+05	1.332E+03	2.970E-02	6.331E-01	-1.420E+00	3.230E-03
0	21	1.240E+07	5.252E-01	7.763E-13	3.765E-01	1.511E+05	1.239E+03	5.324E-03	6.084E-01	-1.533E+00	5.698E-03
0	22	1.369E+07	4.689E-01	2.904E-13	3.912E-01	1.551E+05	1.339E+03	2.533E-02	5.995E-01	-1.581E+00	4.080E-03
0	23	1.479E+07	5.000E-01	6.012E-13	3.572E-01	1.219E+05	1.378E+03	1.552E-02	6.368E-01	-1.368E+00	3.477E-03
0	24	1.317E+07	5.649E-01	6.633E-13	3.508E-01	1.500E+05	1.164E+03	9.723E-03	6.147E-01	-1.718E+00	4.202E-03
0	25	9.175E+06	6.155E-01	3.655E-13	3.869E-01	1.253E+05	1.277E+03	1.362E-02	6.179E-01	-1.748E+00	5.396E-03
0	26	9.963E+06	3.959E-01	9.445E-14	3.891E-01	1.329E+05	1.292E+03	1.300E-02	6.315E-01	-1.689E+00	3.705E-03
0	27	1.146E+07	4.968E-01	4.678E-14	3.798E-01	1.553E+05	1.303E+03	5.589E-03	6.159E-01	-1.673E+00	5.793E-03
0	28	1.185E+07	5.155E-01	6.163E-13	4.233E-01	1.699E+05	1.140E+03	2.473E-02	6.397E-01	-1.403E+00	3.411E-03
0	29	1.295E+07	5.886E-01	1.218E-13	3.971E-01	1.304E+05	1.270E+03	1.516E-02	6.163E-01	-1.312E+00	4.416E-03
0	30	1.374E+07	3.505E-01	3.714E-14	4.114E-01	1.565E+05	1.360E+03	2.214E-02	6.223E-01	-1.539E+00	5.651E-03
0	31	1.070E+07	4.792E-01	2.903E-14	4.132E-01	1.378E+05	1.197E+03	1.152E-02	5.959E-01	-1.471E+00	5.856E-03
0	32	8.959E+06	4.253E-01	1.756E-13	3.779E-01	1.342E+05	1.214E+03	1.468E-02	6.191E-01	-1.387E+00	5.553E-03
0	33	1.437E+07	6.489E-01	8.392E-13	4.006E-01	1.636E+05	1.220E+03	9.367E-03	5.975E-01	-1.706E+00	4.642E-03
0	34	1.030E+07	4.626E-01	1.987E-12	3.735E-01	1.609E+05	1.304E+03	2.741E-02	6.239E-01	-1.364E+00	5.879E-03
0	35	1.176E+07	6.415E-01	4.262E-14	4.034E-01	1.576E+05	1.227E+03	2.253E-02	6.299E-01	-1.703E+00	5.254E-03
0	36	8.794E+06	4.318E-01	9.205E-13	3.631E-01	1.593E+05	1.146E+03	1.435E-02	6.202E-01	-1.633E+00	3.738E-03
0	37	1.052E+07	4.528E-01	3.850E-13	4.250E-01	1.230E+05	1.324E+03	1.667E-02	6.284E-01	-1.571E+00	5.583E-03
0	38	1.087E+07	5.726E-01	1.425E-13	3.625E-01	1.684E+05	1.350E+03	2.640E-02	5.984E-01	-1.238E+00	3.189E-03
0	39	9.312E+06	4.152E-01	4.533E-13	3.538E-01	1.284E+05	1.174E+03	2.893E-02	6.309E-01	-1.755E+00	4.973E-03
0	40	1.196E+07	5.486E-01	4.160E-14	4.199E-01	1.396E+05	1.173E+03	2.306E-02	6.031E-01	-1.281E+00	5.492E-03
0	41	1.224E+07	6.094E-01	6.852E-14	3.860E-01	1.404E+05	1.342E+03	1.702E-02	6.250E-01	-1.338E+00	5.146E-03
0	42	1.104E+07	5.310E-01	3.214E-14	3.646E-01	1.241E+05	1.294E+03	2.385E-02	6.101E-01	-1.514E+00	3.327E-03
0	43	1.392E+07	4.574E-01	5.486E-14	4.169E-01	1.450E+05	1.200E+03	2.695E-02	5.920E-01	-1.549E+00	3.078E-03
0	44	1.280E+07	6.575E-01	1.977E-13	3.744E-01	1.658E+05	1.163E+03	1.967E-02	6.017E-01	-1.228E+00	5.317E-03
0	45	8.208E+06	4.427E-01	1.812E-12	4.297E-01	1.674E+05	1.283E+03	1.621E-02	6.272E-01	-1.508E+00	4.245E-03
0	46	1.330E+07	4.912E-01	2.194E-13	3.825E-01	1.446E+05	1.243E+03	6.618E-03	6.217E-01	-1.450E+00	3.013E-03
0	47	1.164E+07	4.482E-01	2.809E-13	4.101E-01	1.208E+05	1.155E+03	2.118E-02	5.910E-01	-1.351E+00	4.310E-03
0	48	8.619E+06	5.211E-01	1.638E-13	4.063E-01	1.261E+05	1.263E+03	1.888E-02	5.943E-01	-1.731E+00	3.800E-03
0	49	1.212E+07	5.109E-01	7.599E-14	3.718E-01	1.620E+05	1.363E+03	2.416E-02	6.065E-01	-1.432E+00	4.765E-03
0	50	1.270E+07	6.171E-01	2.359E-12	3.919E-01	1.322E+05	1.269E+03	2.071E-02	6.046E-01	-1.260E+00	5.356E-03

1TITLE SDB: PARAMETER_PROD Calc: CRA1 Ver: 1.00 03/03/04 08:00:03

0LATIN HYPERCUBE SAMPLE INPUT VECTORS

RUN NO.		X(11)	X(12)	X(13)	X(14)	X(15)
0	1	1.685E-02	1.276E-14	2.963E-03	4.790E-01	2.967E-03
0	2	2.156E-02	2.895E-14	1.148E-04	7.144E-01	4.495E-03
0	3	2.231E-02	6.468E-14	3.397E-04	6.037E-01	6.266E-03

0	4	2.294E-02	1.106E-15	1.772E-03	3.512E-01	5.363E-03
0	5	2.276E-02	5.972E-15	2.038E-04	3.154E-01	1.143E-03
0	6	2.396E-02	4.733E-15	5.524E-04	4.642E-01	7.859E-03
0	7	1.993E-02	3.692E-15	1.927E-03	2.393E-01	8.030E-03
0	8	1.878E-02	6.229E-14	7.250E-05	6.670E-01	3.641E-03
0	9	2.253E-02	1.178E-14	1.265E-04	7.061E-01	3.765E-03
0	10	2.132E-02	1.562E-14	2.115E-03	4.569E-01	2.439E-03
0	11	2.058E-02	2.319E-14	2.244E-03	2.915E-01	7.032E-03
0	12	2.270E-02	2.239E-14	6.833E-05	3.915E-01	8.913E-03
0	13	2.192E-02	3.264E-15	2.770E-03	4.987E-01	7.622E-03
0	14	1.625E-02	1.583E-15	8.775E-05	7.715E-01	8.465E-03
0	15	2.380E-02	5.577E-15	7.570E-05	6.048E-01	6.021E-03
0	16	1.863E-02	2.571E-15	1.355E-03	1.993E-01	1.571E-03
0	17	1.906E-02	1.609E-15	2.217E-04	2.646E-01	9.205E-03
0	18	1.972E-02	3.163E-14	1.608E-04	9.873E-01	4.740E-03
0	19	1.787E-02	6.925E-14	1.405E-03	7.532E-01	6.770E-03
0	20	2.404E-02	1.032E-14	8.049E-04	1.803E-01	5.260E-03
0	21	2.328E-02	3.541E-15	3.126E-04	9.701E-01	8.690E-03
0	22	1.634E-02	7.737E-15	1.809E-04	6.832E-01	4.383E-03
0	23	1.950E-02	5.704E-14	9.875E-04	3.740E-01	3.109E-03
0	24	1.652E-02	3.989E-14	1.166E-03	1.691E-01	4.848E-03
0	25	2.344E-02	5.064E-14	1.677E-03	4.139E-01	7.201E-03
0	26	1.919E-02	6.539E-15	6.982E-04	6.396E-01	1.471E-03
0	27	1.766E-02	3.406E-14	1.422E-04	1.247E-01	9.898E-03
0	28	2.091E-02	1.990E-14	1.068E-04	8.269E-01	9.505E-03
0	29	1.963E-02	5.076E-15	6.272E-05	5.398E-01	2.088E-03
0	30	1.809E-02	1.035E-15	2.564E-04	6.407E-01	7.799E-03
0	31	1.832E-02	9.031E-14	5.331E-05	1.370E-01	3.218E-03
0	32	1.848E-02	1.834E-15	4.865E-04	8.917E-01	4.147E-03
0	33	2.365E-02	1.439E-14	9.268E-04	8.420E-01	5.106E-03
0	34	2.197E-02	1.598E-14	7.493E-04	9.134E-01	2.480E-03
0	35	2.027E-02	2.096E-15	1.507E-04	7.925E-01	1.814E-03
0	36	1.894E-02	7.268E-15	2.018E-04	5.241E-01	8.265E-03
0	37	1.711E-02	4.560E-14	2.529E-03	9.449E-01	9.408E-03
0	38	1.729E-02	2.877E-15	6.427E-04	8.146E-01	7.367E-03
0	39	2.225E-02	1.211E-15	5.533E-05	3.337E-01	3.408E-03
0	40	2.161E-02	2.582E-14	2.677E-04	5.657E-01	6.213E-03
0	41	1.752E-02	4.205E-15	4.114E-04	9.589E-01	2.652E-03
0	42	1.999E-02	3.805E-14	9.721E-05	8.646E-01	5.775E-03
0	43	2.047E-02	9.364E-15	9.526E-05	2.114E-01	9.651E-03
0	44	1.793E-02	8.755E-15	1.494E-03	4.403E-01	1.298E-03
0	45	2.076E-02	7.904E-14	2.833E-04	3.600E-01	1.940E-03
0	46	2.100E-02	1.401E-15	8.731E-04	2.508E-01	6.561E-03
0	47	2.311E-02	2.356E-15	5.305E-04	7.476E-01	3.958E-03
0	48	1.669E-02	1.828E-14	3.908E-04	8.941E-01	6.657E-03
0	49	2.114E-02	9.381E-14	1.124E-03	5.786E-01	8.950E-03
0	50	1.691E-02	1.973E-15	4.281E-04	1.073E-01	5.616E-03

1TITLE SDB: PARAMETER_PROD Calc: CRA1 Ver: 1.00 03/03/04 08:00:03

0RANKS OF LATIN HYPERCUBE SAMPLE INPUT VECTORS

RUN NO.	X(1)	X(2)	X(3)	X(4)	X(5)	X(6)	X(7)	X(8)	X(9)	X(10)

S1_LO_TRN-4

0	1	40.	3.	24.	37.	26.	3.	12.	24.	13.	18.
0	2	1.	38.	29.	4.	18.	31.	7.	22.	49.	24.
0	3	47.	10.	11.	2.	42.	15.	49.	20.	27.	30.
0	4	4.	37.	10.	31.	35.	37.	11.	13.	16.	3.
0	5	45.	12.	14.	49.	29.	18.	29.	45.	18.	26.
0	6	50.	31.	17.	12.	2.	10.	15.	49.	45.	36.
0	7	3.	32.	45.	41.	6.	11.	42.	29.	33.	28.
0	8	11.	34.	16.	7.	21.	25.	13.	48.	3.	6.
0	9	23.	22.	19.	35.	13.	38.	5.	1.	40.	12.
0	10	24.	6.	34.	11.	31.	20.	6.	7.	12.	17.
0	11	14.	47.	2.	48.	36.	45.	17.	35.	15.	27.
0	12	44.	5.	49.	45.	25.	40.	3.	46.	43.	10.
0	13	16.	4.	1.	6.	32.	14.	27.	37.	29.	32.
0	14	13.	41.	33.	29.	19.	24.	8.	43.	42.	16.
0	15	12.	2.	43.	13.	46.	48.	34.	4.	17.	33.
0	16	33.	7.	41.	28.	30.	49.	26.	23.	26.	35.
0	17	39.	46.	44.	20.	24.	36.	47.	11.	1.	38.
0	18	48.	40.	46.	43.	11.	23.	31.	16.	2.	11.
0	19	19.	9.	42.	33.	9.	9.	46.	18.	50.	20.
0	20	8.	45.	26.	22.	16.	41.	50.	44.	32.	5.
0	21	32.	29.	38.	17.	34.	21.	1.	19.	23.	47.
0	22	41.	20.	28.	26.	37.	42.	41.	10.	19.	19.
0	23	49.	25.	35.	5.	3.	50.	22.	47.	36.	9.
0	24	37.	35.	37.	1.	33.	6.	10.	25.	7.	21.
0	25	9.	43.	30.	24.	7.	29.	18.	28.	5.	42.
0	26	15.	8.	15.	25.	15.	32.	16.	42.	10.	13.
0	27	25.	24.	8.	19.	38.	34.	2.	26.	11.	48.
0	28	28.	27.	36.	46.	50.	1.	40.	50.	34.	8.
0	29	36.	39.	18.	30.	12.	28.	21.	27.	41.	25.
0	30	42.	1.	5.	39.	39.	46.	35.	33.	22.	46.
0	31	20.	21.	3.	40.	20.	12.	14.	6.	28.	49.
0	32	7.	13.	22.	18.	17.	16.	20.	30.	35.	44.
0	33	46.	49.	39.	32.	45.	17.	9.	8.	8.	29.
0	34	17.	19.	48.	15.	43.	35.	45.	34.	37.	50.
0	35	27.	48.	7.	34.	40.	19.	36.	40.	9.	39.
0	36	6.	14.	40.	9.	41.	2.	19.	31.	14.	14.
0	37	18.	17.	31.	47.	4.	39.	24.	39.	20.	45.
0	38	21.	36.	20.	8.	49.	44.	43.	9.	47.	4.
0	39	10.	11.	32.	3.	10.	8.	48.	41.	4.	34.
0	40	29.	33.	6.	44.	22.	7.	37.	14.	44.	43.
0	41	31.	42.	12.	23.	23.	43.	25.	36.	39.	37.
0	42	22.	30.	4.	10.	5.	33.	38.	21.	24.	7.
0	43	43.	18.	9.	42.	28.	13.	44.	3.	21.	2.
0	44	35.	50.	23.	16.	47.	5.	30.	12.	48.	40.
0	45	2.	15.	47.	50.	48.	30.	23.	38.	25.	22.
0	46	38.	23.	25.	21.	27.	22.	4.	32.	30.	1.
0	47	26.	16.	27.	38.	1.	4.	33.	2.	38.	23.
0	48	5.	28.	21.	36.	8.	26.	28.	5.	6.	15.
0	49	30.	26.	13.	14.	44.	47.	39.	17.	31.	31.
0	50	34.	44.	50.	27.	14.	27.	32.	15.	46.	41.

1TITLE SDB: PARAMETER_PROD Calc: CRA1 Ver: 1.00 03/03/04 08:00:03

0RANKS OF LATIN HYPERCUBE SAMPLE INPUT VECTORS

	RUN NO.	X(11)	X(12)	X(13)	X(14)	X(15)
0	1	5.	28.	50.	22.	11.
0	2	34.	37.	11.	35.	20.
0	3	39.	46.	24.	28.	30.
0	4	43.	2.	44.	14.	25.
0	5	42.	20.	18.	12.	1.
0	6	49.	17.	30.	21.	39.
0	7	24.	15.	45.	8.	40.
0	8	17.	45.	5.	32.	15.
0	9	40.	27.	12.	34.	16.
0	10	33.	30.	46.	20.	8.
0	11	28.	35.	47.	11.	34.
0	12	41.	34.	4.	17.	44.
0	13	36.	13.	49.	23.	37.
0	14	1.	5.	7.	38.	42.
0	15	48.	19.	6.	29.	28.
0	16	16.	11.	40.	6.	4.
0	17	19.	6.	19.	10.	46.
0	18	23.	38.	15.	50.	21.
0	19	11.	47.	41.	37.	33.
0	20	50.	26.	34.	5.	24.
0	21	45.	14.	23.	49.	43.
0	22	2.	23.	16.	33.	19.
0	23	21.	44.	37.	16.	12.
0	24	3.	41.	39.	4.	22.
0	25	46.	43.	43.	18.	35.
0	26	20.	21.	32.	30.	3.
0	27	10.	39.	13.	2.	50.
0	28	30.	33.	10.	41.	48.
0	29	22.	18.	3.	25.	7.
0	30	13.	1.	20.	31.	38.
0	31	14.	49.	1.	3.	13.
0	32	15.	7.	28.	44.	18.
0	33	47.	29.	36.	42.	23.
0	34	37.	31.	33.	46.	9.
0	35	26.	9.	14.	39.	5.
0	36	18.	22.	17.	24.	41.
0	37	7.	42.	48.	47.	47.
0	38	8.	12.	31.	40.	36.
0	39	38.	3.	2.	13.	14.
0	40	35.	36.	21.	26.	29.
0	41	9.	16.	26.	48.	10.
0	42	25.	40.	9.	43.	27.
0	43	27.	25.	8.	7.	49.
0	44	12.	24.	42.	19.	2.
0	45	29.	48.	22.	15.	6.
0	46	31.	4.	35.	9.	31.
0	47	44.	10.	29.	36.	17.
0	48	4.	32.	25.	45.	32.

```
0   49        32.        50.        38.        27.        45.
0   50         6.         8.        27.         1.        26.
1   TITLE SDB: PARAMETER_PROD     Calc: CRA1         Ver: 1.00     03/03/04 08:00:03
0  HISTOGRAM FOR VARIABLE NO.  1     UNIFORM         DISTRIBUTION

     MIDPOINT          FREQ.

    7875000.             1    X
    8225000.             1    X
    8574999.             3    XXX
    8924999.             3    XXX
    9274999.             3    XXX
    9624999.             1    X
    9974999.             3    XXX
   0.1032500E+08         2    XX
   0.1067500E+08         3    XXX
   0.1102500E+08         3    XXX
   0.1137500E+08         2    XX
   0.1172500E+08         3    XXX
   0.1207500E+08         3    XXX
   0.1242500E+08         2    XX
   0.1277500E+08         2    XX
   0.1312500E+08         2    XX
   0.1347500E+08         3    XXX
   0.1382500E+08         3    XXX
   0.1417500E+08         2    XX
   0.1452500E+08         3    XXX
   0.1487500E+08         2    XX
0                       50

      MIN            MAX           RANGE           MEAN          MEDIAN        VARIANCE

    8016176.      0.1493875E+08   6922576.      0.1149938E+08  0.1154855E+08  0.4047910E+13

1   TITLE SDB: PARAMETER_PROD     Calc: CRA1         Ver: 1.00     03/03/04 08:00:03
0  HISTOGRAM FOR VARIABLE NO.  2     UNIFORM         DISTRIBUTION

     MIDPOINT          FREQ.

   0.3525000             2    XX
   0.3675000             2    XX
   0.3825001             3    XXX
   0.3975001             1    X
   0.4125001             3    XXX
   0.4275001             3    XXX
   0.4425001             2    XX
   0.4575001             3    XXX
   0.4725001             2    XX
   0.4875002             2    XX
   0.5025002             2    XX
```

S1_LO_TRN-6

```
   0.5175002             3    XXX
   0.5325001             3    XXX
   0.5475001             2    XX
   0.5625001             2    XX
   0.5775001             3    XXX
   0.5925001             2    XX
   0.6075001             2    XX
   0.6225001             3    XXX
   0.6375000             3    XXX
   0.6525000             2    XX
0                       50


      MIN            MAX           RANGE           MEAN          MEDIAN        VARIANCE

   0.3505454      0.6574541      0.3069087      0.5048079      0.5054554      0.7986087E-02

1   TITLE SDB: PARAMETER_PROD     Calc: CRA1         Ver: 1.00     03/03/04 08:00:03
0  HISTOGRAM FOR VARIABLE NO.  3     LOGUNIFORM      DISTRIBUTION

     MIDPOINT          FREQ.

   0.5999999E-13        17    XXXXXXXXXXXXXXXXX
   0.1800000E-12         8    XXXXXXXX
   0.3000000E-12         4    XXXX
   0.4199999E-12         3    XXX
   0.5400000E-12         2    XX
   0.6599999E-12         3    XXX
   0.7799999E-12         2    XX
   0.8999999E-12         1    X
   0.1020000E-11         1    X
   0.1140000E-11         1    X
   0.1260000E-11         1    X
   0.1380000E-11         1    X
   0.1500000E-11         1    X
   0.1620000E-11         1    X
   0.1740000E-11         0
   0.1860000E-11         1    X
   0.1980000E-11         1    X
   0.2100000E-11         1    X
   0.2220000E-11         0
   0.2340000E-11         1    X
0                       50


      MIN            MAX           RANGE           MEAN          MEDIAN        VARIANCE

   0.2569300E-13  0.2359075E-11  0.2333382E-11  0.5253260E-12  0.2320611E-12  0.3791580E-24

1   TITLE SDB: PARAMETER_PROD     Calc: CRA1         Ver: 1.00     03/03/04 08:00:03
0  HISTOGRAM FOR VARIABLE NO.  4     UNIFORM         DISTRIBUTION
```

S1_LO_TRN-8

```
      MIDPOINT          FREQ.

     0.3490499             1    X
     0.3529499             2    XX
     0.3568499             3    XXX
     0.3607499             2    XX
     0.3646499             2    XX
     0.3685499             3    XXX
     0.3724499             3    XXX
     0.3763499             2    XX
     0.3802499             2    XX
     0.3841498             3    XXX
     0.3880498             2    XX
     0.3919498             3    XXX
     0.3958498             2    XX
     0.3997498             2    XX
     0.4036498             3    XXX
     0.4075498             2    XX
     0.4114498             3    XXX
     0.4153498             2    XX
     0.4192498             3    XXX
     0.4231498             2    XX
     0.4270498             2    XX
     0.4309497             1    X
0                         50


       MIN            MAX           RANGE           MEAN          MEDIAN        VARIANCE

    0.3507504      0.4296972      0.7894677E-01  0.3899723      0.3901417      0.5329991E-03

1   TITLE SDB: PARAMETER_PROD     Calc: CRA1         Ver: 1.00     03/03/04 08:00:03
0  HISTOGRAM FOR VARIABLE NO.  5     LOGUNIFORM      DISTRIBUTION

      MIDPOINT          FREQ.

     121250.0             3    XXX
     123750.0             3    XXX
     126250.0             3    XXX
     128750.0             2    XX
     131250.0             3    XXX
     133750.0             3    XXX
     136250.0             2    XX
     138750.0             3    XXX
     141250.0             3    XXX
     143750.0             3    XXX
     146250.0             1    X
     148750.0             3    XXX
     151250.0             3    XXX
     153750.0             1    X
```

```
    156250.0             3    XXX
    158750.0             2    XX
    161250.0             3    XXX
    163750.0             1    X
    166250.0             3    XXX
    168750.0             2    XX
0                       50
```

MIN	MAX	RANGE	MEAN	MEDIAN	VARIANCE
120830.4	169860.5	49030.15	143532.9	142592.2	0.2072117E+09

```
1   TITLE SDB: PARAMETER_PROD     Calc: CRA1         Ver: 1.00     03/03/04 08:00:03
0  HISTOGRAM FOR VARIABLE NO.  6     UNIFORM         DISTRIBUTION

     MIDPOINT          FREQ.

    1146.000             2    XX
    1158.000             3    XXX
    1170.000             3    XXX
    1182.000             2    XX
    1194.000             2    XX
    1206.000             3    XXX
    1218.000             2    XX
    1230.000             3    XXX
    1242.000             3    XXX
    1254.000             2    XX
    1266.000             3    XXX
    1278.000             2    XX
    1290.000             3    XXX
    1302.000             2    XX
    1314.000             3    XXX
    1326.000             2    XX
    1338.000             3    XXX
    1350.000             2    XX
    1362.000             2    XX
    1374.000             3    XXX
0                       50
```

MIN	MAX	RANGE	MEAN	MEDIAN	VARIANCE
1140.107	1377.708	237.6007	1259.746	1260.109	4819.680

```
1   TITLE SDB: PARAMETER_PROD     Calc: CRA1         Ver: 1.00     03/03/04 08:00:03
0  HISTOGRAM FOR VARIABLE NO.  7     UNIFORM         DISTRIBUTION

     MIDPOINT          FREQ.

   0.5399999E-02         2    XX
```

```
   0.6599999E-02         2    XX
   0.7799999E-02         3    XXX
   0.8999999E-02         2    XX
   0.1020000E-01         2    XX
   0.1140000E-01         3    XXX
   0.1260000E-01         3    XXX
   0.1380000E-01         2    XX
   0.1500000E-01         3    XXX
   0.1620000E-01         2    XX
   0.1740000E-01         2    XX
   0.1860000E-01         2    XX
   0.1980000E-01         2    XX
   0.2100000E-01         3    XXX
   0.2220000E-01         3    XXX
   0.2340000E-01         2    XX
   0.2460000E-01         2    XX
   0.2580000E-01         3    XXX
   0.2700000E-01         2    XX
   0.2820000E-01         2    XX
   0.2940000E-01         3    XXX
0                       50


      MIN            MAX           RANGE           MEAN          MEDIAN        VARIANCE

   0.5323772E-02  0.2969946E-01  0.2437569E-01  0.1750332E-01  0.1740441E-01  0.5255701E-04

1   TITLE SDB: PARAMETER_PROD     Calc: CRA1         Ver: 1.00     03/03/04 08:00:03
0  HISTOGRAM FOR VARIABLE NO.  8     UNIFORM         DISTRIBUTION

     MIDPOINT          FREQ.

   0.5912502             3    XXX
   0.5937502             2    XX
   0.5962502             3    XXX
   0.5987502             2    XX
   0.6012502             3    XXX
   0.6037502             2    XX
   0.6062502             2    XX
   0.6087502             3    XXX
   0.6112502             2    XX
   0.6137502             3    XXX
   0.6162502             2    XX
   0.6187502             3    XXX
   0.6212502             3    XXX
   0.6237502             2    XX
   0.6262501             3    XXX
   0.6287501             2    XX
   0.6312501             3    XXX
   0.6337501             2    XX
   0.6362501             3    XXX
```

```
   0.6387501             2    XX
0                       50


      MIN            MAX           RANGE           MEAN          MEDIAN        VARIANCE

   0.5904003      0.6396992      0.4929888E-01  0.6149381      0.6153036      0.2095795E-03

1   TITLE SDB: PARAMETER_PROD     Calc: CRA1         Ver: 1.00     03/03/04 08:00:03
0  HISTOGRAM FOR VARIABLE NO.  9     UNIFORM         DISTRIBUTION

     MIDPOINT          FREQ.

   -1.783500             2    XX
   -1.754500             3    XXX
   -1.725500             2    XX
   -1.696500             3    XXX
   -1.667500             2    XX
   -1.638500             3    XXX
   -1.609500             2    XX
   -1.580500             3    XXX
   -1.551500             2    XX
   -1.522500             2    XX
   -1.493500             2    XX
   -1.464500             3    XXX
   -1.435500             2    XX
   -1.406500             3    XXX
   -1.377500             3    XXX
   -1.348500             2    XX
   -1.319499             2    XX
   -1.290499             3    XXX
   -1.261499             2    XX
   -1.232499             3    XXX
   -1.203499             1    X
0                       50


      MIN            MAX           RANGE           MEAN          MEDIAN        VARIANCE

   -1.788822      -1.200367      0.5884552      -1.499341      -1.503318      0.2971374E-01

1   TITLE SDB: PARAMETER_PROD     Calc: CRA1         Ver: 1.00     03/03/04 08:00:03
0  HISTOGRAM FOR VARIABLE NO. 10     UNIFORM         DISTRIBUTION

     MIDPOINT          FREQ.

   0.3010000E-02         2    XX
   0.3150000E-02         2    XX
   0.3290000E-02         3    XXX
   0.3430000E-02         2    XX
   0.3570000E-02         3    XXX
```

```
   0.3710000E-02         2    XX
   0.3850000E-02         2    XX
   0.3990000E-02         2    XX
   0.4130000E-02         2    XX
   0.4270000E-02         3    XXX
   0.4410000E-02         3    XXX
   0.4550000E-02         2    XX
   0.4690000E-02         2    XX
   0.4830000E-02         3    XXX
   0.4970001E-02         2    XX
   0.5110001E-02         2    XX
   0.5250001E-02         3    XXX
   0.5390001E-02         2    XX
   0.5530001E-02         3    XXX
   0.5670001E-02         2    XX
   0.5810001E-02         3    XXX
0                       50

       MIN            MAX           RANGE           MEAN          MEDIAN        VARIANCE

   0.3012756E-02  0.5879278E-02  0.2866522E-02  0.4445995E-02  0.4431721E-02  0.7293327E-06

1   TITLE SDB: PARAMETER_PROD     Calc: CRA1         Ver: 1.00     03/03/04 08:00:03
0  HISTOGRAM FOR VARIABLE NO. 11     UNIFORM         DISTRIBUTION

      MIDPOINT          FREQ.

   0.1618500E-01         2    XX
   0.1657500E-01         2    XX
   0.1696500E-01         3    XXX
   0.1735500E-01         2    XX
   0.1774500E-01         3    XXX
   0.1813500E-01         2    XX
   0.1852500E-01         2    XX
   0.1891500E-01         3    XXX
   0.1930500E-01         1    X
   0.1969500E-01         3    XXX
   0.2008501E-01         3    XXX
   0.2047501E-01         2    XX
   0.2086501E-01         3    XXX
   0.2125501E-01         2    XX
   0.2164501E-01         2    XX
   0.2203501E-01         2    XX
   0.2242501E-01         3    XXX
   0.2281501E-01         3    XXX
   0.2320501E-01         2    XX
   0.2359501E-01         2    XX
   0.2398501E-01         3    XXX
0                       50
```

S1_LO_TRN-13

```
      MIN            MAX           RANGE           MEAN          MEDIAN        VARIANCE

   0.1624880E-01  0.2404500E-01  0.7796194E-02  0.2014920E-01  0.2012702E-01  0.5426146E-05

1   TITLE SDB: PARAMETER_PROD     Calc: CRA1         Ver: 1.00     03/03/04 08:00:03
0  HISTOGRAM FOR VARIABLE NO. 12     LOGUNIFORM      DISTRIBUTION

     MIDPOINT          FREQ.

   0.2299999E-14        16    XXXXXXXXXXXXXXXX
   0.6899998E-14         8    XXXXXXXX
   0.1150000E-13         4    XXXX
   0.1609999E-13         4    XXXX
   0.2069999E-13         2    XX
   0.2529999E-13         2    XX
   0.2989999E-13         2    XX
   0.3449999E-13         1    X
   0.3909999E-13         2    XX
   0.4369998E-13         1    X
   0.4829998E-13         0
   0.5289998E-13         1    X
   0.5749998E-13         1    X
   0.6209998E-13         1    X
   0.6669998E-13         1    X
   0.7129997E-13         1    X
   0.7589997E-13         0
   0.8049997E-13         1    X
   0.8509997E-13         0
   0.8969997E-13         1    X
   0.9429997E-13         1    X
0                       50


      MIN            MAX           RANGE           MEAN          MEDIAN        VARIANCE

   0.1035020E-14  0.9380977E-13  0.9277475E-13  0.2146078E-13  0.9842687E-14  0.6210209E-27

1   TITLE SDB: PARAMETER_PROD     Calc: CRA1         Ver: 1.00     03/03/04 08:00:03
0  HISTOGRAM FOR VARIABLE NO. 13     LOGUNIFORM      DISTRIBUTION

     MIDPOINT          FREQ.

   0.7500000E-04        13    XXXXXXXXXXXXX
   0.2250000E-03         9    XXXXXXXXX
   0.3750000E-03         5    XXXXX
   0.5250000E-03         3    XXX
   0.6750001E-03         3    XXX
   0.8250001E-03         2    XX
   0.9750001E-03         2    XX
   0.1125000E-02         2    XX
```

S1_LO_TRN-14

```
   0.1275000E-02         0
   0.1425000E-02         3    XXX
   0.1575000E-02         0
   0.1725000E-02         2    XX
   0.1875000E-02         1    X
   0.2025000E-02         0
   0.2175000E-02         2    XX
   0.2325000E-02         0
   0.2475000E-02         1    X
   0.2625000E-02         0
   0.2775000E-02         1    X
   0.2925000E-02         1    X
0                       50


      MIN            MAX           RANGE           MEAN          MEDIAN        VARIANCE

   0.5331121E-04  0.2963364E-02  0.2910053E-02  0.7352161E-03  0.4010968E-03  0.6089885E-06

1   TITLE SDB: PARAMETER_PROD     Calc: CRA1         Ver: 1.00     03/03/04 08:00:03
0  HISTOGRAM FOR VARIABLE NO. 14     UNIFORM         DISTRIBUTION

     MIDPOINT          FREQ.

   0.1100000             2    XX
   0.1540000             2    XX
   0.1979999             3    XXX
   0.2419999             2    XX
   0.2859999             2    XX
   0.3299999             3    XXX
   0.3739999             3    XXX
   0.4179999             1    X
   0.4619999             4    XXXX
   0.5059999             2    XX
   0.5499999             2    XX
   0.5939999             3    XXX
   0.6379998             2    XX
   0.6819998             2    XX
   0.7259998             3    XXX
   0.7699997             2    XX
   0.8139997             3    XXX
   0.8579997             2    XX
   0.9019997             3    XXX
   0.9459996             2    XX
   0.9899996             2    XX
0                       50


      MIN            MAX           RANGE           MEAN          MEDIAN        VARIANCE

   0.1072515      0.9873471      0.8800956      0.5499085      0.5527515      0.6745825E-01
```

1 TITLE SDB: PARAMETER_PROD Calc: CRA1 Ver: 1.00 03/03/04 08:00:03
0 HISTOGRAM FOR VARIABLE NO. 15 UNIFORM DISTRIBUTION

MIDPOINT	FREQ.	
0.1100000E-02	2	XX
0.1540000E-02	2	XX
0.1979999E-02	3	XXX
0.2419999E-02	2	XX
0.2859999E-02	2	XX
0.3299999E-02	3	XXX
0.3739999E-02	3	XXX
0.4179999E-02	2	XX
0.4619999E-02	2	XX
0.5059999E-02	3	XXX
0.5499999E-02	2	XX
0.5939999E-02	2	XX
0.6379999E-02	3	XXX
0.6819999E-02	3	XXX
0.7259999E-02	2	XX
0.7699999E-02	3	XXX
0.8140000E-02	2	XX
0.8579999E-02	2	XX
0.9019999E-02	3	XXX
0.9459998E-02	3	XXX
0.9899998E-02	1	X
0	50	

MIN	MAX	RANGE	MEAN	MEDIAN	VARIANCE
0.1143154E-02	0.9897848E-02	0.8754694E-02	0.5500777E-02	0.5489352E-02	0.6729721E-05

1TITLE SDB: PARAMETER_PROD Calc: CRA1 Ver: 1.00 03/03/04 08:00:03
0CORRELATIONS AMONG INPUT VARIABLES CREATED BY THE LATIN HYPERCUBE SAMPLE FOR RAW DATA PAGE 1

0	1	1.0000													
0	2	-0.0168	1.0000												
0	3	0.0113	-0.0477	1.0000											
0	4	0.0687	-0.0111	0.1350	1.0000										
0	5	0.0799	-0.0574	0.0473	-0.0651	1.0000									
0	6	-0.0369	0.0415	0.0691	-0.0301	0.0683	1.0000								
0	7	0.0168	-0.0232	0.0991	0.0078	0.0650	-0.0140	1.0000							
0	8	-0.0560	-0.0400	0.0123	-0.0219	-0.0932	0.0221	-0.0830	1.0000						
0	9	0.0488	0.0371	0.0764	0.0074	-0.0876	0.0009	0.0812	0.0183	1.0000					
0	10	0.0272	0.0075	0.0765	-0.0049	0.0713	-0.0263	0.0497	-0.0269	0.0254	1.0000				
0	11	-0.0186	-0.0434	0.0229	-0.0363	0.0378	-0.0355	-0.0116	0.0477	0.0162	-0.0320	1.0000			
0	12	-0.0649	-0.0522	0.0015	-0.0109	-0.0072	0.0531	0.0005	0.0101	-0.0287	0.0360	-0.0644	1.0000		
0	13	-0.1171	-0.0925	-0.0759	0.0306	-0.0357	-0.0463	-0.1135	0.0227	-0.0755	0.0427	-0.0565	0.0215	1.0000	
0	14	-0.0687	0.0234	-0.0851	0.0026	-0.0034	0.0272	0.0677	-0.0466	0.0826	0.0105	-0.0453	-0.0528	-0.1541	1.0000
0	15	0.0041	0.0358	0.0515	0.0512	0.0370	0.0163	0.0474	-0.0121	0.0204	-0.0192	0.0173	0.0332	0.0097	-0.0025	1.0000

```
0            1       2       3       4       5       6       7       8       9      10      11      12      13      14      15
0VARIABLES
0THE VARIANCE INFLATION FACTOR FOR THIS MATRIX IS  1.09
1TITLE SDB: PARAMETER_PROD     Calc: CRA1         Ver: 1.00     03/03/04 08:00:03
0CORRELATIONS AMONG INPUT VARIABLES CREATED BY THE LATIN HYPERCUBE SAMPLE FOR RANK DATA                          PAGE   1
0    1  1.0000
0    2 -0.0149  1.0000
0    3 -0.0161 -0.0312  1.0000
0    4  0.0699 -0.0097  0.0029  1.0000
0    5  0.0813 -0.0571 -0.0315 -0.0685  1.0000
0    6 -0.0357  0.0450 -0.0143 -0.0338  0.0708  1.0000
0    7  0.0202 -0.0161  0.0191  0.0075  0.0449 -0.0077  1.0000
0    8 -0.0570 -0.0396  0.0022 -0.0160 -0.0939  0.0274 -0.0806  1.0000
0    9  0.0460  0.0339  0.0338  0.0059 -0.1008  0.0025  0.0827  0.0225  1.0000
0   10  0.0252  0.0058 -0.0389 -0.0020  0.0729 -0.0273  0.0533 -0.0330  0.0294  1.0000
0   11 -0.0160 -0.0420  0.0067 -0.0358  0.0297 -0.0281 -0.0093  0.0443  0.0137 -0.0248  1.0000
0   12 -0.0108 -0.0129 -0.0038  0.0338 -0.0175  0.0080 -0.0540 -0.0090 -0.0574 -0.0605 -0.0175  1.0000
0   13 -0.0433  0.0107  0.0526 -0.0397  0.0043  0.0084 -0.0341 -0.0133  0.0087  0.0740 -0.0223  0.0153  1.0000
0   14 -0.0637  0.0255  0.0204 -0.0003 -0.0153  0.0327  0.0621 -0.0424  0.0848  0.0147 -0.0456  0.0342 -0.1071  1.0000
0   15 -0.0035  0.0362  0.0177  0.0480  0.0357  0.0120  0.0544 -0.0132  0.0222 -0.0151  0.0157  0.0247 -0.0294  0.0024  1.0000
0            1       2       3       4       5       6       7       8       9      10      11      12      13      14      15
0VARIABLES
0THE VARIANCE INFLATION FACTOR FOR THIS MATRIX IS  1.05
```

Appendix S1_HI_TRN

The following is a excerpt from the LHS transfer file "LHS2_DRS_SENS1_HI.TRN" that gives tabular data regarding the LHS sampling for high-pressure runs in Sensitivity Study 1.


```
1

    TITLE SDB: PARAMETER_PROD     Calc: CRA1         Ver: 1.00     03/04/04 10:47:58

    RANDOM SEED =   921196800

    NUMBER OF VARIABLES =  15

    NUMBER OF OBSERVATIONS =   50
0   THE SAMPLE INPUT VECTORS WILL BE PRINTED ALONG WITH THEIR CORRESPONDING RANKS
0   HISTOGRAMS OF THE ACTUAL SAMPLE WILL BE PLOTTED FOR EACH INPUT VARIABLE
0   THE CORRELATION MATRICES (RAW DATA AND RANK CORRELATIONS) WILL BE PRINTED
1

    TITLE SDB: PARAMETER_PROD     Calc: CRA1         Ver: 1.00     03/04/04 10:47:58

    VARIABLE  DISTRIBUTION          RANGE           LABEL
0       1     UNIFORM           1.2000E+07 TO   1.5000E+07  SPALLMOD  REPIPRES
0       2     UNIFORM           0.3500     TO   0.6600      SPALLMOD  REPIPOR
0       3     LOGUNIFORM        2.4000E-14 TO   2.4000E-12  SPALLMOD  REPIPERM
0       4     UNIFORM           0.3500     TO   0.4300      SPALLMOD  POISRAT
0       5     LOGUNIFORM        1.2000E+05 TO   1.7000E+05  SPALLMOD  TENSLSTR
0       6     UNIFORM            1140.     TO    1380.      SPALLMOD  INITMDEN
0       7     UNIFORM           5.0000E-03 TO   3.0000E-02  SPALLMOD  MUDVISCO
0       8     UNIFORM           0.5900     TO   0.6400      SPALLMOD  MUDSOLMX
0       9     UNIFORM           -1.800     TO   -1.200      SPALLMOD  MUDSOLVE
0      10     UNIFORM           2.9600E-03 TO   5.9300E-03  SPALLMOD  DRILRATE
0      11     UNIFORM           1.6100E-02 TO   2.4200E-02  SPALLMOD  MUDPRATE
0      12     LOGUNIFORM        1.0000E-15 TO   1.0000E-13  SPALLMOD  DDZPERM
0      13     LOGUNIFORM        5.0000E-05 TO   3.1000E-03  SPALLMOD  ANNUROUG
0      14     UNIFORM           0.1000     TO    1.000      SPALLMOD  SHAPEFAC
0      15     UNIFORM           1.0000E-03 TO   1.0000E-02  SPALLMOD  PARTDIAM
1TITLE SDB: PARAMETER_PROD     Calc: CRA1         Ver: 1.00     03/04/04 10:47:58
0LATIN HYPERCUBE SAMPLE INPUT VECTORS

 RUN NO.  X(1)       X(2)       X(3)       X(4)       X(5)       X(6)       X(7)       X(8)       X(9)       X(10)
0    1  1.436E+07  3.626E-01  2.120E-13  4.085E-01  1.431E+05  1.152E+03  1.085E-02  6.130E-01 -1.650E+00  3.993E-03
0    2  1.201E+07  5.821E-01  3.215E-13  3.558E-01  1.358E+05  1.285E+03  8.024E-03  6.112E-01 -1.220E+00  4.380E-03
0    3  1.479E+07  4.090E-01  6.029E-14  3.526E-01  1.607E+05  1.208E+03  2.924E-02  6.094E-01 -1.477E+00  4.738E-03
0    4  1.223E+07  5.786E-01  5.621E-14  3.986E-01  1.522E+05  1.316E+03  1.004E-02  6.024E-01 -1.610E+00  3.093E-03
```

S1_HI_TRN-2

0	5	1.465E+07	4.242E-01	8.474E-14	4.268E-01	1.468E+05	1.224E+03	1.948E-02	6.344E-01	-1.584E+00	4.447E-03
0	6	1.497E+07	5.388E-01	1.100E-13	3.688E-01	1.214E+05	1.183E+03	1.209E-02	6.387E-01	-1.268E+00	5.051E-03
0	7	1.217E+07	5.475E-01	1.513E-12	4.145E-01	1.249E+05	1.188E+03	2.579E-02	6.186E-01	-1.407E+00	4.618E-03
0	8	1.262E+07	5.550E-01	9.834E-14	3.598E-01	1.382E+05	1.257E+03	1.145E-02	6.373E-01	-1.769E+00	3.312E-03
0	9	1.336E+07	4.840E-01	1.368E-13	4.051E-01	1.307E+05	1.318E+03	7.422E-03	5.904E-01	-1.330E+00	3.638E-03
0	10	1.341E+07	3.826E-01	5.473E-13	3.675E-01	1.485E+05	1.233E+03	7.958E-03	5.961E-01	-1.661E+00	3.930E-03
0	11	1.283E+07	6.375E-01	2.670E-14	4.255E-01	1.532E+05	1.353E+03	1.319E-02	6.240E-01	-1.625E+00	4.520E-03
0	12	1.459E+07	3.759E-01	2.099E-12	4.206E-01	1.421E+05	1.330E+03	6.080E-03	6.353E-01	-1.289E+00	3.522E-03
0	13	1.293E+07	3.747E-01	2.569E-14	3.586E-01	1.498E+05	1.204E+03	1.841E-02	6.266E-01	-1.453E+00	4.812E-03
0	14	1.277E+07	6.011E-01	4.977E-13	3.963E-01	1.361E+05	1.254E+03	8.709E-03	6.323E-01	-1.304E+00	3.884E-03
0	15	1.269E+07	3.589E-01	1.238E-12	3.701E-01	1.650E+05	1.370E+03	2.195E-02	5.936E-01	-1.600E+00	4.878E-03
0	16	1.394E+07	3.889E-01	1.012E-12	3.937E-01	1.475E+05	1.371E+03	1.779E-02	6.126E-01	-1.499E+00	5.025E-03
0	17	1.430E+07	6.305E-01	1.362E-12	3.807E-01	1.412E+05	1.310E+03	2.826E-02	6.008E-01	-1.789E+00	5.192E-03
0	18	1.482E+07	5.926E-01	1.615E-12	4.174E-01	1.294E+05	1.248E+03	2.050E-02	6.051E-01	-1.777E+00	3.598E-03
0	19	1.309E+07	4.057E-01	1.111E-12	4.027E-01	1.271E+05	1.183E+03	2.794E-02	6.077E-01	-1.200E+00	4.094E-03
0	20	1.246E+07	6.234E-01	2.448E-13	3.848E-01	1.334E+05	1.332E+03	2.970E-02	6.331E-01	-1.420E+00	3.230E-03
0	21	1.388E+07	5.252E-01	7.763E-13	3.765E-01	1.511E+05	1.239E+03	5.324E-03	6.084E-01	-1.533E+00	5.698E-03
0	22	1.444E+07	4.689E-01	2.904E-13	3.912E-01	1.551E+05	1.339E+03	2.533E-02	5.995E-01	-1.581E+00	4.080E-03
0	23	1.491E+07	5.000E-01	6.012E-13	3.572E-01	1.219E+05	1.378E+03	1.552E-02	6.368E-01	-1.368E+00	3.477E-03
0	24	1.421E+07	5.649E-01	6.633E-13	3.508E-01	1.500E+05	1.164E+03	9.723E-03	6.147E-01	-1.718E+00	4.202E-03
0	25	1.250E+07	6.155E-01	3.655E-13	3.869E-01	1.253E+05	1.277E+03	1.362E-02	6.179E-01	-1.748E+00	5.396E-03
0	26	1.284E+07	3.959E-01	9.445E-14	3.891E-01	1.329E+05	1.292E+03	1.300E-02	6.315E-01	-1.689E+00	3.705E-03
0	27	1.348E+07	4.968E-01	4.678E-14	3.798E-01	1.553E+05	1.303E+03	5.589E-03	6.159E-01	-1.673E+00	5.793E-03
0	28	1.365E+07	5.155E-01	6.163E-13	4.233E-01	1.699E+05	1.140E+03	2.473E-02	6.397E-01	-1.403E+00	3.411E-03
0	29	1.412E+07	5.886E-01	1.218E-13	3.971E-01	1.304E+05	1.270E+03	1.516E-02	6.163E-01	-1.312E+00	4.416E-03
0	30	1.446E+07	3.505E-01	3.714E-14	4.114E-01	1.565E+05	1.360E+03	2.214E-02	6.223E-01	-1.539E+00	5.651E-03
0	31	1.316E+07	4.792E-01	2.903E-14	4.132E-01	1.378E+05	1.197E+03	1.152E-02	5.959E-01	-1.471E+00	5.856E-03
0	32	1.241E+07	4.253E-01	1.756E-13	3.779E-01	1.342E+05	1.214E+03	1.468E-02	6.191E-01	-1.387E+00	5.553E-03
0	33	1.473E+07	6.489E-01	8.392E-13	4.006E-01	1.636E+05	1.220E+03	9.367E-03	5.975E-01	-1.706E+00	4.642E-03
0	34	1.298E+07	4.626E-01	1.987E-12	3.735E-01	1.609E+05	1.304E+03	2.741E-02	6.239E-01	-1.364E+00	5.879E-03
0	35	1.361E+07	6.415E-01	4.262E-14	4.034E-01	1.576E+05	1.227E+03	2.253E-02	6.299E-01	-1.703E+00	5.254E-03
0	36	1.234E+07	4.318E-01	9.205E-13	3.631E-01	1.593E+05	1.146E+03	1.435E-02	6.202E-01	-1.633E+00	3.738E-03
0	37	1.308E+07	4.528E-01	3.850E-13	4.250E-01	1.230E+05	1.324E+03	1.667E-02	6.284E-01	-1.571E+00	5.583E-03
0	38	1.323E+07	5.726E-01	1.425E-13	3.625E-01	1.684E+05	1.350E+03	2.640E-02	5.984E-01	-1.238E+00	3.189E-03
0	39	1.256E+07	4.152E-01	4.533E-13	3.538E-01	1.284E+05	1.174E+03	2.893E-02	6.309E-01	-1.755E+00	4.973E-03
0	40	1.370E+07	5.486E-01	4.160E-14	4.199E-01	1.396E+05	1.173E+03	2.306E-02	6.031E-01	-1.281E+00	5.492E-03
0	41	1.382E+07	6.094E-01	6.852E-14	3.860E-01	1.404E+05	1.342E+03	1.702E-02	6.250E-01	-1.338E+00	5.146E-03
0	42	1.330E+07	5.310E-01	3.214E-14	3.646E-01	1.241E+05	1.294E+03	2.385E-02	6.101E-01	-1.514E+00	3.327E-03
0	43	1.454E+07	4.574E-01	5.486E-14	4.169E-01	1.450E+05	1.200E+03	2.695E-02	5.920E-01	-1.549E+00	3.078E-03
0	44	1.406E+07	6.575E-01	1.977E-13	3.744E-01	1.658E+05	1.163E+03	1.967E-02	6.017E-01	-1.228E+00	5.317E-03
0	45	1.209E+07	4.427E-01	1.812E-12	4.297E-01	1.674E+05	1.283E+03	1.621E-02	6.272E-01	-1.508E+00	4.245E-03
0	46	1.427E+07	4.912E-01	2.194E-13	3.825E-01	1.446E+05	1.243E+03	6.618E-03	6.217E-01	-1.450E+00	3.013E-03
0	47	1.356E+07	4.482E-01	2.809E-13	4.101E-01	1.208E+05	1.155E+03	2.118E-02	5.910E-01	-1.351E+00	4.310E-03
0	48	1.227E+07	5.211E-01	1.638E-13	4.063E-01	1.261E+05	1.263E+03	1.888E-02	5.943E-01	-1.731E+00	3.800E-03
0	49	1.377E+07	5.109E-01	7.599E-14	3.718E-01	1.620E+05	1.363E+03	2.416E-02	6.065E-01	-1.432E+00	4.765E-03
0	50	1.401E+07	6.171E-01	2.359E-12	3.919E-01	1.322E+05	1.269E+03	2.071E-02	6.046E-01	-1.260E+00	5.356E-03

1TITLE SDB: PARAMETER_PROD Calc: CRA1 Ver: 1.00 03/04/04 10:47:58

0LATIN HYPERCUBE SAMPLE INPUT VECTORS

S1_HI_TRN- 3

RUN	NO.	X(11)	X(12)	X(13)	X(14)	X(15)
0	1	1.685E-02	1.276E-14	2.963E-03	4.790E-01	2.967E-03
0	2	2.156E-02	2.895E-14	1.148E-04	7.144E-01	4.495E-03
0	3	2.231E-02	6.468E-14	3.397E-04	6.037E-01	6.266E-03
0	4	2.294E-02	1.106E-15	1.772E-03	3.512E-01	5.363E-03
0	5	2.276E-02	5.972E-15	2.038E-04	3.154E-01	1.143E-03
0	6	2.396E-02	4.733E-15	5.524E-04	4.642E-01	7.859E-03
0	7	1.993E-02	3.692E-15	1.927E-03	2.393E-01	8.030E-03
0	8	1.878E-02	6.229E-14	7.250E-05	6.670E-01	3.641E-03
0	9	2.253E-02	1.178E-14	1.265E-04	7.061E-01	3.765E-03
0	10	2.132E-02	1.562E-14	2.115E-03	4.569E-01	2.439E-03
0	11	2.058E-02	2.319E-14	2.244E-03	2.915E-01	7.032E-03
0	12	2.270E-02	2.239E-14	6.833E-05	3.915E-01	8.913E-03
0	13	2.192E-02	3.264E-15	2.770E-03	4.987E-01	7.622E-03
0	14	1.625E-02	1.583E-15	8.775E-05	7.715E-01	8.465E-03
0	15	2.380E-02	5.577E-15	7.570E-05	6.048E-01	6.021E-03
0	16	1.863E-02	2.571E-15	1.355E-03	1.993E-01	1.571E-03
0	17	1.906E-02	1.609E-15	2.217E-04	2.646E-01	9.205E-03
0	18	1.972E-02	3.163E-14	1.608E-04	9.873E-01	4.740E-03
0	19	1.787E-02	6.925E-14	1.405E-03	7.532E-01	6.770E-03
0	20	2.404E-02	1.032E-14	8.049E-04	1.803E-01	5.260E-03
0	21	2.328E-02	3.541E-15	3.126E-04	9.701E-01	8.690E-03
0	22	1.634E-02	7.737E-15	1.809E-04	6.832E-01	4.383E-03
0	23	1.950E-02	5.704E-14	9.875E-04	3.740E-01	3.109E-03
0	24	1.652E-02	3.989E-14	1.166E-03	1.691E-01	4.848E-03
0	25	2.344E-02	5.064E-14	1.677E-03	4.139E-01	7.201E-03
0	26	1.919E-02	6.539E-15	6.982E-04	6.396E-01	1.471E-03
0	27	1.766E-02	3.406E-14	1.422E-04	1.247E-01	9.898E-03
0	28	2.091E-02	1.990E-14	1.068E-04	8.269E-01	9.505E-03
0	29	1.963E-02	5.076E-15	6.272E-05	5.398E-01	2.088E-03
0	30	1.809E-02	1.035E-15	2.564E-04	6.407E-01	7.799E-03
0	31	1.832E-02	9.031E-14	5.331E-05	1.370E-01	3.218E-03
0	32	1.848E-02	1.834E-15	4.865E-04	8.917E-01	4.147E-03
0	33	2.365E-02	1.439E-14	9.268E-04	8.420E-01	5.106E-03
0	34	2.197E-02	1.598E-14	7.493E-04	9.134E-01	2.480E-03
0	35	2.027E-02	2.096E-15	1.507E-04	7.925E-01	1.814E-03
0	36	1.894E-02	7.268E-15	2.018E-04	5.241E-01	8.265E-03
0	37	1.711E-02	4.560E-14	2.529E-03	9.449E-01	9.408E-03
0	38	1.729E-02	2.877E-15	6.427E-04	8.146E-01	7.367E-03
0	39	2.225E-02	1.211E-15	5.533E-05	3.337E-01	3.408E-03
0	40	2.161E-02	2.582E-14	2.677E-04	5.657E-01	6.213E-03
0	41	1.752E-02	4.205E-15	4.114E-04	9.589E-01	2.652E-03
0	42	1.999E-02	3.805E-14	9.721E-05	8.646E-01	5.775E-03
0	43	2.047E-02	9.364E-15	9.526E-05	2.114E-01	9.651E-03
0	44	1.793E-02	8.755E-15	1.494E-03	4.403E-01	1.298E-03
0	45	2.076E-02	7.904E-14	2.833E-04	3.600E-01	1.940E-03
0	46	2.100E-02	1.401E-15	8.731E-04	2.508E-01	6.561E-03
0	47	2.311E-02	2.356E-15	5.305E-04	7.476E-01	3.958E-03
0	48	1.669E-02	1.828E-14	3.908E-04	8.941E-01	6.657E-03

```
0   49  2.114E-02  9.381E-14  1.124E-03  5.786E-01  8.950E-03
0   50  1.691E-02  1.973E-15  4.281E-04  1.073E-01  5.616E-03
1TITLE SDB: PARAMETER_PROD     Calc: CRA1         Ver: 1.00     03/04/04 10:47:58
0RANKS OF LATIN HYPERCUBE SAMPLE INPUT VECTORS
```

Appendix S2_TRN

The following is a listing of the LHS transfer file "LHS2_DRS_SENS2.TRN" that gives tabular data regarding the LHS sampling for Sensitivity Study 2.

```
1

    TITLE SDB: PARAMETER_PROD     Calc: CRA1         Ver: 1.00     02/27/04 07:35:19

    RANDOM SEED =   921396800

    NUMBER OF VARIABLES =   5

    NUMBER OF OBSERVATIONS =  100
0   THE SAMPLE INPUT VECTORS WILL BE PRINTED ALONG WITH THEIR CORRESPONDING RANKS
0   HISTOGRAMS OF THE ACTUAL SAMPLE WILL BE PLOTTED FOR EACH INPUT VARIABLE
0   THE CORRELATION MATRICES (RAW DATA AND RANK CORRELATIONS) WILL BE PRINTED
1

    TITLE SDB: PARAMETER_PROD     Calc: CRA1         Ver: 1.00     02/27/04 07:35:19

    VARIABLE  DISTRIBUTION          RANGE            LABEL
0       1     UNIFORM            8.0000E+06 TO   1.5000E+07  SPALLMOD  REPIPRES
0       2     UNIFORM            0.3500     TO   0.6600      SPALLMOD  REPIPOR
0       3     LOGUNIFORM         2.4000E-14 TO   2.4000E-12  SPALLMOD  REPIPERM
0       4     LOGUNIFORM         1.0000E+04 TO   1.0000E+06  SPALLMOD  TENSLSTR
0       5     LOGUNIFORM         1.0000E-03 TO   0.1000      SPALLMOD  PARTDIAM
1TITLE SDB: PARAMETER_PROD     Calc: CRA1         Ver: 1.00     02/27/04 07:35:19
0LATIN HYPERCUBE SAMPLE INPUT VECTORS

 RUN NO.  X(1)       X(2)       X(3)       X(4)       X(5)
0    1  9.962E+06  5.327E-01  1.409E-12  4.961E+04  1.497E-03
0    2  9.426E+06  4.241E-01  4.809E-14  6.235E+05  9.494E-02
0    3  1.029E+07  4.563E-01  8.098E-13  1.057E+04  1.860E-03
0    4  1.348E+07  6.106E-01  1.911E-13  3.179E+05  1.816E-03
0    5  1.393E+07  4.022E-01  3.836E-13  1.530E+05  2.542E-03
0    6  1.069E+07  4.310E-01  8.486E-14  1.200E+05  4.218E-02
0    7  1.085E+07  6.152E-01  3.529E-13  2.280E+04  1.574E-03
0    8  1.441E+07  5.285E-01  1.237E-12  3.918E+05  6.586E-02
0    9  9.317E+06  4.698E-01  6.594E-13  5.311E+04  5.446E-02
0   10  8.023E+06  6.070E-01  4.776E-13  7.618E+05  4.700E-03
0   11  1.329E+07  4.107E-01  5.925E-14  2.821E+05  1.176E-02
0   12  1.250E+07  5.110E-01  1.392E-13  6.428E+04  2.800E-03
0   13  8.420E+06  6.250E-01  1.136E-13  8.510E+04  3.067E-02
0   14  9.822E+06  3.970E-01  1.175E-12  1.114E+05  1.078E-02
0   15  1.266E+07  6.264E-01  1.738E-13  1.038E+05  8.814E-03
0   16  1.302E+07  3.555E-01  1.571E-12  1.720E+05  6.043E-03
0   17  9.949E+06  4.782E-01  1.043E-12  1.806E+04  1.603E-03
0   18  1.183E+07  5.042E-01  5.657E-13  1.823E+04  3.009E-02
0   19  9.596E+06  5.261E-01  5.081E-14  1.826E+05  7.972E-03
0   20  1.484E+07  5.569E-01  1.000E-12  2.276E+05  4.830E-02
0   21  8.592E+06  6.398E-01  4.906E-13  7.353E+04  3.124E-03
0   22  1.200E+07  3.602E-01  1.340E-12  2.084E+05  8.171E-02
0   23  1.358E+07  6.201E-01  4.019E-13  2.307E+04  1.109E-03
0   24  1.120E+07  5.931E-01  2.886E-13  1.295E+04  5.194E-03
0   25  1.406E+07  4.938E-01  7.930E-13  2.163E+04  1.049E-03
0   26  1.227E+07  4.449E-01  3.144E-14  3.022E+04  2.116E-03
0   27  8.903E+06  5.662E-01  5.064E-13  3.761E+04  1.632E-02
0   28  8.193E+06  6.436E-01  1.784E-12  4.373E+04  1.782E-02
0   29  8.359E+06  4.984E-01  9.395E-13  9.846E+04  7.621E-02
0   30  9.086E+06  4.280E-01  5.740E-14  4.253E+04  4.105E-02
0   31  8.101E+06  4.674E-01  6.975E-14  3.779E+05  1.984E-02
0   32  1.050E+07  3.659E-01  5.293E-13  6.760E+05  8.610E-03
0   33  8.995E+06  4.403E-01  4.379E-13  1.035E+04  7.307E-03
0   34  8.553E+06  5.856E-01  2.201E-13  1.172E+04  6.045E-02
0   35  1.287E+07  4.831E-01  3.598E-14  2.929E+04  9.474E-03
0   36  1.173E+07  4.990E-01  1.610E-12  5.017E+05  1.215E-02
```

```
0   37  1.362E+07  4.188E-01  6.188E-14  7.609E+04  1.098E-02
0   38  1.398E+07  5.151E-01  2.081E-13  3.228E+04  6.801E-02
0   39  1.160E+07  4.855E-01  1.526E-13  1.393E+05  3.400E-03
0   40  1.144E+07  4.504E-01  3.053E-13  2.184E+05  5.502E-02
0   41  8.717E+06  3.871E-01  2.561E-13  5.080E+04  2.447E-02
0   42  1.459E+07  5.684E-01  2.805E-14  1.369E+04  2.094E-02
0   43  1.103E+07  6.189E-01  2.532E-14  8.817E+05  4.903E-03
0   44  1.426E+07  3.831E-01  4.164E-14  1.637E+04  1.408E-02
0   45  1.321E+07  3.576E-01  4.261E-13  1.119E+04  3.661E-03
0   46  1.343E+07  4.746E-01  2.375E-12  9.734E+05  2.600E-02
0   47  9.655E+06  4.905E-01  3.686E-13  5.883E+05  7.425E-02
0   48  1.421E+07  3.503E-01  8.797E-14  6.614E+04  6.003E-02
0   49  8.772E+06  5.708E-01  3.846E-14  1.559E+04  5.687E-03
0   50  8.938E+06  4.167E-01  1.023E-13  9.295E+04  1.449E-02
0   51  8.685E+06  4.120E-01  4.513E-14  1.256E+05  3.309E-03
0   52  1.142E+07  3.750E-01  1.078E-12  1.917E+04  1.991E-03
0   53  1.131E+07  5.540E-01  7.640E-14  2.424E+04  2.694E-03
0   54  1.039E+07  5.780E-01  1.254E-13  8.540E+05  6.446E-03
0   55  1.370E+07  6.027E-01  1.134E-12  7.475E+05  1.721E-03
0   56  1.096E+07  5.479E-01  8.619E-13  3.568E+05  2.762E-02
0   57  9.787E+06  5.404E-01  6.980E-13  6.991E+04  4.101E-03
0   58  1.238E+07  3.943E-01  2.972E-14  5.565E+05  2.052E-03
0   59  1.211E+07  3.796E-01  3.211E-13  3.950E+04  9.563E-02
0   60  1.474E+07  5.450E-01  3.347E-14  8.230E+05  2.287E-02
0   61  1.308E+07  5.796E-01  8.258E-14  4.750E+05  1.233E-03
0   62  1.411E+07  5.126E-01  6.878E-14  1.976E+05  7.078E-03
0   63  1.458E+07  6.580E-01  9.351E-14  2.576E+05  8.980E-02
0   64  1.125E+07  6.379E-01  6.555E-14  4.013E+05  1.373E-03
0   65  1.333E+07  6.009E-01  5.994E-13  5.771E+04  3.594E-03
0   66  1.386E+07  6.545E-01  1.291E-13  7.953E+04  2.315E-02
0   67  1.278E+07  5.613E-01  2.159E-12  4.189E+05  3.384E-02
0   68  1.296E+07  4.864E-01  4.352E-14  1.313E+05  8.692E-02
0   69  1.275E+07  4.255E-01  3.773E-14  6.971E+05  1.155E-03
0   70  1.008E+07  4.388E-01  2.443E-14  2.676E+05  5.087E-02
0   71  1.073E+07  3.640E-01  3.461E-13  2.991E+05  2.194E-03
0   72  1.261E+07  5.490E-01  1.472E-13  2.525E+04  3.966E-03
0   73  9.690E+06  6.075E-01  6.879E-13  1.397E+04  4.431E-02
0   74  8.235E+06  6.485E-01  1.910E-12  1.321E+05  1.735E-02
0   75  1.216E+07  6.459E-01  6.101E-13  6.174E+04  2.062E-02
0   76  1.022E+07  6.309E-01  1.080E-13  1.632E+05  2.738E-02
0   77  1.248E+07  3.925E-01  2.059E-12  6.546E+05  2.435E-03
0   78  1.467E+07  6.332E-01  5.410E-14  1.239E+04  3.509E-02
0   79  1.499E+07  5.231E-01  1.321E-13  5.586E+04  1.294E-02
0   80  1.189E+07  4.606E-01  7.322E-13  3.401E+05  1.551E-02
0   81  1.445E+07  4.633E-01  1.465E-12  1.743E+05  5.253E-03
0   82  1.490E+07  5.742E-01  1.677E-12  2.084E+04  9.739E-03
0   83  1.379E+07  4.366E-01  2.150E-13  8.986E+04  5.991E-03
0   84  1.315E+07  5.375E-01  1.191E-13  2.665E+04  3.824E-02
0   85  1.193E+07  5.581E-01  1.314E-12  1.472E+04  3.727E-02
0   86  9.247E+06  4.549E-01  2.755E-14  4.494E+05  4.199E-03
0   87  1.112E+07  5.067E-01  1.873E-12  2.458E+05  1.331E-02
0   88  1.226E+07  4.078E-01  2.242E-12  3.042E+05  7.915E-03
0   89  1.089E+07  3.725E-01  8.842E-13  1.463E+05  1.031E-02
0   90  1.168E+07  6.516E-01  2.308E-13  4.805E+05  2.316E-03
0   91  1.064E+07  5.907E-01  1.831E-13  4.767E+04  6.988E-02
0   92  9.490E+06  4.483E-01  2.652E-13  1.705E+04  3.177E-02
0   93  1.437E+07  5.853E-01  2.479E-13  3.603E+04  4.370E-03
0   94  1.033E+07  5.188E-01  4.662E-14  4.134E+04  6.629E-03
0   95  1.013E+07  5.358E-01  2.835E-13  1.073E+05  1.837E-02
0   96  1.056E+07  5.960E-01  7.521E-14  9.241E+05  1.423E-03
0   97  8.311E+06  3.714E-01  9.665E-14  2.874E+04  1.035E-03
0   98  9.348E+06  4.035E-01  1.789E-13  3.398E+04  1.281E-03
0   99  1.153E+07  3.873E-01  1.642E-13  5.351E+05  2.918E-03
0  100  9.186E+06  4.715E-01  3.272E-14  2.333E+05  4.665E-02
1TITLE SDB: PARAMETER_PROD     Calc: CRA1         Ver: 1.00     02/27/04 07:35:19
0RANKS OF LATIN HYPERCUBE SAMPLE INPUT VECTORS

 RUN NO.     X(1)       X(2)       X(3)       X(4)       X(5)
0    1        29.        59.        89.        35.         9.
0    2        21.        24.        16.        90.        99.
0    3        33.        35.        77.         2.        14.
```

0	4	79.	85.	46.	76.	13.
0	5	85.	17.	61.	60.	21.
0	6	39.	27.	28.	54.	82.
0	7	41.	86.	59.	18.	10.
0	8	92.	58.	86.	80.	91.
0	9	19.	39.	72.	37.	87.
0	10	1.	83.	65.	95.	34.
0	11	76.	20.	20.	73.	54.
0	12	65.	52.	39.	41.	23.
0	13	7.	89.	34.	47.	75.
0	14	27.	16.	85.	53.	52.
0	15	67.	90.	43.	51.	48.
0	16	72.	2.	91.	62.	40.
0	17	28.	42.	82.	13.	11.
0	18	55.	50.	69.	14.	74.
0	19	23.	57.	17.	64.	46.
0	20	98.	67.	81.	68.	85.
0	21	9.	94.	66.	44.	25.
0	22	58.	4.	88.	66.	96.
0	23	80.	88.	62.	19.	3.
0	24	46.	79.	55.	6.	36.
0	25	87.	47.	76.	17.	2.
0	26	62.	31.	6.	25.	17.
0	27	13.	70.	67.	29.	61.
0	28	3.	95.	94.	33.	63.
0	29	6.	48.	80.	50.	95.
0	30	16.	26.	19.	32.	81.
0	31	2.	38.	24.	79.	65.
0	32	36.	6.	68.	92.	47.
0	33	15.	30.	64.	1.	44.
0	34	8.	77.	49.	4.	90.
0	35	70.	43.	9.	24.	49.
0	36	54.	49.	92.	86.	55.
0	37	81.	23.	21.	45.	53.
0	38	86.	54.	47.	26.	92.
0	39	52.	44.	41.	58.	27.
0	40	50.	33.	56.	67.	88.
0	41	11.	12.	52.	36.	70.
0	42	95.	71.	4.	7.	67.
0	43	44.	87.	2.	98.	35.
0	44	90.	11.	12.	11.	58.
0	45	75.	3.	63.	3.	29.
0	46	78.	41.	100.	100.	71.
0	47	24.	46.	60.	89.	94.
0	48	89.	1.	29.	42.	89.
0	49	12.	72.	11.	10.	38.
0	50	14.	22.	32.	49.	59.
0	51	10.	21.	14.	55.	26.
0	52	49.	9.	83.	15.	15.
0	53	48.	66.	26.	20.	22.
0	54	35.	74.	36.	97.	41.
0	55	82.	82.	84.	94.	12.
0	56	43.	64.	78.	78.	73.
0	57	26.	62.	74.	43.	31.
0	58	63.	15.	5.	88.	16.
0	59	59.	10.	57.	30.	100.
0	60	97.	63.	8.	96.	68.
0	61	73.	75.	27.	84.	5.
0	62	88.	53.	23.	65.	43.
0	63	94.	100.	30.	71.	98.
0	64	47.	93.	22.	81.	7.
0	65	77.	81.	70.	39.	28.
0	66	84.	99.	37.	46.	69.
0	67	69.	69.	98.	82.	77.
0	68	71.	45.	13.	56.	97.
0	69	68.	25.	10.	93.	4.
0	70	30.	29.	1.	72.	86.
0	71	40.	5.	58.	74.	18.
0	72	66.	65.	40.	21.	30.
0	73	25.	84.	73.	8.	83.
0	74	4.	97.	96.	57.	62.

```
0   75        60.        96.        71.        40.        66.
0   76        32.        91.        33.        61.        72.
0   77        64.        14.        97.        91.        20.
0   78        96.        92.        18.         5.        78.
0   79       100.        56.        38.        38.        56.
0   80        56.        36.        75.        77.        60.
0   81        93.        37.        90.        63.        37.
0   82        99.        73.        93.        16.        50.
0   83        83.        28.        48.        48.        39.
0   84        74.        61.        35.        22.        80.
0   85        57.        68.        87.         9.        79.
0   86        18.        34.         3.        83.        32.
0   87        45.        51.        95.        70.        57.
0   88        61.        19.        99.        75.        45.
0   89        42.         8.        79.        59.        51.
0   90        53.        98.        50.        85.        19.
0   91        38.        78.        45.        34.        93.
0   92        22.        32.        53.        12.        76.
0   93        91.        76.        51.        28.        33.
0   94        34.        55.        15.        31.        42.
0   95        31.        60.        54.        52.        64.
0   96        37.        80.        25.        99.         8.
0   97         5.         7.        31.        23.         1.
0   98        20.        18.        44.        27.         6.
0   99        51.        13.        42.        87.        24.
0  100        17.        40.         7.        69.        84.
1   TITLE SDB: PARAMETER_PROD     Calc: CRA1         Ver: 1.00     02/27/04 07:35:19
0  HISTOGRAM FOR VARIABLE NO.  1     UNIFORM         DISTRIBUTION

     MIDPOINT          FREQ.

    7875000.             1    X
    8225000.             5    XXXXX
    8574999.             5    XXXXX
    8924999.             5    XXXXX
    9274999.             5    XXXXX
    9624999.             5    XXXXX
    9974999.             5    XXXXX
   0.1032500E+08         4    XXXX
   0.1067500E+08         5    XXXXX
   0.1102500E+08         6    XXXXXX
   0.1137500E+08         5    XXXXX
   0.1172500E+08         5    XXXXX
   0.1207500E+08         4    XXXX
   0.1242500E+08         5    XXXXX
   0.1277500E+08         5    XXXXX
   0.1312500E+08         6    XXXXXX
   0.1347500E+08         5    XXXXX
   0.1382500E+08         5    XXXXX
   0.1417500E+08         4    XXXX
   0.1452500E+08         6    XXXXXX
   0.1487500E+08         4    XXXX
0                      100


      MIN            MAX           RANGE           MEAN          MEDIAN        VARIANCE

    8023228.      0.1499233E+08   6969099.      0.1149958E+08  0.1148257E+08  0.4091160E+13

1   TITLE SDB: PARAMETER_PROD     Calc: CRA1         Ver: 1.00     02/27/04 07:35:19
0  HISTOGRAM FOR VARIABLE NO.  2     UNIFORM         DISTRIBUTION

     MIDPOINT          FREQ.

   0.3525000             3    XXX
   0.3675000             5    XXXXX
   0.3825001             5    XXXXX
   0.3975001             5    XXXXX
   0.4125001             5    XXXXX
   0.4275001             4    XXXX
   0.4425001             5    XXXXX
```

```
   0.4575001             5    XXXXX
   0.4725001             5    XXXXX
   0.4875002             5    XXXXX
   0.5025002             4    XXXX
   0.5175002             5    XXXXX
   0.5325001             5    XXXXX
   0.5475001             5    XXXXX
   0.5625001             5    XXXXX
   0.5775001             4    XXXX
   0.5925001             5    XXXXX
   0.6075001             5    XXXXX
   0.6225001             5    XXXXX
   0.6375000             5    XXXXX
   0.6525000             5    XXXXX
0                      100


      MIN            MAX           RANGE           MEAN          MEDIAN        VARIANCE

   0.3502551      0.6580150      0.3077599      0.5049728      0.5054672      0.8010331E-02

1   TITLE SDB: PARAMETER_PROD     Calc: CRA1         Ver: 1.00     02/27/04 07:35:19
0  HISTOGRAM FOR VARIABLE NO.  3     LOGUNIFORM      DISTRIBUTION

     MIDPOINT          FREQ.

   0.5999999E-13        35    XXXXXXXXXXXXXXXXXXXXXXXXXXXXXXXXXX
   0.1800000E-12        15    XXXXXXXXXXXXXXX
   0.3000000E-12         9    XXXXXXXXX
   0.4199999E-12         6    XXXXXX
   0.5400000E-12         5    XXXXX
   0.6599999E-12         4    XXXX
   0.7799999E-12         3    XXX
   0.8999999E-12         3    XXX
   0.1020000E-11         3    XXX
   0.1140000E-11         2    XX
   0.1260000E-11         2    XX
   0.1380000E-11         2    XX
   0.1500000E-11         1    X
   0.1620000E-11         3    XXX
   0.1740000E-11         1    X
   0.1860000E-11         2    XX
   0.1980000E-11         0
   0.2100000E-11         2    XX
   0.2220000E-11         1    X
   0.2340000E-11         1    X
0                      100


      MIN            MAX           RANGE           MEAN          MEDIAN        VARIANCE

   0.2443127E-13  0.2375084E-11  0.2350653E-11  0.5167137E-12  0.2393595E-12  0.3609148E-24

1   TITLE SDB: PARAMETER_PROD     Calc: CRA1         Ver: 1.00     02/27/04 07:35:19
0  HISTOGRAM FOR VARIABLE NO.  4     LOGUNIFORM      DISTRIBUTION

     MIDPOINT          FREQ.

    23999.99            34    XXXXXXXXXXXXXXXXXXXXXXXXXXXXXXXXXX
    71999.98            15    XXXXXXXXXXXXXXX
    120000.0             9    XXXXXXXXX
    168000.0             6    XXXXXX
    215999.9             5    XXXXX
    263999.9             4    XXXX
    311999.9             3    XXX
    359999.9             3    XXX
    407999.9             3    XXX
    455999.9             2    XX
    503999.9             2    XX
    551999.9             2    XX
    599999.9             2    XX
```

```
    647999.9             1    X
    695999.9             2    XX
    743999.9             2    XX
    791999.9             0
    839999.9             2    XX
    887999.9             1    X
    935999.9             1    X
    983999.9             1    X
0                      100


      MIN            MAX           RANGE           MEAN          MEDIAN        VARIANCE

    10354.82       973430.8       963076.0       214599.1       101129.8      0.6195354E+11

1   TITLE SDB: PARAMETER_PROD     Calc: CRA1         Ver: 1.00     02/27/04 07:35:19
0  HISTOGRAM FOR VARIABLE NO.  5     LOGUNIFORM      DISTRIBUTION

     MIDPOINT          FREQ.

   0.2349999E-02        34    XXXXXXXXXXXXXXXXXXXXXXXXXXXXXXXXX
   0.7049998E-02        14    XXXXXXXXXXXXXX
   0.1175000E-01        10    XXXXXXXXXX
   0.1645000E-01         6    XXXXXX
   0.2114999E-01         5    XXXXX
   0.2584999E-01         4    XXXX
   0.3054999E-01         3    XXX
   0.3524999E-01         3    XXX
   0.3994999E-01         3    XXX
   0.4464999E-01         2    XX
   0.4934999E-01         2    XX
   0.5404998E-01         2    XX
   0.5874998E-01         2    XX
   0.6344998E-01         0
   0.6814998E-01         3    XXX
   0.7284997E-01         1    X
   0.7754997E-01         1    X
   0.8224997E-01         1    X
   0.8694997E-01         1    X
   0.9164996E-01         1    X
   0.9634996E-01         2    XX
0                      100


      MIN            MAX           RANGE           MEAN          MEDIAN        VARIANCE

   0.1035236E-02  0.9562719E-01  0.9459195E-01  0.2147832E-01  0.1002459E-01  0.6236890E-03

1TITLE SDB: PARAMETER_PROD     Calc: CRA1         Ver: 1.00     02/27/04 07:35:19
0CORRELATIONS AMONG INPUT VARIABLES CREATED BY THE LATIN HYPERCUBE SAMPLE FOR RAW DATAPAGE
1
0    1  1.0000
0    2  0.0340  1.0000
0    3  0.0537 -0.0343  1.0000
0    4  0.0368  0.0180  0.1108  1.0000
0    5 -0.0121 -0.0340 -0.0370 -0.0588  1.0000
0           1       2       3       4       5
0VARIABLES
0THE VARIANCE INFLATION FACTOR FOR THIS MATRIX IS  1.02
1TITLE SDB: PARAMETER_PROD     Calc: CRA1         Ver: 1.00     02/27/04 07:35:19
0CORRELATIONS AMONG INPUT VARIABLES CREATED BY THE LATIN HYPERCUBE SAMPLE FOR RANK DATA PAGE
1
0    1  1.0000
0    2  0.0348  1.0000
0    3 -0.0013  0.0121  1.0000
0    4  0.0293 -0.0442 -0.0318  1.0000
0    5 -0.0300  0.0110  0.0126 -0.0116  1.0000
0           1       2       3       4       5
0VARIABLES
0THE VARIANCE INFLATION FACTOR FOR THIS MATRIX IS  1.00
```

Appendix SPALL_TABLE

Reproduced here is the ASCII table of spall release volumes produced for the WIPP PA CUTTINGS code. The format is as follows:

```
# of vectors per scenario
# of scenarios
REPIPRES(S1)        REPIPRES(S2) ….
(S1) vector #       runtime       SPLVOL2
…..

(S2) vector #       runtime       SPLVOL2
…..
```

```
50
4
10000000  12000000  14000000  14800000
 1.000000E+00  6.000000E+02  0.000000E+00
 2.000000E+00  6.000000E+02  0.000000E+00
 3.000000E+00  6.000000E+02  0.000000E+00
 4.000000E+00  6.000000E+02  0.000000E+00
 5.000000E+00  6.000000E+02  0.000000E+00
 6.000000E+00  6.000000E+02  0.000000E+00
 7.000000E+00  6.000000E+02  0.000000E+00
 8.000000E+00  6.000000E+02  0.000000E+00
 9.000000E+00  6.000000E+02  0.000000E+00
 1.000000E+01  6.000000E+02  0.000000E+00
 1.100000E+01  6.000000E+02  0.000000E+00
 1.200000E+01  6.000000E+02  0.000000E+00
 1.300000E+01  6.000000E+02  0.000000E+00
 1.400000E+01  6.000000E+02  0.000000E+00
 1.500000E+01  6.000000E+02  0.000000E+00
 1.600000E+01  6.000000E+02  0.000000E+00
 1.700000E+01  6.000000E+02  0.000000E+00
 1.800000E+01  6.000000E+02  0.000000E+00
 1.900000E+01  6.000000E+02  0.000000E+00
 2.000000E+01  6.000000E+02  0.000000E+00
 2.100000E+01  6.000000E+02  0.000000E+00
 2.200000E+01  6.000000E+02  0.000000E+00
 2.300000E+01  6.000000E+02  0.000000E+00
 2.400000E+01  6.000000E+02  0.000000E+00
 2.500000E+01  6.000000E+02  0.000000E+00
 2.600000E+01  6.000000E+02  0.000000E+00
 2.700000E+01  6.000000E+02  0.000000E+00
 2.800000E+01  6.000000E+02  0.000000E+00
 2.900000E+01  6.000000E+02  0.000000E+00
 3.000000E+01  6.000000E+02  0.000000E+00
 3.100000E+01  6.000000E+02  0.000000E+00
 3.200000E+01  6.000000E+02  0.000000E+00
 3.300000E+01  6.000000E+02  0.000000E+00
 3.400000E+01  6.000000E+02  0.000000E+00
 3.500000E+01  6.000000E+02  0.000000E+00
 3.600000E+01  6.000000E+02  0.000000E+00
 3.700000E+01  6.000000E+02  0.000000E+00
 3.800000E+01  6.000000E+02  0.000000E+00
 3.900000E+01  6.000000E+02  0.000000E+00
 4.000000E+01  6.000000E+02  0.000000E+00
 4.100000E+01  6.000000E+02  0.000000E+00
 4.200000E+01  6.000000E+02  0.000000E+00
 4.300000E+01  6.000000E+02  0.000000E+00
 4.400000E+01  6.000000E+02  0.000000E+00
```

4.500000E+01	6.000000E+02	0.000000E+00
4.600000E+01	6.000000E+02	0.000000E+00
4.700000E+01	6.000000E+02	0.000000E+00
4.800000E+01	6.000000E+02	0.000000E+00
4.900000E+01	6.000000E+02	0.000000E+00
5.000000E+01	6.000000E+02	0.000000E+00
1.000000E+00	6.000000E+02	0.000000E+00
2.000000E+00	6.000000E+02	1.219309E+00
3.000000E+00	6.000000E+02	0.000000E+00
4.000000E+00	6.000000E+02	5.647984E-01
5.000000E+00	6.000000E+02	0.000000E+00
6.000000E+00	6.000000E+02	0.000000E+00
7.000000E+00	6.000000E+02	0.000000E+00
8.000000E+00	6.000000E+02	0.000000E+00
9.000000E+00	6.000000E+02	0.000000E+00
1.000000E+01	6.000000E+02	0.000000E+00
1.100000E+01	6.000000E+02	0.000000E+00
1.200000E+01	6.000000E+02	0.000000E+00
1.300000E+01	6.000000E+02	0.000000E+00
1.400000E+01	6.000000E+02	0.000000E+00
1.500000E+01	6.000000E+02	0.000000E+00
1.600000E+01	6.000000E+02	1.708426E+00
1.700000E+01	6.000000E+02	0.000000E+00
1.800000E+01	6.000000E+02	0.000000E+00
1.900000E+01	6.000000E+02	6.072450E-01
2.000000E+01	6.000000E+02	7.934533E-03
2.100000E+01	6.000000E+02	0.000000E+00
2.200000E+01	6.000000E+02	0.000000E+00
2.300000E+01	6.000000E+02	1.665951E-01
2.400000E+01	6.000000E+02	0.000000E+00
2.500000E+01	6.000000E+02	0.000000E+00
2.600000E+01	6.000000E+02	1.392531E-01
2.700000E+01	6.000000E+02	0.000000E+00
2.800000E+01	6.000000E+02	3.465368E-02
2.900000E+01	6.000000E+02	0.000000E+00
3.000000E+01	6.000000E+02	7.000460E+00
3.100000E+01	6.000000E+02	9.779406E-02
3.200000E+01	6.000000E+02	0.000000E+00
3.300000E+01	6.000000E+02	0.000000E+00
3.400000E+01	6.000000E+02	0.000000E+00
3.500000E+01	6.000000E+02	0.000000E+00
3.600000E+01	6.000000E+02	1.828914E-01
3.700000E+01	6.000000E+02	0.000000E+00
3.800000E+01	6.000000E+02	0.000000E+00
3.900000E+01	6.000000E+02	0.000000E+00
4.000000E+01	6.000000E+02	0.000000E+00
4.100000E+01	6.000000E+02	0.000000E+00
4.200000E+01	6.000000E+02	0.000000E+00
4.300000E+01	6.000000E+02	0.000000E+00
4.400000E+01	6.000000E+02	0.000000E+00
4.500000E+01	6.000000E+02	0.000000E+00
4.600000E+01	6.000000E+02	0.000000E+00
4.700000E+01	6.000000E+02	2.443149E-01
4.800000E+01	6.000000E+02	2.241325E-01
4.900000E+01	6.000000E+02	0.000000E+00
5.000000E+01	6.000000E+02	0.000000E+00
1.000000E+00	6.000000E+02	3.969786E-01
2.000000E+00	6.000000E+02	7.2180000+00
3.000000E+00	6.000000E+02	0.000000E+00
4.000000E+00	6.000000E+02	1.288459E+00
5.000000E+00	6.000000E+02	7.992458E-02
6.000000E+00	6.000000E+02	7.098113E-02
7.000000E+00	6.000000E+02	0.000000E+00
8.000000E+00	6.000000E+02	0.000000E+00
9.000000E+00	6.000000E+02	1.893962E-01
1.000000E+01	6.000000E+02	0.000000E+00
1.100000E+01	6.000000E+02	2.772627E-01
1.200000E+01	6.000000E+02	4.027504E-02
1.300000E+01	6.000000E+02	1.027906E-01

1.400000E+01	6.000000E+02	3.571318E-02
1.500000E+01	6.000000E+02	1.126825E-01
1.600000E+01	6.000000E+02	3.130843E+00
1.700000E+01	6.000000E+02	9.304333E-02
1.800000E+01	6.000000E+02	6.011905E-01
1.900000E+01	6.000000E+02	4.405089E+00
2.000000E+01	6.000000E+02	2.248029E-01
2.100000E+01	6.000000E+02	0.000000E+00
2.200000E+01	6.000000E+02	2.612711E-02
2.300000E+01	6.000000E+02	1.788106E+00
2.400000E+01	6.000000E+02	4.610163E-01
2.500000E+01	6.000000E+02	6.482388E-02
2.600000E+01	6.000000E+02	1.033008E+00
2.700000E+01	6.000000E+02	0.000000E+00
2.800000E+01	6.000000E+02	7.382768E-01
2.900000E+01	6.000000E+02	3.845654E-01
3.000000E+01	6.000000E+02	9.452960E+00
3.100000E+01	6.000000E+02	6.942384E-01
3.200000E+01	6.000000E+02	2.364516E-02
3.300000E+01	6.000000E+02	1.207344E-01
3.400000E+01	6.000000E+02	4.061748E-01
3.500000E+01	6.000000E+02	2.688929E-01
3.600000E+01	6.000000E+02	9.488029E-01
3.700000E+01	6.000000E+02	0.000000E+00
3.800000E+01	6.000000E+02	5.156692E-02
3.900000E+01	6.000000E+02	2.100307E-01
4.000000E+01	6.000000E+02	0.000000E+00
4.100000E+01	6.000000E+02	9.508261E-03
4.200000E+01	6.000000E+02	3.110759E-01
4.300000E+01	6.000000E+02	1.570537E-01
4.400000E+01	6.000000E+02	6.952912E-02
4.500000E+01	6.000000E+02	4.843711E-01
4.600000E+01	6.000000E+02	2.243195E-01
4.700000E+01	6.000000E+02	1.809723E+00
4.800000E+01	6.000000E+02	1.336131E+00
4.900000E+01	6.000000E+02	0.000000E+00
5.000000E+01	6.000000E+02	3.235973E-01

1.000000E+00	6.000000E+02	5.573982E-01
2.000000E+00	6.000000E+02	7.297470E+00
3.000000E+00	6.000000E+02	0.000000E+00
4.000000E+00	6.000000E+02	1.610650E+00
5.000000E+00	6.000000E+02	2.073942E-01
6.000000E+00	6.000000E+02	1.825025E-01
7.000000E+00	6.000000E+02	0.000000E+00
8.000000E+00	6.000000E+02	0.000000E+00
9.000000E+00	6.000000E+02	3.403259E-01
1.000000E+01	6.000000E+02	0.000000E+00
1.100000E+01	6.000000E+02	3.810624E-01
1.200000E+01	6.000000E+02	9.223854E-02
1.300000E+01	6.000000E+02	2.163116E-01
1.400000E+01	6.000000E+02	1.372680E-01
1.500000E+01	6.000000E+02	2.696921E-01
1.600000E+01	6.000000E+02	3.952352E+00
1.700000E+01	6.000000E+02	3.760077E-01
1.800000E+01	6.000000E+02	1.170028E+00
1.900000E+01	6.000000E+02	5.317553E+00
2.000000E+01	6.000000E+02	3.182866E-01
2.100000E+01	6.000000E+02	0.000000E+00
2.200000E+01	6.000000E+02	1.082159E-01
2.300000E+01	6.000000E+02	2.248536E+00
2.400000E+01	6.000000E+02	6.337715E-01
2.500000E+01	6.000000E+02	1.654469E-01
2.600000E+01	6.000000E+02	1.206204E+01
2.700000E+01	6.000000E+02	0.000000E+00
2.800000E+01	6.000000E+02	1.452345E+00
2.900000E+01	6.000000E+02	4.869126E-01
3.000000E+01	6.000000E+02	1.206204E+01
3.100000E+01	6.000000E+02	1.427621E+00
3.200000E+01	6.000000E+02	9.781100E-02
3.300000E+01	6.000000E+02	2.572754E-01

3.400000E+01	6.000000E+02	6.018938E-01
3.500000E+01	6.000000E+02	4.417713E-01
3.600000E+01	6.000000E+02	1.670775E+00
3.700000E+01	6.000000E+02	0.000000E+00
3.800000E+01	6.000000E+02	1.609376E-01
3.900000E+01	6.000000E+02	3.452956E-01
4.000000E+01	6.000000E+02	0.000000E+00
4.100000E+01	6.000000E+02	8.979040E-02
4.200000E+01	6.000000E+02	5.206025E-01
4.300000E+01	6.000000E+02	3.251399E-01
4.400000E+01	6.000000E+02	1.797236E-01
4.500000E+01	6.000000E+02	6.526521E-01
4.600000E+01	6.000000E+02	4.319749E-01
4.700000E+01	6.000000E+02	3.105359E+00
4.800000E+01	6.000000E+02	2.329654E+00
4.900000E+01	6.000000E+02	0.000000E+00
5.000000E+01	6.000000E+02	5.460343E-01

Appendix VG

The following tables comprise a glossary of CAMDAT variable names.

Table VG-1. CAMDAT Property Names

Property Name	DRSPALL Input Parameter
SURFELEV	Land elevation
REPOSTOP	Repository top
REPOSTCK	Total thickness
DRZTCK	DRZ thickness
DRZPERM	DRZ permeability
REPOTRAD	Outer radius
REPIPRES	Initial gas pressure
FFPORPRS	Far-field Pore Pressure
FFSTRESS	Far-field In-Situ Stress
REPIPOR	Repository initial porosity
REPIPERM	Repository initial permeability
FRCHBETA	Forchheimer beta
BIOTBETA	Biot beta
POISSRAT	Poisson's ratio
COHESION	Cohesion
FRICTANG	Friction angle
TENSLSTR	Tensile strength
CHARLEN	Characteristic failure length
PARTDIAM	Particle diameter
GASBSDEN	Gas base density
GASVISCO	Gas viscosity
INITMDEN	Initial mud density
MUDVISCO	Mud viscosity
PIPEROUG	Pipe roughness
ANNUROUG	Annulus roughness
MUDSOLMX	Max mud solids vol. Fraction
MUDSOLVE	Mud solids viscosity exponent
BITDIAM	Bit diameter
PIPEDIAM	Pipe diameter
COLRDIAM	Collar diameter
PIPEID	Pipe inside diameter
COLRLNGT	Collar length

Property Name	DRSPALL Input Parameter
EXITPLEN	Exit pipe length
EXITPDIA	Exit pipe diameter
DRILRATE	Drilling rate
BITABOV	Initial bit above repository
MUDPRATE	Mud pump rate
MAXPPRES	Mud pump pressure
DDZTHICK	DDZ thickness
DDZPERM	DDZ permeability
STPDVOLR	Stop drilling exit volume rate
STPPVOLR	Stop pumping exit volume rate
STPDTIME	Stop drilling time
REPODR	Initial repository cell length
REPODDR	Repository cell growth rate
WELLDZ	Initial wellbore cell length
WELLDDZ	Well cell growth Rate
GEOMEXP	Geometry exponent
ALLOWFLD	Fluidization flag
WELLSTAB	Well stability factor
REPOSTAB	Repository stability factor
MASSDIFF	Mass diffusion factor
MOMDIFF	Momentum diffusion factor
VALIDTC	Validation test case flag
PI	Pi
REFPRES	Atmospheric pressure
GRAVACC	Gravity
RGAS	Gas constant
TREPO	Repository temperature
H2OCOMP	Water compressibility
WASTDENS	Waste density
SALTDENS	Salt density
SHAPFAC	Shape factor
TENSVEL	Tensile velocity
BITNZNO	Bit nozzle number
BITNZDIA	Bit nozzle diameter
CHOKEFF	Choke efficiency
CAVRAD0	Initial cavity radius
MINCHVEL	Minimum characteristic velocity
MINNUMLT	Minimum number of zones per characteristic length

Table VG-2. CAMDAT History Variable Names

Index	History Variable Name	Description
1	PUMPRS	Pump pressure
2	BOTPRS	Well bottom pressure
3	CAVPRS	Cavity pressure
4	DRILLRAD	Equivalent Drilled radius
5	CAVRAD	Equivalent Cavity radius
6	TENSRAD	Equivalent Tensile radius
7	CUTRAD	Maximum Equivalent Cuttings radius (constant)
8	WBSUPVEL	Waste boundary pore velocity
9	FLUIDVEL	Fluidization velocity
10	MUDEJVEL	Mud ejection velocity
11	WASWELL	Waste in Well
12	WASEJCT	Waste ejected at surface
13	CUTMASMX	Maximum Cuttings mass
14	GASINJ	Gas injected into well
15	WELLGAS	Gas in Well
16	GASEJCT	Gas ejected at surface
17	GASPOSN	Gas position in well
18	WASPOSN	Waste position in well
19	CPUTIME	CPU time
20	RUNSTEP	Run step index
21	VOLSTORE	Volume failed/drilled material in storage(released from repository but not in well)
22	GASTORE	Gas mass in temporary storage
23	WASTORE	Waste mass in temporary storage
24	WASINJ	Waste injected into well
25	GASCAV	Cavity gas mass
26	SWELLGAS	Sum of well gas mass/cell
27	SREPOGAS	Sum repository gas mass/cell
28	GASTOTAL	(16)+(22)+(25)+(26)+(27)
29	GASFROMW	Total gas from waste
30	CUTMASS	Mass of cuttings
31	SPLMASS	Mass of spalled material
32	TOTMASS	Total mass of material removed
33	CUTVOLEQ	Equivalent uncompacted cuttings volume
34	SPLVOLEQ	Equivalent uncompacted spall volume

Index	History Variable Name	Description
35	TOTVOLEQ	Equivalent uncompacted total volume
36	CUTRUVOL	True cuttings volume
37	CUTRUMAS	True cutting mass
38	PUMPRATE	Mud pump rate
39	SHEARRAD	Maximum radius of shear failure
40	NOZLVEL	Nozzle fluid velocity
41	WBUPVEL	Fluid velocity near well bottom
42	FLUIDTIM	Characteristic fluidization time
43	SWELLWAS	Sum well waste mass /cell
44	WASFROMR	Total waste mass from repository
45	WASTOTAL	Total waste in system (removed from repository)
46	PITGAIN	Pit gain = Σ ($\Delta m\ \rho - R_p\ \Delta t$), Δm = ejected mud mass; ρ mud density; R_p= mud pump rate; Δt = time increment
47	MUDEJCT	Accumulated mud mass ejected at surface
48	SPLVOL2	Incremental equivalent uncompacted spalled volume
49	SPLMAS2	Incremental equivalent spalled mass
50	BEDDEPTH	Bed depth TENSRAD-CAVRAD
51	FORCHRAT	Forchheimer test ratio

Table VG-3. CAMDAT Element Variable Names

Index	Element Variable Name	Domain	Description
1	POREPRS	Repository	Repository pressure
2	RADEFSTR	Repository	Radial effective stress
3	TANEFSTR	Repository	Tangential effective stress
4	POREVEL	Repository	Pore velocity
5	RADELSTR	Repository	Radial elastic stress
6	TANELSTR	Repository	Tangential elastic stress
7	RADSPSTR	Repository	Radial seepage stress
8	TANSPSTR	Repository	Tangential seepage stress
9	FLUDSTRT	Repository	Fluidization start time
10	FLUDSTOP	Repository	Fluidization stop time
11	FAILSTRT	Repository	Failure start time
12	SUPRVEL	Repository	Superficial velocity
13	WELLPRS	Wellbore	Pressure
14	WELLVEL	Wellbore	Mixture velocity
15	WELLGSMS	Wellbore	Gas mass
16	WELLWSMS	Wellbore	Waste mass
17	WELLRHO	Wellbore	Mixture density
18	WELLWSVF	Wellbore	Waste volume fraction
19	WELLGSVF	Wellbore	Gas volume fraction
20	WELLSAVF	Wellbore	Salt volume fraction
21	WELLWSMF	Wellbore	Waste mass fraction
22	WELLGSMF	Wellbore	Gas mass fraction
23	WELLMDMF	Wellbore	Mud mass fraction
24	WELLVOL	Wellbore	Cell volume
25	COORD	Repository, Wellbore	Repository and well coordinate positions (center of cell)

WASTE ISOLATION PILOT PLANT (WIPP)
Distribution List
(Revised 7/27/2005)

Federal Agencies

1 Department of Energy
Office of Civilian Radioactive Waste Mgmt.
Attn: Deputy Director, RW-2
Forrestal Building
Washington, DC 20585

7 US Department of Energy
Carlsbad Field Office
Attn: D. Moody
G. Basabilvazo
S. Casey
D. Mercer
R. Nelson
R. Patterson
Mailroom
P.O. Box 3090
Carlsbad, NM 88221-3090

1 US Department of Energy
Office of Environmental Restoration and Waste Management
Attn: P. Bubar, EM-20
Forrestal Building
Washington, DC 20585-0002

1 US Department of Energy
Office of Environmental Restoration and Waste Management
Attn: Mary Bisesi/Lynne Smith, EM-23
Washington, DC 20585-0002

2 US Environmental Protection Agency
Radiation Protection Programs
Attn: B. Forinash
ANR-460
Washington, DC 20460

Boards

1 Defense Nuclear Facilities Safety Board
Attn: D. Winters
625 Indiana Ave. NW, Suite 700
Washington, DC 20004

State Agencies

1 Attorney General of New Mexico
P.O. Drawer 1508
Santa Fe, NM 87504-1508

2 Environmental Evaluation Group
Attn: Library
7007 Wyoming NE
Suite F-2
Albuquerque, NM 87109

1 NMED Hazardous Waste Bureau
WIPP Project Leader
2905 Rodeo Park Dr E., Bldg 1
Santa Fe, NM 87505-6303

1 NM Bureau of Geology & Mineral Resources
801 Leroy Place
Socorro, NM 87801

Laboratories/Corporations

1 Battelle Pacific Northwest Laboratories
Battelle Blvd.
Richland, WA 99352

1 Los Alamos National Laboratory
Attn: B. Erdal, INC-12
P.O. Box 1663
Los Alamos, NM 87544

3 Washington TRU Solutions
Attn: Library, GSA-214
P.O. Box 2078
Carlsbad, NM 88221

Universities

1 University of New Mexico
Geology Department
Attn: Library
141 Northrop Hall
Albuquerque, NM 87131

Libraries

1 Eastern New Mexico University
Golden Library
Regional Federal Depository
University & Avenue K
Portales, NM 88130-7402

1 Farmington Public Library
Regional Federal Depository
2101 Farmington Avenue
Farmington, NM 87401-6420

1 New Mexico Highlands University
Thomas C. Donnelly Library
Regional Federal Depository
12th & National
Las Vegas, NM 87701

1 New Mexico Inst. of Mining & Technology
Joseph R. Skeen Library
Regional Federal Depository
Bullock & Leroy Streets
Socorro, NM 87801-4696

1 New Mexico Junior College
Pannell Library
Regional Federal Depository
5317 Lovington Highway
Hobbs, NM 88240-9121

1 New Mexico State University
Branson Library
Regional Federal Depository
801 Leroy Place
Las Cruces, NM 88003-8006

1 New Mexico State Library
Regional Federal Depository
1209 Camino Carlos Rey
Santa Fe, NM 87507-5166

1 New Mexico Supreme Court
Law Library
Regional Federal Depository
237 Don Gaspar Avenue
Santa Fe, NM 87501

1 University of New Mexico
Government Information/General Library
Regional Federal Depository
1 University of New Mexico
Albuquerque, NM 87131-0001

1 University of New Mexico
School of Law Library
Regional Federal Depository
1117 Stanford Drive NE
Albuquerque, NM 87131-1441

1 Western New Mexico University
J. Cloyd Miller Library
Regional Federal Depository
1000 West College Avenue
Silver City, NM 88062-0680

Consultants

1 Golder Associates, Inc.
Attn: Bill Thompson
44 Union Boulevard, Suite 300
Lakewood, CO 80228

1 TerraTek
Attn: Mao Bai
Pioneer Business Park
1935 S. Fremont Drive
Salt Lake City, UT 84104

1 Mike Gross
415 Riviera Drive
San Rafael, CA 94901-1530

1 ASRC Energy Services
E&P Technology Inc.
Attn: John McLennan
1419 McClelland Street
Salt Lake City, UT 84105

1 John F. Schatz Research & Consulting
4636 South Lane
Del Mar, CA 92014

2 GRAM, Inc.
Attn: Krishan Wahi
8500 Menaul Blvd, NE
Suite B-335
Albuquerque, NM 87112

Foreign Addresses
(Note: Not needed for all documents)

2 Francois Chenevier
ANDRA
Parc de la Croix Blanche
1-7 rue Jean Monnet
92298 Chatenay-Malabry Cedex
FRANCE

1 Commissariat a L'Energie Atomique
Attn: D. Alexandre
Centre d'Etudes de Cadarache
13108 Saint Paul Lez Durance Cedex
FRANCE

1 Bundesanstalt fur Geowissenschaften und Rohstoffe
Attn: M. Wallner
Postfach 510 153
D-30631 Hannover
GERMANY

1 Bundesministerium fur Forschung und Technologie
Postfach 200 706
5300 Bonn 2
GERMANY

1 Gesellschaft fur Anlagen und Reaktorsicherheit (GRS)
Attn: B. Baltes
Schwertnergasse 1
D-50667 Cologne
GERMANY

1 Dr.-Ing. Klaus Kuhn
TU Clausthal Institut fur Bergbau
Erzstr. 20
D-38678 Clausthal-Zellerfeld
GERMANY

1 Dr. Susumu Muraoka
Nuclear Material Control Center
Tokai-Mura, Ibaraki-Ken, 319-11
JAPAN

2 Nationale Genossenschaft fur die Lagerung Radioaktiver Abfalle
Attn: NAGRA Library
Hardstrasse 73
CH-5430 Wettingen
SWITZERLAND

1 AEA Technology
Attn: W. R. Rodwell
424-4 Harwell
Didcot, Oxfordshire OX11 OQJ
UNITED KINGDOM

Internal

	MS	Org.	
1	0701	6100	P. B. Davies
2	0731	6034	823 Library
1	0771	6800	D. Berry
1	1395	6821	D. S. Kessel
1	1395	6822	M. Rigali
1	1395	6821	E.D. Vugrin
1	1395	6821	M.B. Nemer
1	1395	6821	G.R. Kirkes
1	0776	6852	J.S. Stein
10	0706	6113	D. L. Lord
1	1165	5101	C.W. Hansen
1	0771	6853	F.D. Hansen
1	0136	0216	M.K. Knowles
8	1395	6034	WIPP Library
2	1395	6034	WIPP Records
2	9018	8945-1	Central Technical Files
2	0899	4536	Technical Library


Sandia National Laboratories